WT-1335 — *SAN*

OPERATION REDWING — PROJECT 5.9 —

WEAPON EFFECTS ON MISSILE STRUCTURES AND MATERIALS (U),
Sanitized Version

WARNING!
All pages of this document will be
afforded ... the over-
... on the cover of
the document.

C. J. Cosenza, Lt, USAF, Project Officer
G. W. Mills
G. J. Roth

Aircraft Laboratory
Wright Air Development Center
Wright-Patterson Air Force Base
Dayton, Ohio

3—4

F C/ 04601011

THIS PAGE LEFT INTENTIONALLY BLANK.

FOREWORD

This report presents the final results of one of the projects participating in the military-effect programs of Operation Redwing. Overall information about this and other military-effect projects can be obtained from WT-1344, the "Summary Report of the Commander, Task Unit 3." This technical summary includes: (1) tables listing each detonation with its yield, type, environment, meteorological conditions, etc.; (2) maps showing shot locations; (3) discussion of results by programs; (4) summaries of objectives, procedures, results, etc., for all projects; and (5) a listing of project reports for the military-effect programs.
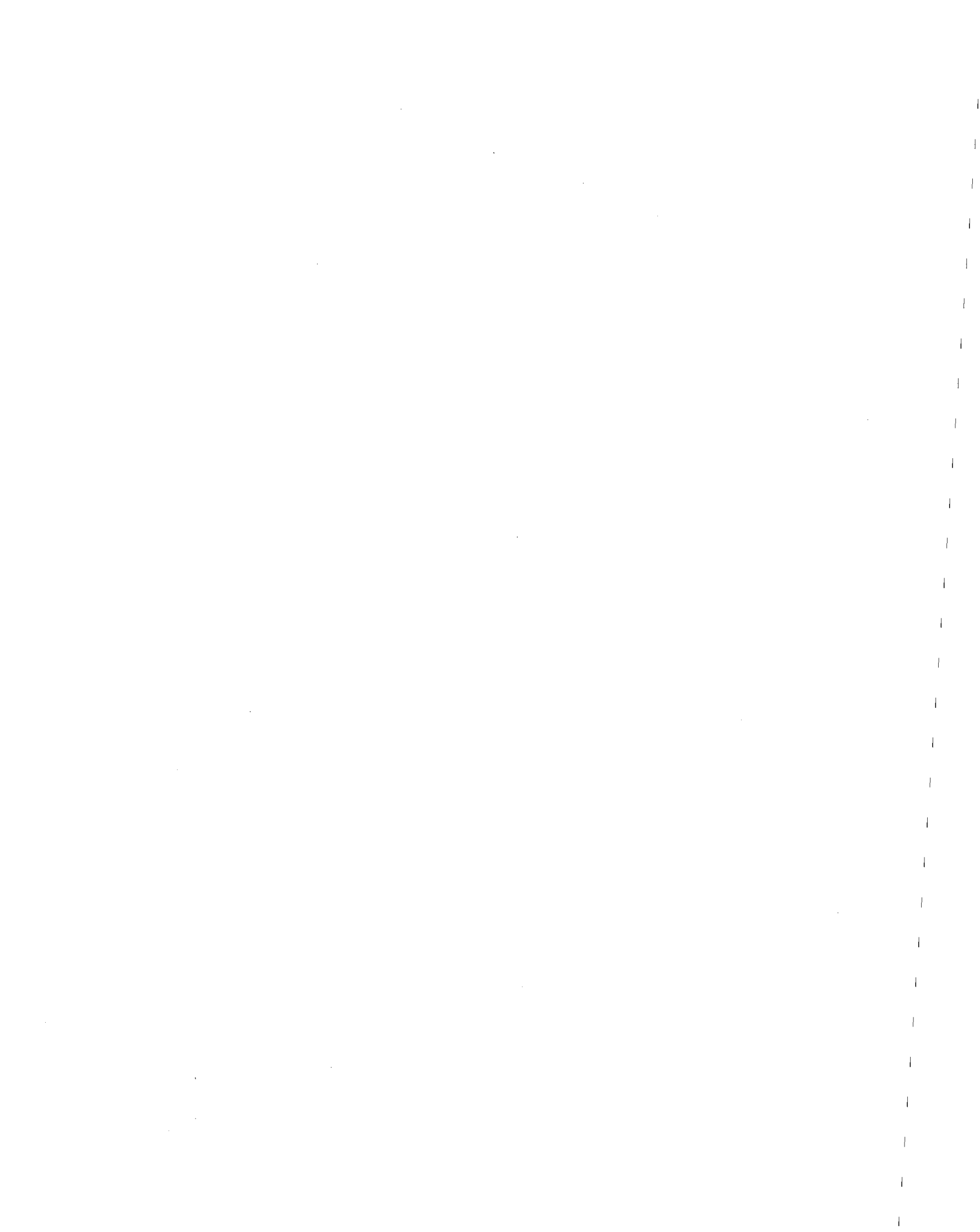
ABSTRACT

The objective of Project 5.9 was to investigate the vulnerability of basic missile structures and materials to fireball and associated phenomena of a nuclear detonation.

Tests consisted of exposing a total of 103 specimens, comprising over 30 different designs, within the fireballs of Shots Erie and Mohawk. On Shot Erie, exposures were made at seven locations ranging from 25 to 300 feet from the burst point; on Shot Mohawk, specimens were exposed at two elevations on a tower 525 feet from ground zero. As much as possible, the specimens were designed so that the effects of each of the several mechanisms causing thermal damage could be evaluated individually.

Eighty-eight of the 103 specimens which were exposed were recovered: 79 out of 94 from Shot Erie and all 9 from Shot Mohawk. The high radiation level after the shots delayed the major recovery effort for approximately 3 months. Results of the material evaluation studies showed that 8-inch-diameter spheres of stainless steel, molybdenum, and titanium sustained approximately equal mass ablation which was 0.08 psi at 100 feet and 0.06 psi at the 200-foot range. Copper sustained 2 to 4 times the mass ablation of the above three metals, and plastic experienced substantially less than any of the metals for the exposure conditions on Shot Erie. The existence of an attenuating vapor layer was substantiated by the data, and a few specimens indicated that the removal of this vapor layer by hydrodynamic means had affected the ablation. The apparent anomaly of approximately equal ablation experienced by the 12-inch-diameter steel spheres at Stations 150, 200, 250, and 300 on Shot Erie could, for the most part, be explained on the basis of ablation by melting after emergence from the fireball. It was shown that removal of a molten layer by spinning off drops of the material could be significant to total ablation and would be important to ICBM destruction if the missile had an appreciable angular velocity.

The electrically instrumented Operation Redwing specimens have shown that it is feasible to record data electrically inside the fireball of a nuclear detonation with a system similar to that used on Redwing. The velocity-distance impact gages which were adequately protected from the effects of overpressure and material ablation operated satisfactorily and yielded apparently reliable velocity versus distance data. It has been shown also that ball-crusher gages may be successfully employed to observe experimentally peak fireball pressures and accelerations, provided the approximate shape of the dynamic input is known.

6

PREFACE

In the interest of maintaining an adequate system for defending against modern implements of war, the U. S. Air Force has been charged with evaluating the feasibility of using nuclear weapons in defense against intercontinental ballistic missiles. Such an evaluation requires a determination of the vulnerability of an incoming missile to a nuclear detonation.

FC/ 04601011

CONTENTS

10

12

14

Chapter 1
INTRODUCTION

1.1 OBJECTIVE

The objective of this project was to investigate the vulnerability of basic missile structures and materials to fireball and associated phenomena of a nuclear detonation. Specifically, the project was to determine: (1) comparative susceptibility of certain ballistic missile materials to fireball environment; (2) characteristic gust accelerations, overpressures, and thermal energy produced by the fireball; (3) response of basic structural configurations to the fireball and associated phenomena, primarily to evaluate the mechanism causing material loss as well as parameters producing other types of destruction; and (4) response of hypersonic test vehicle nose cones in static exposures for comparison with results obtained from similar vehicles in dynamic exposures.

1.2 MILITARY SIGNIFICANCE

Since this project had basic objectives nearly identical to those of Project 5.4 of Operation Teapot, the military significance of the earlier test also applied here. The following was taken from Paragraph 1.2 of the Final Report of Project 5.4, Operation Teapot:

> The fact that intercontinental ballistic missiles are nearly reality, with the consequent threat to the security of the nation, makes the development of an adequate defense system an urgent requirement. Considerable thought has been given to the problem of protecting against hostile intercontinental ballistic missiles; however, partly because of the scarcity of vulnerability data, there is at present no positive method of defense. Because of the very high velocity and the variety of evasive tactics that can be employed, the problem of intercepting and destroying a ballistic missile of the Atlas type imposes severe requirements on the hypothetical defense system. Because of the magnitude of the anticipated average miss-distance, it is doubtful that conventional warheads have sufficiently large lethal radii to give a reasonable overall probability of successful interception.

> It has been speculated that a nuclear warhead of nominal yield, or larger, may have a greater lethal range of destruction than conventional warheads in the application of ballistic missile defense. However, because of the lack of factual information on the capabilities of nuclear weapons employed in this manner, it was suggested that an experimental test be conducted.

1.3 BACKGROUND AND THEORY

The feasibility of using nuclear or thermonuclear weapons as defensive measures against intercontinental ballistic missiles is currently being studied from a theoretical standpoint by several agencies. The results of at least one of these studies indicate that the use of such a

weapon appears to be more effective when defending against an enemy missile carrying a
nuclear warhead than against one bearing a conventional high explosive charge. [REDACTED]

[illegible redacted text]
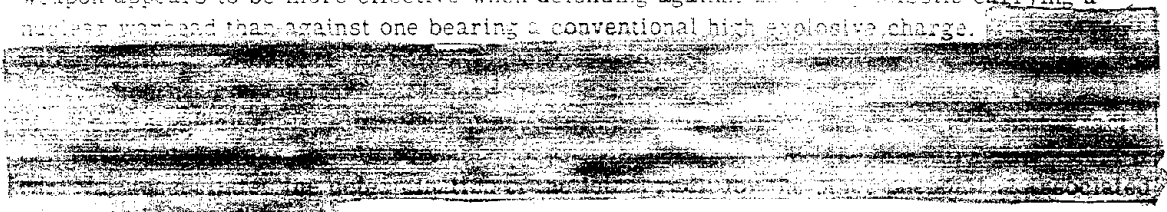
On Operation Teapot, Project 5.4 exposed several steel and aluminum specimens on towers
at various ranges within the fireball of Shot 12. The experiment was limited in scope, since it
was not certain that the test articles would be recovered; however, all the tower specimens
were found and the objective of the test accomplished. Consequently, a more extensive test
was planned with confidence for Operation Redwing.

Material loss parameters selected for investigation were type of material, surface curva-
ture, orientation, thermal attenuation by the metallic vapors given off by the object, and
spalling. Project 5.9 was designed to investigate the effects of all the above mechanisms and,
in addition, the effects of blast and overpressure.

SECRET

Chapter 2
PROCEDURE

A total of 103 specimens comprising over 30 different types, materials, and sizes were exposed within the fireballs of Shots Erie and Mohawk of Operation Redwing. Basically, the test consisted of mounting the specimens near the burst points atop lightweight towers, recovering them after the explosion, and later determining the type and degree of the resulting damage.

The test was designed to accomplish the specific Objectives 1, 2, and 3 listed in Section 1.1. Objective 4, to determine the response of hypersonic test vehicle nose cones in static exposures for comparison with results obtained from similar vehicles in dynamic exposures, was deleted from the program because the project which was to furnish the dynamic exposure data was cancelled.

2.1 SHOT ERIE

Six tower sites were planned for this shot, the locations and tower heights being such that the approximate slant ranges from the burst point varied from 50 feet to 300 feet in 50-foot increments. However, during the erection of the towers and the mounting of specimens an accident occurred in which the two towers at the 50-foot station were destroyed. Consequently, a mounting rig was devised and attached to the shot tower so that the test specimens could be positioned at approximately the same points in space as had been planned originally. The lines from the burst point through the specimen arrays were on different azimuths from the shot tower, and each was at an angle of approximately 45 degrees to the horizontal. One additional array of specimens was mounted on the side of the shot tower, 25 feet from the burst point. The location of this array was such that the specimens would be propelled downward at an angle of approximately 38 degrees from the vertical. A drawing showing the locations and heights of all stations is presented in Figure 2.1.

Because of the accumulative weight of the specimens exposed at the first three tower stations, two towers were required at each. Similarly, although the total weight was not excessive, two towers were erected at the fourth tower station because of the large unbalanced moments which would have been present in a single tower with cross-beam arrangement when the instrumented sphere described in Section 2.5 was lowered to the ground. At all stations, except Station 50 where the improvised rig was made of steel, the superstructures for mounting the specimens consisted of aluminum beams. From Station 50 through Station 200 three cross beams, or tiers, were required; at Stations 250 and 300 one tier at each was sufficient. The specimens were mounted above and below the cross beams with aluminum and steel brackets. These were designed to fail in such a way that the moments introduced into the specimens during failure would be sufficiently low to minimize undesirable tumbling effects. A typical specimen array is shown in Figure 2.2.

A complete summary of the specimen exposures is presented in Section 2.7, following the detailed descriptions of the specimens themselves.

17

Station & Slant Range (ft)	Ground Range (ft)	Tower Height (ft)
25	—	—
50	35	—
100	71	230
150	106	195
200	142	159
250	177	124
300	212	89
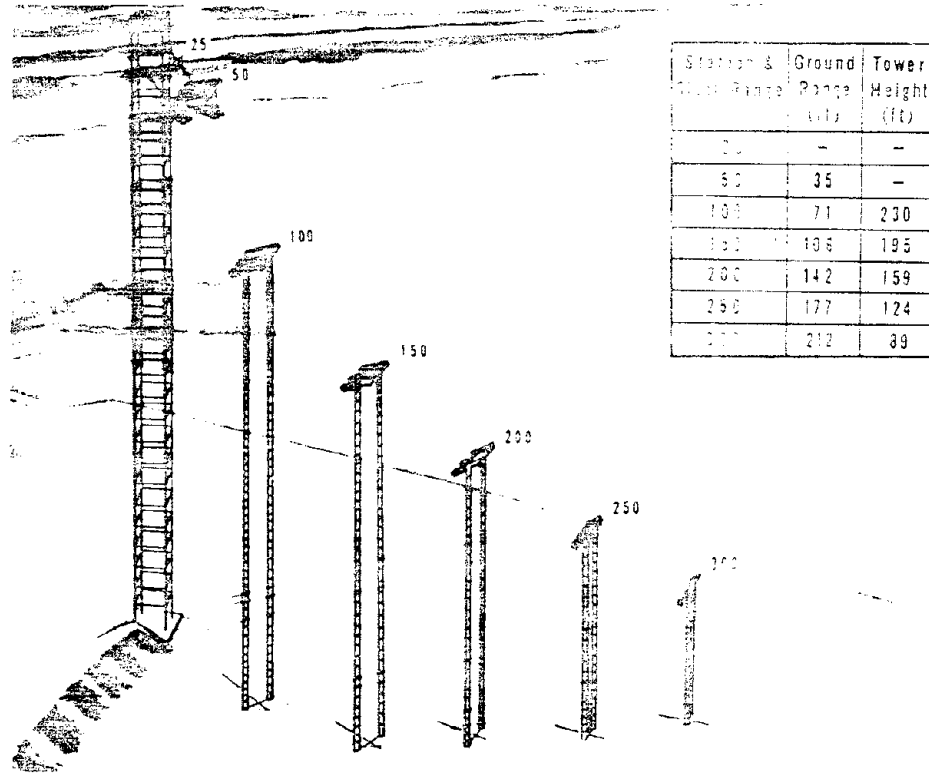
Figure 2.1 Station layout for Shot Erie, showing slant ranges, ground ranges, and tower heights.
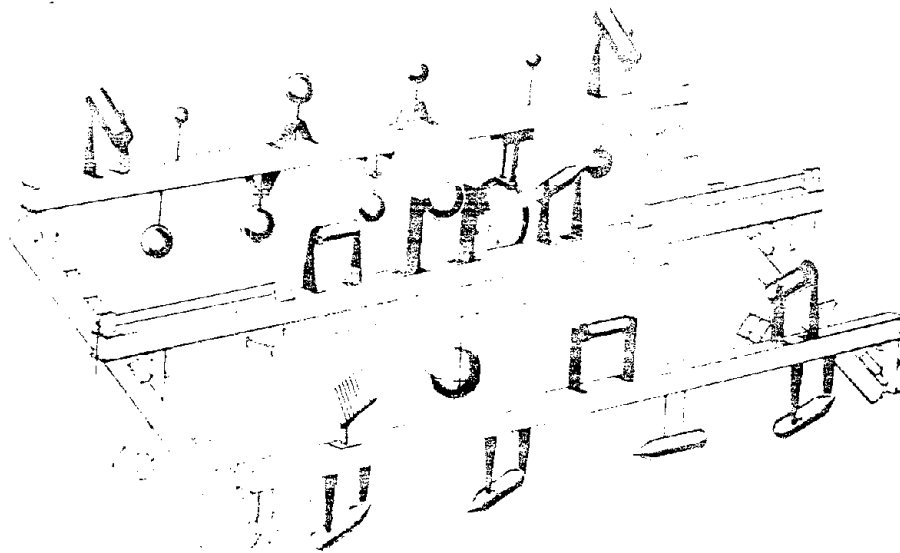
Figure 2.2 Specimen array for Shot Erie Station 50. (Other stations similar except for support of mounting structures.)

18

The purpose of the specimen exposures during this shot was to determine the comparative effectiveness of the lower temperature, coupled with longer time exposure within the fireball, from a higher yield weapon during the latter stages of fireball development. A specimen exposure tower 150 feet high was erected at a ground range of 525 feet. Seven spheres, as shown schematically in Figure 2.3, were exposed at the top of the tower, which was 545 feet from the burst point; and two spheres were exposed at an elevation of 70 feet on the tower, which was 575 feet from the burst point. Using the cube root scaling law to scale damage (in the absence of a known method of scaling metal loss data), the damage to the specimens exposed during ~~........................~~) should have been roughly comparable to that damage which the specimens received at Station 200 during ~~....................~~
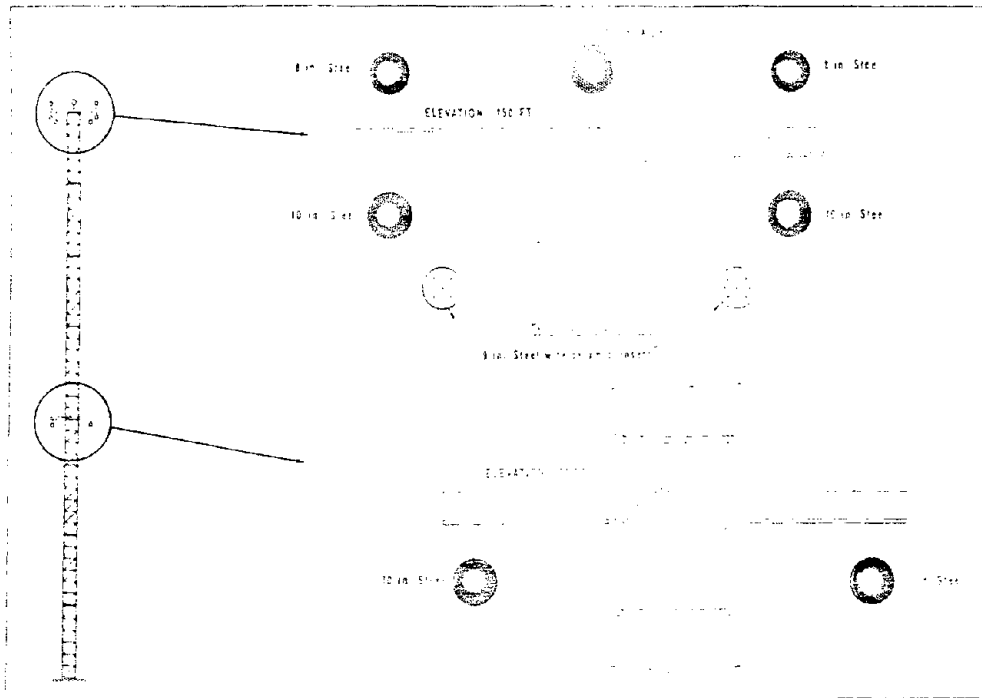
Figure 2.3 Specimen exposure for Shot Mohawk.

2.3 PASSIVE SPECIMENS

The majority of specimens were designed to accomplish the test objective by providing a means for determining the effect of configuration, orientation, and type of material involved on the amount of surface material removed. Wherever possible, the designs were such that the effects of the parameter under investigation were maximized, and the effects of the others were minimized.

2.3.1 Steel Spheres. Spherical specimens of mild steel were exposed to Shot Erie for two reasons: (1) to obtain data required for establishing a range-yield scaling procedure for any given thermal damage level, and (2) to determine variation in material loss with radius of curvature. To accomplish the first, 10-inch-diameter spheres were exposed at the 25-foot, 50-foot, and 100-foot ranges, where the material loss would be large and hence measurable with a fair degree of accuracy. The resulting data, in conjunction with comparable information obtained during Operation Teapot, was to permit attainment of the objective. Additional data on range scaling procedure could also be obtained from the instrumented spheres (Section 2.4)

19

and the overpressure spheres (Section 2.5.2) which were 12 inches in diameter and located at Stations 100 through 300. To determine the variation in material loss with radius, spheres of 4-, 6-, 8-, 10-, 12-, and 16-inch diameters were exposed, together with the 20-inch segment of a 33-inch-diameter sphere. All these specimens were located at the 50-foot range.

On Shot Mohawk, all the nine specimens involved were spherical. However, because of the flat trajectories anticipated and the associated recovery problems, the diameters and elevations were varied, as indicated in Figure 2.3.

2.3.2 Composites. To determine the effect of shape and orientation of a specimen on the amount of material lost from its surface, solid cylinders and cones were exposed in various orientations in addition to the spheres enumerated in the previous paragraph. In the interest of economy, however, the composite specimen shown in Figure 2.4 was adopted. Comprising both

Figure 2.4   Composite specimen combining conical, cylindrical, and spherical surfaces.

a cylindrical and a 60-degree conical surface, as well as a hemispherical end, the specimen provided a means of obtaining a large amount of information from a relatively small number of specimens. The specimens were made either of steel or aluminum and were 6 inches in diameter. Those of steel were exposed in various orientations at four ranges. At each of these ranges, an aluminum specimen was mounted in a nose-on orientation. Nearly all these specimens contained the device described in Section 2.5.1 for measuring specimen velocity.

To provide a means of determining material loss resulting from the passage of the high-density (though relatively cool) shock wave over an object, three aluminum composite specimens were exposed in a special manner; each was housed in a shield (Figure 2.5) having a large frontal area, so that the shields would separate from the specimens either during or just after the passage of the shock front. Thus, the specimens would be protected from a considerable portion of the blast although completely exposed within the fireball. The difference between the material lost by the unshielded and shielded specimens at the same range was to be an indication of the damage inflicted by the shock wave.

2.3.3 Flat Plates. Flat steel and aluminum plates were exposed; (1) to extend data on the material loss versus radius for a sphere of infinite radius, (2) to understand better the thermal attenuation afforded by metallic vapors, and (3) to evaluate the effectiveness of the hydrodynamic sweeping away of the vapors.

Two of the specimens are shown in Figure 2.6. The flat areas were 10 inches square; the nose angles were 33 degrees and the thicknesses were $2\frac{3}{8}$ and $2\frac{1}{8}$ inches for the steel and
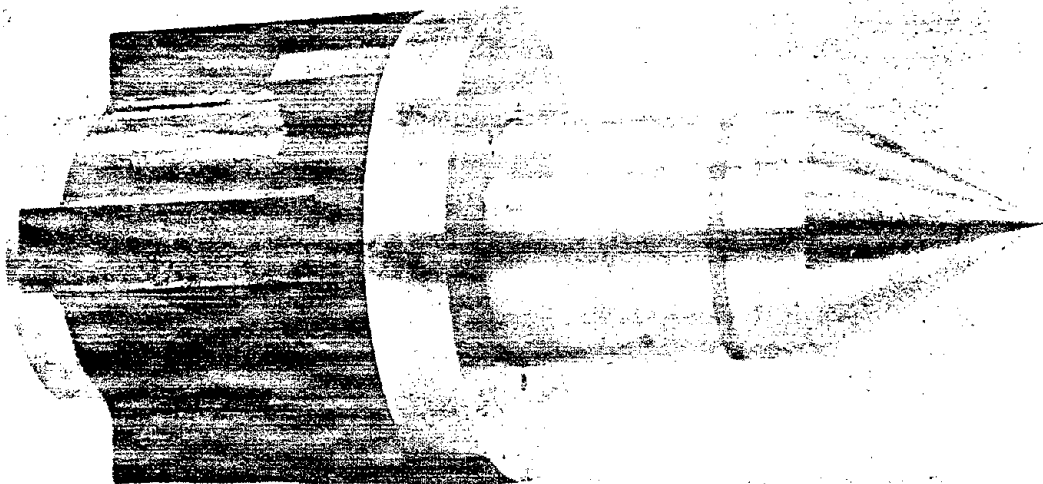
Figure 2.5 Composite specimen with shield.
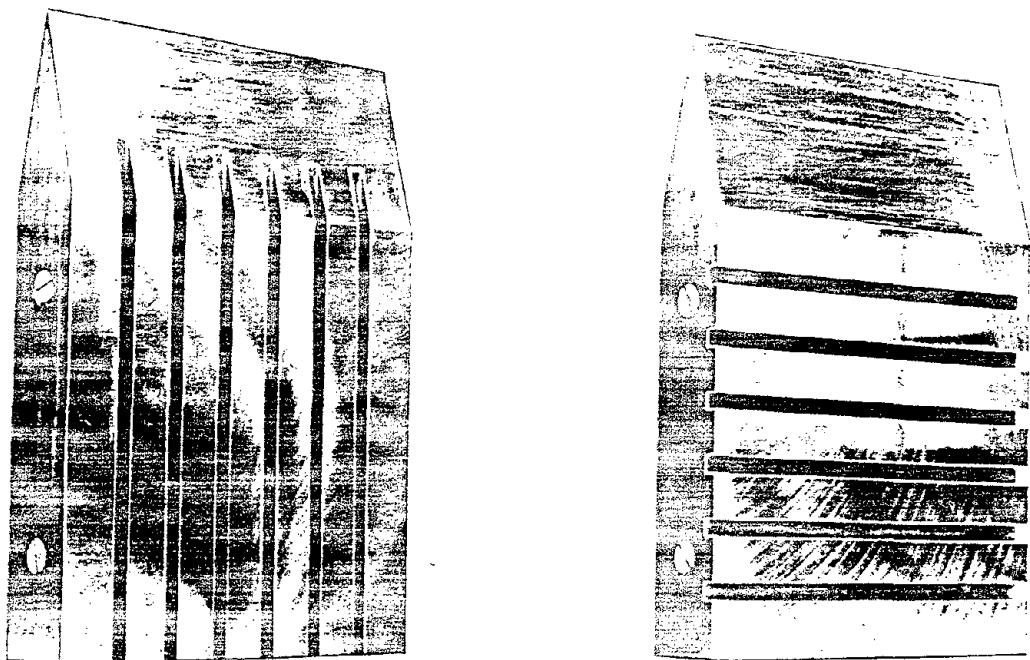
Figure 2.6 Flat plates showing longitudinal and transverse grooves.

21

aluminum specimens, respectively. During exposure, the plates were mounted in a vertical plane with the tapered edge toward the burst point.

The plain surface was to yield data for the study of material loss versus radius, and the grooved areas were for the remaining two investigations. As shown in the figure, the grooves existed in directions both longitudinal and transverse to the direction of shock propagation. In size, the grooves were 0.4 inch wide and 0.4 inch deep and were 1.0 inch apart.

Although any analyses concerning the grooves must consider both types of specimens, the transversely grooved plates were intended primarily for the study of the thermal attenuation properties of vapors, and the longitudinally grooved specimen was intended for hydrodynamic study.

One of the transversely grooved plates was exposed at each of the following stations: 50, 100, 150, and 200; the transversely grooved aluminum plate and the longitudinally grooved steel plate were both at Station 150.

2.3.4 Laminated Cylinders. Among various mechanisms from which damage to a structure may result is thermal spalling, where a strong shock wave, induced in the material by the thermal radiation, may cause relatively large bits of material to be ejected from the surface of the structure. It appears likely that comparatively thin-skin structures may be more vulnerable to this type of damage than would solid objects because of the smaller shear area involved in the spalling process.

Since water-cooled, thin-skin structures have been considered as possible missile bodies, it was deemed advisable to explore their vulnerability to this mechanism. Therefore, six cylinders of aluminum laminations having tubular shapes pressed over solid steel cores were constructed. The thicknesses of the layers varied from $\frac{1}{8}$ to $\frac{3}{8}$ inch, with the number of laminations being so chosen that the total thickness outside the core of any one specimen was approximately twice the expected metal loss for a solid aluminum specimen at the same range. Figure 2.7 shows a laminated cylinder made up of four layers, each $\frac{3}{8}$ inch thick. In all cases, the overall diameter and length of the specimens were 5 inches and $11\frac{1}{2}$ inches, respectively.

2.3.5 Hollow Cylinders. In an attempt to determine the crushing forces attributable to overpressure and the combination of overpressure and dynamic pressure, one of each of the hollow cylinders shown in Figure 2.8 was exposed at Station 50. The pointed cylinder was oriented with the cone end toward the burst point; the other was mounted for a side-on exposure. Both specimens were made of mild steel.

2.3.6 Ballistic and Dynamic-Pressure Cylinders. The objective of the exposure of the ballistic cylinders was to verify certain calculations regarding blow-off pressure. The term blow-off pressure as used here means the force per unit area on the surface of a specimen caused by the vaporization of material from the surface. The name ballistic cylinders was assigned to the specimens, since the trajectories of the cylindrical specimens were to be the basis for obtaining the desired information. A typical specimen is shown in Figure 2.9. Two specimens were 7 inches in diameter, 11 inches long, and were made of solid mild steel with a bakelite plastic disk, $\frac{1}{2}$ inch thick and $5\frac{1}{2}$ inches in diameter, embedded in one end. A third specimen, a solid steel cylinder of the same size but containing no plastic, was similarly exposed for purposes of comparison.

All these cylinders were exposed at Station 100. One of the two with plastic was oriented with its axis in a vertical plane and normal to the direction of shock propagation with the plastic disk facing upward. The other was oriented with its axis along the line to the burst point and with the plastic disk facing away from the burst point.

Preliminary calculations indicated that the blow-off pressure resulting from the vaporization of the plastic should be greater than that resulting from the vaporization of the steel on the opposite end. The unbalanced force would then deflect the specimens from the trajectories which would normally be traversed. To determine these deflections, the third specimen was mounted at the same range and with the same orientation as the first. The deflections thus determined were used to calculate the relative blow-off pressures.

As the name dynamic pressure implies, certain cylindrical specimens were exposed in an attempt to obtain some time-history data on the dynamic pressure within the fireball. These

22
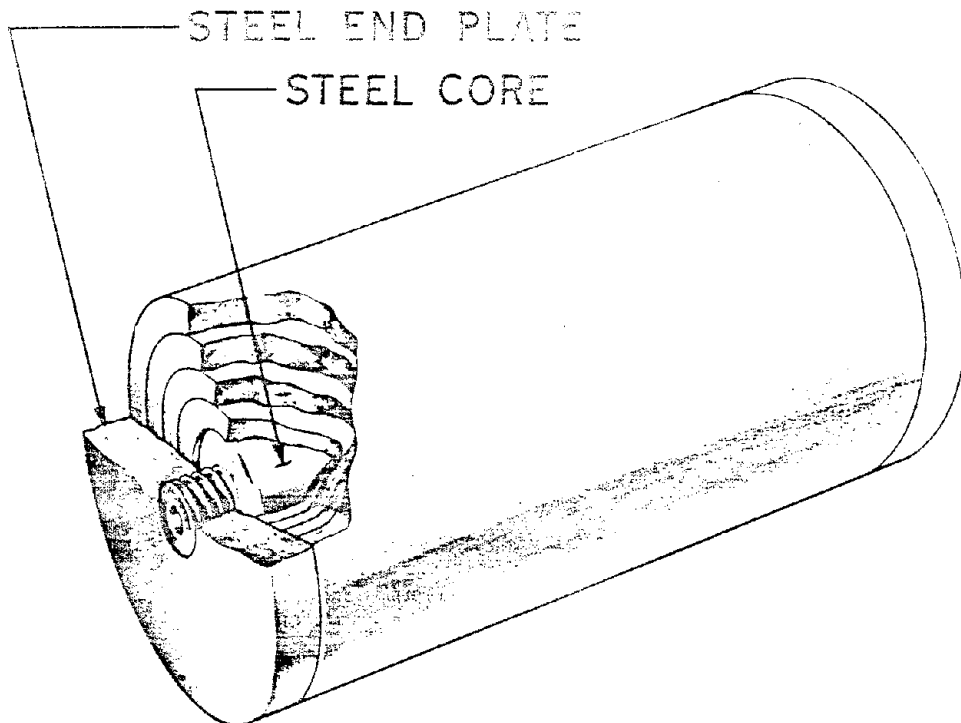
Figure 2.7 Laminated cylinder.
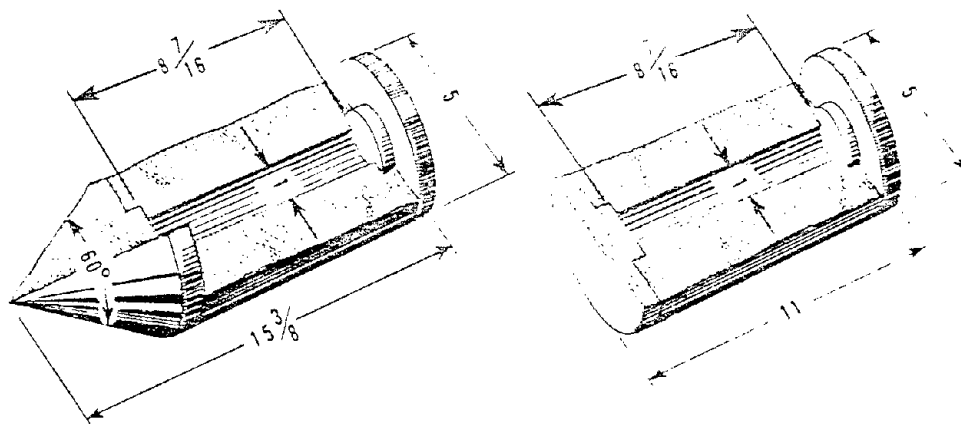
Figure 2.8 Hollow cylinder to investigate effects of overpressure (left) and dynamic pressure (right).

specimens were also exposed to obtain data on the effect of shape and orientation on the material loss. The specimens employed were cylinders 7 inches in diameter and 14 inches long, each containing a mechanical device designed to provide information on specimen velocity as a function of specimen travel. The velocity-distance impact gage used for this purpose is described in Section 2.5.1. One specimen was exposed in an end-on orientation at each of the

Figure 2.9 Ballistic cylinder with bakelite disk.

three ranges, 50, 150, and 250 feet. In addition, two specimens similar to the dynamic-pressure cylinders, except with bakelite plastic disks in one end, as with the ballistic cylinders, were mounted at the 150-foot range. The cylinders were exposed in an end-on orientation with the plastic disks toward the burst point. In this way, the blow-off pressure would add an additional propelling force to the specimen, thus causing a steeper rise in the velocity-distance curve and a correspondingly greater acceleration measurement. By a comparison, then, between the cylinders with and without the bakelite, an additional determination of the blow-off pressure should be possible.

2.3.7 Material Evaluation. As a means for determining the depth of metal loss as a function of the material involved, numerous specimens were exposed at various stations. Materials under investigation were copper, titanium, tantalum, stainless steel, molybdenum, reinforced plastic, and graphite. To determine material loss by the simplest of measurements, all the materials, with the exception of tantalum, were exposed as 8-inch-diameter solid spheres. Copper was used for the control specimen, with one sphere being placed at each of the first six ranges. In the interest of economy, only three or four spheres of each of the other materials were employed; the locations varied from the nearest to the most remote ranges. The station locations of all specimens are shown in Table 2.4.

In addition to the material loss information for the copper spheres, a determination of the maximum temperature attained versus depth below the surface was also desirable. This information was obtained by the method described in Section 2.5.3.

24

The extreme cost of tantalum precluded the possibility of exposing this material in a spherical form; and hence, the specimen shown in Figure 2.10 was designed as an alternate. Tantalum sheets of two thicknesses, 0.050 and 0.100 inch, were welded into cylindrical shells 3 inches in diameter and 4 inches long. These were filled with molten copper, machined, and
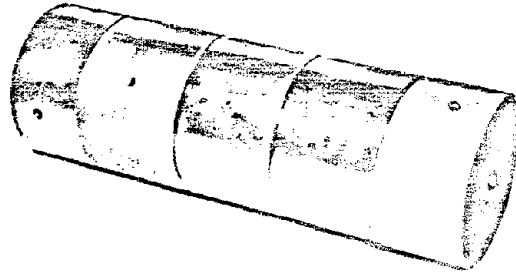
Figure 2.10   Tantalum specimen.

Figure 2.11   Plastic sphere.

assembled, together with solid copper disks, as shown in the figure. No direct measurements of material loss could be made on these specimens, but a determination of the relative susceptibility of tantalum was assumed possible by observation of the shielding afforded to the copper by the two thicknesses of tantalum.

Since not only the material but also the shape and fabricating technique might affect the overall vulnerability of a plastic specimen, cylinders of a similar material, though fabricated by different technique, were exposed in addition to the spheres. The spheres, shown in Figure 2.11, were molded into shape by the Cincinnati Testing and Research Laboratories, Cincinnati,

25

Ohio, using macerated Volan-A finished, 181 weave, fiberglas cloth and CTL-91-LD resin. The cylinders were fabricated by Narmco, Incorporated, of San Diego, using Conolon 506 resin and 181 weave, Volan-A cloth. A ½-inch-diameter mandrel was molded first, and the desired diameter of 5 inches finally obtained after a step-by-step process of rewrapping, curing, and machining.
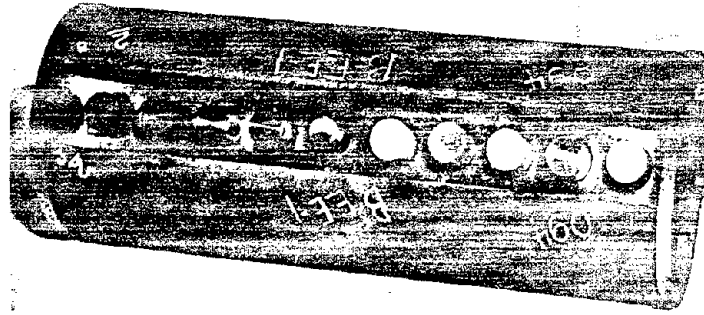
Figure 2.12 Cylindrical holder for ceramic and alloy samples.
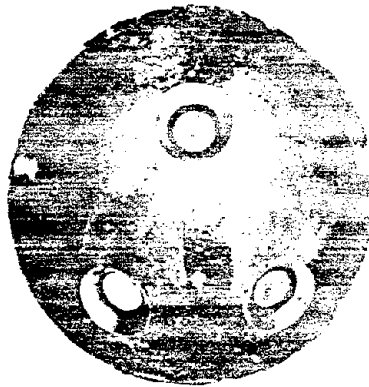
Figure 2.13 Spherical holder for ceramic and alloy samples.

Several cylindrical and spherical holders for samples of special purpose alloys and ceramics were designed and fabricated by the Missile and Ordnance Systems Department of the General Electric Company, Schenectady, New York, for use in determining the thermal effects on these materials. For Shot Erie, six of the cylindrical holders shown in Figure 2.12 were employed. Each was 6 inches in diameter and 16 inches long and contained samples of 10 materials. The materials involved, as well as the exposure ranges, are listed in Table 2.1. For Shot Mohawk, two 9-inch-diameter spheres (Figure 2.13) were used as specimen holders. Each contained 14 inserts of the materials being tested. These materials are also listed in Table 2.1.

26

TABLE 2.1 SUMMARY OF CERAMIC AND SPECIAL A LOY EXPOSURES

Sample Material	Specimen Holder and Range							
	EMIT Test						MOHAWK Test	
	#1-Cyl 25 ft.	#2-Cyl 50 ft.	#3-Cyl 50 ft.	#4-Cyl 100 ft	#5-Cyl 200 ft	#6-Cyl 200 ft	#1-Sph 545 ft	#2-Sph 545 ft
Mo + Cr Plate	X	X		X			X	
Al$_2$O$_3$. TiO$_2$			X		X			X
Mo		X				X		X
S-816 Co - base alloy	X	X		X				
MgO + binder (Norton)			X		X		X	
M-252 Ni-base alloy		X				X		
"hydrocal" pottery plaster and graphite	X	X		X			X	
BN + Si$_3$N$_4$			X		X		X	
Cu		X				X		
Refrax 10 - SiC bonded with Si$_3$N$_4$	X	X		X				X
Q - felt + polyester			X		X		X	
Graphite		X				X		
Al(OH)$_3$ + fiberglas + polyester	X	X		X				
B$_4$C + polyester			X		X		X	
Carboloy (GE tungsten carbide cermet)		X				X		X
Sintered and extruded alum.+ Al$_2$O$_3$-powder metal product	X			X		X		
Phenolic asbestos felt			X		X			
Graphite + Cr plate	X			X		X	X	
MgO + binder (Carborundum)			X		X			X
K 162 B Kentanium (TiC cermet)	X			X		X	X	
Glass cloth and melamine			X		X			X
Durhy - Si impregnated into SiC	X			X		X	X	X
Glass mat and polyester			X		X			X
Cu + Cr plate	X			X		X		X
Mo, Ceramic Coated							X	X
Molded compound phenolic asbestos			X		X			
Ni + 10% (vol) Al$_2$O$_3$							X	
SiC (KT fine)							X	X
Quartz rod								X
MgO + ZrO$_2$								X
Al$_2$O$_3$ (Norton)							X	
ZrO$_2$ (Carborundum)								X
Rokide C coated graphite							X	

The General Electric Company also prepared two specimens for exposure to high neutron flux. The specimens consisted of sections of 4-inch pipe approximately 2 feet long which contained samples of various electronic components. Among the articles enclosed in the pipes were transistors, diodes, resistors, capacitors, ferrite cores, crystals, and peak-temperature indicating devices. The pipes were buried about 18 inches below ground level, 35 feet from Shot Erie ground zero.

2.4 ELECTRICALLY INSTRUMENTED SPECIMENS

Appendix B, Electrical Recording Within the Fireball, describes in detail the recording system and specimen design used in Project 5.9 and presents an evaluation of the results obtained. A brief abstract of Appendix B is included in this report for the reader who requires only general knowledge of the electrical instrumentation system.

Six electrically instrumented specimens, each containing a miniature tape recorder, were exposed inside the fireball of Shot Erie. Five were spheres 12 inches in diameter and were exposed at slant ranges of approximately 100, 150, 200, 250, and 300 feet from the detonation point. The sixth specimen was a 16-inch-diameter sphere exposed at a slant range of 50 feet. The addition of 4 inches to its diameter was required at the 50-foot range because calculations indicated the 12-inch design did not provide adequate mechanical protection.

A spherical shape was chosen for the instrumented specimens because it was the configuration most capable, structurally, of withstanding the crushing forces. Its drag coefficient was independent of orientation, and the ballistics of a sphere were somewhat predictable, thus facilitating specimen recovery after the test. The main body of the container and all external caps were made of high strength steel. Since the strongest specimen possible would have been a solid sphere, the container was designed to approach this ideal as nearly as possible. Figure 2.14 illustrates the 12- and 16-inch container design. The 16-inch specimen was essentially one of the 12-inch specimens with a 2-inch-thick shell completely enclosing it. This shell was fabricated in two pieces which could be screwed together and was machined and ground to close tolerances so that it would fit tightly around the inside sphere.

The recorders employed were miniature magnetic tape recorders developed primarily for use in experimental rockets and manufactured by North American Instruments Inc. Recorders of this design were reported to have operated satisfactorily under axial accelerations up to 500 grams and angular accelerations up to 200 radians/sec^2. The recorders were 4 inches in diameter and 6 inches long including their own battery power. Eight channels of data were recorded on the $\frac{1}{2}$-inch-wide Mylar recording tape. The specimens were instrumented to record time histories of acceleration, depth of melting of the surface material, and specimen temperatures near the surface. The direct recording of low power fluctuating direct current on magnetic tape was accomplished by partially erasing a prerecorded alternating-current signal as described in Appendix B, Section B.2.2. That section also describes the frequency response of the entire system which was flat within 10 percent from 0 to 55 cps.

Each instrumented sphere contained two accelerometers: one measured the acceleration along the radial line from the burst point through the specimen and the other, mounted normal to the first, measured the acceleration in the plane of the shot tower and the specimen. Statham Laboratories Type A5A-1000-50 accelerometers of the unbonded strain gage type with a range of ±1000 grams were used for all specimens. Calibration of each accelerometer channel was accomplished by introducing given millivolt steps into the recording head and measuring the resultant deflection on the playback oscillograms. This information combined with the calibration factor relating grams and millivolts supplied with each instrument by the manufacturer permitted a calibration curve of grams versus millivolts to be drawn for each channel.

The depth-of-melt (DOM) transducer was designed to put out a pulse when the specimen melting had reached a predetermined depth below the surface. It consisted of two insulated conductors connected in series with a battery and recording head and located at a predetermined depth below the surface of the specimen. When the specimen melted to the depth of the conductors, contact would be established by the molten metal and a pulse recorded on the tape. This would provide an indication of the time required for the specimen to melt to that depth.

28

A triplet DOM consisted of three depth-of-melt transducers at different depths connected together with a suitable circuit and recorded on one channel. The only calibration required for a single DOM channel was the determination of the polarity of the signal produced when the two conductors were shorted. Calibration of the triplet DOM channel, however, required the determination of the relative pulse heights from each channel as well as the polarity of the signals.
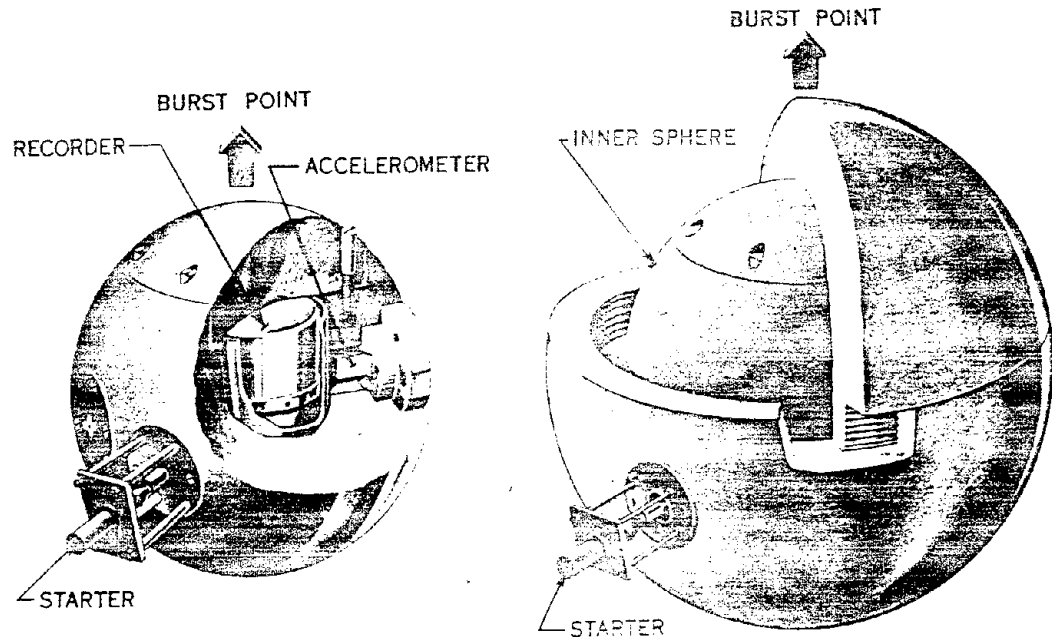
Figure 2.14   Twelve- and sixteen-inch instrumented spheres.

Thermocouples were of the chromel-alumel type and were designed to measure the temperature at various depths below the surface of the specimen as described in Appendix B, Section B.2.3. Calibration of the thermocouple channels was accomplished by accepting the standard chromel-alumel thermocouple tables of millivolts versus temperature and establishing the millivolt sensitivity of each channel by the method described above for the accelerometers.

The primary timing reference consisted of a 1000-cps transistor oscillator which furnished timing information that was relatively independent of external influences. A secondary timing reference, consisting of recording the output of a pulse transformer connected in series with the armature of the tape drive motor, was utilized because of the recognized vulnerability of transistors to neutron bombardment.

Table 2.2 lists the data recorded on each channel of the recorder for all ranges.

The reduction of the test data was accomplished by playing back the test tape on a modified Ampex playback unit and recording these data on a Consolidated Electrodynamics oscillograph. The Ampex equipment was also used for checking out the tape recorders and for prerecording the test tapes.

29

TABLE 2.2 CHANNEL DISTRIBUTION FOR MAGNETIC RECORDERS

	Station					
Channel	50 Ft.	100 Ft.	150 Ft.	200 Ft.	250 Ft.	300 Ft.
1	1 kc Timing	1 kc Timing	1 kc Timing	1 kc Timing	1 kc Timing	1 kc Timing
2	DOM[a]	DOM	DOM	DOM	DOM	DOM
3	Motor Timing	Motor Timing	Acc.	Motor Timing	Motor Timing	Motor Timing
4	DOM	DOM	DOM	T.C.[b]	T.C.	T.C.
5	Acc.[c]	Acc.	Acc.	Acc.	Acc.	Acc.
6	DOM	Triplet DOM	DOM	T.C.	T.C.	T.C.
7	Acc.	Acc.	Motor Timing	Acc.	Acc.	Acc.
8	DOM	Triplet DOM	DOM	T.C.	T.C.	T.C.

[a] DOM—Depth of melt.
[b] T.C.—Thermocouple.
[c] Acc.—Accelerometer.

2.5 MECHANICALLY INSTRUMENTED SPECIMENS

Several of the specimens were equipped with passive type instrumentation which was of the peak reading or point value type. These gages were designed in attempts to measure: (1) specimen velocity as a function of distance moved, (2) peak overpressure at each tower station, and (3) peak temperature variation of a copper sphere.

2.5.1 Velocity-Distance Impact Gages. The device employed to obtain the velocity-distance data consisted of a number of blunt-end, steel plungers arranged to penetrate a soft aluminum target block after the specimen had moved a prescribed distance. A cutaway drawing of a specimen containing a gage is shown in Figure 2.15 and a similar drawing of the gage itself in Figure C.1. Under the influence of dynamic pressure, the specimen moved away from the burst point, while the plunger, because of its inertia, was assumed to stay stationary in space. The specimen, while moving through the distance separating the plunger and target block, attained a particular velocity, and the amount of penetration of the plunger into the target block was approximately proportional to the square of this velocity. The insert in each specimen contained several plungers, each maintained at a different distance from its target block by an adjustable spacer. Thus, the velocity of each specimen could be determined at several distinct points. The dynamic-pressure cylinders and the composite specimens, oriented nose-on, from Stations 100 to 250 feet, each had seven plungers. The composite specimens at the 25- and 50-foot stations each contained five plungers. Preliminary calculations showed that, assuming an exponential decay of dynamic pressure, the specimen velocities would approach a maximum rapidly, under some conditions, even within a few inches. Consequently, most of the plungers were positioned rather close to their target blocks.

Shields for the shielded composite specimens were also equipped with velocity-distance plungers. The main purpose of their use in the shields was for a determination of the rate of separation between the shield and the specimen.

Because of various specimens and ranges involved, numerous types of plungers were required. Trial tests were performed using the calibration device described in Appendix C. Results of these tests indicated the proper plunger-tip diameter to use to obtain an optimum penetration for any preassigned expected velocity calculated from the theoretical impulse data. After the sizes of the plungers were determined, a complete calibration was performed
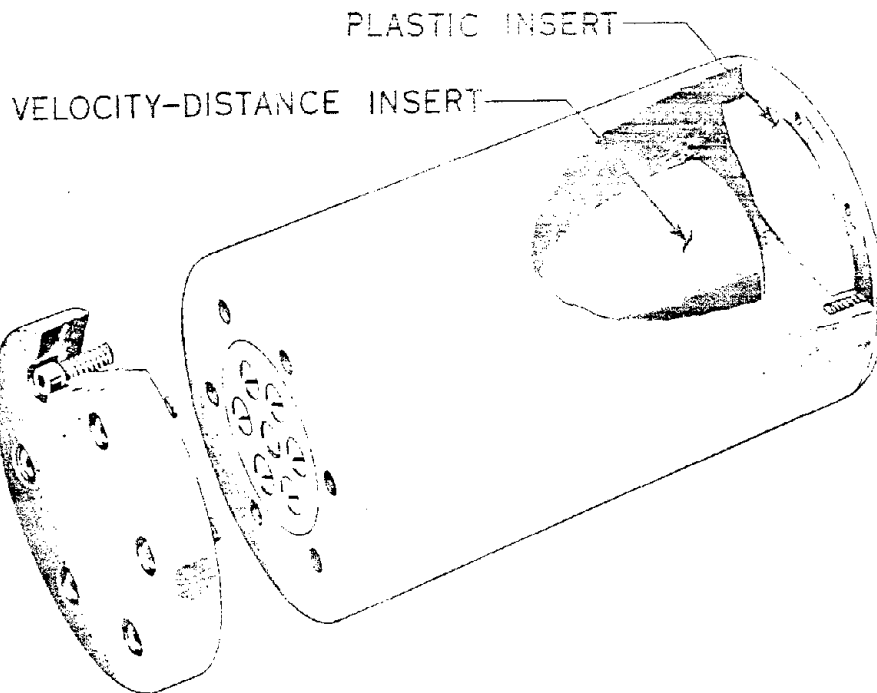
Figure 2.15 Dynamic pressure cylinder showing velocity-distance insert.
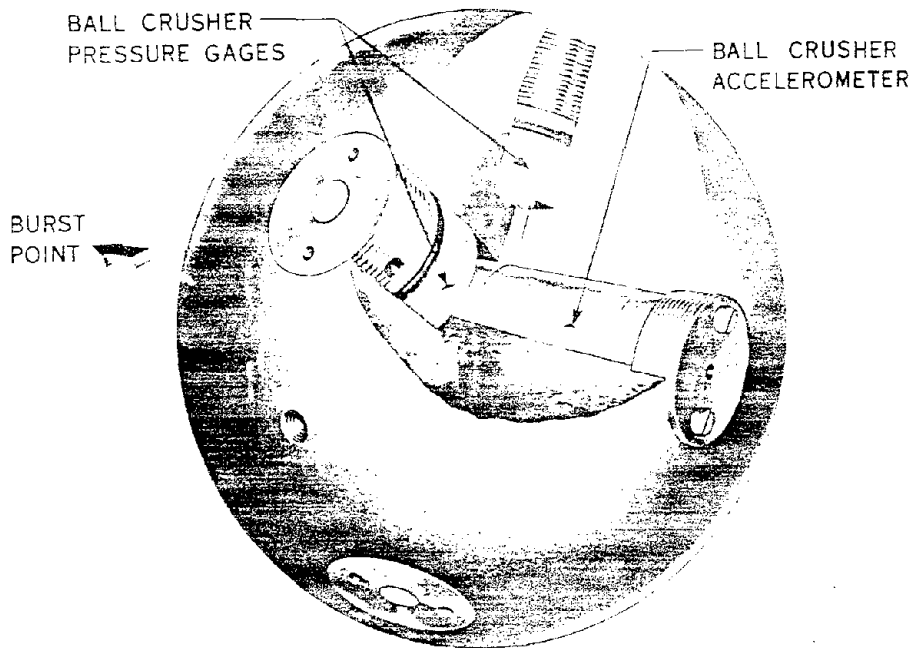
Figure 2.16 Overpressure sphere.

for each. The results agreed quite closely with theory and showed a reproducibility of within a few percentage points. A more complete description of the velocity-distance impact gage is presented in Appendix C.

2.5.2 Overpressure Spheres. For measurement of peak overpressure and its variation with range inside the fireball, an additional spherical specimen was exposed at each station, except the first. The specimens, one of which is shown in Figure 2.16, were instrumented with ball-crusher gages. Two types of gages were involved, one for the measurement of peak overpressure and one for the measurement of maximum specimen acceleration. Detailed drawings of both types are shown in Figures D.1 and D.2. Each spherical specimen contained four pressure gages and two accelerometers. The former were equally spaced around the sphere in a plane normal to the direction of shock propagation, and the latter were at the rear of the specimen with their axes parallel to this direction.

The design, fabrication, and calibration of both devices, as well as the basic design of the specimen itself, were accomplished by personnel of Allied Research Associates, Inc., of Boston, Massachusetts. Appendix D, Ball-Crusher Gages for the Measurement of Pressure and Acceleration Within the Fireball of a Nuclear Detonation, describes the theory upon which the design of the gages is based. The basic principle involved is that, within relatively wide limits, the plastic deformation of the balls is proportional to the forces exerted on them by the sliding pistons. This linearity exists, in connection with annealed copper balls, for deformation up to 30 percent of the ball diameter; the limit is somewhat lower for other materials. Because of the extreme forces involved, aluminum balls were used in the pressure gages at Station 50; at all other stations, however, annealed copper balls were employed. Dynamic calibrations were conducted using a drop-test apparatus to obtain accurate values for deformation constants. By use of these values, the desired information was obtained.

In an exploratory attempt to determine whether the pressure exerted on a body as a result of the vaporization process, i.e., the blow-off pressure, is appreciable, the front surface of one of the pressure gages at Station 150 was altered, as follows: the exposed piston was cut down and threaded, and a $\frac{1}{2}$-inch-thick piece of Micarta plastic was screwed onto the end. Also, to minimize the edge effects, the central portion of the cylinder face was recessed and plugged with Micarta. The lightweight plastic was expected to be blown off with more momentum than steel, thus causing a force to act on the ball which would be larger than those forces experienced in the other three gages at that station.

2.5.3 Copper Sphere Peak Temperature Determination. In addition to the material loss information for the copper sphere, a determination of the maximum-temperature-attained versus depth-below-the-surface was also desirable. For this purpose, each copper sphere was fitted with a large tapered pin in which were embedded small slugs of various pure metals and eutectic alloys. The pin was to be removed after recovery, and the maximum temperatures attained at various depths were to be determined by observing which of the slugs had melted.

2.6 SPECIMEN MATERIALS AND PROPERTIES

A complete listing of the materials and mechanical properties of the specimens is given in Table 2.3.

2.7 SUMMARY OF SPECIMEN EXPOSURE

Figure 2.17 shows pictorially the exact location of all specimens including type, slant range, tower site, tier, and location on the tier. The orientation of the specimens may also be determined by considering the burst point to be at the top of the chart.

A summary of the specimen exposure for Shots Erie and Mohawk arranged according to specimen type is presented in Table 2.4.

TABLE 2.3   SUMMARY OF MATERIALS AND MECHANICAL PROPERTIES

Code	Material	Ultimate tensile strength, psi	Tensile yield strength, psi	Code	Material	Ultimate tensile strength, psi	Tensile yield strength, psi
A	1045 steel	98,000[a]	59,000[a]	Q	1045 steel	98,000[a]	59,000[a]
B	2017-T4 aluminum	55,000[b]	32,000[b]	R	Conolon 506 resin with 181 weave fiberglas cloth	–	–
C	2017-T4 aluminum	55,000[b]	32,000[b]				
D	1045 steel	98,000[a]	59,000[a]				
E	Cast aluminum	–	–	S	Tantalum, commercially pure	–	–
F	1045 steel	98,000[a]	59,000[a]	T	2017-T4 aluminum	55,000[b]	32,000[b]
G	CTL-91-LD resin with macerated 181 weave fiberglas cloth	12–15,000	–	U	1045 steel	98,000[a]	59,000[a]
				V	1045 steel	98,000[a]	59,000[a]
				W	1045 steel	98,000[a]	59,000[a]
H	Speer grade 6095	–	–	X	4340 steel heat treated Rockwell C43-46	190,000	180,000
I	99.99% molybdenum	–	–				
J	416 stainless steel	85,000[a]	50,000[a]				
K	99.9% titanium type A-70	95,000[c]	84,100[c]	Y	4340 steel heat treated Rockwell C43-46	190,000	180,000
L	OFHC electrolytic tough pitch copper	–	–	Z	1045 steel	98,000[a]	59,000[a]
				AA	1045 steel	98,000[a]	59,000[a]
M	1045 steel	98,000[a]	59,000[a]	BB	1045 steel	98,000[a]	59,000[a]
N	1045 steel	98,000[a]	59,000[a]	CC	1045 steel	98,000[a]	59,000[a]
O	1045 steel	98,000[a]	59,000[a]				
P	1045 steel	98,000[a]	59,000[a]	DD	Bakelite plastic cotton fiber	–	–
				EE	See Table 2.1		

[a] Joseph T. Ryerson and Son, Inc.
[b] Alcoa Structural Handbook.
[c] Rem-Cru Titanium, Inc.

STATION & NOMINAL SLANT RANGE (ft.)		UPPER TIER	MIDDLE TIER	LOWER TIER
25	ABOVE BEAM		S 22.6; L 22.6; A 22.9; EE 23.5	
	BELOW BEAM		N 24.3; K 24.2; J 24.4; I 24.8	
50	ABOVE BEAM	EE 45.2; Q 44.9; P 44.7; L 44.7; Q 44.9; EE 45.2	V 44.0; Z 43.7; W 44.0	U 43.8; R 43.4; D 43.7
	BELOW BEAM	H 46.7; M 46.3; O 46.2; H 46.4; G 46.6	Y 46.3	B 45.6; A 45.5; A 45.8; A 45.3
100	ABOVE BEAM	T 95.8; T 95.8; EE 95.8; T 95.9; D 95.7		I 95.4; L 95.3; DD 95.3; K 95.3; CC 95.4
	BELOW BEAM	A 97.5; A 97.7; B 97.6; S 97.7	X 97.9	N 97.6; J 97.4; CC 97.4; BB 97.4; Z 97.7
150	ABOVE BEAM	L 156; G 156; T 156; T 156; T 156		D 156; E 156; R 156; F 156
	BELOW BEAM	A 158; B 158; C 159; A 158	X 159	H 159; AA 158; Z 159; AA 159; U 159
200	ABOVE BEAM	EE 202; B 202; S 202; EE 202; DD 202		K 202; L 202; D 201
	BELOW BEAM	C 204; C 204; A 204; A 204	X 205	I 204; Z 204; J 204
250	ABOVE BEAM		U 254; Z 254; I 254	
	BELOW BEAM		G 257; X 257; H 257	
300	ABOVE BEAM		G 304	
	BELOW BEAM		Z 306; X 306	

Figure 2.17   Specimen distribution as to station and tier for Shot Erie. Code letters refer to those given in Table 2.4 and numbers are the actual specimen slant ranges in feet.

TABLE 2.4   SUMMARY OF TEST SPECIMEN EXPOSURE

			ERIE							
CODE	SPECIMEN	MATERIAL	STATION							TOTAL
			25	50	100	150	200	250	300	
A	Composite Specimen	Steel	1	3	2	2	2			10
B	Composite Specimen	Aluminum		1	1	1	1			4
C	Composite Specimen-Shielded	Aluminum				1	2			3
D	Flat Plate-Grooved-Transverse	Steel		1	1	1	1			4
E	Flat Plate-Grooved-Transverse	Aluminum				1				1
F	Flat Plate-Grooved-Parallel	Steel				1				1
G	Sphere	Plastic		1		1		1	1	4
H	Sphere	Graphite		1		1		1		3
I	Sphere	Moly	1		1		1			3
J	Sphere	S. Steel	1		1		1			3
K	Sphere	Titanium	1		1		1			3
L	Sphere	Copper	1	1	1	1	1	1		6
M	Sphere 32"	Steel			1					1
N	Sphere 10"	Steel	1	1	1					3
O	Sphere 8"	Steel		1						1
P	Sphere 6"	Steel		1						1
Q	Sphere 4"	Steel		2						2
R	Cylinder	Plastic		1		1				2
S	Cylinder	Tantalum	1		1		1			3
T	Laminated Cylinder	Aluminum			3	3				6
U	Dynamic Pressure Cylinder	Steel		1		1		1		3
V	Hollow Cylinder (Pointed)	Steel		1						1
W	Hollow Cylinder (Blunt End)	Steel		1						1
X	Instrumented Sphere 12"	Steel			1	1	1	1	1	5
Y	Instrumented Sphere 16"	Steel		1						1
Z	Overpressure Sphere	Steel		1	1	1	1	1	1	6
AA	Dynamic Pressure Cyl. (w/plastic insert)	Steel					2			2
BB	Ballistic Cylinder	Steel			1					1
CC	Ballistic Cyl. (w/plastic insert)	Steel			2					2
DD	Bakelite Cylinder	Bakelite			1		1			2
EE	Cylinders with Ceramic Inserts	Steel	1	2	1		2			6
	(TOTALS)		8	22	20	19	16	6	3	94

			MOHAWK		
CODE	SPECIMEN	MATERIAL	ELEVATION		TOTAL
			70 FT	150 FT	
N	Sphere 10"	Steel	2	2	4
O	Sphere 8"	Steel		2	2
FF	Spheres with Ceramic Inserts	Steel		2	2
GG	Sphere 10"	Aluminum		1	1
	(TOTALS)		2	7	9

35
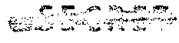
Chapter 3
RESULTS

3.1 SHOT AND RECOVERY DATA

Of the 103 specimens exposed in fireballs by Project 5.9, 88 were recovered. Table 3.1 lists all the specimens exposed to Shot Erie and indicates the 79 which were recovered from that shot, as well as those which were not. All nine specimens exposed to Shot Mohawk were recovered. This chapter summarizes specimen damage; Appendix A contains a detailed discussion of each recovered specimen.

3.1.1 Shot Erie. Shot Erie was detonated at 0615:30 hours atop a 300-foot tower on 31 May 1956. ~~~~~~ Figure 3.1 shows the Shot Erie fireball at 1, 4, 7, and 14 msec after detonation. Table 3.2 is a tabulation of the Shot Erie fireball dimensions and positions from 25 msec to approximately 1 second. At 1600 hours on shot day, i.e., H hour plus 10, an aerial survey team flew over the specimen-impact area for purposes of observation and photography. The photographs were intended to preserve, for use during the recovery program, any visible evidence of specimen penetration into the ground. The level of residual radiation, however, was extremely high, and a minimum flight altitude of 200 feet was designated by the Radiological Safety Unit. As a consequence, the photographs did not possess sufficient detail for the intended purpose, and the effort was repeated at 1100 hours on 1 June at an altitude of 100 feet.

Reliable radiation readings, obtainable only at ground level, were not available until 4 days after the shot, at which time they indicated a value of 13.5 r/hr. However, the following day after a heavy rainfall, a value of 5 r/hr was obtained; apparently the rain had leached some of the fallout material into the ground.

On 7 June, 7 days after detonation, a party entered the impact area to recover at least one instrumented sphere, as well as any other specimens which were visible. Although the radiation level was approximately 3 r/hr and the permissible time in the area was correspondingly short, the mission was successful. The instrumented sphere from Station 300 was found and removed from the area.

On 19 June, 19 days after the shot, another recovery party entered the impact area and recovered nine additional specimens. The radiation level at that time was 1 r/hr, which was too high for an extended recovery effort. Arrangements were made with Rad-Safe to supply Project 5.9 with weekly radiation level readings of the impact area. This arrangement afforded the opportunity for Project 5.9 personnel to return to the United States to await a reasonably low radiation level before attempting full scale recovery. Figure 3.2 shows the radiation decay of the Shot Erie impact area as plotted from the Rad-Safe readings.

On 13 September 1956, after the level of radiation had decayed to approximately 200 mr/hr, Project 5.9 personnel returned to the test site and attempted to recover the specimens by hand digging; however, when only seven additional specimens had been recovered after

TABLE 8.1 SUMMARY OF RECOVERED SPECIMENS SHOT KNEE

CODE	SPECIMEN	MATERIAL	IMPACT 25	50	100	150	200	250	300	RECOVERED 25	50	100	150	200	250	300	TOTAL EXP.	REC.
A	Composite Specimen	Steel	1	3	2	2	2				2	2ᵃ	2	2ᵇ			10	8
B	Composite Specimen	Aluminum		1	1	1	1										4	0
C	Comp. Spec. Shielded	Aluminum				1						1ᶜ	2ᶜ				3	3
D	Flat Pl. Grooved Trans.	Steel		1	1	1	1						1	1			4	3
E	Flat Pl. Grooved Trans.	Aluminum				1											1	0
F	Flat Pl. Grooved Parallel	Steel				1						1					1	1
G	Sphere	Plastic		1		1			1			1ᵈ		1			4	2
H	Sphere	Graphite		1		1						●		●			3	2
I	Sphere	Mo.	1		1					f	1		1				3	3
J	Sphere	S. Steel	1		1					d	1		1				3	3
K	Sphere	Titanium	1		1						1		1				3	2
L	Sphere	Copper	1	1	1	1	1	1		1	1	1	1	1			6	5
M	Sphere 32"	Steel		1													1	0
N	Sphere 10"	Steel	1	1	1						1						3	2
O	Sphere 8"	Steel		1													1	1
P	Sphere 6"	Steel		1													1	0
Q	Sphere 4"	Steel		2													2	1
R	Cylinder	Plastic		1		1											2	0
S	Cylinder	Ta. Cu.	1		1						1		1				3	2
T	Laminated Cylinder	Aluminum			3	3						1ᵍ	2ᵍ				6	3
U	Dyn. Press. Cylinder	Steel		1		1					1		1		1		3	3
V	Hollow Cylinder (Pt.)	Steel		1													1	0
W	Hollow Cylinder (Bl. End)	Steel		1													1	0
X	Instr. Sphere 12"	Steel			1	1	1	1	1		1	1	1	1	1		5	5
Y	Instr. Sphere 16"	Steel		1													1	1
Z	Overpressure Sphere	Steel		1	1	1	1	1	1	1	1	1	1	1	1		6	6
AA	Dynamic Pressure Cyl.	Steel			2							2ʰ					2	2
BB	Ballistic Cylinder	Steel			1						1						1	1
CC	Ballistic Cylinder	Steel			2						2						2	2
DD	Bakelite Cylinder	Steel		1		1							1ʲ				2	1
EE	Cylinder With Ceramic Inserts	Steel	1		1	2					1		2				6	3
	Unidentified V-S Capsule	Steel																5
	(TOTALS)		8	21	20	19	15	5	3	2	11	15	14	13	6	2	94	79

ᵃ Without Insert, Cone and Sphere
ᵇ Without Cone
ᶜ Only the Shield was Recovered
ᵈ Approximately 1/2 of Sphere
ᵉ Several Large Pieces Recovered But Not Identified
f Part of a Specimen
ᵍ Steel End Caps Missing
ʰ Without Plastic Disc
ʲ Approximately 1/2 of Cylinder

2 days, it was decided to use heavy equipment. Carryalls (pans) were used to remove about 6 inches of the surface at a pass and then to spread out the material in layers about 2 inches thick. By this method, specimens could be recovered either in the impact area or in the dumping area.

A few specimens were found on the surface, but the remaining ones were found at depths ranging from a few inches to 5 feet. It is estimated that the heavy equipment moved on the order of 100,000 yd³ of soil during recovery. After removing 6 to 8 feet of soil from all areas that specimens could reasonably have impacted, it was decided that the time and expense to search a larger area could not be justified, in view of the low probability of success. The recovery effort therefore was terminated on 1 November 1955.
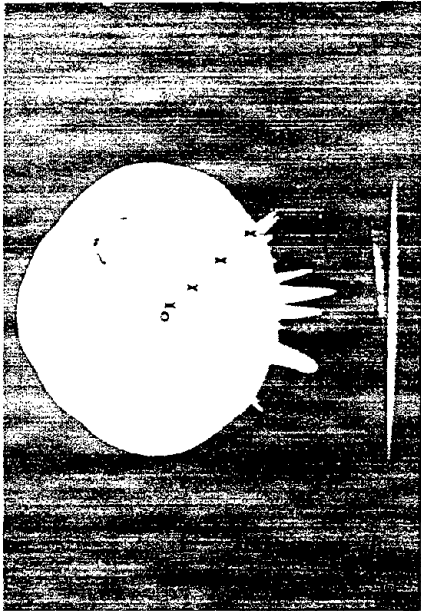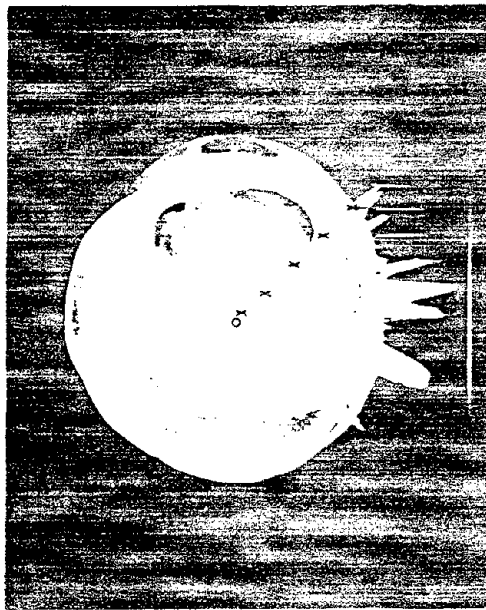
4 MILLISECONDS

14 MILLISECONDS

1 MILLISECOND

7 MILLISECONDS

Figure 3.1 Shot Erie fireball growth.

38

TIME AFTER DETONATION	FIREBALL DIMENSIONS					
	a	b	c	d	e	f
MSEC	FT	FT	FT	FT	FT	FT
25	0	643	0	0	264	600
35	448	738	30	30	262	619
45	511	765	48	48	251	649
55	641	835	49	76	264	664
65	684	865	56	75	251	662
75	598	902	71	109	267	697
85	724	862	95	114	286	722
95	667	984	106	106	270	730
145	805	1081	156	156	322	810
195	860	1116	171	171	389	868
295	1046	1257	221	221	427	957
495	1071	1379	219	219	524	1052
745	1413	1413	106	106	596	1149
995	1365	1365	87	87	640	1176

Data obtained from Edgerton, Germeschausen and Grier motion pictures (1000 frames/sec.) by Allied Research Associates, Inc.

3.1.2 Shot Mohawk. Shot Mohawk was detonated on 3 July 1956 at 0606 hours. ▒▒▒▒▒▒ ▒▒▒▒▒▒▒▒▒▒▒▒▒▒▒▒▒▒ No immediate recovery was attempted because of the high level of radiation. On 4 July, an aerial survey team flew over the specimen impact area for the purpose of observation and photography. Shot Mohawk radiation decay data were supplied to Project 5.9 personnel in the United States by the Rad-Safe unit of Eniwetok. Figure 3.3 shows the Shot Mohawk impact area radiation decay as a function of time after the detonation as plotted from these data. These radiation data are for Site Sally, approximately 3,000 feet from the detonation point, because it was expected that the specimens would be carried there; however, the specimens traveled only 400 feet or less, and were, therefore, found on the shot island, Site Ruby, which has a much higher radiation level.
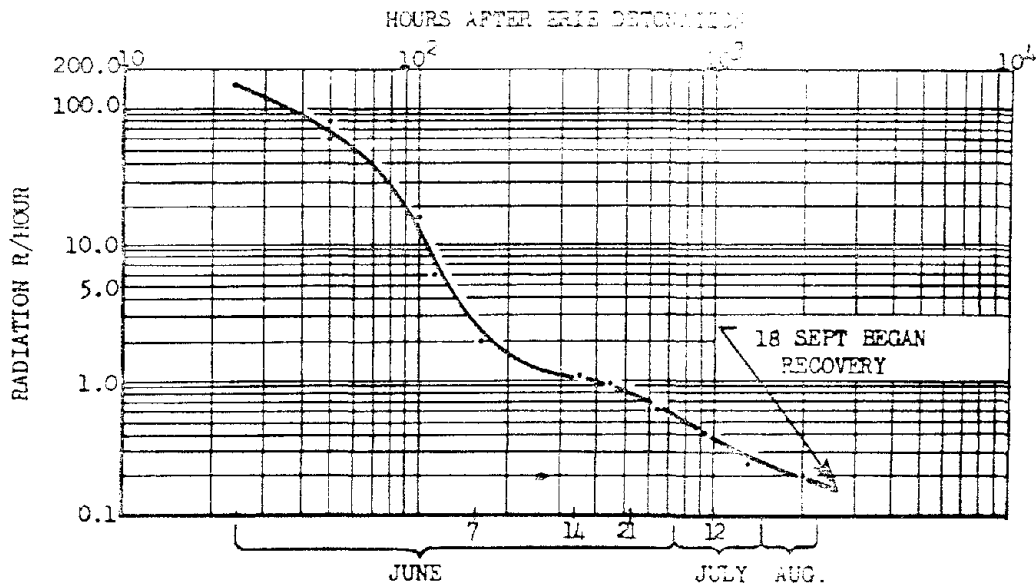
Figure 3.2 Radiation decay of Site Yvonne.

HOURS AFTER MOHAWK DETONATION
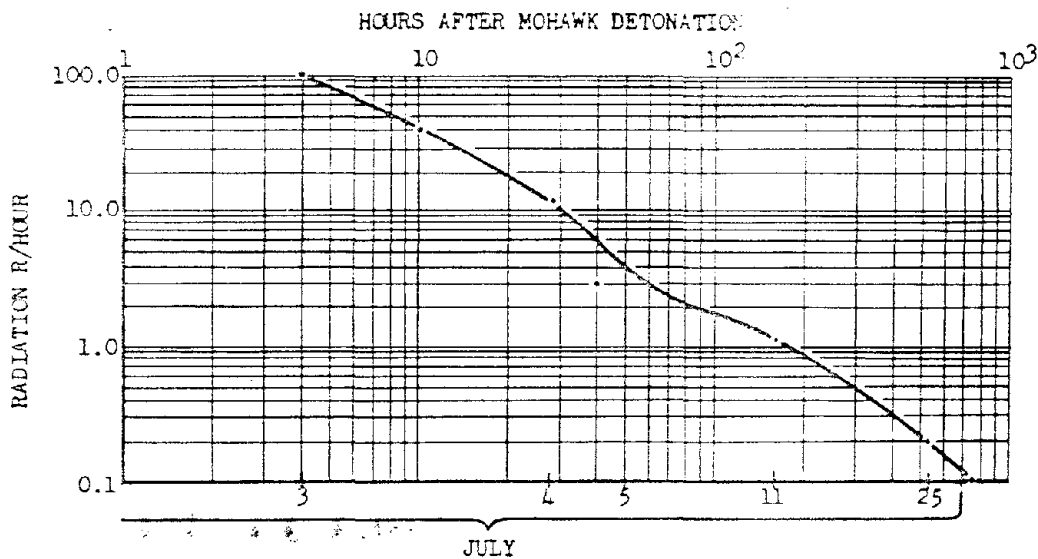
Figure 3.3 Radiation decay of Site Sally.
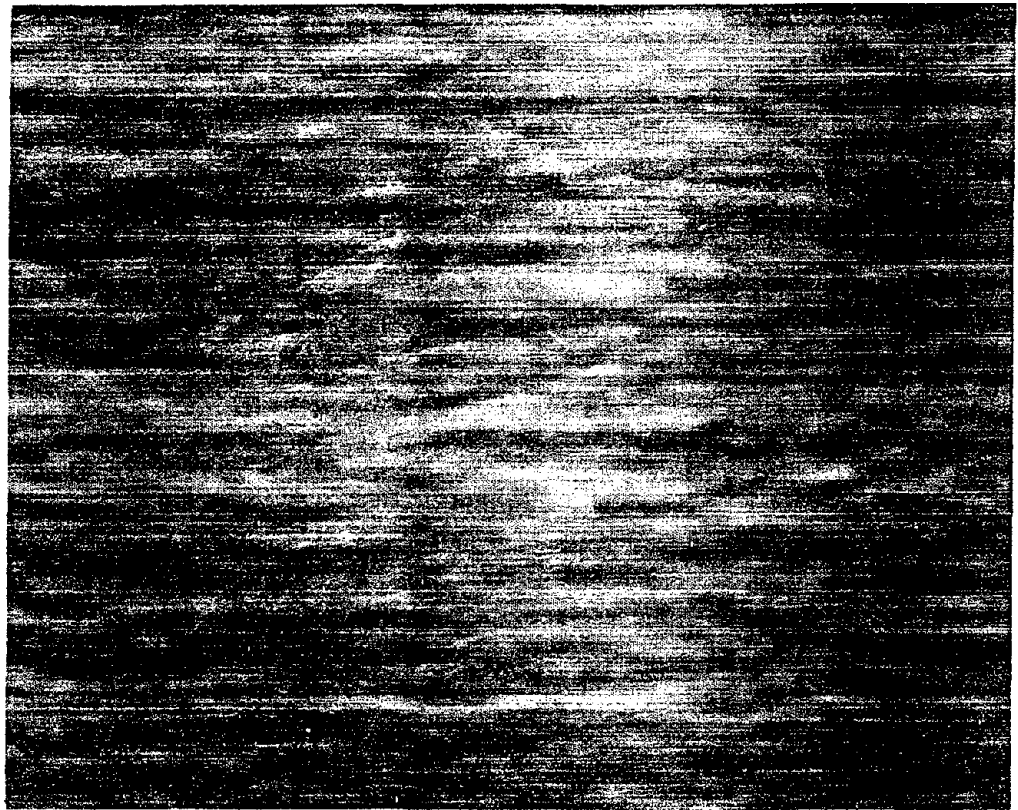
On the day the specimens were recovered, the area was reading 1 r/hr; but since all 9 of the specimens were lying on top of the ground, no trouble was experienced in locating and recovering them.

3.1.3 **Recovered Specimens Summary.** Table 3.1 lists the specimens, or parts of specimens, recovered from Shot Erie. Forty-four of these specimens were recovered in their impact locations, and the remainder were found in the dumping area. Figure 3.5 shows the recovery locations of the majority of these 44 specimens with respect to their original positions and the burst point. A table listing the preshot and postshot coordinates of each specimen found in the impact area is also included in Figure 3.5.

3.2 PASSIVE SPECIMENS

In general, the specimens retained their original shape but were reduced in size because of loss of material from the surface; however, a few specimens either had irregular metal loss

41

STATION	CODE	STATION	CODE
50		200	
100		250	
150		300	

STATION	SPECIMEN CODE	PRE-SHOT X FEET	PRE-SHOT Y FEET	HEIGHT FEET	POST-SHOT X FEET	POST-SHOT Y FEET
25	J	17.7	-3.2	262.0	259	-37
50	A	20.0	26.2	277.8		250
	A	13.7	30.0	278.0	111	232
	D	20.0	26.2	280.9	-10	368
	L	18.7	33.4	286.4	158	370
	M	20.0	37.8	283.4	144	356
	U	9.7	31.6	282.8	99	299
	T	16.2		279.5	127	302
	Z	16.2		283.5	108	283
100	A	58.6	44.8	245.5	178	154
	I	55.3	45.9	245.2	132	148
	J	51.0	45.0	239.4	97	134
	X	54.6	42.6	247.7	210	182
	L	51.6	43.8	247.7	117	156
	M	49.2	47.0	239.7	94	149
	T	50.8	41.8	248.7	175	154
	Z	55.4	37.4	239.4	144	140
	BB	53.9	41.4	239.8	155	194
	CC	55.0	39.4	242.7	168	166
	DD	57.4		235.0	129	146
	EE	54.6	49.6	243.3	160	211
150	A	96.6	47.0	194.9	120	75
	A	96.6	54.9	195.0	219	140
	CC	96.0	47.6	194.3	233	135
	D	95.5	50.0	192.6	-200	290
	F	96.3	44.4	197.4	300	270
	G	95.7	52.2	197.8	193	164
	U	96.2	43.5	189.3	137	115
	X	96.2	48.9	191.3	169	130
	Z	95.6	47.6	188.9	165	116
200	A	137.4	44.4	165.9	136	108
	A	138.3	42.0	166.0	253	95
	CC	136.6	47.1	165.3	255	124
	DD	135.2	51.0	165.3	263	133
	D	137.6	40.8	163.4	146	404
	L	134.8	43.2	163.1	159	140
	S	137.3	45.0	168.8	252	95
	X	134.4	45.5	160.9	212	110
	Z	131.3	44.6	159.9	211	102
	EE	136.5	47.2	168.3	266	137
250	L	173.6	34.4	126.5	310	140
	X	173.2	36.3	122.9	257	69
	Z	173.1	36.4	127.0	260	77
300	X	211.0	14.0	88.59	342	0

a End-on
b Approximate distance
c Side-on
d Shields only

Figure 3.5   Recovery locations with a table of preshot and postshot coordinates of those specimens which were found in the impact area, Shot Erie.

42

SECRET

Figure 3.5 Recovery locations with a table of preshot and postshot coordinates of those specimens which were found in the impact area, Shot Erie.

Legend:

STATION	CODE	STATION	CODE
50	○	200	▭
100		250	△
150	▢	300	

STATION	SPECIMEN CODE	PRE-SHOT X FEET	PRE-SHOT Y FEET	HEIGHT FEET	POST-SHOT X FEET	POST-SHOT Y FEET
25	J			243.0	259	-32
50	A [a]			227.8	-8 [b]	250
	A [c]			278.0	111	232
	D			280.9	-10 [b]	360
	L	18.7		286.4	158	370
	N			333.4	144	356
	U			281.8	99	299
	Y			271.5	127	304
	Z			283.5	108	283
100	A [c]			245.5	178	184
	I			247.7	132	148
	J			239.8	97	134
	L			247.7	210	182
	N			243.7	117	156
	Y			248.2	94	146
	Z			239.4	175	154
	BB	53.6		239.8	144	146
	CC			247.7	155	174
	CC			237.3	168	182
	EE			249.3	129	146
					160	211
150	A [a]			194.9	120	75
	A [c]			195.0	219	140
	C [d]	46.0		194.3	233	135
	D			192.4	-20 [b]	255
	F			197.4	306	270 [b]
	G			197.8	193	164
	U			189.3	137	115
	Y			191.3	169	130
	Z			198.9	165	116
200	A [a]	137.4		165.9	136	108
	A [c]	138.7		166.0	253	95
	C [d]	136.6		165.3	255	124
	C [d]	135.2		165.3	263	133
	D			163.4	146	104
	L	131.8		163.1	159	140
	S			166.8	252	95
	X			166.9	212	110
	U			164.9	211	102
	EE			166.9	266	137
250	L			116.6	310	140
	X			222.9	257	69
	Z		36.8	107.0	260	77
300	X	211.0		88.59	342	6

[a] End-on
[b] Approximate distance
[c] Side-on
[d] Shield only

or were distorted by the pressure forces, so that they did not retain their shapes. The profiles of the specimens were measured with a specially designed gage which measured the distance and azimuth of any point on the surface from a reference point within the specimen. The maximum error in these measured distances was ¼ of an inch. A few pertinent comments regarding specimen shapes follows:

(1) The 10-inch steel sphere at the 50-foot station was distorted so that at some places there was an increase in the radius and at other places a decrease, with the result that the specimen was much out of round.

(2) The forward end of the dynamic-pressure cylinder at the 50-foot station was mushroomed by the pressure forces, so that it was larger in diameter than it was before the shot.

(3) The copper spheres at the 50- and 150-foot stations were either distorted or had an irregular pattern of material loss, leaving the specimen more elliptical than spherical.

In addition to the profile determinations, the weight loss of each specimen was calculated. Also, an attempt was made to determine the postshot densities of some specimens. The weight loss of each specimen was determined by subtracting the postshot weight from the preshot weight. Both these measurements had tolerances of $\pm\frac{1}{4}$ pound; therefore, the weight loss data could have been in error by as much as $\pm\frac{1}{2}$ pound. The postshot density of the specimens from the close-in stations was measured by dividing their weight in air by their volume as determined from their loss of weight when submerged in water; however, any change in density, if any, was so small that it was less than the expected error of the measurements.

The weight loss and other pertinent information are presented in the ensuing paragraphs, and a detailed description of the specimen damage, surface conditions, and depth of metal loss as determined from the profile measurements is presented for each specimen in Appendix A.

3.2.1   Steel Spheres.   Sixteen of the 20 steel spheres exposed in the Shot Erie fireball were recovered. Those which were not recovered were the 10-inch-diameter steel sphere at the 25-foot station and the 6-inch-diameter sphere, a 4-inch-diameter sphere, and the 20-inch segment of the 32-inch-diameter sphere at the 50-foot station.

With the exception of the specimens exposed at the 50-foot station, where the surfaces facing the burst point were severely pockmarked, the steel spheres from Shot Erie had almost the same amount of metal loss over their entire surfaces. Figures 3.6 and 3.7 are typical examples of specimens which had pockmarks.

Weight losses of the steel spheres are summarized in Table 3.3. The table also lists the average reduction in radius of the specimens as determined from the postshot weight. This average is the difference between the preshot radius and the radius of a sphere of equal density that would have the same weight as the postshot weight of the specimen.

All eight of the steel spheres from Shot Mohawk were recovered. The weight losses of these spheres are also presented in Table 3.3. All the 8- and 10-inch diameter spheres which were exposed at the 150-foot level on the specimen tower had two peculiar grooves, about $\frac{1}{16}$ inch deep and $\frac{1}{2}$ to $\frac{3}{4}$ inch wide extending around the sphere. These grooves were about $1\frac{1}{2}$ inches apart. There was no correlation of the plane of the grooves with the direction of the shock wave. A photograph and profile drawing of one of these specimens is shown in Figure 3.8.

One of the 10-inch-diameter steel spheres at the 70-foot level on the specimen tower for Shot Mohawk had an interesting pattern of resolidified metal: its flow lines started at the two poles of the specimen and spiraled around, ending in a line at the equator. More details on this phenomenon as well as a photograph are presented in Appendix A.

3.2.2   Composites.   Four of the five steel composite specimens oriented cone forward, and all four of those with side-on exposures, were recovered. The one steel specimen oriented hemisphere forward, the steel specimen with its cone forward at 25 feet, and all seven of the aluminum specimens were not recovered. Six velocity-distance inserts from composite specimens were found separated from the composite shells. Only the separated insert from the cone-forward steel composite specimen at 200 feet could be positively identified. One of the remaining five inserts could have been from the cone-forward steel specimen at 100 feet, and the remaining four inserts could have been from aluminum composites; or all five could have been from aluminum specimens.

43
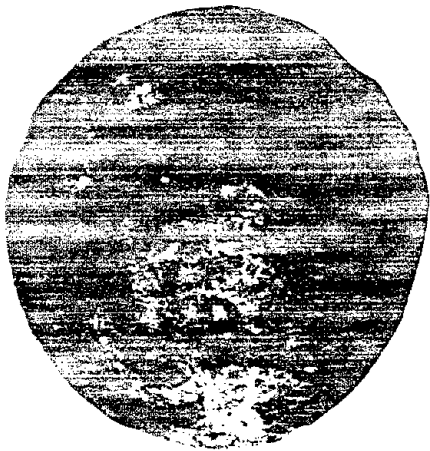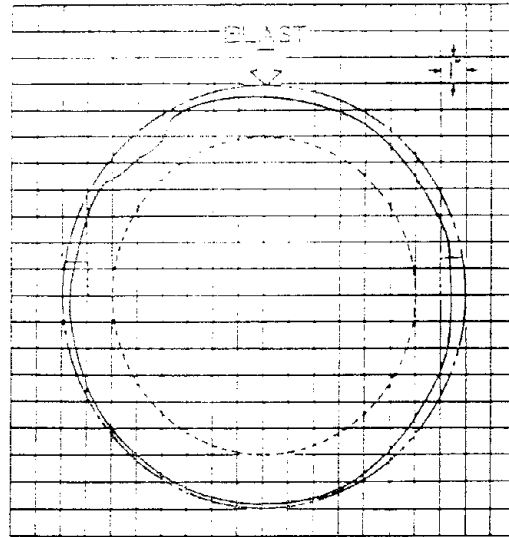
(a) as viewed from burst point   (b) vertical profile

Figure 3.6   Instrumented sphere at the 50-foot station from Shot Erie.
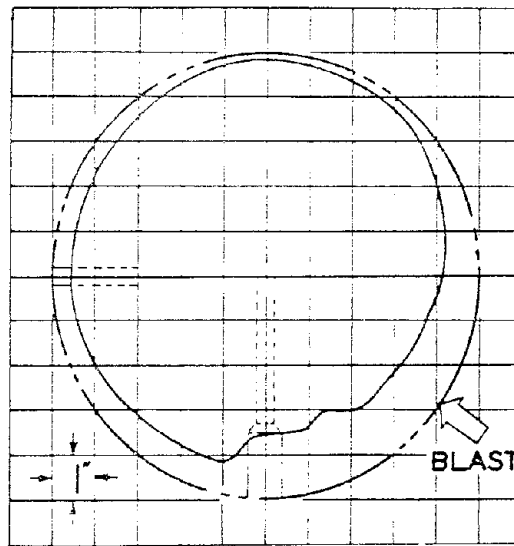
(a) as viewed from burst point   (b) vertical profile

Figure 3.7   Ten-inch-diameter steel sphere at the 50-foot station from Shot Erie.

44

Table 3.4 is a summary of the weight loss of each recovered composite specimen.

The cone of the specimen oriented cone forward at the 200-foot station was not recovered. Since the cone was not recovered, the total weight loss can only be given as an estimate. Assuming that the cone lost the same depth of metal as the cylinder, the postshot weight of the cone would have been 6¼ pounds. This assumption led to an estimated weight loss for the entire specimen of 60 pounds.

Both the composite specimens at the 50-foot station were badly damaged. The cone-forward specimen was crushed by the pressure forces; the side-on specimen was severely pockmarked in the top rear quadrant, tangent to the blast, and the bottom rear quadrant, shielded from the blast. was badly honeycombed. A photograph of the honeycombing is presented in Figure 3.9. More details about these damages are presented in Appendix A.

3.2.3 Flat Plates. Of the six specimens of this type originally exposed, only the aluminum plate, exposed at the 150-foot station and the steel plate grooved transversely, exposed at 100 feet, were not recovered. The recovery location of the flat plate, Type D, at the 200-foot station is shown in Figure 3.5. The approximate recovery coordinates of the other flat plates are also in Figure 3.5. Note that the specimens were found far to the left, clockwise, from the line-of-sight through the specimens and the burst point. A summary of the preshot and postshot weights is given in Table 3.5.

In general, the plain side of the plate lost about the same depth of metal as did the bottom of the grooves, and the top of the grooves lost an additional $^{3}/_{16} \pm ^{1}/_{16}$ inch of metal. A plot of the preshot and postshot profiles of a section through the center of the transversely-grooved plates is presented in Figure 3.10 and those for the longitudinally grooved plate in Figure 3.11. The latter had more loss on the top of the grooves than the bottom, but both areas lost more toward the front than the rear. This variation is also shown in the figure.

3.2.4 Laminated Cylinders. Three of the six exposed cylinders were recovered. A summary of their weights is given in Table 3.6. All three were recovered without the steel end caps; and, since no reliable estimate could be made of the weights of these caps, the postshot weights listed in the table were the actual weights of the specimens as recovered, and the weight loss data included the loss of both the steel and aluminum.

All the laminated cylinders had pockmarks on the outside lamination. These pockmarks were large in area but not very deep. Only on the cylinder at the 100-foot station were the pockmarks as deep as the thickness of the lamination on which they appeared.

3.2.5 Hollow Cylinders. The two hollow cylinders were exposed at the 50-foot station, but neither was recovered.

3.2.6 Ballistic and Dynamic-Pressure Cylinders. All the ballistic and dynamic-pressure cylinders were recovered. The recovery locations of the ballistic cylinders are shown in Figure 3.5. It may be noted that the two cylinders which were side-on, one Type BB and one Type CC, were found at approximately the same distance from their original position and that the one which was end-on did not travel as far. The side-on cylinder with the plastic disk (CC) was found at a range of 185 feet, the one without the plastic (BB) was found at 184 feet, and the end-on cylinder (CC) was found at 129 feet.

Table 3.7 is a summary of the specimen weights and recovery information.

The dynamic-pressure cylinder at the 50-foot station was badly damaged by pressure forces. Details of this damage are presented in Appendix A.

3.2.7 Material Evaluation Specimens. Fourteen complete specimens and parts of six others of the 29 material evaluation specimens were recovered. Table 3.1 lists the recovered specimens, and Table 3.8 is a tabulation of the preshot and postshot weights.

Recovery locations of those specimens found in their original impact points are shown in Figure 3.5.

Average reduction in radius of the spherical specimens is also presented in Table 3.8.

The plastic sphere at the 150-foot station broke apart along a horizontal plane; and the surface was severely canyoned, as shown in Figure 3.12. Since there was no material loss

45

TABLE 3.3 SUMMARY OF PRESHOT AND POSTSHOT WEIGHTS OF STEEL SPHERES

Type	Diameter, inches	Slant range Nominal, feet	Slant range Actual, feet	Weight Preshot, pounds	Weight Postshot, pounds	Weight loss, pounds	Average reduction in radius, inches
				SHOT ERIE			
Y	16	50	46.3	$584\frac{1}{2}$	$466\frac{1}{4}$	$55\frac{1}{4}$	0.41
X	12	100	97.9	225	$194\frac{3}{4}$	$30\frac{1}{4}$	0.25
X	12	150	158.9	$225\frac{1}{4}$	$200\frac{1}{2}$	$24\frac{3}{4}$	0.20
X	12	200	205.2	$225\frac{1}{4}$	$199\frac{3}{4}$	$25\frac{1}{2}$	0.21
X	12	250	257.1	225	$202\frac{1}{4}$	$22\frac{3}{4}$	0.18
X	12	300	306.4	225	200	25	0.20
Z	12	50	43.7	$251\frac{1}{4}$	206	$45\frac{1}{4}$	0.39
Z	12	100	97.7	252	$217\frac{1}{4}$	$34\frac{3}{4}$	0.29
Z	12	150	158.7	$252\frac{1}{4}$	$227\frac{1}{2}$	$24\frac{3}{4}$	0.20
Z	12	200	204.0	$253\frac{3}{4}$	233	$20\frac{3}{4}$	0.17
Z	12	250	254.2	254	$232\frac{1}{2}$	$21\frac{1}{2}$	0.17
Z	12	300	306.0	$252\frac{1}{4}$	$232\frac{1}{2}$	$19\frac{3}{4}$	0.16
N	10	50	46.4	$148\frac{1}{4}$	$107\frac{3}{4}$	$40\frac{1}{2}$	0.51
N	10	100	97.5	$148\frac{3}{4}$	$126\frac{1}{2}$	$22\frac{1}{4}$	0.22
O	8	50	46.2	76	$43\frac{1}{2}$	$32\frac{1}{2}$	0.68
Q	4	50	44.9	9.4	0.8	8.6	1.12
				SHOT MOHAWK			
N	10	545	–	$148\frac{3}{4}$	$98\frac{1}{2}$	$50\frac{1}{4}$	0.64
N	10	545	–	$148\frac{1}{2}$	$108\frac{1}{2}$	40	0.50
N	10	575	–	$148\frac{3}{4}$	$144\frac{1}{2}$	$4\frac{1}{4}$	0.05
N	10	575	–	149	$127\frac{1}{2}$	$21\frac{1}{2}$	0.25
FF	9	545	–	105	77	28	0.44
FF	9	545	–	$105\frac{3}{4}$	$76\frac{1}{4}$	$29\frac{1}{2}$	0.47
O	8	545	–	76	53	23	0.45
O	8	545	–	$76\frac{1}{4}$	$55\frac{1}{4}$	21	0.41

TABLE 3.4 SUMMARY OF PRESHOT AND POSTSHOT WEIGHT OF STEEL COMPOSITE
SPECIMENS, TYPE A

Orientation	Slant range Nominal, feet	Slant range Actual, feet	Weight Preshot, pounds	Weight Postshot, pounds	Weight loss, pounds
Nose-on	50	45.8	$147\frac{3}{4}$	$61\frac{1}{4}$	$86\frac{1}{2}$
Nose-on	100	97.7	$145\frac{3}{4}$	$9\frac{3}{4}$ [a]	–
Nose-on	150	158.2	$145\frac{3}{4}$	$84\frac{1}{2}$	$61\frac{1}{4}$
Nose-on	200	203.5	$145\frac{1}{4}$	$36\frac{1}{4}$ [b]	60 [c]
Side-on	50	45.3	$156\frac{3}{4}$	$111\frac{1}{2}$	$45\frac{1}{4}$
Side-on	100	97.5	$156\frac{1}{4}$	$114\frac{1}{4}$	42
Side-on	150	158.1	$156\frac{1}{4}$	$109\frac{3}{4}$	$46\frac{1}{2}$
Side-on	200	203.6	156	$128\frac{1}{4}$	$27\frac{3}{4}$

[a] The velocity-distance insert, cone, and sphere were not recovered.

[b] Specimen not complete; the velocity-distance insert and cone were separated from cylinder.

[c] Estimated weight loss (weight loss of insert 0.0 lbs, estimated loss of cone 6.2 lbs).
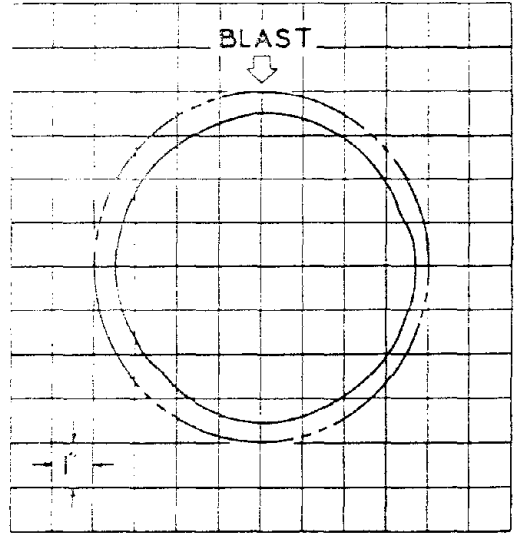
Figure 3.8   Eight-inch-diameter steel sphere at 545-foot slant range, Shot Mohawk.
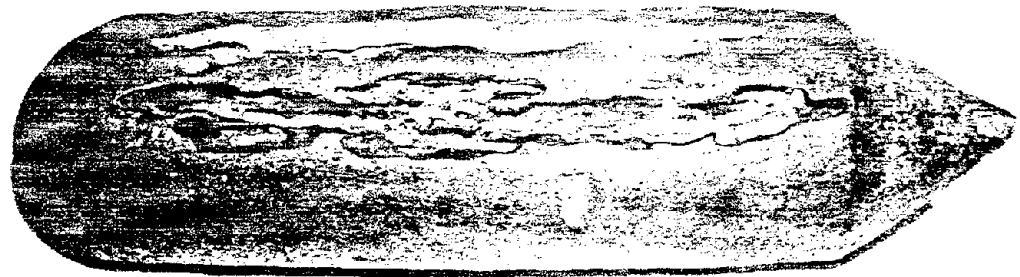
Figure 3.9   Side-on composite, 50-foot range, showing honeycomb.

TABLE 3.5 SUMMARY OF PRESHOT AND POSTSHOT WEIGHTS OF FLAT PLATES

Type	Grooves	Slant range Nominal, feet	Slant range Actual, feet	Weight Preshot, pounds	Weight Postshot, pounds	Weight loss, pounds
D	Transverse	50	43.7	76¾	19¾	57
D	Transverse	150	156.2	77½	29½	48
D	Transverse	200	201.5	77½	43¼	34¼
F	Longitudinal	150	156.3	77¼	26½	50¾

TABLE 3.6 SUMMARY OF PRESHOT AND POSTSHOT WEIGHTS OF LAMINATED CYLINDERS

Slant range Nominal, feet	Slant range Actual, feet	Laminations Number	Laminations Thickness, inches	Weights Preshot, pounds	Weights Postshot, pounds	Weight loss,[a] pounds
100	95.9	12	⅛	33½	11½	22
150	156.1	5	¼	37¼	15	22¼
150	156.2	4	⅜	34¼	13½	20¾

[a]Includes weights of missing steel end caps.

TABLE 3.7 SUMMARY OF PRESHOT AND POSTSHOT WEIGHTS OF DYNAMIC-PRESSURE AND BALLISTIC CYLINDERS

Type	Slant range Nominal, feet	Slant range Actual, feet	Orientation	Weight Preshot, pounds	Weight Postshot, pounds	Weight recovery Loss, pounds	Weight recovery Range, feet[a]
U	50	43.8	End-on	143¾	91½	52¼	283
U	150	158.6	End-on	144¼	104½	39¾	101
U	250	254.5	End-on	144¼	126½	17¾	b
AA	150	158.0	End-on	141¾	109½	32¼[c]	b
AA	150	158.5	End-on	142½	114	28½[d]	b
CC	100	95.4	End-on	114¾	81¼	33½[c]	129
BB	100	97.4	Side-on	112	91¼	20¾	184
CC	100	97.4	Side-on	115½	84¾	30¾[e]	185

[a]Horizontal distance from original position.
[b]Found in dumping area.
[c]Includes 0.57 pounds loss of plastic disk.
[d]Includes 0.22 pounds loss of plastic disk.
[e]Includes 0.20 pounds loss of plastic disk.
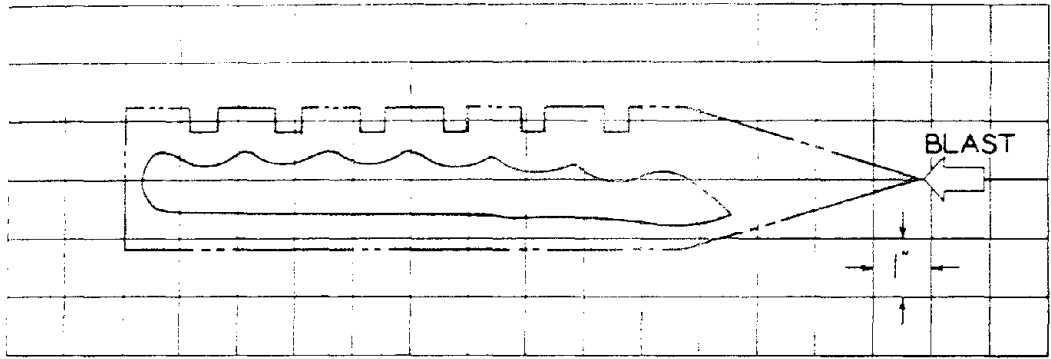
50-foot station
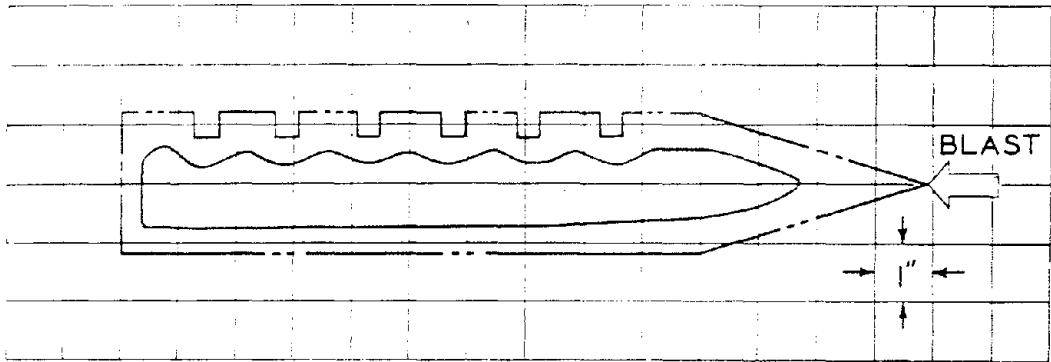
150-foot station
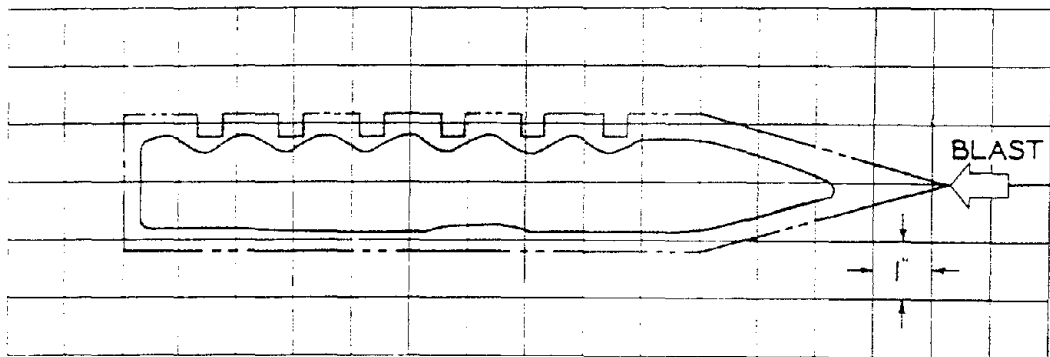
200-foot station

Figure 3.10 Profile plots of transversely grooved steel plates.

49
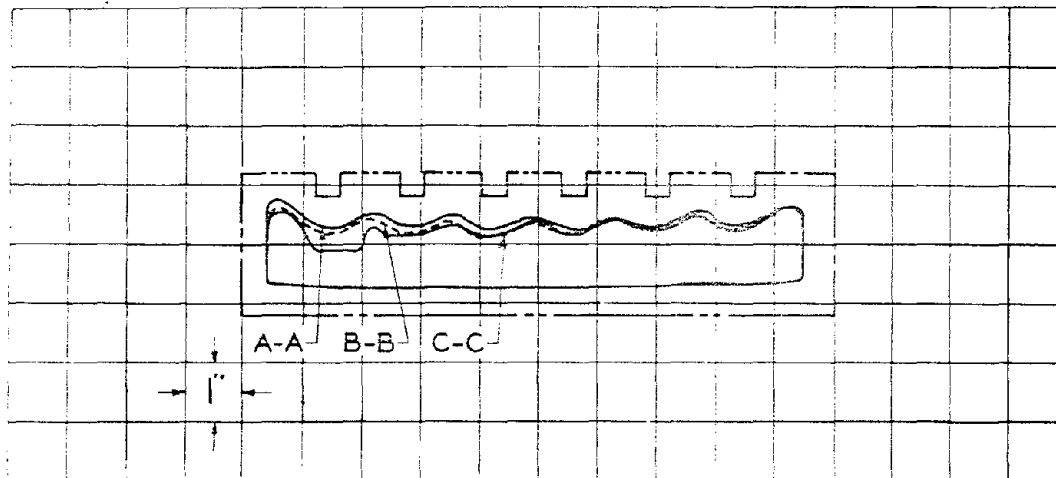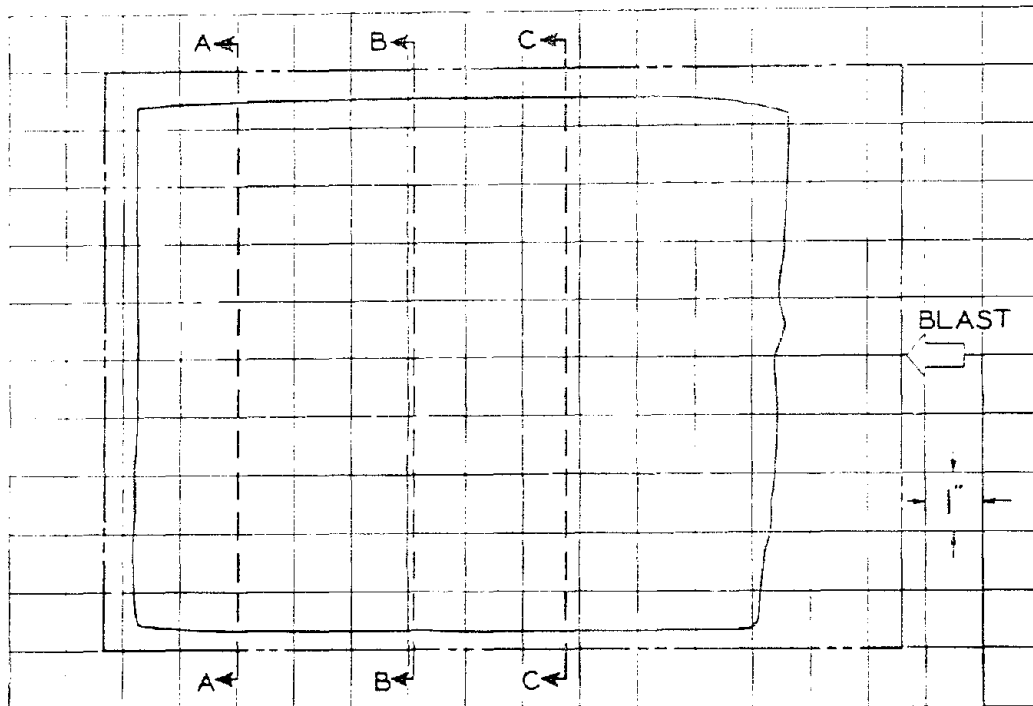
Figure 3.11 Flat plate grooved longitudinally, 150-foot station, Shot Erie.

Figure 3.12 Plastic sphere, 150-foot station.
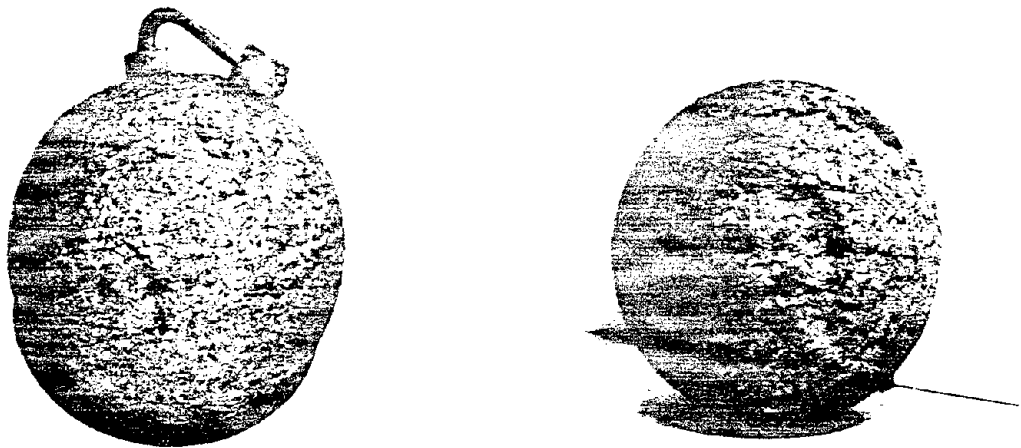
L 10   11   1F 1   ▼ 2   ▼ 3   ▼ 4   ▼ 5   ▼ 6   ▼ 7   ▼ 8   ▼ 9

Figure 3.13 Plastic sphere, 250-foot station.

51

under the locking nut, the material loss of the exposed area could be compared to that of the unexposed area and measured directly, as recorded in Table 3.8.

The plastic sphere from the 250-foot station was one of the least damaged specimens of those recovered. Figure 3.13 is a photograph of this specimen as it was found; it is to be

TABLE 3.8 SUMMARY OF PRESHOT AND POSTSHOT WEIGHTS OF MATERIAL-EVALUATION SPECIMENS

Type	Material	Slant range		Weight		Weight loss, pounds	Average reduction in radius, inches
		Nominal, feet	Actual, feet	Preshot, pounds	Postshot, pounds		
G	Plastic	150	156.0	17	$8^3/_4$	a	0.05
G	Plastic	250	256.6	$16^3/_4$	$15^1/_2$	$^1/_4$	0.02
H	Graphite	b	-	-	-	-	-
I	Molybdenum	25	24.8	$99^1/_2$	$7^1/_4$	c	-
I	Molybdenum	100	95.3	$98^1/_2$	82	$16^1/_2$	0.24
I	Molybdenum	200	203.9	$99^3/_4$	87	$12^3/_4$	0.18
J	Stainless steel	25	24.3	$73^3/_4$	$29^3/_4$	a	-
J	Stainless steel	100	97.4	$73^3/_4$	$56^1/_4$	$17^1/_2$	0.34
J	Stainless steel	200	203.5	74	$62^1/_4$	$11^3/_4$	0.22
K	Titanium	100	95.3	$43^3/_4$	$27^1/_4$	16	0.56
K	Titanium	200	201.6	44	$33^1/_2$	$10^1/_2$	0.35
L	Copper	50	44.7	87	$27^3/_4$	$59^1/_4$	1.27
L	Copper	100	95.3	$86^1/_2$	$44^3/_4$	$41^3/_4$	0.79
L	Copper	150	156.1	$86^1/_2$	30^2	$56^1/_2$	1.19
L	Copper	200	201.6	$86^1/_2$	$44^1/_2$ e	42	0.80
L	Copper	250	254.4	87	$49^3/_4$	$37^1/_4$	0.68
S	Tantalum copper	100	97.7	$156^3/_4$	$83^1/_4$	$73^1/_2$ f	
S	Tantalum copper	200	201.6	156	$101^1/_2$	$54^1/_2$ f	
DD	Bakelite cyl.	200	201.7	$20^1/_4$	13	a	-
EE	Cylinder with ceramic inserts	100	95.8	$113^3/_4$	74	$44^3/_4$	-
EE	Cylinder with ceramic inserts	200	201.6	$120^1/_2$	83	$37^1/_4$	-
EE	Cylinder with ceramic inserts	200	201.7	$115^3/_4$	88	$27^3/_4$	-
FF	Sphere with ceramic insert	545 g	545	105	77	28	-
FF	Sphere with ceramic insert	545 g	545	$105^3/_4$	$76^1/_4$	$29^1/_2$	-
GG	Aluminum	545 g	545	51	$28^1/_2$	$22^1/_2$	0.88

a Approximately $^1/_2$ of specimen was recovered.
b Several large pieces recovered but not identified.
c Only a small part of specimen recovered (see text).
d Specimen not positively identified, could be from 200 foot station.
e Specimen not positively identified, could be from 150 foot station.
f Combined loss of tantalum, copper, and steel.
g Exposed to Mohawk.

noted that the mounting bolt was still attached to the specimen. The front sector of the sphere had some large, but shallow, sections broken out. Except for the shallow sections missing from the front face, there was no structural failure of the specimen.

The molybdenum sphere from the 25-foot station also broke apart, and only part of it was recovered. The depth of metal loss was determined by measuring the profile of the recovered

part and then fitting the best radius to the profile plot. Using this method, the metal loss was estimated to be 0.74 inch in a radial direction. Assuming equal metal loss over the entire surface of the sphere, the weight loss of the entire specimen, had it remained in one piece, would have been approximately 45 pounds.

Both the spheres and three of the six cylinders which held the special purpose alloys were recovered. Comments on the postshot conditions of the inserts are presented in Appendix A.

3.3 ELECTRICALLY INSTRUMENTED SPECIMENS

All six instrumented spheres exposed on Shot Erie were recovered. The magnetic recording tapes from the three farthest specimens, Stations 200, 250, and 300, were played back after the test. Although heat had damaged the tapes, some time-history data from Stations 250 and 300 are presented. The recorder at Station 200 stopped at shock arrival so no data was recorded. The tapes of the remaining specimens, Stations 50, 100, 150, were so brittle that playback was impossible. However, it was determined by weighing the take-up and pay-out spools, that the Station 150 recorder had operated for at least 6 seconds after time zero.

Damage to the specimen container, recorder, and transducers varied from minor damage at the farthest ranges to heavy damage at the close ranges. Appendix B, Section B.3, describes in detail the damage sustained by all electrically instrumented specimens.

3.3.1 Station 200. The magnetic recording tape in the Station 200 recorder stopped when the shock wave and fireball engulfed the specimen. The exact reason for this recorder failure was unknown; however, the specimen was subjected to a peak acceleration of approximately 11,000 grams and this appeared to be the most probable cause.

The only significant damage to the Mylar recording tape was caused by heat. It is estimated that the tape was subjected to a temperature of approximately 500F sometime after the specimen had impacted the ground. This relatively high temperature caused the oxide binder to become soft and sticky and ultimately caused part of the oxide to be transferred from its normal side of the tape to the adjacent back side of the tape on the take-up reel. This oxide transfer (called blocking) was evident on the entire Station 200 tape, except in the area that was between the pay-out and take-up reel, i.e., that area which could not block because there was no adjacent surface to which the oxide could be transferred. The heat had caused some signal disturbance in this unblocked area; however, there was sufficient signal remaining to determine time zero and shock arrival times. It took 5 msec for the fireball to expand and engulf the instrumented sphere at Station 200. Time zero was determined from disturbances on the motor timing, depth-of-melt, and transistor oscillator channels. Shock arrival was determined from the two accelerometer channels and the transistor oscillator channel. Accuracy of this shock arrival time was estimated to be ±20 percent.

Transistors are known to be sensitive to neutrons, and it was suspected that the transistor oscillator might fail at time zero. However, it continued to operate through time zero and failed at shock arrival. A slight disturbance was noted at time zero, but the oscillator frequency and amplitude showed no significant change until shock arrival.

The nuclear radiation experienced by the specimen at Station 200 apparently caused no disturbance or loss of signal on the magnetic recording tape.

3.3.2 Station 250. The recorder at Station 250 operated satisfactorily, and the recording tape ran all the way through. The tape had evidently been exposed to high temperature, because it was badly blocked. This blocking occurred on the tape in the vicinity of time zero and the oxide had transferred so completely that it was necessary to play back the reverse side of the tape as well as the normal side. This reverse side playback introduced many problems in the reduction of the data. It was necessary to add together the deflection readings from the normal and reverse side playback of a channel to obtain the actual recorded information. The necessity of this type of data reduction reduced the reliability of the information obtained from this specimen; however, most of the data was of sufficient interest to warrant presentation in this report.

The time base used on all the curves presented from this station was obtained from the transistor oscillator. The accuracy of this time base was better than ±1 percent before shock arrival when the oscillator stopped. In the absence of an independent time base subsequent to this time, the recorder speed after shock arrival was assumed to be the same as before. Even on the basis of this assumption the accuracy of the time base after shock arrival was estimated to be ±2 percent or ±1 msec, whichever was greater. The motor timing channel was sensitive to recorder shock loads and provided indications of initial shock wave engulfment and impact of the specimen with the ground. The two accelerometer channels, as well as the motor timing channel, indicated that the specimen from Station 250 impacted the ground 1.27 ± 0.03 seconds after shock wave engulfment.

It is important to note that the transistor oscillator in this specimen also operated through time zero and stopped at shock arrival. Some disturbance was noted on the oscillator channel at time zero, but the frequency showed no significant change.

R a d i a l   A c c e l e r a t i o n .   Figure 3.14 presents the recorded time history of the radial acceleration experienced by the instrumented sphere at Station 250. The ordinate scale has been omitted from this curve because of the uncertainty introduced by the addition of the signals played back from the normal and reverse sides of the tape. Although the ordinate scale is in doubt, the general wave shape is considered a reasonable representation of the acceleration experienced by the specimen within the frequency response limits of the recording circuit. Shock arrival time of 9 ± 1 msec was determined from this curve. A slight disturbance can be observed at time zero, but it is so small that is is of the same order as the normal signal variations and cannot definitely be attributed to time zero phenomena.

N o r m a l   A c c e l e r a t i o n .   The recorded normal acceleration time history at Station 250 is presented in Figure 3.15. This curve is also presented without an ordinate scale because of the uncertainty introduced by the addition of the signals played back from the normal and reverse sides of the tape. Signal variations known as drop outs, caused by dust or imperfections on the tape, also contributed to the uncertainty of recorded data. The variation in the curve prior to time zero illustrates a particularly large extraneous signal. It is possible that time zero phenomena such as electromagnetic disturbances or neutron bombardment caused the rapid signal variation observed at time zero. If this were a time zero phenomena, it caused no permanent damage in the accelerometer or recording head because both were found in operating condition after the shot. Although the amplitude of this curve was questionable, the time base was considered good. Reflected shock arrival time of 36 msec was determined from this curve.

T e m p e r a t u r e   o f   S t e e l   a t   a   D e p t h   o f   0 . 0 1 6   I n c h .   Figure 3.16 presents the recorded temperature time history of the rear surface of a steel diaphragm 0.016 inch thick whose front surface was exposed to the thermal energy within the fireball and isothermal sphere. Temperature scale accuracy on this curve was estimated to be ±30 percent. The chromel-alumel thermocouples were reliable to only 2400 F, and hence no data is presented above this temperature. It is possible that some of the rapid signal variations could have been caused by an intermittent thermocouple; however, if the circuit had opened completely for 4 msec or more, the signal would have dropped to zero. The disturbance observed at time zero may have been caused by time zero phenomena; however, if this were true, it was of such a low magnitude that it caused no circuit damage.

The depth-of-melt channel at a depth of 0.016 inch below the surface of the sphere indicated a completed circuit at 17 msec after detonation. This was the only such indication recorded on this channel during the period of interest except for the time zero pulse.

T e m p e r a t u r e   o f   S t e e l   a t   a   D e p t h   o f   0 . 0 3 1   I n c h .   The recorded temperature time history of the rear surface of a steel diaphragm 0.031 inch thick is presented in Figure 3.17. Accuracy of the temperature scale is estimated to be ±30 percent. Although an intermittent thermocouple was possible on some of the quick signal variations, the relatively short time constant of approximately 1.3 msec reduced the probability of such circuit disturbances. No time zero disturbances were observed on this channel.

T e m p e r a t u r e   o f   S t e e l   a t   a   D e p t h   o f   0 . 0 6 0   I n c h .   Figure 3.18 shows the recorded temperature time history of the rear surface of a steel diaphragm 0.060 inch thick
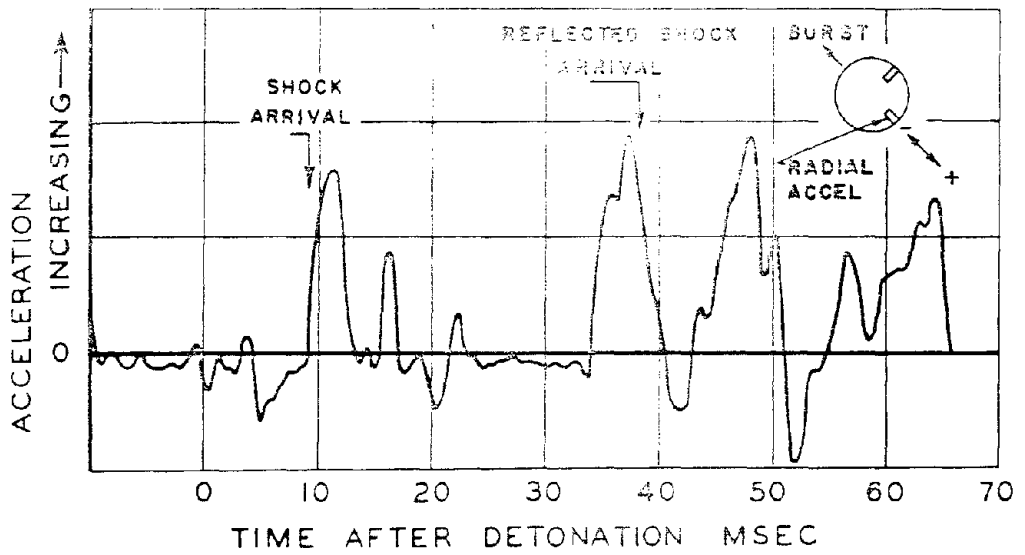
Figure 3.14 Radial acceleration versus time of instrumented sphere at Station 250.
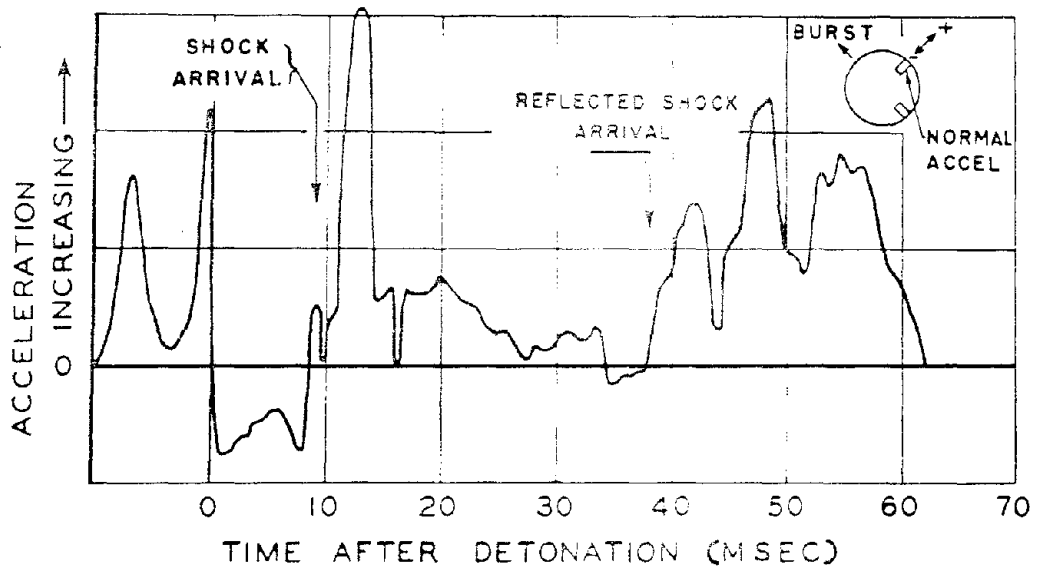
Figure 3.15 Normal acceleration versus time of instrumented sphere at Station 250.

55
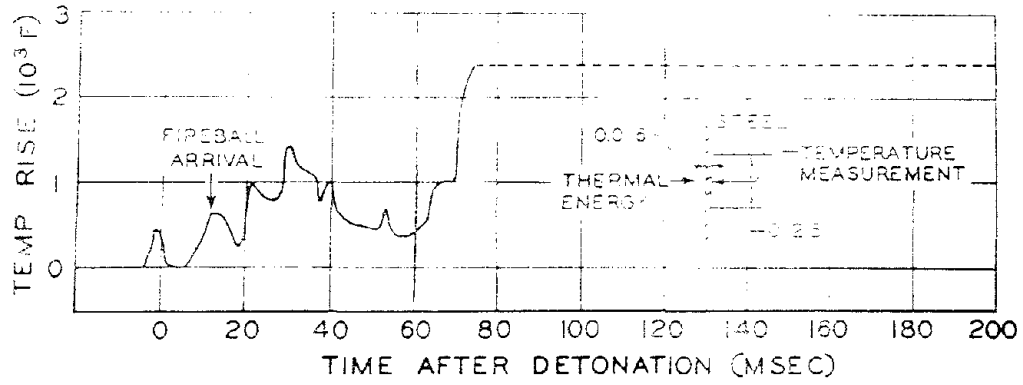
Figure 3.16 Temperature rise of steel versus time at a depth of 0.016 inch below surface of the instrumented sphere at Station 250.
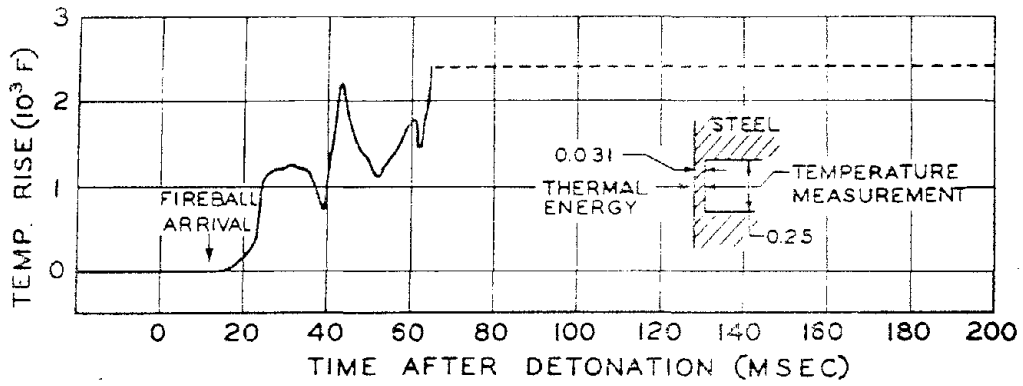
Figure 3.17 Temperature rise of steel versus time at a depth of 0.031 inch below surface of the instrumented sphere at Station 250.
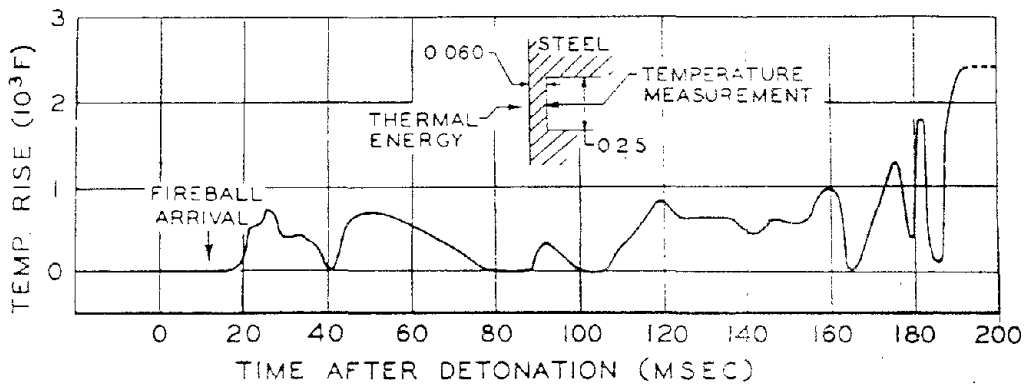
Figure 3.18 Temperature rise of steel versus time at a depth of 0.060 inch below surface of the instrumented sphere at Station 250.

whose front surface was exposed to the thermal energy inside the fireball and isothermal sphere. The accuracy of the temperature scale is estimated to be ±40 percent. Again, some of the rapid signal variations after 160 msec could have been due to an intermittent thermocouple, but it is doubtful that the situation existed before this time. No disturbances due to time zero phenomena were observed.

Figure 3.19 shows the orientation of the thermocouples and depth-of-melt transducers with respect to the direction of the direct shock wave from the detonation. This figure may be of assistance in the interpretation of the temperature time history curves.

3.3.3 Station 300. Approximately 6 seconds of recording tape ran through the recorder after time zero at Station 300. The tape apparently jammed because the neoprene sleeve on the pinch roll became enlarged and caused a malfunction of the capstan assembly. The enlargement of the pinch roll could have been due to the neutron bombardment. The capstan itself continued to rotate for some time, as evidenced by a spot on the recording tape that was rubbed bare of oxide.

The Mylar recording tape showed blocking at both ends; however, in the area of interest the blocking was minor and most of the oxide was on the normal side of the tape. A small portion of a few channels required the addition of data from both sides of the tape.

The transistor oscillator stopped at time zero, and the error in the timing reference before time zero was estimated to be less than ±1 percent. Since no time base was recorded after time zero, the recorder was assumed to operate at a constant speed through time zero and until it jammed. Time base error after time zero was estimated to be within ±2 percent or ±1 msec, whichever was greater. The motor timing channel was helpful in determining time zero and shock arrival. The depth-of-melt channel was the primary factor in the accurate determination of time zero for the even-numbered channels.

Radial Acceleration. Figure 3.20 presents the recorded time history of the radial acceleration experienced by the instrumented sphere at Station 300. The possibility of dropouts, as well as the relatively low frequency response (flat dc to 50 cps), indicates an estimated accuracy of ±40 percent of the acceleration scale, except for the two large peaks immediately after shock arrival. The low frequency response of the recording system probably prevented accurate recordings of these peaks and their possible error is therefore greater. A shock arrival time of 13 ± 1 msec was determined from this channel. If the slight disturbance at time zero was due to time zero phenomena, it was insignificant as far as damage to the channel was concerned.

Normal Acceleration. The recorded normal acceleration time history at Station 300 is presented in Figure 3.21. The amplitude of this curve was reduced by some time zero phenomena to approximately $\frac{2}{3}$ of its original preshot dimension. This amplitude change and low frequency response of the recording circuit, along with the possibility of drop-outs, indicates an estimated overall acceleration scale accuracy for this channel of ±50 percent, except in the vicinity of initial and reflected shock arrival where the low frequency response could introduce a larger error. This amplitude change is one of the few recorded disturbances which can definitely be attributed to time zero phenomena.

Temperature at a Depth of 0.011 Inch. Figure 3.22 presents the recorded temperature time history of the rear of a 0.011-inch-thick steel diaphragm positioned with the front surface exposed to the thermal energy within the fireball. The temperature scale accuracy of this curve was estimated to be ±30 percent. The curve indicated that the temperature rise, having exceeded 2400F (which was the thermocouple limit) at approximately 48 msec, dropped below this temperature at 50 msec or 2 msec later. No time zero disturbances were observed on this channel.

The 0.011-inch-deep depth-of-melt channel at this station recorded a pulse at 29 msec after detonation. This was the first pulse after the time zero indication.

Temperature at a Depth of 0.021 Inch. The recorded temperature time history of the rear of a 0.021-inch-thick steel diaphragm having its front surface exposed to the thermal energy within the fireball is presented in Figure 3.23. The accuracy of the temperature scale on this curve is estimated to be ±20 percent. The possibility exists that the thermo-
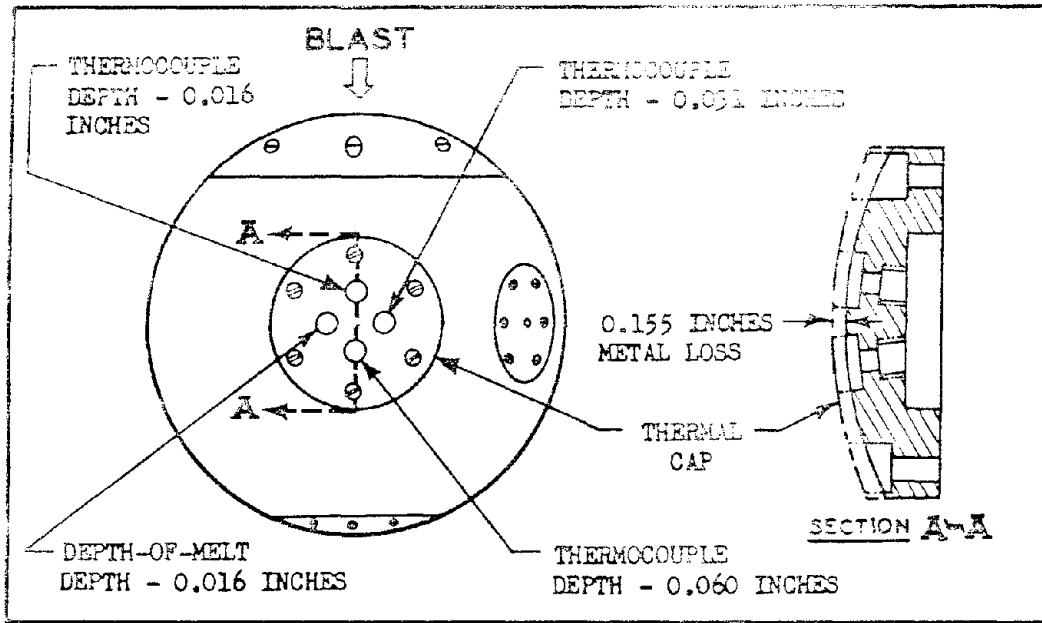
Figure 3.19 Orientation of thermocouple and depth-of-melt transducers with respect to shock wave for instrumented sphere at Station 250.
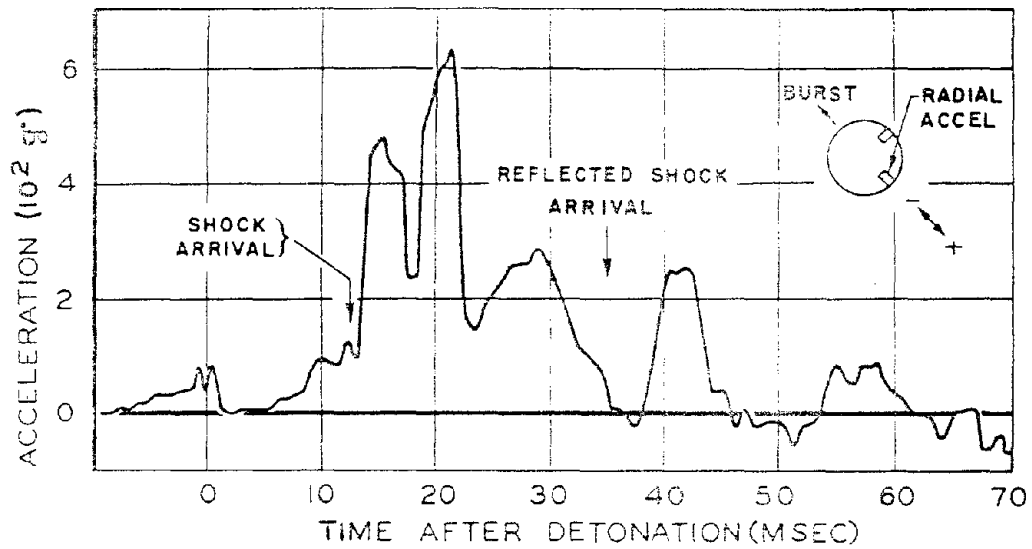
Figure 3.20 Radial acceleration versus time of instrumented sphere at Station 300.
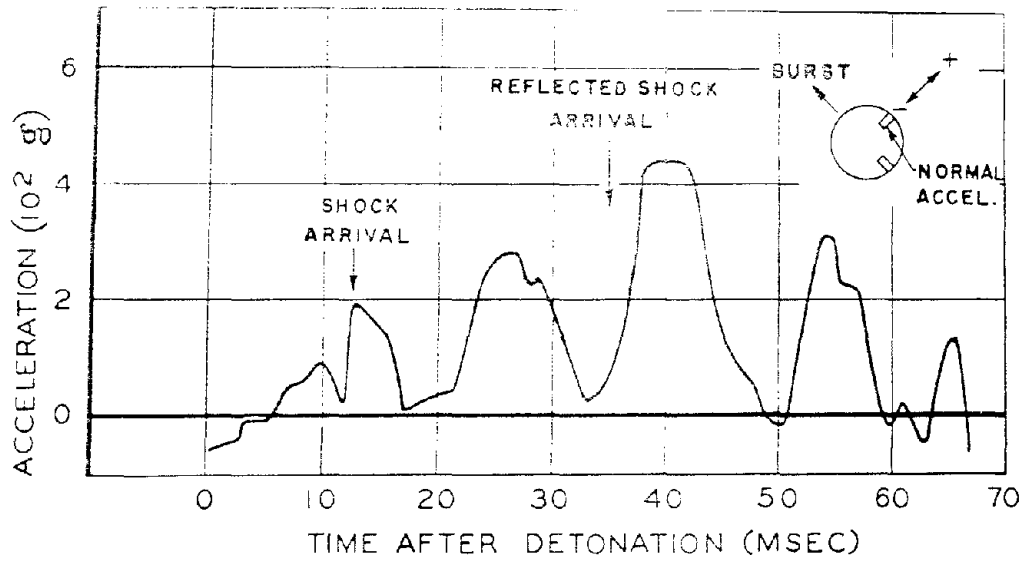
Figure 3.21 Normal acceleration versus time of instrumented sphere at Station 300.
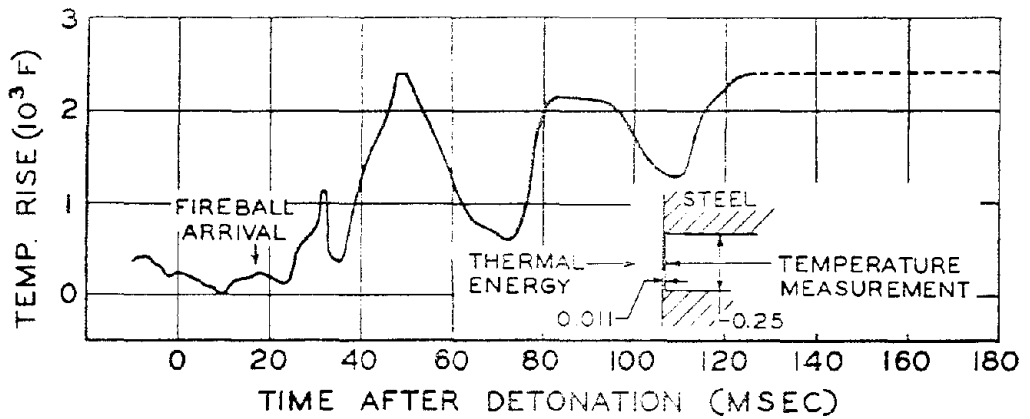
Figure 3.22 Temperature rise of steel versus time at a depth of 0.011 inch below surface of instrumented sphere at Station 300.

59

couple circuit was open prior to the steep rise which occurred at about 30 msec. This channel showed no significant time zero disturbances.

Temperature at a Depth of 0.041 Inch. Figure 3.24 presents the recorded temperature time history of the rear of a 0.041-inch-thick steel diaphragm having its front surface exposed to the thermal energy within the fireball. The temperature scale accuracy of this curve is estimated to be ±20 percent. The disturbances at time zero may have been due to time zero phenomena; however, if this were true, they were much too small to harm the recording circuit.

Figure 3.25 indicates the orientation of the thermocouple and depth-of-melt transducers with respect to the direction of the shock wave. This figure may aid in the interpretation of the temperature time history curves.

3.4 MECHANICALLY INSTRUMENTED SPECIMENS

Mechanically instrumented specimens were those which were designed to contain passive type instrumentation which were either peak reading or point value gages, the velocity-distance gages being point value gages, and the ball-crusher gages and temperature measuring gages being of the peak value type.

Eleven of the 20 specimens containing the velocity-distance gages were recovered; seven of the eleven yielded reliable data. All six of the specimens containing the ball-crusher gages were recovered; however, the one from the 50-foot station had been crushed so severely that only one gage has been removed from the specimen. Five of the six peak temperature specimens were recovered.

3.4.1 Velocity-Distance. Only one of the 11 recovered specimens failed to yield reliable data due to malfunctioning of the velocity-impact gage. Three other recovered specimens failed to yield usable data because of overpressure and material ablation effects which resulted in destruction of the specimens.

The specimen velocity data obtained by applying the calibration data to the depth of penetration readings must be corrected to account for the effects of specimen acceleration during plunger penetration, since the calibration data was obtained for zero specimen acceleration. The derived equation to effect these corrections is

$$V_0^2 = V_c^2 - 2 \int_0^{\delta \, max} \ddot{X}_s \, d\delta, \qquad (3.1)$$

where: V_0 = Actual impact velocity,

V_c = Impact velocity as indicated from calibration data.

$\ddot{X}_s$ = Specimen acceleration,

δ = Plunger penetration.

A complete analysis of the velocity-impact gage including a derivation of the above equation is presented in Appendix C. If the specimen acceleration during plunger penetration were appreciable, i.e., of the order of 9,000 grams for the larger sized plungers, a correction would have to be applied to the indicated impact velocity to determine the actual impact velocity, which was the actual specimen velocity. Theoretical calculations and inspection of the test results indicated that these high accelerations occurred during extremely short periods of time at the beginning of specimen travel for specimen movements of approximately $\frac{1}{4}$ inch. Consequently, only the data points between zero and $\frac{1}{4}$-inch specimen travel were appreciably affected by the acceleration corrections.

The data points obtained from the plungers spaced at farther distances could be somewhat in error due to Coulomb friction on the plungers as they moved relative to the tube. This effect would have been negligible had the specimens been accelerated in a direction parallel to the longitudinal axis of the gages. Application of the data presented in Figure 4.3, however, showed that the specimens located at the 150-foot station were accelerated in a direction 12 degrees from the longitudinal axis of the gage. The specimens located at the farther ranges came closer to being accelerated in the desired direction but were still somewhat in error:
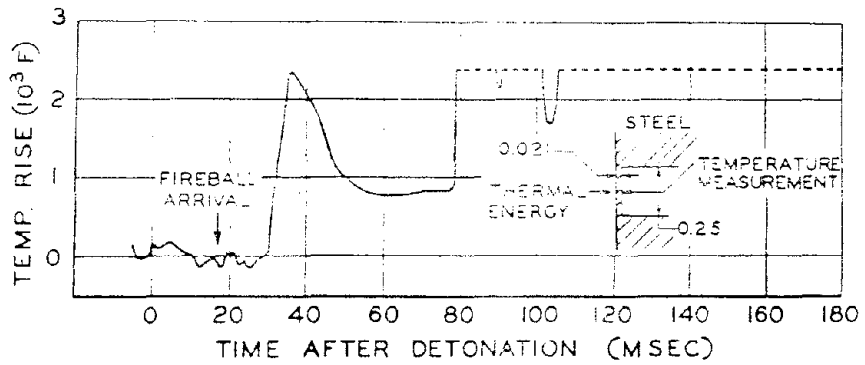
Figure 3.23 Temperature rise of steel versus time at a depth of 0.021 inch below surface of instrumented sphere at Station 300.
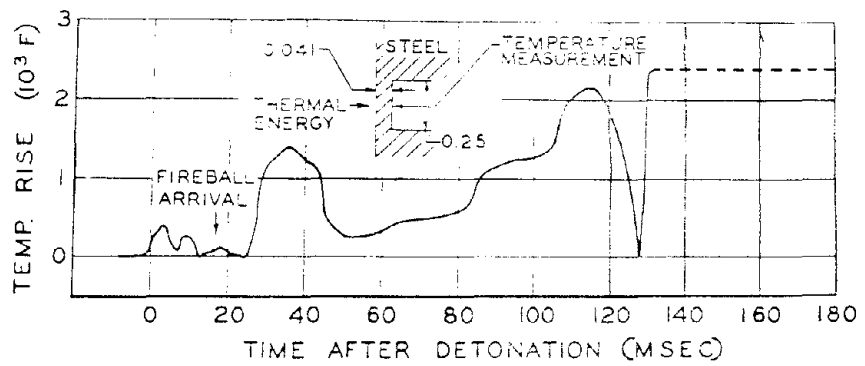
Figure 3.24 Temperature rise of steel versus time at a depth of 0.041 inch below surface of instrumented sphere at Station 300.
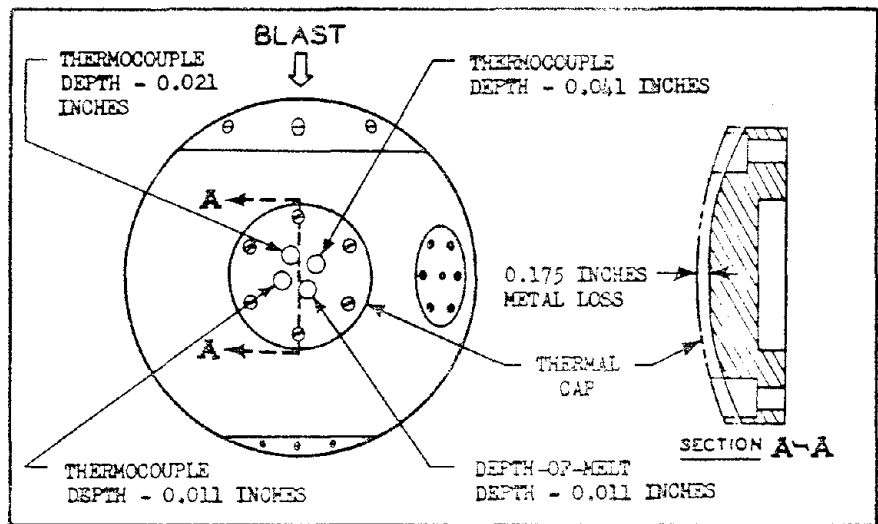
Figure 3.25 Orientation of the thermocouple and depth-of-melt transducers with respect to shock wave for instrumented sphere at Station 300.

9 degrees at the 200-foot station and 7 degrees at the 250-foot station. As a result of these side accelerations, large normal forces were developed between the plungers and the tubes; consequently, relatively large Coulomb friction forces acted upon the plungers as they moved relative to the tubes. The readings from the plungers located at the longer distances from the target blocks were thus suspected to be low, with the effect more pronounced on the specimens at the closer ranges.

Composite Specimens. All the composite specimens which were oriented end-on contained the velocity-distance impact gages. Only two of these specimens remained intact, and only one other velocity-distance insert could be identified. The cone-forward steel specimens at the 50- and 150-foot stations were recovered complete; but the one from the 50-foot station was so severely crushed by the pressure forces that the gages were damaged, and no data were obtained. The specimen from the 150-foot station had two broken plungers which did not penetrate, and the other plungers had only a few thousandths of an inch penetration. The cone-forward steel composite at the 200-foot station came apart, and the velocity-distance insert was found separated from the specimen; this specimen also had plungers which experienced little, or no, penetration.

Dynamic-Pressure Cylinders. The dynamic-pressure cylinder at the 50-foot station was so badly damaged (Section A.1.5) that the velocity-distance gages were destroyed.

The other four cylinders, two with plastic disks and two without, were recovered and yielded good velocity-distance data. Figure 3.26 is a plot of the data for the dynamic-pressure cylinders without plastic disks and Figure 3.27 is a plot for the cylinders with plastic disks. The data points representing a distance traveled of 0.250 and 0.500 inch on the four curves presented in Figures 3.26 and 3.27 are considered to be reliable measures of the actual specimen velocities within an estimated ±10 percent, since the acceleration corrections were small for these points. The lower velocity readings for the 4.00 and 7.95 inches distance traveled data points, especially at the 150-foot stations, could have been the result of Coulomb friction on the plungers, since acceleration corrections were negligible in this region and since it is not believed that a negative acceleration was experienced by the specimens at that time (of the order of 5 msec). It is believed that the specimens at the 150-foot range nearly attained their maximum velocity before they had traveled $\frac{1}{4}$ inch. The velocity of the specimens at the greater ranges was more gradually built up as evidenced by the velocity curve, Figure 3.26, of the dynamic-pressure cylinder located at the 250-foot range. The data for all four curves presented in Figures 3.26 and 3.27 was only qualitatively determined by the methods presented in Appendix C in the region from zero to $\frac{1}{8}$ inch distance traveled and consequently are presented in dashed form.

Shields From Composite Specimens. The shields from the three composite specimens were recovered, but the specimens were not. The velocity-distance data is of little value without the specimen but is presented here as evidence that the shields did accelerate at a high rate and should have accomplished their objective if the aluminum composites had been recovered.

The velocity-distance curves for all three shields are presented in Figure 3.28. The shield at the 150-foot station and the one on the left-hand side at the 200-foot station were designed to slide off the specimen at the same time interval after shock arrival, and the shield on the right-hand side at the 200-foot station was to require twice as long. As shown by the data, the two shields which were to slide off the specimen in the same interval reached the same velocity at approximately the same distance traveled, and the one designed to require twice as long to clear the specimen had attained only $\frac{1}{2}$ this velocity at the same distance.

Two of the plungers in the shield on the right-hand side at the 200-foot station penetrated almost completely through the aluminum target block and trapped some aluminum between the plunger and the steel plate which was backing up the target block. Therefore, the values given on the graph are minimum values for these two points and the curve is correspondingly low.

The curves presented in Figure 3.28 for the shield on the right-hand side of the 200-foot station should be used in a qualitative sense only, since no acceleration corrections were made on the data. The curves from the specimens at the 150-foot station and 200-foot station (left-hand side) have been corrected by the method presented in Appendix C.

62
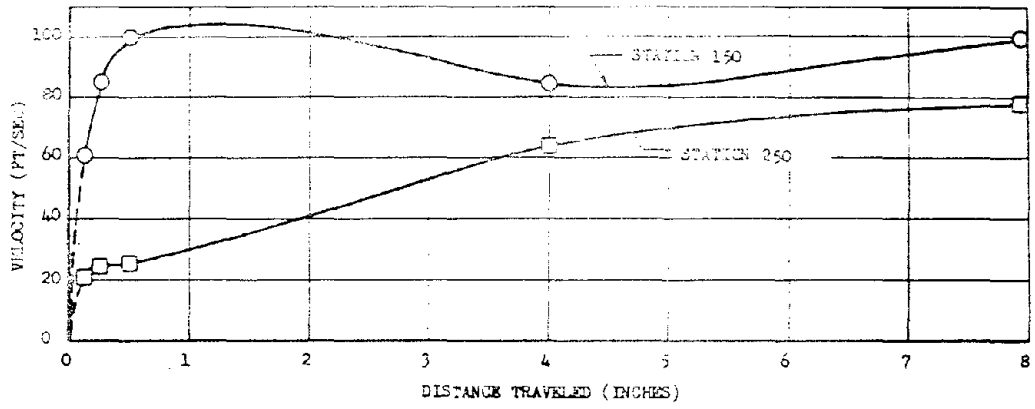
Figure 3.26   Specimen velocity versus distance traveled, dynamic pressure cylinders without plastic disk.
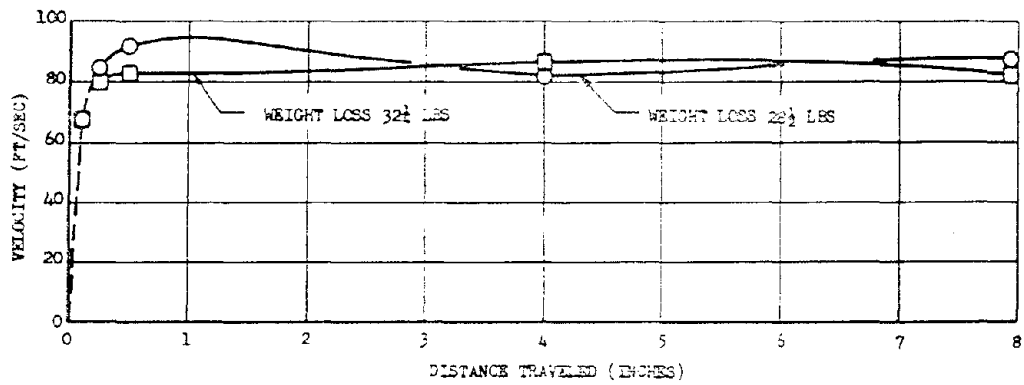
Figure 3.27   Specimen velocity versus distance traveled for the two dynamic pressure cylinders with plastic disks, Station 150.
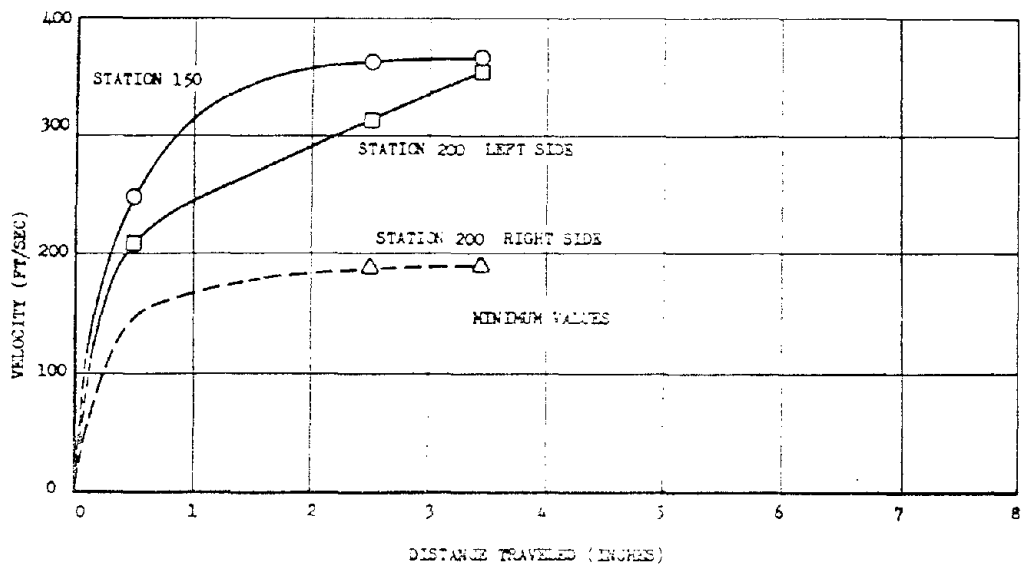
Figure 3.28   Velocity versus distance traveled, shields for composite specimen.

83
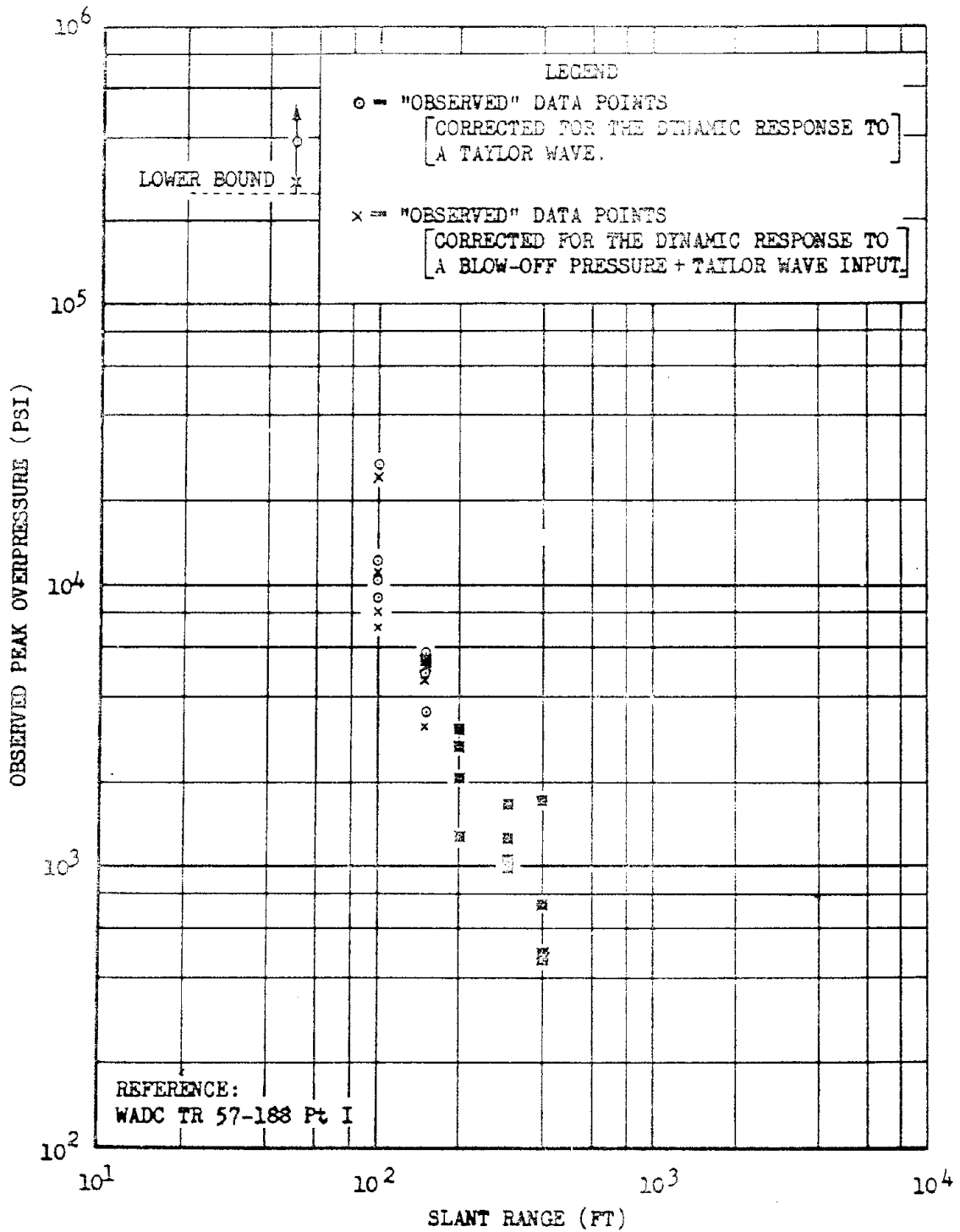
Figure 3.29 Observed peak pressures from ball-crusher gages at various slant ranges, Shot Erie.

3.4.2 Overpressure and Acceleration. A detailed description and analysis of the ball-crusher gage, as well as an analysis of the test results, is contained in Reference 1. Appendix D of this report is a summary of information contained in the reference. To determine the peak value of the forcing function, the experimental data was analyzed by using the gage responses for the various postulated dynamic inputs to the gages. These postulated inputs are presented in Appendix D. The peak pressures are shown in Figure 3.29 for two of the postulated inputs, namely the Taylor Wave and the Taylor Wave plus the blow-off pressure. From the figure, it can be seen that, for a given ball deformation, a smaller peak pressure (at the closer ranges) is calculated when the combined Taylor Wave plus blow-off pressure response of the gage is used instead of the Taylor Wave response alone, since the blow-off pressure is also acting to increase the deformation. Only one data point is given for the 50-foot station, since at this time the other gages had not been removed from the specimen. The lower bound shown in the figure for the 50-foot station is given as the ultimate strength of the steel used in the gage (250,000 psi), since the gage failed from pressure loading.

TABLE 3.9 PEAK ACCELERATION FROM BALL-CRUSHER DATA FOR
VARIOUS DYNAMIC INPUTS TO THE OVERPRESSURE SPHERES

Station		100	150	200	250	300
Gust	g Peak	2.81×10^4	1.03×10^4	6.27×10^3	2.89×10^3	1.035×10^3
Diffraction plus gust	g Peak	5.9×10^4	1.82×10^4	9.46×10^3	4.43×10^3	1.81×10^3

It is not possible to quote any degree of accuracy for the ball-crusher data, since the results are based on the dynamic response of the gage to a postulated input; however, it can be said that the observed pressures agree to within a factor of three with the theoretical predictions based on a simple Taylor Wave model.

The data from the ball-crusher accelerometers was reduced in much the same way as the overpressure gages. The dynamic input for these gages was assumed to be either a combination of the diffraction loading plus the gust loading or gust loading only. The observed peak accelerations from these inputs are shown in Table 3.9. The data shows that for a given ball deformation the existence of the diffraction input leads to a larger apparent peak acceleration.

3.4.3 Copper Sphere Temperature Distributions. Five of the six copper spheres containing the peak temperature devices were recovered and the tapered pins were removed. A study of the metallic slugs in the pins indicated that, except for a few near the surface, all the slugs had melted. This indicated that the peak temperatures attained at various depths below the surface were higher than predicted. This higher temperature could have been a result of the fact, that the copper sphere lost approximately twice the amount of metal, as predicted. Since almost all the slugs melted, no conclusions can be drawn as to what the peak temperatures actually were at various depths.

Chapter 4

DISCUSSION

In general, the damage sustained by the specimers exposed in
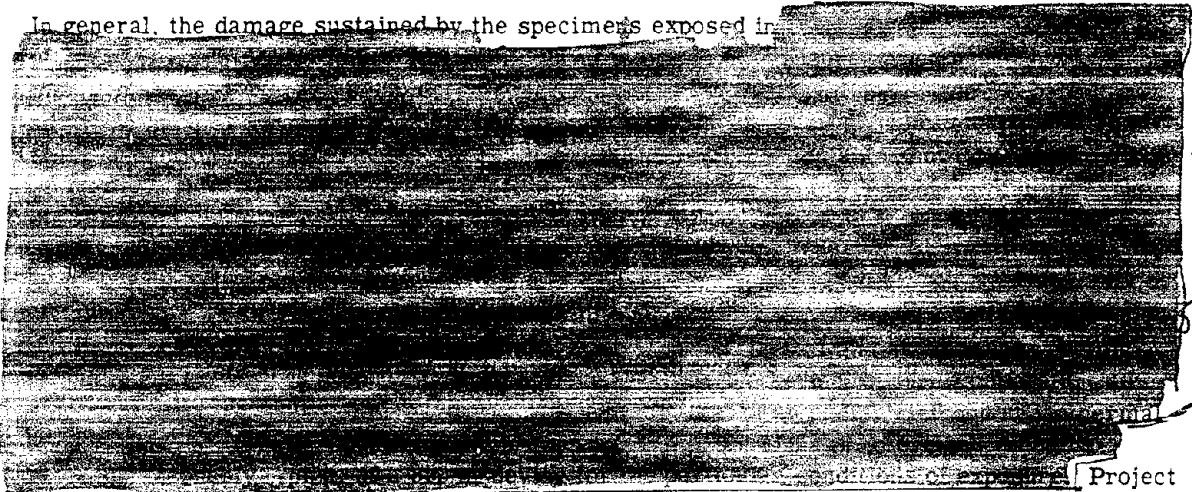
Project
5.9 specimens were exposed to the fireballs of particular nuclear detonations in a specialized
manner, and it is recommended that any attempt to extrapolate these data to other exposure
conditions take into account the complex nature of the various damage mechanisms discussed
in this chapter.

4.1 THERMAL DAMAGE

Thermal energy caused more damage to specimens within the fireballs of Shots Erie and
Mohawk than the other two general nuclear detonation phenomena: blast and nuclear radiation.
This damage was primarily material ablation, the most important contributing factors to which
were probably the temperature of the isothermal sphere at the time of engulfment and the tem-
perature time history of the specimen from the time of engulfment to ground impact. A theo-
retical curve of the temperature time history of the isothermal sphere for a 20 kt device was
obtained from Reference 2. This curve was scaled to 15.5 kt (Shot Erie) by scaling time by the
cube root of the yield ratio and is presented in Figure 4.1.

4.1.1 Specimen Engulfment Times. Ablation of material by a nuclear fireball is un-
doubtedly a strong function of the specimen engulfment time. This engulfment time is deter-
mined by the speed and trajectory of the specimen and the fireball growth and position with
respect to the specimen.

Only spherical specimen trajectories and engulfment times were calculated because of the
unpredictable paths associated with nonspherical specimens. Since all the specimens were
mounted in such a manner that the mounts would introduce no significant forces to the speci-
mens upon engulfment, the trajectory calculations were made without consideration of these

66

forces. The trajectory calculations also were based upon the assumption that the specimen receives its total impulse in a relatively short time, before it can experience any appreciable motion.

If the specimen follows a ballistic trajectory and the above assumptions are realistic, the position of the specimen at any time, t, is described by the following two equations:

$$y = \frac{gt^2}{2} + V_0 t \sin A'; \tag{4.1}$$

$$x = V_0 t \cos A'; \tag{4.2}$$

where: V_0 = Initial velocity, (ft/sec);
    t = Time, (sec);
    g = Acceleration due to gravity, (ft/sec^2);
    A' = Departure angle, (degrees), (see Figure 4.3);
    y = Vertical distance traveled in time t, (ft);
    x = Horizontal distance traveled in time t, (ft).

Figure 4.2 shows the physical correspondence of the factors in the above equation. Since the specimen preshot height above ground and its postshot recovered range are both know, it remains only to determine the departure angle so that both V_0 and t may be calculated.

The departure angle of the specimen is dependent upon the direction of the impulse received from the expanding fireball and shock wave and from the shock wave reflected by the ground. On Shot Erie the effect of the reflected shock wave, because of its relatively long path, was considered negligible for specimens closer than 150-foot slant range. The direction of the expanding fireball impulse for Shot Erie was determined from the fireball growth pictures of Figure 3.1. These photographs clearly show Project 5.9 specimen towers as well as the growth of the fireball. The impulse from the fireball was assumed to act in a direction normal to the surface of the fireball. The departure angles were determined from the pictures in Figure 3.1 by constructing a normal to the surface of the fireball in the vicinity of the specimens. This departure angle, A, is presented as a function of slant range in Figure 4.3. An estimation of the effect of the reflected shock on the departure angle is presented as A' in Figure 4.3. This estimation was based on the impact time recorded by the instrumented sphere, using Equations 4.1 and 4.2 in the following manner: if preshot height, postshot impact distance, and impact time are substituted in Equations 4.1 and 4.2, there remain only two unknowns, V_0 and A', in the two equations which can then be solved simultaneously. Thus, the impact time recorded by the instrumented sphere at Station 250 had assisted in a determination of the initial velocity and departure angle for that specimen.

Having determined the departure angle A', the initial velocities V_0 and impact times t_i were calculated for all Shot Erie spherical specimens for which impact distances were known by using Equations 4.1 and 4.2. These data are tabulated in Figure 4.6.

Since spherical specimens having the same diameter, even though different masses, should receive equal impulses from the shock wave when exposed at the same range, it was desirable, for correlation purposes, to convert the velocities and masses of these specimens to impulse. The following equation was used to calculate specimen impulse:

$$I_0 = V_0 M; \tag{4.3}$$

where: I_0 = Total specimen impulse, (lb-sec);
    V_0 = Initial velocity, (ft/sec);
    M = Specimen mass, (lb-sec^2/ft).

The specimen impulse, thus calculated, is compared to similar specimens at other ranges in Figure 4.4. This figure correlated the impulses received by the 12-inch- and 8-inch-diameter specimens and also shows how the 10-inch and 16-inch specimen impulses compare with the

67
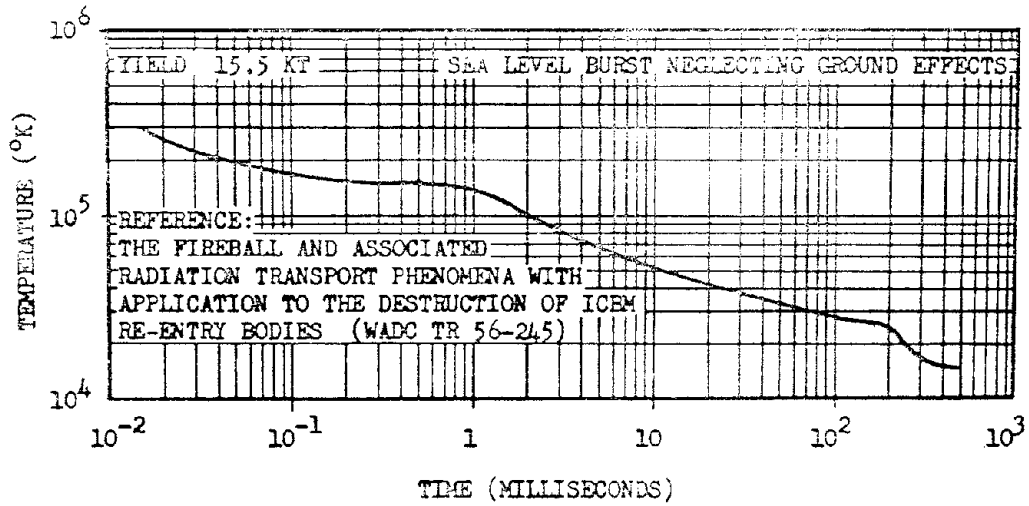
Figure 4.1 Isothermal sphere temperature versus time for 15.5 kt at sea level.
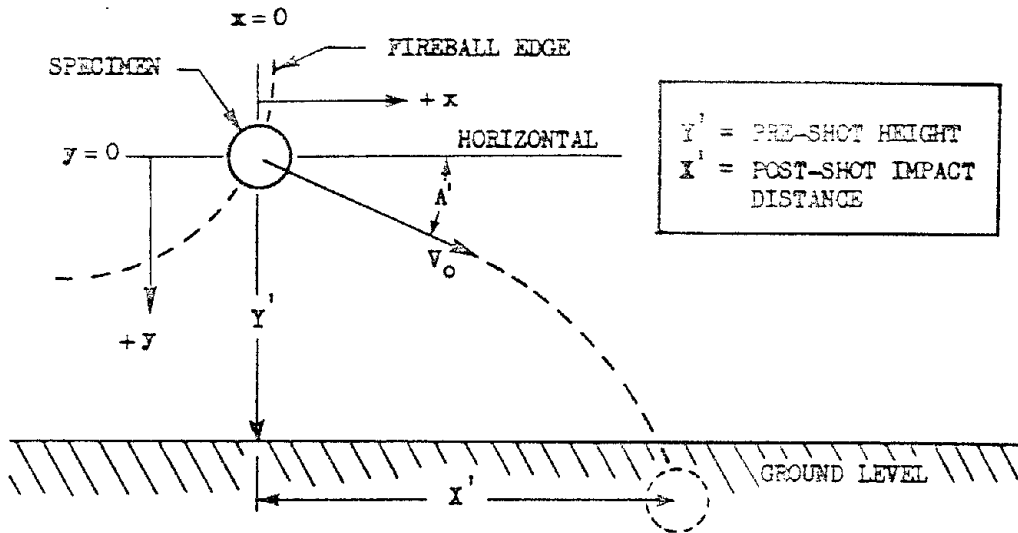
Figure 4.2 Explanation of symbols in trajectory equations.
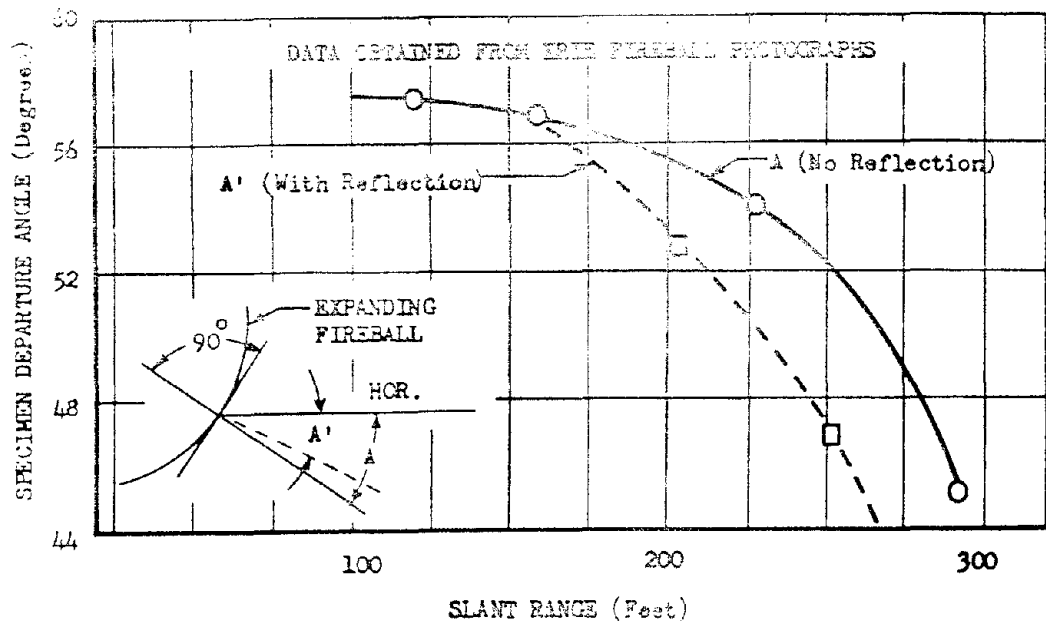
Figure 4.3   Specimen departure angle as a function of slant range, Shot Erie.
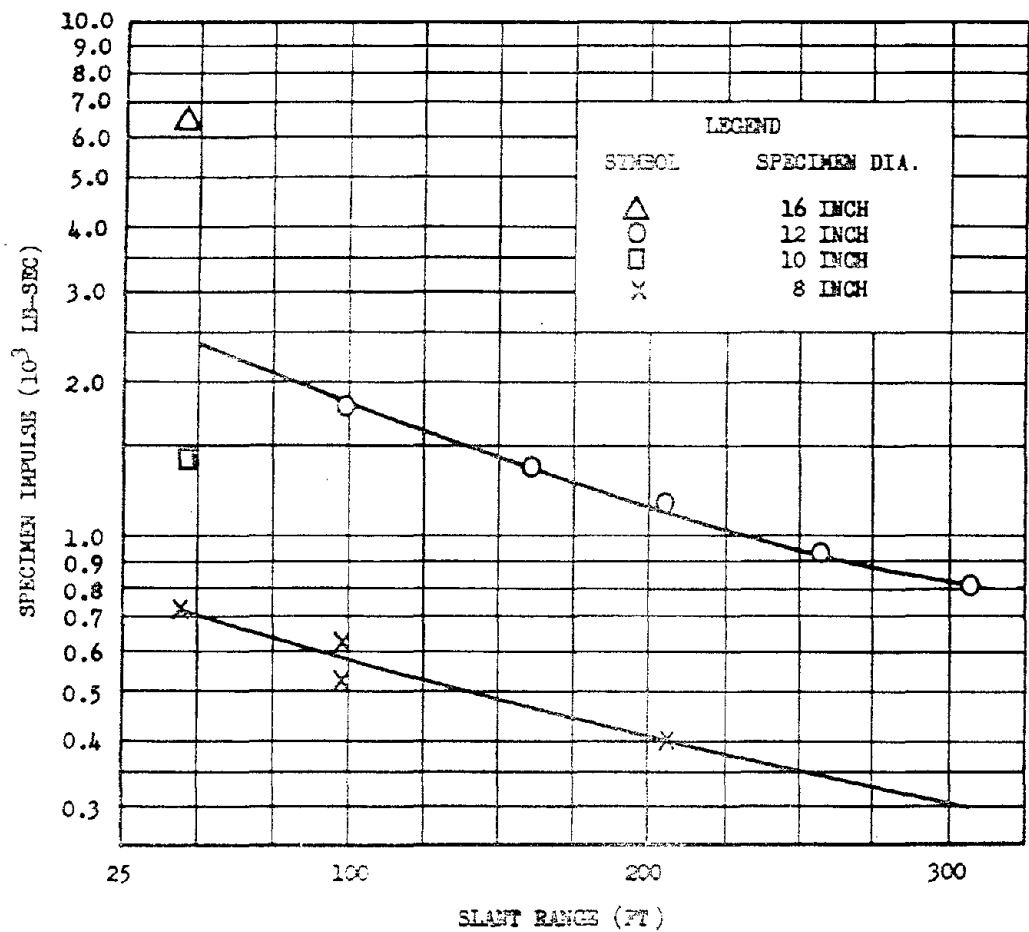
Figure 4.4   Specimen impulse as a function of slant range, Shot Erie.

69

other diameters. Having thus determined the impulses for various diameter spheres, it is now possible to calculate V_0 and t_i for those spherical specimens for which impact distances are not known. These data are also tabulated in Figure 4.6.

Inspection of the data contained in Table 3.2 presents the possibility that the reflected shock wave rebounding from the ground beneath the shot may have hollowed out the fireball and isothermal sphere. This hollowing-out, or cupping, would not have been particularly noticeable on the motion picture frames from which these data were obtained. Various opinions have been expressed as to the probability of cupping and its effect on the specimen engulfment times. Since the cupping would only affect the specimen exit time, and this is probably much less important than the entrance time, the effect of any cupping is probably slight. In view of the lack of any actual data and the probability that the effect of cupping is negligible, this phenomena has not been considered in the computation of engulfment times which follows.

Engulfment times for the spherical specimens exposed in Shot Erie were obtained from curves similar to Figure 4.5. This figure shows the time history of the location of the fireball and isothermal sphere above ground along a 45 degree line formed by the specimen locations. The fireball data were obtained from Figure 3.1 and Table 3.2 in the Results Chapter of the main report. The isothermal sphere location inside the fireball was scaled from data contained in Reference 2. Typical time histories of the vertical location of each specimen are illustrated in Figure 4.5 and were obtained from the trajectory data above. The engulfment times for all Shot Erie spherical specimens are shown in Figure 4.6. These times were computed from curves similar to Figure 4.5.

4.1.2   Ablation Mechanisms.   The ablation of material from a specimen within the fireball by thermal means can be accomplished by several mechanisms, namely: vaporization, melting, and spalling. However, the determination of the magnitude of each of these mechanisms on a given specimen by postshot analysis is difficult. If all the mechanisms were contributive, any observable effects due to one could be obliterated by the effects of any subsequent mechanism. Each of the above three mechanisms is discussed in the following paragraphs with the object of presenting briefly current thinking to provide an appreciation of the various parameters which affect these mechanisms. Project 5.9 data is used throughout the discussion of each mechanism to support or contradict the explanations of the mechanisms.

Vaporization.   The mechanism of vaporization of metal specimens within the high energy region of a nuclear fireball is complex. The radiant energy available inside an isothermal sphere at 100,000K is sufficient to vaporize many times the material which was actually removed from the specimens. Since the measured loss was much less than the available energy would indicate, it follows that some phenomena must have retarded the process of vaporization. The most probable and reasonable explanation for this retarding action is that the initial vapors from the specimen effectively shield the specimen and attenuate or reduce the energy incident on the surface at any subsequent time.

Consider a metal specimen which has just been engulfed by the isothermal sphere of a nuclear detonation as shown in Figure 4.7. Upon engulfment, the extremely high energy level of the isothermal sphere caused the outer surface of the specimen to vaporize almost immediately. This results in a minute amount of material loss and the formation of the vapor layer illustrated in Figure 4.7. The specimen surface is thus shielded from the high energy of the isothermal sphere by the relatively cool vapor. The objectives of several Project 5.9 specimens were directed toward understanding the action of this vapor layer and its associated shielding characteristics. If the vapor layer were swept away by the action of the moving material surrounding the specimen, it would reduce the shielding effect of the layer and thus be important to the mechanism of ablation by vaporization. Theoretical calculations have indicated that sweeping is negligible; however, the longitudinally grooved flat plate was exposed in an effort to determine experimentally the effectiveness of this hydrodynamic sweeping.

The longitudinally grooved plate recovered from the 150-foot station showed more metal loss toward the front than it did toward the rear on both the grooved and flat sides. The grooved side averaged between 10 and 25 percent more metal loss on the front than on the rear, and the variation along the flat side was approximately 10 percent.

70

VERTICAL DISTANCE FROM GROUND TO 45° LINE (FT.)

TIME AFTER DETONATION (MSEC)

LEGEND

☐ RAPATRONIC DATA
◯ E.G.&G. MOTION PICTURE DATA
☐ FIREBALL
▨ ISOTHERMAL SPHERE

STA 50

HEIGHT OF SPECIMEN ABOVE GROUND

STA 100

STA 150

STA 200

STA 250

STA 300

BURST POINT

× FIREBALL EDGE

45°

GROUND

VERTICAL DISTANCE FROM GROUND TO 45° LINE
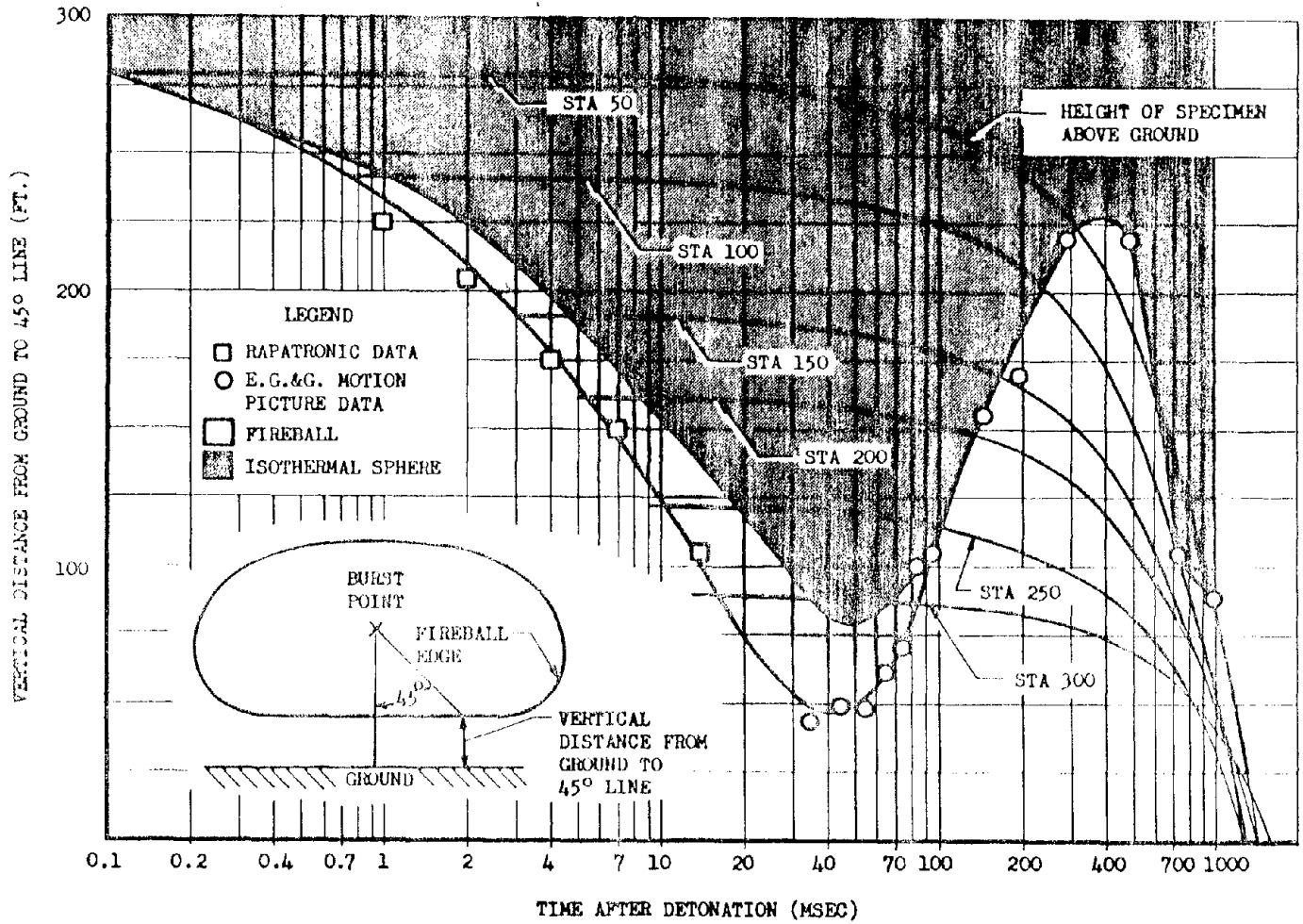
Figure 4.5   Engulfment time determination for the electrically instrumented specimens.

SPECIMEN				TRAJECTORY DATA			FIREBALL AND ISOTHERMAL SPHERE ENGULFMENT TIMES MSEC
Station	Code	Diameter	Material	Velocity V_0	Departure Angle A	Impact Time t_i	
		inches		ft/sec	degrees	seconds	
50	T	16	Steel	277	40.2[a]	1.39	
	Z	12	Steel	141	35.8[x]	2.35	
	N	10	Steel	243	34.2[a]	1.73	
	L	8	Copper	207	31.0[a]	2.06	
	O	8	Steel	237[b]	34.1[x]	1.76	
100	Z	12	Steel	181	57.5	1.37	
	X	12	Steel	202[b]	57.5	1.26	
	N	10	Steel	105	57.5	1.99	
	I	8	Molybdenum	160	57.5	1.53	
	L	8	Copper	156	57.5	1.54	
	J	8	S. Steel	95	57.5	1.99	
	K	8	Titanium	360	57.5	1.09	
150	Z	12	Steel	135	56.6	1.35	
	X	12	Steel	152	56.6	1.33	
	L	8	Copper	136[b]	56.6	1.44	
	G	8	Plastic	694[b]	56.6	0.34	
200	Z	12	Steel	105	52.6	1.54	
	X	12	Steel	118	52.6	1.43	
	I	8	Molybdenum	101[b]	52.6	1.53	
	L	8	Copper	117	52.6	1.42	
	J	8	S. Steel	137[b]	52.6	1.25	
	K	8	Titanium	210[b]	52.6	0.82	
250	Z	12	Steel	92	47.2	1.53	
	X	12	Steel	104	47.2	1.27	
	L	8	Copper	98[b]	47.2	2.59	
	G	8	Plastic	510[b]	47.2	0.33	
300	Z	12	Steel	80[b]	21.0	1.62	
	X	12	Steel	90	21.0	1.57	

[a] Line-of-sight angle from specimen through burst point.

[b] No impact data, velocity computed from assumed impulse.

Figure 4.6   Engulfment times for Shot Erie spherical specimens.

Further, the cone-forward steel composite specimens from the 50-, 150-, and 200-foot stations also showed a greater depth of metal loss toward the front (cone) end than toward the rear (hemispherical) end. In general, the difference was under 10 percent; however, since all three specimens showed the same trend, it was believed to be significant. The fact that both the flat plate and composite specimens show more metal loss toward the front tends to substantiate the existence of an attenuating vapor layer and that some sweeping of this layer did occur.

Another objective of the flat plate exposure was a more complete understanding of the vapor layer, its thickness, and its attenuating characteristics. To date, the analysis of the metal loss sustained by the flat plates has yielded no conclusive results concerning the magnitude of the shielding properties of the vapor layer. Further analysis may provide some tentative data on the thickness of the attenuating vapor layer.

Acceptance of the vapor layer attenuation theory leads to the conclusion that the shape of the specimen may affect its ablation by vaporization. Consider three specimen shapes: a plane surface, a cylindrical surface, and a spherical surface of the same radius as the cylinder. Assuming that the average directions of the vaporized molecules are normal to the surfaces and that the average molecular velocities are equal for the three surfaces, it can be shown that for equal depths of metal loss the average vapor density of cylindrical surfaces is less than plane surfaces and greater than spherical surfaces of the same radius. Since lower average density indicates a smaller attenuation, which would result in more ablation, it would be reasonable to expect more material loss on a spherical surface than on a cylindrical surface of the same radius, all other parameters being equal. Similarly, due to this radius of curvature effect, the material loss on a plane surface should be less than either a cylinder or sphere. The composite specimen offers the best comparison of cylindrical and spherical surfaces, since these surfaces were on the same specimen and therefore experienced the same time history. Only side-on steel composite specimens were considered because the cone-forward composites showed some sweeping effects which complicate the comparisons. The spherical surfaces of all recovered side-on composites showed more metal loss than their cylindrical surfaces. This data tends to support the radius of curvature theory developed above.

Extending the radius of curvature arguments to spherical specimens of different radii would lead one to expect more ablation by vaporization on smaller radius specimens. This effect was noted at the 50-foot station on Shot Erie, as shown in Figure 4.8. This data is for 1045 steel spheres with the exception of the 8-inch radius which was 4340 steel. The plane side of the flat plate (sphere of infinite radius) at the same range lost an average of 0.56 inch of steel; however, it may have had a longer engulfment time and hence the loss may be high compared to the spheres. The values given in the figure are actual loss, and no attempt has been made to correct this data for differences in engulfment times since the duration of the engulfments as shown by Figure 4.5 are approximately equal.

The measured metal loss on 4- and 5-inch-radius steel specimens exposed in Shot Mohawk seems to contradict the radius of curvature theory, because the larger sphere lost a greater depth of metal than the smaller one as shown in Table 3.3. Future theory development should attempt to explain this apparent reversal of the radius of curvature effect for the larger yield device.

Since the corners of the flat plates and cylinders could be considered as areas of near zero radius, the radius of curvature effect would predict a large material loss for these areas leaving them rounded to a considerable extent. In this regard, the Teapot and Redwing data are somewhat contradictory. Inspection of the cylindrical specimens exposed in Operation Teapot showed that their corners were rounded to a radius of about 1 inch, thus supporting the above hypothesis. However, with only a few exceptions, the corners of the flat plates and cylinders exposed during Operation Redwing remained comparatively sharp with the average radius of the flat plate corners being between 0.1 and 0.4 inch, as presented in Table 4.1. Although the lack of significant corner rounding on the Redwing specimens does not support the vapor attenuation and radius of curvature theories, it does not completely contradict them either. Further theory development should take into account this corner rounding data and attempt to correlate this phenomenon with the general material ablation theory.

73
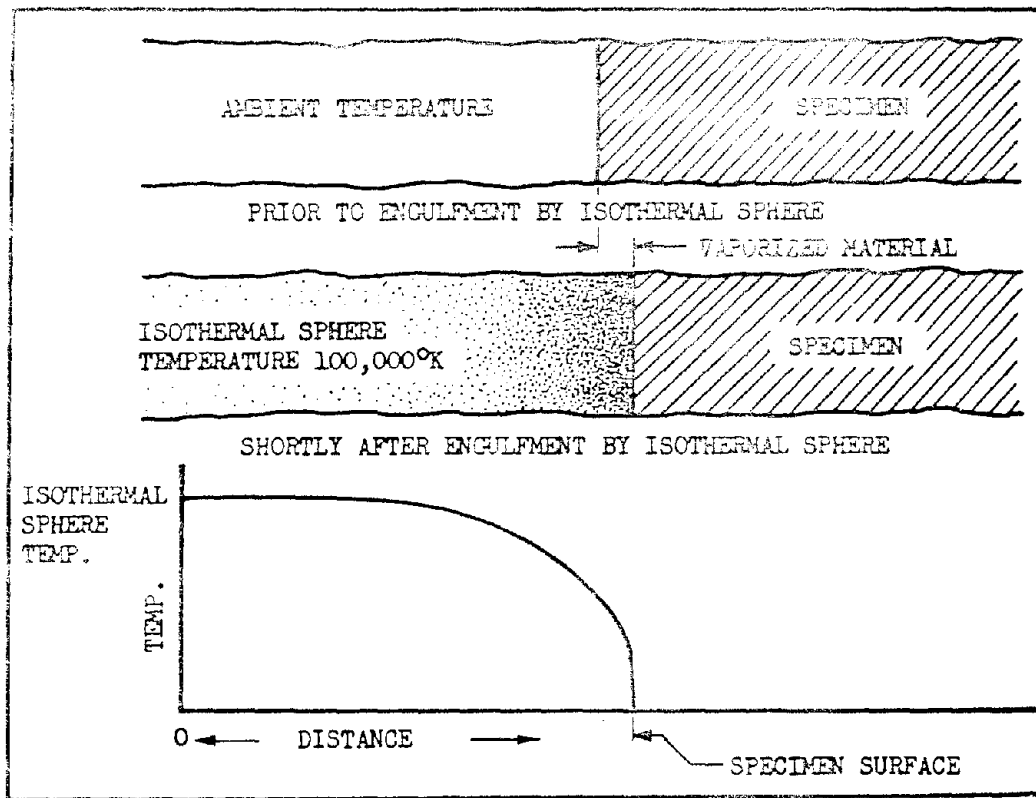
Figure 4.7 Vapor layer attenuation.
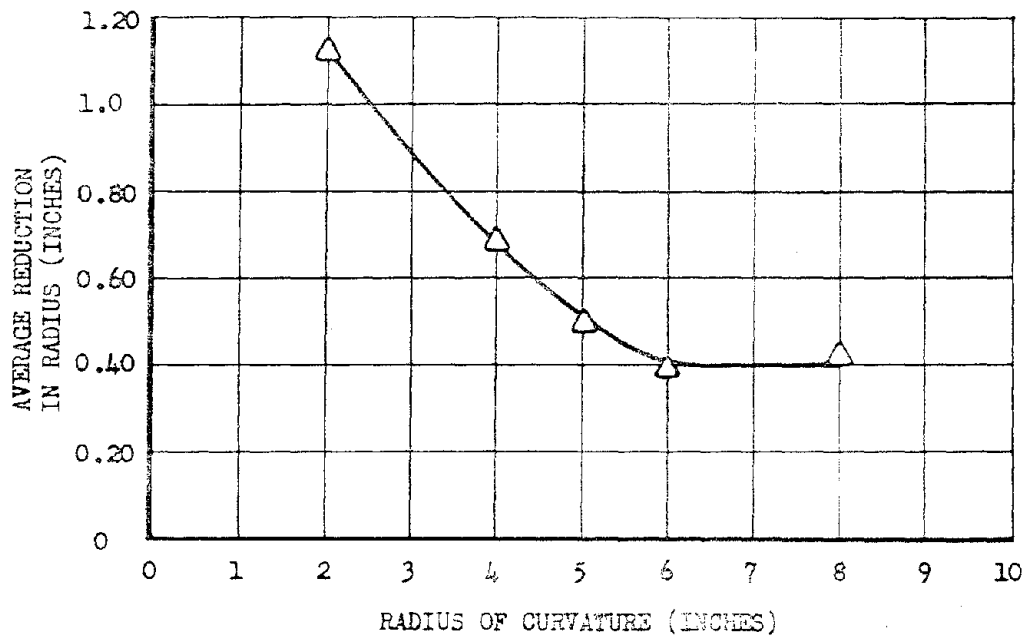
Figure 4.8 Radius of curvature effect for spherical specimens at the 50-foot station, Shot Erie.

74

Figure 4.9 illustrates an interesting phenomenon observed on Shot Erie. The specimens shown in the figure all show excessive metal loss at the junction of two pieces of metal. The width of these slots probably varied from a few thousandths to 30 thousandths of an inch. This phenomenon was observed in Redwing and Teapot on the cylindrical specimens. The spherical specimens on Redwing which had metal junctions of the same type showed no evidence of this metal loss phenomenon. Excessive metal loss in the vicinity of the junction of two pieces of metal seems to be a phenomenon associated with cylindrical shapes and it is apparent at slant ranges as great as 250 feet for exposure conditions similar to those of Shot Erie.

In general, the data collected by Project 5.9 supports the presence of a radius of curvature effect which in turn lends support to the vapor layer attenuation theory.

The effects of shape and orientation on the material ablation sustained by Project 5.9 specimens is evident from examination of the tables in Appendix A, which show that the steel spheres had approximately $\frac{1}{2}$ the depth of metal loss experienced by both the cylinders oriented side-on and the blunt ended cylinders oriented end-on and about $\frac{1}{3}$ the loss of the composite specimens oriented cone-forward. The major portion of these differences can probably be attributed to engulfment time variation between various types of specimens. The importance of the duration of the engulfment was emphasized by the fact that the steel locking nut on the plastic sphere from the 150-foot station (engulfment time of 113 msec) lost only 0.07 inch of metal, although the heavier steel specimens at the same station (engulfment time 150 msec) lost an average of 0.2 inch.

Except for the radius of curvature effect and the excessive metal loss noted at the junction of two pieces of metal on the cylinders, the shape of a specimen probably has little effect on the depth of material ablation, if all other exposure conditions are the same.

In general, most specimens sustained more ablation on the surface facing toward the burst point. All but a few of the spherical metal specimens exposed within the fireball of Shot Erie showed from 10 to 150 percent more metal loss on the side facing the detonation than on the rear or opposite side. The nonspherical specimens such as composites and cylinders, in general, also showed more material loss on the surface facing the burst but to a lesser degree than the spherical specimens.

The cone-forward composite specimens experienced approximately twice the metal loss of the side-on composites at the same ranges. Again, this difference can probably be attributed to the substantially different engulfment times caused by the specimen orientation. The velocity for the side-on specimen was probably much greater than that for the cone-forward specimen because of the much larger frontal area presented to the shock wave.

The predominant effect of orientation on the material ablation of specimens is a probable increase in the depth of material loss on the surface facing the burst point.

Melting. Data were recorded from thermocouples installed at various depths below the surface of the electrically instrumented spheres at Stations 250 and 300. These data were used to plot a curve of depth of melt in steel as a function of time after detonation, as described in Section 4.5.1, Figures 4.19 and 4.20. Assuming the molten layer was thin and of relatively constant thickness, these depth-of-melt curves were a close approximation to depth of metal loss as a function of time, and their slope was a measure of the rate of metal loss as a function of time. Figure 4.10 presents this rate of metal loss from Stations 250 and 300 instrumented spheres as determined from the slope of the mean curves in Figures 4.19 and 4.20.

The isothermal sphere exit time for the Station 250 instrumented specimen was 100 msec, and its total postshot depth of metal loss was approximately 0.155 inch. Figure 4.19 shows that at the time of exit, the specimen had melted or vaporized only to a depth of approximately 0.048 inch or approximately 30 percent of its ultimate depth of metal loss. Therefore, the remaining 70 percent material ablation must have been accomplished between isothermal sphere exit time and ground impact time. Investigation of the energy available to the specimen from the large hot fireball surrounding it during this period indicated that for most of this time sufficient energy was available to melt approximately 2 to 4 $(gm\ cm^2)$/sec of steel. This rate of melting for the times involved plus the material already ablated resulted in a total depth of melt approximately that of the observed postshot depth of metal loss. Removal of this molten layer could have been accomplished by a number of methods, such as sweeping, spinning-off,

75
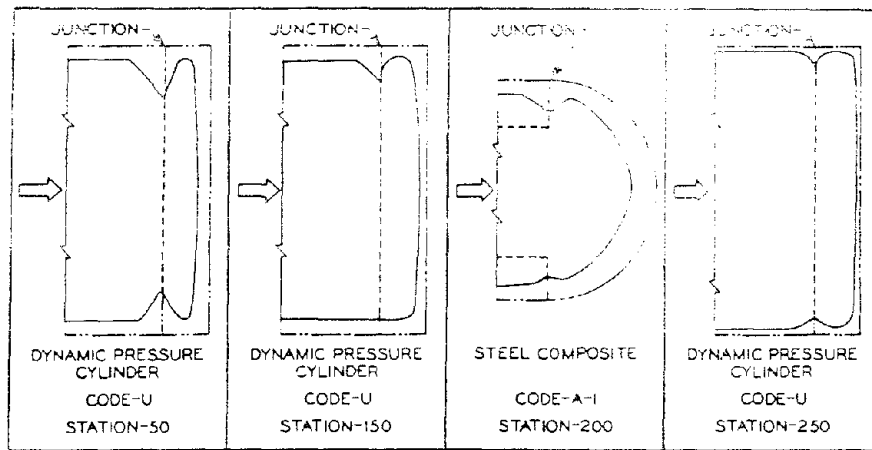
Title	Code	Station	Orientation	Damage at junction
Steel composite	A-1	50	Cone-forward	Yes
Steel composite	A-1	150	Cone-forward	Yes
Steel composite	A-1	200	Cone-forward	Yes
Dynamic pressure cylinder[a]	U	50	End-on	Yes
Dynamic pressure cylinder[a]	U	150	End-on	Yes
Dynamic pressure cylinder[a]	U	250	End-on	Yes
Dyn. pres. cyl. with plastic	AA	150	End-on	Yes
Dyn. pres. cyl. with plastic	AA	150	End-on	Yes

[a]Indicates specimen shown.

Figure 4.9   Excessive metal loss in the vicinity of the junction of two pieces of metal.
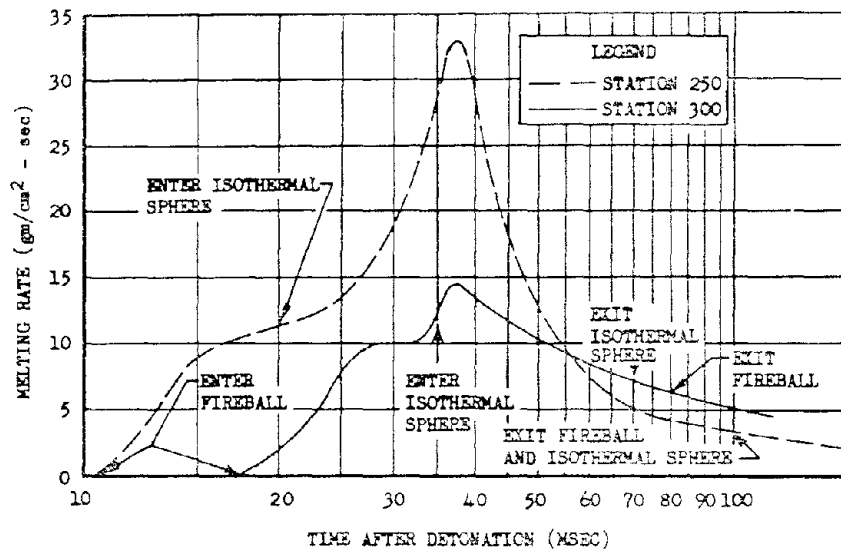
Figure 4.10   Rate of melting as a function of time for instrumented spheres at Stations 250 and 300. Shot Erie.

76

oxidation, or any combination of these or other methods. It was therefore concluded that it was possible for the instrumented specimen at Station 250 to have lost up to 70 percent of its total metal loss by melting, after emerging from the isothermal sphere.

Fireball exit time for the Station 300 instrumented specimen was 80 msec. Figure 4.20 indicates that at that time the depth of melting or vaporization was approximately 0.030 of an inch; however, the total postshot depth of metal loss was determined to be approximately 0.175 inch. At fireball exit time, therefore, the depth of metal loss was approximately 20 percent of the observed postshot total depth of metal loss.

The Station 300 instrumented specimen had approximately the same energy available for specimen melting as the Station 250 specimen after emerging from the fireball. Two factors, however, indicated that the Station 300 specimens should have had an equal or greater depth of melt than Station 250 specimens. The first was that the rates of material loss, or rates of melt, for Stations 250 and 300 were equal at approximately 55 msec, as indicated by Figure 4.10; and thereafter the Station 250 rate was less than that of Station 300. A possible explanation for this was that the vapor layer generated by the relatively high initial rate of vaporization at Station 250 produced an attenuation for this specimen much greater than that of Station 300 which entered the isothermal sphere at a much cooler temperature and, therefore, had a vapor layer which attenuated to a lesser degree. The second factor which indicated an equal or greater depth of material loss for Station 300 compared to Station 250 was that the impact time for the Station 300 specimen was approximately 300 msec later than that of the Station 250 specimen. Although the energy input to the specimen was relatively low during these 300 msec, because of the cooling of the fireball, enough energy was available to continue melting. The above analysis indicates that up to 80 percent of the total ablation sustained by the instrumented sphere at Station 300 could have been due to melting after the specimen had emerged from the fireball.

The above discussion offers an explanation for the fact that the instrumented sphere at Station 300 experienced approximately the same total material ablation as the instrumented sphere at Station 250. However, Figure 4.11 shows that these two specimens were not the only ones to experience approximately the same ablation since the overpressure spheres at Stations 250 and 300 also showed approximately the same total metal loss. Furthermore, Figure 4.11 indicates that the instrumented and overpressure spheres at Stations 150, 200, 250, and 300 all showed approximately the same metal loss. This result was unexpected since the isothermal sphere engulfment temperatures were much higher and engulfment times much longer for Station 150 than for Station 300. Although the ablation-by-melting (after emergence from the fireball) theory discussed above may not fully explain the approximately equal ablation of the 12-inch steel spheres from Stations 150 and 300, it is believed that it does explain a significant portion of this apparent anomaly.

Removal of Molten Layer. Ablation by vaporization depends primarily on supplying the specimen surface with sufficient energy to vaporize the specimen material. Ablation by melting, however, not only depends on providing the surface with sufficient energy to cause melting but also on some method for removing this melted material. Molten material may be removed from the specimen by a number of methods, such as sweeping, centrifugal force, and oxidation.

Current theory, Reference 2, states that vaporization is the predominant ablation mechanism for isothermal sphere temperatures above approximately 7,000K. However, it is possible that a significant molten layer exists between the vaporizing material and the solid material of the specimen for these high temperatures. At isothermal sphere temperatures below 7,000K but above the melting point of the specimen material, the predominant effect is specimen melting. The removal of the above mentioned molten layers is the subject of the following discussion.

Molten material can be removed by a sweeping action in two ways: (1) by the action of the moving material behind the direct and reflected shock fronts, and (2) upon impact with the ground. Ablation of molten material by the sweeping action associated with the material velocity behind a shock front presupposes the existence of a molten layer during the time this

77

TABLE 4.1 FLAT PLATE CORNER RADII, SHOT ERIE
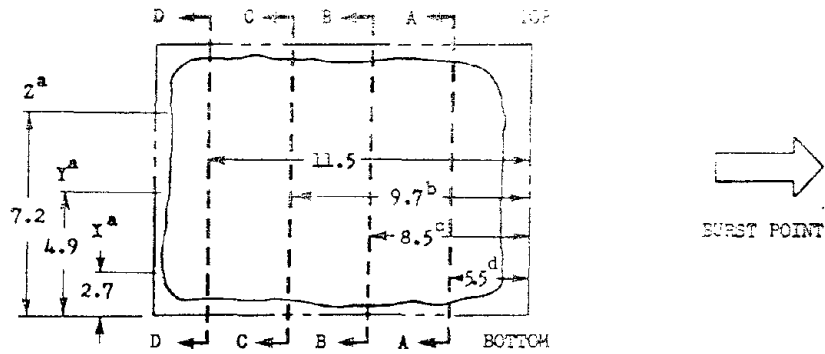
| Type | Slant Range | | Radii | | | | | | | | X^a | Y^a | Z^a |
| | Nominal Ft | Actual Ft | Section AA | | Section BB | | Section CC | | Section DD | | In. | In. | In. |
			Top In.	Bottom In.	Top In.	Bottom In.	Top In.	Bottom In.	Top In.	Bottom In.			
F	150	156	0.25	0.30	0.25	0.25	0.25	0.25	0.20	0.25	0.20	0.20	0.20
D	50	43.7	0.15	0.15	0.15	0.15	0.15	0.20	0.15	0.20	0.15	0.15	0.15
D	150	156	0.20	0.20	0.25	0.20	0.20	0.25	0.20	0.25	0.25	0.25	0.25
D	200	201	0.25	0.25	0.25	0.25	0.25	0.25	0.20	0.30	0.25	0.25	0.25

[a] Radii at X, Y, and Z were taken at rear of specimens.
[b] Measurements were taken at 8.5 inches on Type F (grooved longitudinally).
[c] Measurements were taken at 5.8 inches on Type F (grooved longitudinally).
[d] Measurements were taken at 4.4 inches on Type F (grooved longitudinally).
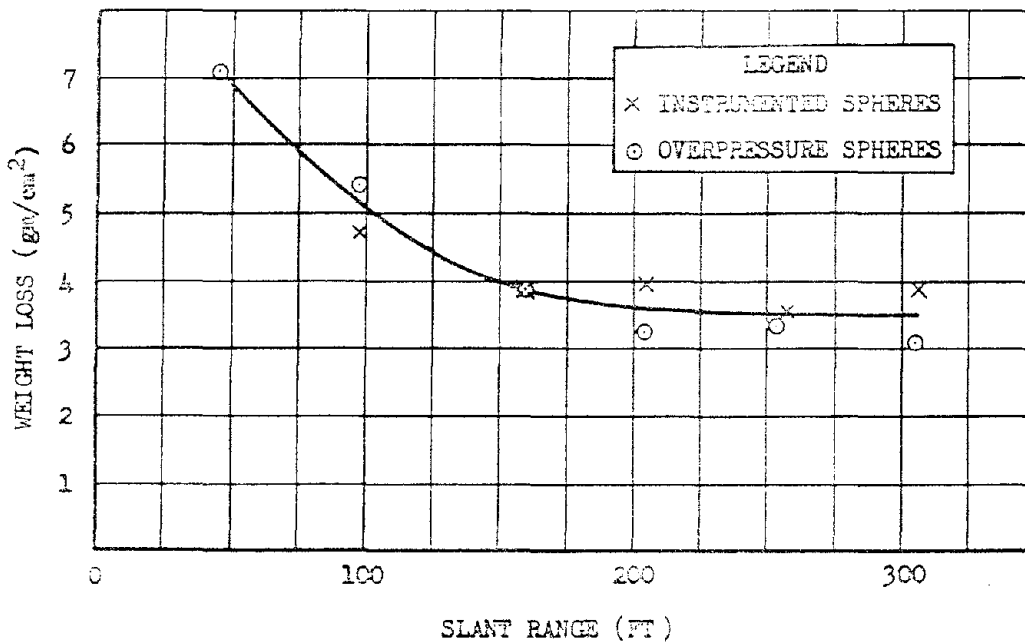
Figure 4.11   Weight loss as a function of slant range for 12-inch steel spheres, Shot Erie.

material velocity is operating. If this type of sweeping is important, it is believed that the shock wave reflected from the ground is more important to material removal than the direct shock wave, because the high temperature of the isothermal sphere and longer engulfment time will have provided a thicker layer of material subject to such removal even though the material velocity of the reflected shock is smaller. Unfortunately, however, the specimens recovered by Project 5.9 yielded no direct information which would indicate the existence of importance of material velocity sweeping of a molten layer.

Removal of molten material upon ground impact was observed on few specimens exposed by Project 5.9. The effect of this method of molten layer removal was relatively small on the specimens involved and, therefore, was considered negligible as far as the total metal loss was concerned. Removal of the molten layer by this method is important only to ground tests similar to Redwing and obviously has no application to the high-altitude destruction of an ICBM by a nuclear detonation.

If a spherical specimen engulfed by an isothermal sphere has acquired a rotational velocity, a molten layer on the surface of the specimen would experience a centrifugal force tending to throw it from the specimen. The magnitude of this force would depend on the rotational speed as well as the radius of the specimen and would have its maximum effect at the equator of rotation. The molten layer would have a tendency to run toward the rotational equator from all other points on the surface and, if the rotational speed were of sufficient magnitude, would be spun off at the equator in relatively small droplets.

Assuming a hemispherical shape for the drops of metal which are flung off and a surface tension of 1000 dynes/cm for the molten metal, it would require approximately 55 radians/sec angular rotation to remove a drop 0.080 inch in diameter from an 8-inch copper or 10-inch steel sphere. Inspection of the mounting arrangement for such specimens reveals that rotational speeds of this magnitude were possible. The shape of the 8-inch sphere at Station 150 on Shot Erie (Figure A.20) strongly suggests that molten copper may have been spun off in the manner described above. The 10-inch diameter steel sphere from the 575-foot range on Shot Mohawk, Figure A.46, has a pattern of resolidified metal which substantiates this method of molten metal loss. This specimen has spiral flow lines emanating from the poles of the axis of rotation and ending in a ridge of metal at the equator as shown in Figure A.46. Little droplets of metal, approximately 0.080 inch in diameter, are in evidence on this equator ridge. This flow pattern exactly fits the theory of the spun-off metal developed above. Although the metal loss sustained by this specimen is possibly unrepresentative of the 350 kt shot in which it was exposed, the flow pattern discussed above is believed to be representative of this type of molten metal removal.

The removal of a molten layer by spinning off drops of the material could be important to high-altitude ICBM destruction if the missile were metal and had an appreciable angular velocity.

Spalling. Ablation of material from a specimen by thermal spalling depends on a strong shock wave, induced by thermal radiation, causing relatively large pieces to be ejected from the surface of the specimen.

Investigation of thermal spalling was one of the major reasons for exposing the laminated cylinders in Shot Erie. Inspection of the three recovered laminated cylinders, one from Station 100 and two from Station 150, indicated no thermal spalling damage. However, the relatively large material loss experienced by these cylinders may have obliterated any spalling damage, since the spalling damage would have probably occurred before the vaporization or melting ablation.

Thermal spalling may have caused the recovered portions of the molybdenum and stainless steel specimens at Station 25 to break away from the other part of the specimen. Both these pieces were from the rear of their respective specimens, which was the area that would be subject to spalling. This evidence was not conclusive, however, because of the other damage mechanisms which were operating at this relatively close exposure range.

Pockmarks were observed on recovered specimens from the close ranges (inside 150 feet) on Shot Erie, Operation Redwing and Shot Met, Operation Teapot. It is possible that these pock-

79

marks were due to some effect similar to thermal spalling; however, they were generally found on the specimen surface facing the detonation point, and this location indicates that they were probably not due to thermal spalling as the mechanism is currently understood.

Thermal spalling could be a significant damage mechanism at close ranges (25 to 50 feet) and is probably insignificant at farther ranges (200 to 300 feet) for specimens and exposure conditions similar to Shot Erie.

4.1.3 Effect of Material on Ablation. A number of 8-inch-diameter spheres of various materials were exposed within the fireball of Shot Erie with the objective of determining their relative susceptibility to ablation. The materials exposed were copper, steel, stainless steel, molybdenum, titanium, and plastic; and since their total ablation vulnerability was the objective, no particular attempt will be made to separate the ablation mechanisms.

Figure 4.12 presents the results of this study in the form of a graph which shows the weight loss per unit area of the original surface as a function of slant range. All the data shown in Figure 4.12 were obtained from 8-inch-diameter specimens. Inspection of the graph indicates that stainless steel, molybdenum, and titanium specimens sustained approximately the same mass ablation when exposed at equal slant ranges. Copper, however, sustained approximately two to four times the mass loss of the other metals when exposed at the same slant range, and the plastic specimens showed practically no ablation for the two slant ranges from which specimens were recovered. Only half the plastic specimen from the 150-foot range was recovered, and the mass loss per unit area was estimated from this portion. The curve for copper neglected the specimen at the 150-foot range because of its odd shape, as well as the probability that a portion of the metal loss was due to molten metal being spun off by centrifugal force. Since the copper specimens at the 150- and 200-foot ranges were not positively identified, the possibility exists that they should be interchanged. Neglecting the specimen now plotted at 150 feet permits the specimen now at 200 feet to be plotted at either 200 or 150 feet with little or no effect to the curve. The copper sphere at the 50-foot station also was irregularly shaped, but to a lesser degree, and could have experienced some metal loss similar to that at the 150-foot station.

The 10-inch-diameter steel and aluminum specimens exposed to Shot Mohawk on top of the specimen tower indicated that the steel lost approximately twice the mass which was lost by the aluminum specimen. A possible explanation for this apparent inconsistency with Operation Teapot and Shot Erie data is that the two types of specimens experienced significantly different engulfment times. The aluminum specimen, being lighter than the steel, would have a shorter engulfment time, resulting in a smaller loss of material.

The aluminum laminated cylinders lost between 0.84 and 1.10 inches, and steel cylinders exposed at the same respective ranges lost between 0.30 and 0.44 inch of metal. Assuming that engulfment times for the two types of specimens were approximately equal, aluminum was approximately $2\frac{1}{2}$ times more vulnerable than steel in terms of depth loss. If this were converted to mass loss, aluminum and steel would be within approximately 10 percent of being equally vulnerable. None of the aluminum composites exposed to Shot Erie were recovered; and, assuming that the aluminum lost $2\frac{1}{2}$ times the depth loss of the steel, which varied from 0.92 inch at 50 feet to 0.56 inch at 200 feet, it is probable that all the cylindrical sections of the composites were ablated, since the aluminum sides were only 1 inch thick and should have lost between 2.3 and 1.4 inches.

The material loss on the 8-inch-diameter plastic specimens could have been affected by the somewhat shorter engulfment time experienced by these specimens; however, Figure 4.6 indicates that this difference was small. Additional information on the vulnerability of plastic was obtained from the plastic disks attached to the dynamic cylinders and ballistic cylinders. The specimens were recovered with the disks still attached, and the plastic had approximately $^2\!/_5$ the depth of material loss sustained by the steel on the same specimen.

Results of Operation Teapot tests showed that when measured in terms of mass loss, aluminum and steel were of equal vulnerability when exposed as 10-inch-diameter spheres under Operation Teapot test conditions. The Redwing data from Shot Erie indicated that for these particular exposure conditions stainless steel, molybdenum, and titanium had approximately

equal vulnerability when exposed as 8-inch-diameter spheres and that aluminum and steel were roughly equal when exposed as side-on cylinders. On Shot Erie the vulnerability of copper was from two to four times that of other metals tested and the vulnerability of plastic was much less than that of all metals tested for the particular conditions of exposure.

4.2 SHOCK DAMAGE

The damage to a specimen by the shock wave of a nuclear detonation could be of three types: overpressure crushing, acceleration, and material erosion. Each of these mechanisms is discussed separately in the following paragraphs.

4.2.1 Overpressure and Blow-Off Pressure. The only recovered steel specimens from Shot Erie which showed evidence of overpressure crushing damage were those exposed at the 50-foot range. The structural damage to the nose-on composite and instrumented sphere at the 50-foot station was studied and an attempt was made to determine what static overpressure would be required to cause the failures.

The overpressure figures quoted below for the 16-inch instrumented sphere were computed by finding the static pressure required to bring the steel up to a stress of 180,000 psi. Crushing of the sphere at this station was observed in a direction normal to the direction of the shock wave; and, therefore, was attributed to overpressure. Assuming that the 16-inch outer shell did not leak pressure, it would require 155,000 psi overpressure to yield the inner sphere; but if the outer shell leaked pressure (a better assumption), only 135,000 psi static overpressure would cause the inner sphere to yield.

The composite specimen oriented nose-on at the 50-foot station had a hardened steel velocity-distance insert which had a compression yield strength of 400,000 psi. This insert was severly broken at the front end but had only two small cracks on the rear end. Since the front end contained the soft aluminum target blocks, it would be weaker to external pressure than the rear which had the 2024S-T4 aluminum spacers. A static overpressure of 105,000 psi would be required to yield the front end and 121,000 psi to yield the rear end.

The above analysis indicated that the value for overpressure at the 50-foot station was at least 105,000 psi.

Figure 4.13 shows a plot of peak overpressure versus slant ranges extrapolated from data obtained from Reference 3. The overpressure values computed from the above damage analysis are plotted on this graph and, as expected, are somewhat low. The other data are limits obtained from the ball-crusher gages described in Appendix D.

The ballistic cylinders were exposed in Shot Erie in an attempt to verify some calculations which indicated that the blow-off pressure resulting from vaporization of plastic would be greater than that from steel. These differences in blow-off pressure were to be detected by exposing two identical specimens (except for a plastic disk on the end of one) in exactly the same manner and noting the differences in their trajectories and resulting impact locations. The two specimens, however, were recovered at essentially the same range, 185 feet, after the test. This would seem to indicate that there was little or no difference in the blow-off pressure of plastic and steel; however, because of the inconsistencies in impact locations noted on even spherical specimens, it is believed that this conclusion is not completely justified.

Three end-on dynamic-pressure cylinders with the velocity distance impact gage at the 150-foot station yielded some information relative to the blow-off pressure of plastic and steel. Figure 4.14 shows the three specimens, their preshot weights, and velocities as measured by their respective velocity distance impact gages. The two specimens with the plastic disks were found in the dumping area and their impact locations are unknown. Since all three specimens were practically identical as to size, shape, and weight, except for the plastic disks on the front surface of two of them, and since they were all at the same slant range, it is possible that the difference in their velocities was due to the difference in the blow-off pressures of steel and plastic. This line of reasoning indicates that steel has a larger blow-off pressure than plastic. However, because the difference between the velocities of the two specimens with plastic is equal to the difference between the all-steel specimen and the high velocity plastic disk specimen, the basis for this conclusion may be the normal errors associated with data of this type.

81
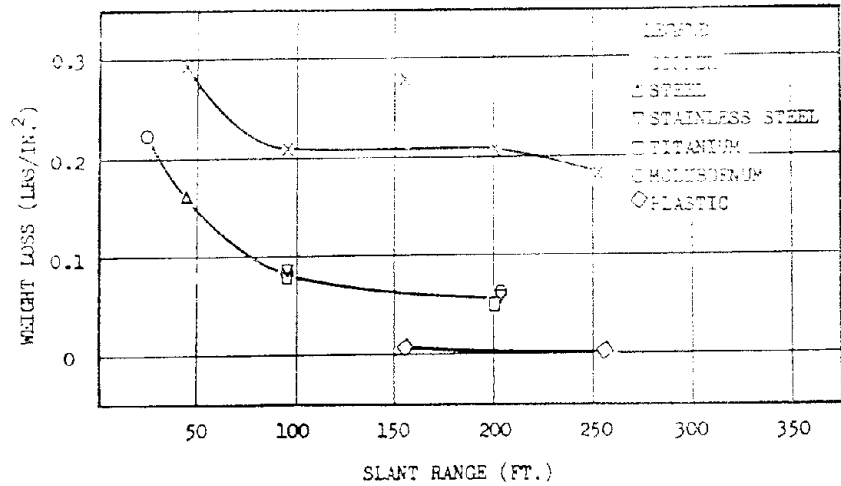
Figure 4.12   Ablation of 8-inch-diameter spheres as a function of slant range for Shot Erie.
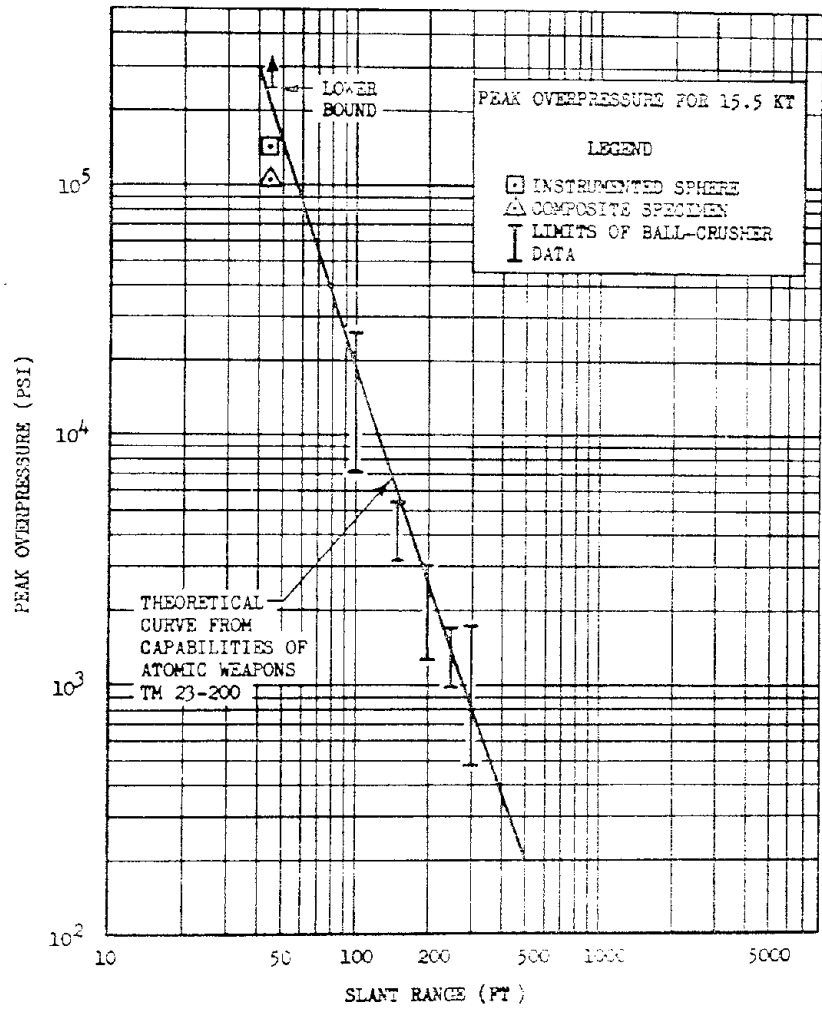
Figure 4.13   Overpressure as a function of slant range for Shot Erie.

82

4.2.2 Dynamic Pressure and Inertial Effects. The damage to a nonrigidly mounted specimen by dynamic pressure is usually a combination of the force on the specimen and the resistance of this force by the inertia of the specimen. The force is the sum of the overpressure from the time of shock arrival at the exposed surface until complete engulfment, the diffraction of the shock wave, and the drag force resulting from the material velocity of the shock wave.

Three attempts were made on Shot Erie to determine these forces. One of these attempts was the measurement of peak specimen acceleration with the use of the ball-crusher gages described in Appendix D, another was the measurement of specimen velocity as a function of distance traveled by the velocity-distance impact gages described in Appendix C, and the third was the measurement of the time history of specimen acceleration with the tape recorders described in Appendix B. The force on the specimen was then to be determined from its mass and acceleration.

TABLE 4.2   SUMMARY OF THE ACCELERATING FORCE ON THE INSTRUMENTED SPECIMENS

Specimen		Slant Range, feet	Weight, pounds	Projected frontal area, In.^{2}	Peak acceleration, grams	Peak force, pounds
Type	Code					
Inst sphere	Y	46.3	$584\frac{1}{2}$	202	7.5×10^{4a}	4.4×10^7
Inst sphere	X	97.9	225	113	6.5×10^{4a}	1.5×10^7
Inst sphere	X	158.9	$225\frac{1}{4}$	113	2.6×10^{4a}	5.7×10^6
Inst sphere	X	205.2	$225\frac{1}{4}$	113	1.1×10^{4a}	2.5×10^6
Inst sphere	X	257.1	225	113	4.7×10^{3a}	1.1×10^6
Inst sphere	X	306.4	225	113	1.8×10^{3a}	4.1×10^5
Overpressure sphere	Z	98.7	$251\frac{1}{4}$	113	5.9×10^4	1.5×10^7
Overpressure sphere	Z	159.7	252	113	1.8×10^4	4.6×10^6
Overpressure sphere	Z	204.0	$252\frac{1}{4}$	113	9.5×10^3	2.4×10^6
Overpressure sphere	Z	254.2	$253\frac{3}{4}$	113	4.4×10^3	1.1×10^6
Overpressure sphere	Z	306.1	254	113	1.8×10^3	4.6×10^5

[a] Value obtained by scaling curve presented in Figure 4.21 to actual weights and sizes.

The ball-crusher accelerometer data presented in Section 3.4.2 and an analysis of the damage to the components of the electrically instrumented sphere presented in Appendix B were all used to estimate the peak total force acting on the front of the specimens. These estimations were the product of the peak acceleration and the mass of the specimen and are presented in Table 4.2. The limitations of the data presented in the table are discussed in Chapter 3 and Appendixes B and D. It should be noted that the values given for the instrumented spheres were taken from the curve in Figure 4.21 but that the data for the instrumented spheres have been scaled from the weight and area of the overpressure spheres to actual weight and area of the instrumented spheres. This was accomplished by multiplying the value on the curve by the ratio of the mass of the overpressure sphere to the instrumented sphere and also by the ratio of the projected frontal area of the instrumented sphere to the overpressure sphere.

The extremely high forces and resulting accelerations caused some structural damage to the specimens at the 50-foot station and to the electrical recorders and transducers from the 50- to the 200-foot stations, inclusive. The details of the damage to the recorders and transducers are presented in Appendix B, Figure B.9. The extrusion of the front of the dynamic-pressure cylinder and composite specimen at the 50-foot station into the velocity-distance

insert was a result of the pressure on the front of the specimen. Although the overpressure was probably enough to cause the extrusions, the fact that the extrusions on the front were longer than those on the rear indicated that the difference must have been caused by diffraction and dynamic pressure. The mushrooming of the dynamic-pressure cylinder at the 50-foot station was probably a result of either diffraction, dynamic pressure, or both.

4.2.3 Material Loss by Erosion. The loss of material by erosion caused by the dense high velocity shock wave passing over the specimen could be a damage mechanism; however, this would occur early in the exposure and consequently might be obscured by later vaporization and melting. An attempt was made to investigate this phenomenon by shielding part of three aluminum composite specimens during the passage of the shock wave and then exposing the entire specimen after the wave had passed. Aluminum was chosen for these shielded specimens because its greater vulnerability would show the damage gradation as the shield was removed from the specimen.

The three shields were recovered after the test, but unfortunately none of the aluminum composite specimens were found. Consequently no analysis could be performed. Since the velocity-distance impact gages indicated that the shields had attained a velocity of approximately 350 ft/sec after $2\frac{1}{2}$ inches of travel and since the low drag composite specimens could not have attained nearly this velocity, it is believed that this method of investigation was satisfactory and that the shields did separate either during or shortly after the passage of the shock wave.

The pockmarks observed on the specimens at the 50-foot station might possibly have been due to erosion or to the impingement of high velocity particles behind the shock wave; however, they could have also been caused by a form of thermal spalling or some other phenomena. Consequently, pockmarks cannot be definitely attributed to erosion.

There was no definite evidence of erosion observed on any of the specimens. It is believed that any additional ablation of material caused by the shock wave was not in the form of erosion but more in the sweeping away of the vapor layer, which allowed more energy to reach the specimen.

4.3 NUCLEAR RADIATION DAMAGE

Two types of nuclear radiation damage are considered here: heating of materials due to neutron absorption and physical damage due directly to the nuclear radiation causing physical changes in the structure of the materials.
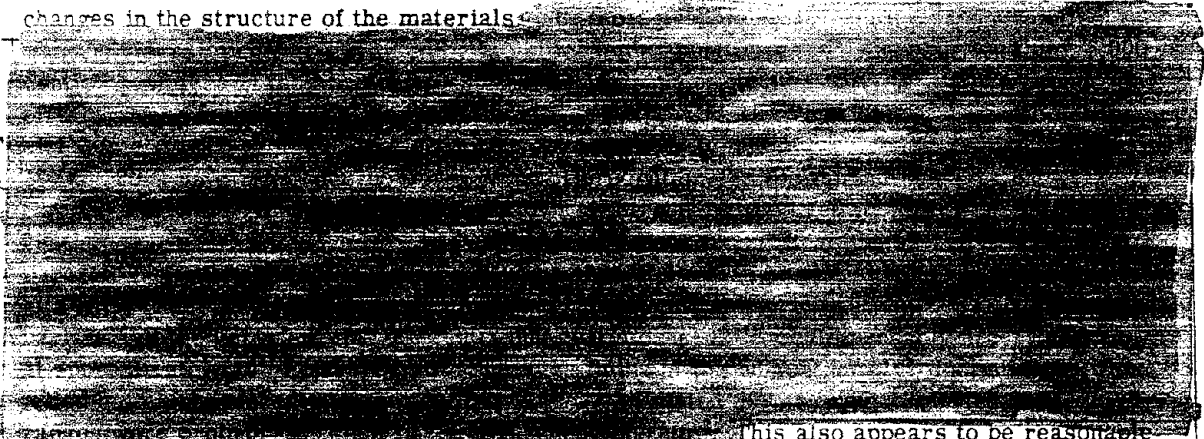
This also appears to be reasonable in comparison with the curve of estimated neutron flux as shown in Figure 4.15. This curve and the curve of estimated gamma dosage shown in Figure 4.16 were both calculated from the data and curves of "Capabilities of Atomic Weapons," TM-23-200, and are presented to show primarily the order of magnitude of the inputs to be expected in the fireball.

Nuclear radiation effects were not nearly as pronounced on other materials as on the DC-200 fluid and were, for the most part, nearly impossible to isolate from heat effects. One effect which could clearly be attributed to neutrons, however, was the melting of the vitreous
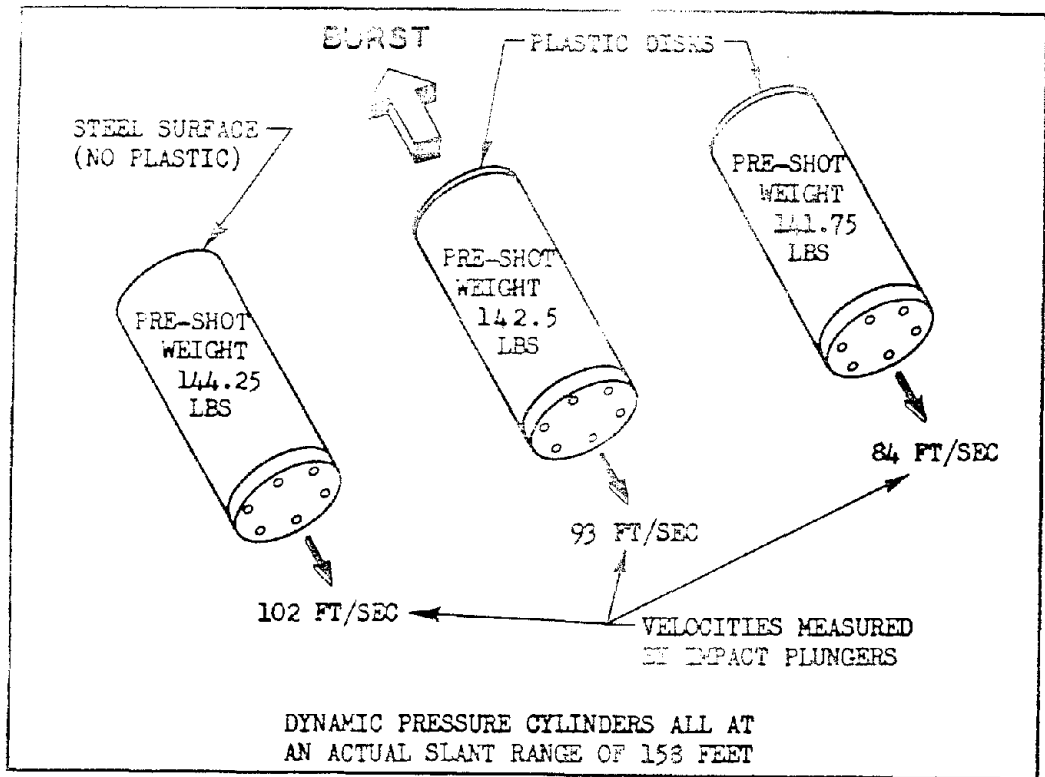
Figure 4.14 Weights and velocities of dynamic pressure cylinders at Station 150.
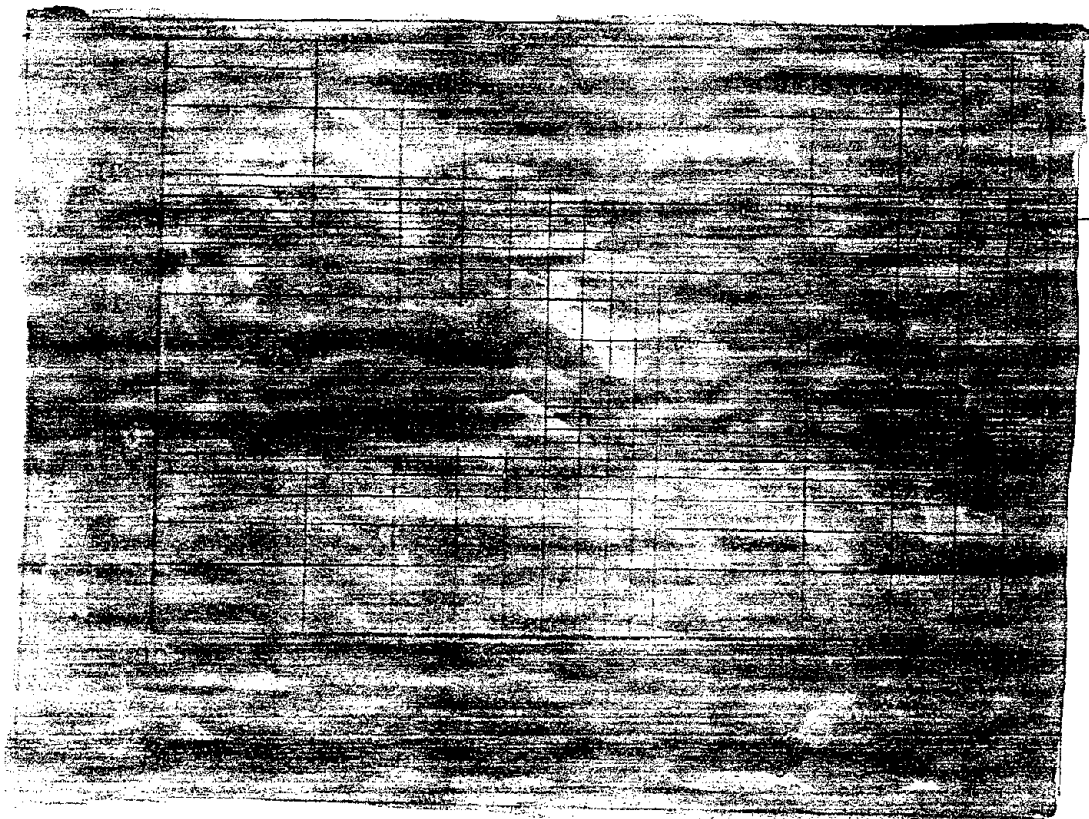
enamel coating on the Blue Jacket resistors, as described in Appendix B, Section B.3.2. This coating contained from [illegible] and although no calculation of the neutron flux was possible from these data, there was little doubt that this melting was due to neutron heating.

It is believed that almost all the damage incurred on the recorder and components was caused by heat. This heating of the recorder inside the sphere may have been caused, in part, by neutron heating; however, it is believed that conduction of heat contained in the molten metal layer on the surface of the specimen was the primary cause. If the temperature rise had been due to neutron heating, the amount of heating would be proportional to the neutron flux which in turn should be proportional to the inverse square of the distance from the burst point. The estimated temperature rises in the closer instrumented spheres were somewhat larger than at the farther ranges, but there was no obvious inverse-square relationship between the various specimens.

Postshot analyses of transistors used in the oscillators of the timing circuits showed that they were all inoperative as transistors and, in view of past performances of similar components in radiation environments, it is almost certain that the time zero failure at Station 300, and perhaps also the shock arrival time failures at Stations 200 and 250, were the result of neutron irradiation. The possibility still remains, however, that these latter two failures resulted from mechanical shock.

4.4 METAL LOSS SCALING

One of the main purposes of exposing the steel spheres in the various shots was to attempt to learn the variation of metal loss of such specimens when exposed in the fireballs of nuclear devices of various sizes. Available for comparison were metal loss versus range data for steel spheres for two device yields, 23 kt (Shot Met) and 15.5 kt (Shot Erie). In addition, usable metal loss data were available from four steel spheres, all at the same range, from a 355 kt device (Shot Mohawk). All these data were scaled down to 1 kt burst by dividing both the range and the metal loss by the cube root of the yield and are shown plotted in Figure 4.17. Use of the cube root scaling was derived theoretically, assuming that the rate at which material ablates is proportional to $k_1 T^n - k_2$, where k_1, k_2, and n are constants and T is the temperature of the isothermal sphere. The power n was introduced only to generalize the theory since the simple case $n = 1$ gave a reasonably good fit of the experimental data obtained during Operations Teapot and Redwing. The calculation was further simplified by assuming constant-gamma, adiabatic expansion of the isothermal sphere. The end result of the calculation was that $m/w^{1/3}$ (scaled mass loss) versus $R/w^{1/3}$ (scaled range) was completely independent of yield.

A curve is shown through the data for 12-inch spheres of Shot Erie in Figure 4.17. Most of the data for 10-inch-diameter spheres lie above this curve, as would be expected from radius of curvature considerations. The main exceptions are the 10-inch-diameter sphere from Shot Erie and the two farther out data points from Shot Met. According to Reference 2, the farther-out spheres from Shot Met were not in the isothermal sphere for a long period, if for any time at all, hence they would not be expected to exhibit as much metal loss.

Unfortunately the yields of Shots Erie and Met were not sufficiently different to expect any appreciable difference in material ablation; hence the fact that the data scale by the cube root of the yield lends little support to this scaling procedure. The fact that Shot Mohawk data being from a much larger yield device scale down quite nicely, however, does help to support this method of scaling. Of course, this scaling method does not take into account effects peculiar to particular shots such as the rapid fireball rise experienced during Shot Met, thus causing the specimens to appear to leave the fireball early.

4.5 INSTRUMENTATION

The instrumentation effort of Project 5.9 represented one of the first attempts to collect data by electrical and mechanical means from within the fireball of a nuclear detonation. An

Figure 4.16   Estimated gamma radiation dosage as a function of slant range for Shot Erie.

evaluation of the data and the system from which it was obtained are contained in the following sections.

4.5.1 Electrical. The results of the electrical instrumentation system used by Project 5.9 on Operation Redwing showed that it is feasible to record data electrically within the fireball of a nuclear detonation. The basic Redwing system, with improvements indicated by the experience gained on Redwing, should be capable of recording data successfully at slant ranges in the vicinity of 150 feet for shot and exposure conditions similar to those of Shot Erie. Detailed information concerning the Redwing instrumentation system is contained in Appendix B.

The accuracy and reliability of the ten time history curves from Stations 250 and 300 presented in Section 3.3 were materially reduced by the heat damage sustained by the recording tapes at the two stations. Although these data have a relatively low accuracy and reliability compared to data collected under less severe environmental conditions, there was general overall consistency and reasonable correlation with some known values such as shock arrival time.

The low frequency response of the accelerometer recording circuits probably caused significant reductions in the peak values recorded by the instrumented specimens. However, the acceleration time history curves presented in Section 3.3 are believed to represent the general shape of the acceleration pulse experienced by their respective specimens, and the time scale is estimated to be accurate to within ±2 percent. Figure 4.18 shows the correlation of shock arrival times obtained from the specimens at Stations 200, 250, and 300 and the reflected shock arrival times from Stations 250 and 300. Figure 4.18 indicates the theoretical location of the expanding shock front as a function of time after the detonation. The vertical heights and times at which the reflected shock front intercepts the trajectories are indicated on the trajectories for Station 250 and Station 300 specimens. These values were computed assuming no increase in speed of shock propagation upon reflection due to its passage through a heated medium.

Figure 4.18 shows the excellent correlation obtained for the initial shock arrival time for Stations 200, 250, and 300. The reflected shock arrival times for Stations 250 and 300 both occur a short time before the theoretical points shown. This result was expected because the reflected shock would have to travel a significant portion of its path through the air preheated by the fireball and isothermal sphere, and this would result in an increase in its velocity. In general, the acceleration time histories recorded at Stations 250 and 300 and presented in this report show excellent time correlation with known values but have relatively poor accuracy and reliability for the acceleration values presented.

The frequency response of the thermocouple recording circuits which was flat from 0 to 50 cps was considered adequate for the recording of this phenomenon and probably introduced no significant errors in the time history curves presented in Section 3.3. Since thermocouple type transducers are basically rugged and relatively insensitive to most of the inputs experienced by the instrumented specimens and since no external power such as batteries is required for their operation, the reliability and accuracy of thermocouples is inherently better than transducers such as accelerometers. Inspection of the temperature time history curves presented in Section 3.3 shows a number of temperature fluctuations which are difficult to interpret. It is possible that some of these could be due to such things as intermittent thermocouples and drop outs during playback; however, it is the opinion of the author that an appreciable number of the fluctuations were actually present and faithfully recorded.

The temperature time history curves presented in Section 3.3 were the source of the data in Table 4.3. The minimum and maximum times at which the melting point (2800F) of steel could logically have been attained were noted in each of the curves and entered in Table 4.3. The depth-of-melt pulse was used for the minimum probable time for the 0.016 and 0.011 depths at Stations 250 and 300, respectively, because it was the earliest melting time indicated for these depths. It is believed that the actual melting time for each depth listed lies between the minimum and maximum values presented in Table 4.3.

Figures 4.19 and 4.20 present Table 4.3 data in the form of depth-of-melt versus time curves for Stations 250 and 300. The possible error due to the uncertainty of the times is in-
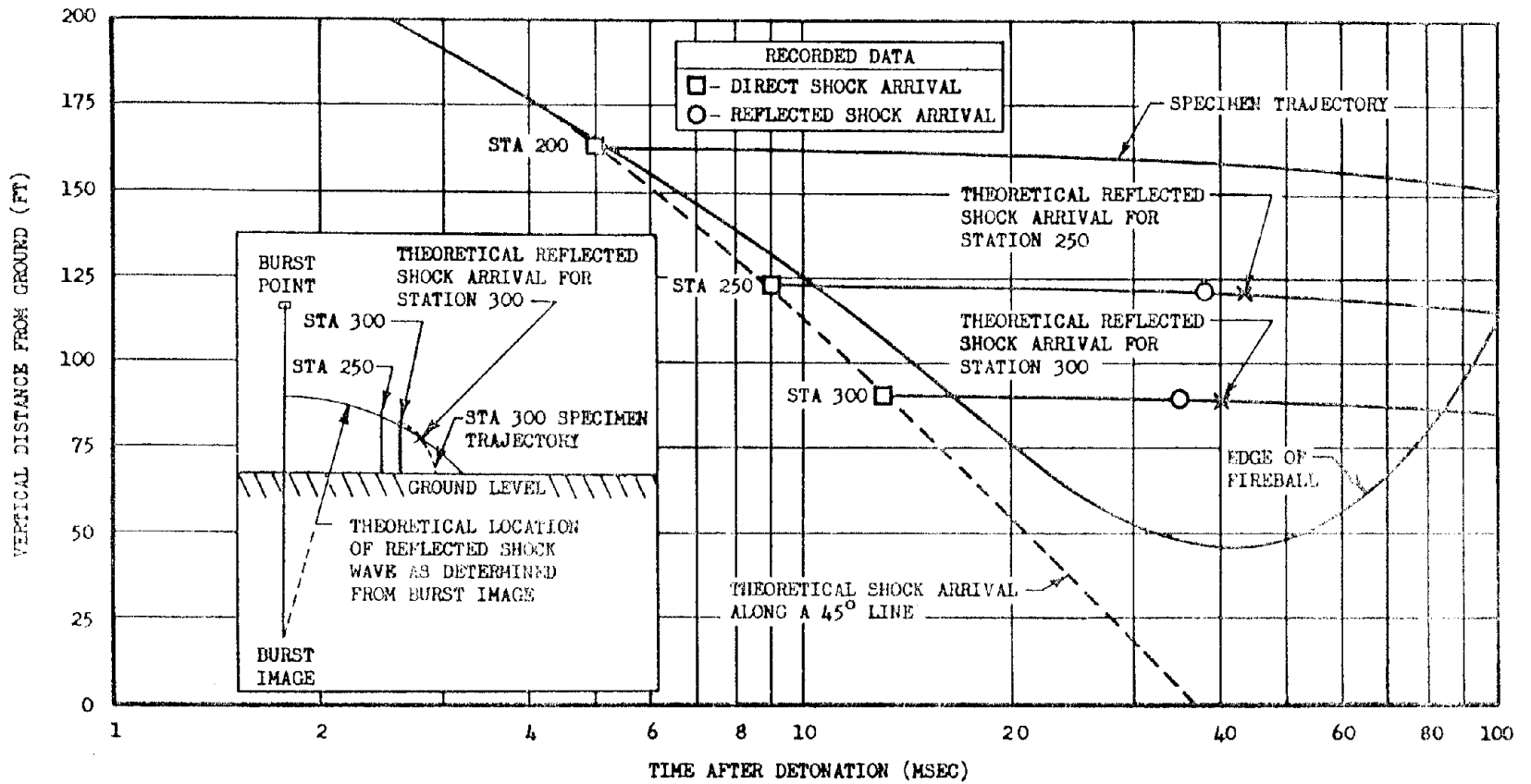
Figure 4.18 Correlation of electrically recorded and theoretical shock arrival times for the instrumented spheres at Stations 200, 250, and 300, Shot Erie.

dicated by the shaded portion, and a mean is drawn through the center of the time spread at each depth. Figure 4.11, Section 4.1.2, presented the slopes of these mean curves, which are the rates of specimen melting, as a function of time after detonation.

TABLE 4.3 TIMES REQUIRED FOR STEEL TO MELT TO VARIOUS DEPTHS

Times obtained from recorded temperature time history data.
Melting temperature of steel assumed to be 2800F.

| | | Depth below original surface in inches | | | | | |
		0.011	0.016	0.021	0.031	0.041	0.060
Station 250	Minimum Time msec		17[a]			28	180
	Maximum Time msec		50			64	195
Station 300	Minimum Time msec	29[a]		36		118	
	Maximum Time msec	48		78		130	

[a] Time obtained from depth-of-melt pulse.

The feasibility of recording data electrically within the fireball of a nuclear detonation with a system similar to that used on Redwing was thus demonstrated by the electrically instrumented specimens. An electrical recording system similar to that used on Redwing and with improvements indicated by Redwing experience should be capable of recording data accurately and reliably at slant ranges in the vicinity of 150 feet on yields comparable to Shot Erie.

Redwing indicated that two out of the three transistor oscillators at Stations 200, 250, and 300 operated through time zero and stopped at shock arrival. It is, therefore, concluded that transistor oscillators, properly shock mounted, thermally insulated, and using radiation resistant transistors may be capable of use as the time base for future recorders.

4.5.2 Mechanical. Velocity-Distance. It was anticipated that from the velocity-distance data presented in Section 3.4.1 it would be possible to determine an acceleration time history. Since the first portion of the curve, from 0- to $\frac{1}{4}$-inch displacement, is questionable, and it is the slope of this section that determines the higher accelerations, and also since the time must be determined from the summation of times after shock arrival as discussed in Appendix C, it was impossible to determine the acceleration-time curve. However, the velocity-distance curves for the dynamic-pressure cylinders at the 150-foot station, Figures 3.26 and 3.27 are believed to be correct in the region from $\frac{1}{4}$ to $\frac{1}{2}$ inch of travel, after which the specimen receives relatively little additional impulse. It is also believed that the decrease in the observed velocity after $\frac{1}{2}$ inch of travel is probably due to friction on the plunger.

Each specimen had one plunger which was in contact and one which was $\frac{1}{16}$ inch away from the target block; but since the amount of penetration was a function of both the impact velocity and the acceleration of the target during the penetration and the acceleration was extremely high while these plungers were penetrating, it is believed that the velocities indicated by these plungers are too high and therefore are not shown on the plots.

The results of the Redwing experiment indicate that the velocity-distance gage is a satisfactory method of describing the later portion of the specimen velocity as a function of distance traveled.

Overpressure and Acceleration Measurements by Ball-Crusher Gages. Analysis of the overpressure and acceleration measurements by ball-crusher gages is presented in Appendix D. Since the response of the overpressure gage was fast enough to

90
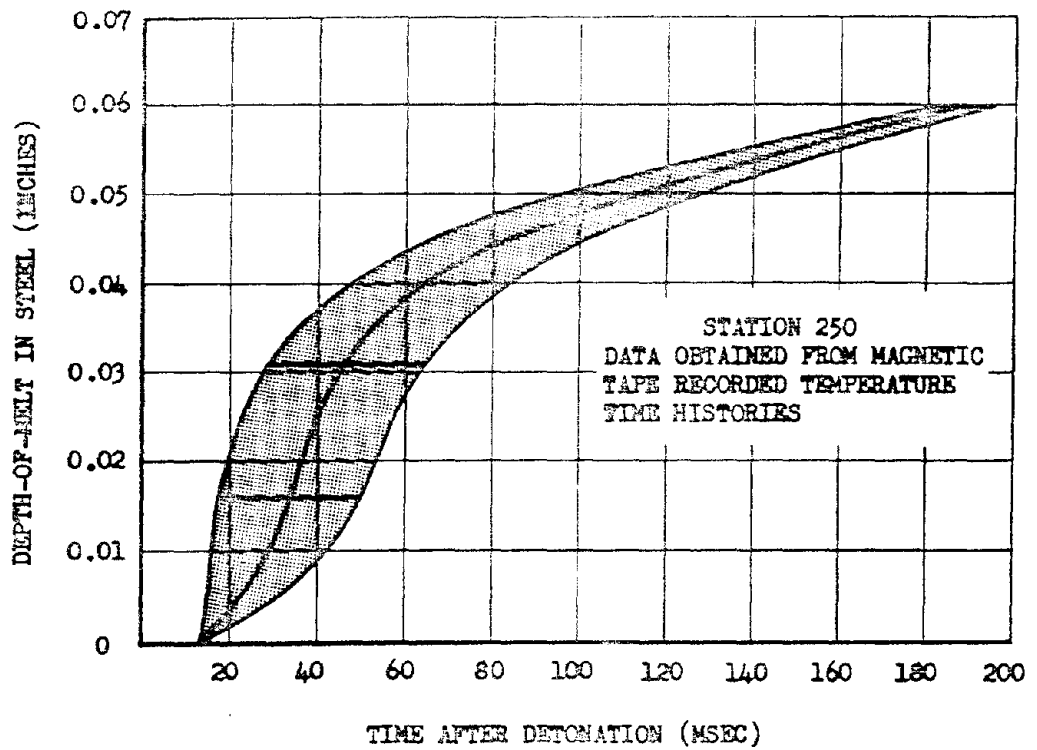
Figure 4.19   Depth of melt as a function of time for Station 250 instrumented sphere.
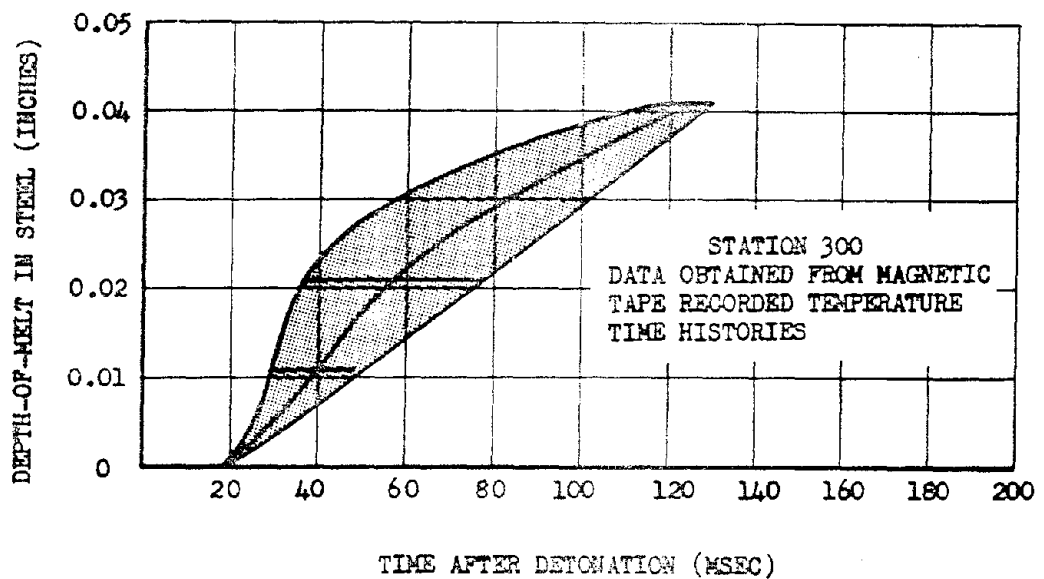
Figure 4.20   Depth of melt as a function of time for Station 300 instrumented sphere.
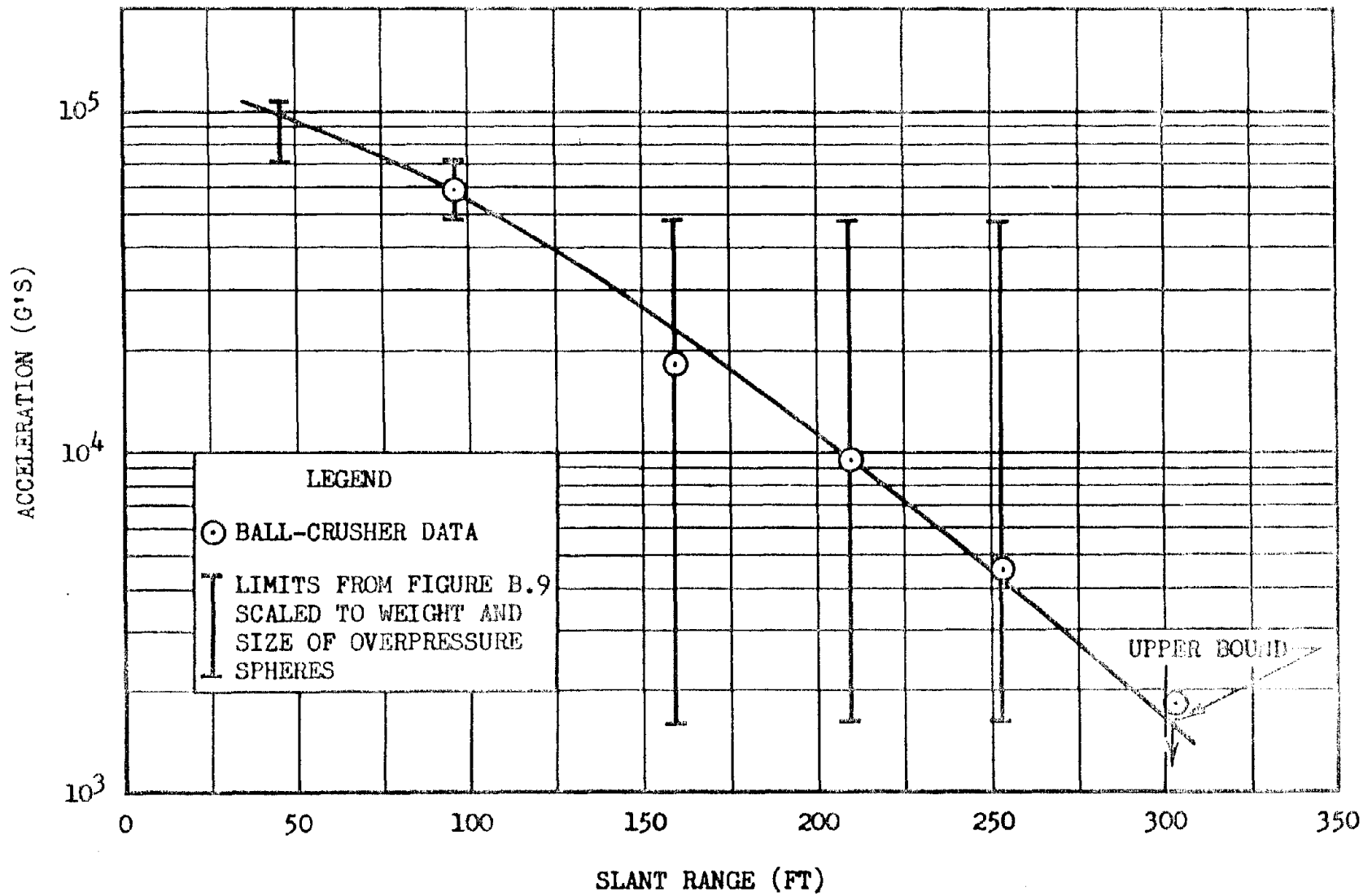
Figure 4.21   Observed peak acceleration as a function of slant range, Shot Erie.

respond to the shock overpressure, the maximum deformation of the ball was probably caused by the shock front overpressure and not blow-off pressure. A plot of the maximum and minimum observed values of peak pressure is presented in Figure 4.13. The curve drawn in the figure is a theoretical curve extrapolated from Reference 3. As can be seen in the figure, the observed values agree well with the theoretical values. The large spread in the ball-crusher data at any one station could be caused by a spike around the specimen, causing local pressures that may vary in magnitude by a factor of 2 or 3. The spike would be similar to those formed on guy wires and the shot tower and would be caused by preheating of the air around the sphere. The mechanism of this preheating is that a small amount of metal is vaporized from the specimen and advances into the air, effectively heating the air. This temperature rise increases the local shock front velocity in an unpredictable and unstable manner and causes different shock diffraction effects on various sections of the surface.

The response of the gages used in the ball-crusher accelerometers was not fast enough to observe completely the diffraction phase of the shock wave; however, there was good agreement between the observed ball-crusher data and the calculated accelerations based on the damage to the transducers and tape recorder in the instrumented spheres. Figure 4.21 is a plot of the ball-crusher data using a postulated input of diffraction plus gust loading as presented in Table D.3; also shown in the figure are the maximum and minimum values calculated for the instrumented spheres by scaling the data in Figure B.9 to the same weight and area as the overpressure spheres. A study of the figure would show that there were only a limited number of curves which could be drawn through the limits of the instrumented sphere data. One of these curves is drawn in the figure, and it can be seen that the two sets of data agree quite well.

In general, it can be said that the peak pressures observed by the ball-crusher gages in Shot Erie have good agreement with the theoretical values based on a Taylor Wave plus blow-off pressure and that the observed accelerations agree with theoretical values calculated from a gust plus diffraction loading.

Peak Temperature. The method used to measure the peak temperature at various depths below the surface of the copper spheres was not satisfactory. Most of the metal slugs melted; and, therefore, no data were obtained. However, it is believed that a different distribution of the metal slugs, so that some of the higher melting metals would have been further below the surface, would have yielded data.

Chapter 5

CONCLUSIONS and RECOMMENDATIONS

5.1 CONCLUSIONS

1. Eight-inch-diameter spherical specimens of stainless steel, molybdenum, and titanium sustained approximately the same mass ablation when exposed at equal slant ranges under the conditions of Shot Erie.

2. Spherical copper specimens, 8 inches in diameter, sustained approximately 2 to 4 times the mass loss of other metals exposed to 8-inch-diameter spheres at equal slant ranges under the conditions of Shot Erie.

3. The 8-inch-diameter spherical plastic specimens experienced substantially less mass ablation at the 150- and 250-foot slant ranges than any of the metals which were exposed at the same slant ranges under the conditions of Shot Erie.

4. In general, Project 5.9 data tend to support the existence of an attenuating vapor layer on test specimens within the fireball of a nuclear detonation.

5. Hydrodynamic sweeping of the vapor layer probably affected the ablation of the flat plate and cone-forward steel composite specimens in Shot Erie.

6. The radius of curvature effect, which predicts greater material ablation for specimens of small radii, was substantiated by the various radii of the spherical specimens exposed in Shot Erie at the 50-foot range.

7. In general, the corners of the flat plates and cylindrical specimens exposed in Shot Erie showed less rounding than would be expected from the radius of curvature effect and Operation Teapot data.

8. The specimen shape apparently had little effect on the depth of material ablation sustained from exposure within the fireball of Shot Erie, except for engulfment time differences, radius of curvature effect, and the excessive metal loss noted at the junction of two pieces of metal on the cylinders.

9. The predominant effect of orientation on material ablation of the specimens within the fireball of Shot Erie was an increase in the depth of material loss for most of the specimens on the surface facing toward the burst point.

10. The apparent anomaly of approximately equal ablation for the 12-inch-diameter steel spheres at Stations 150, 200, 250, and 300 on Shot Erie can, for the most part, be explained on the basis of ablation by melting after emergence from the fireball. Approximately $^3/_4$ of the total ablation sustained by the instrumented spheres at Stations 250 and 300 on Shot Erie could have been due to melting after emerging from the fireball.

11. The removal of a molten layer by spinning off drops of the material could be significant to total ablation and would be important to ICBM destruction, if the missile had an appreciable angular velocity.

12. Thermal spalling could be a significant damage mechanism at close ranges (25 to 50 feet) and is probably insignificant at farther ranges (200 to 300 feet) for specimens and exposure conditions similar to Shot Erie.

13. No conclusive data were obtained on the blow-off pressure of steel and plastic within the fireball of Shot Erie.

14. Overpressure crushing damage and extensive structural damage due to acceleration can be expected at slant ranges of 50 feet or less for specimens and exposure conditions similar to those of Shot Erie.

15. The electrically instrumented Redwing specimens have shown that it is feasible to record data electrically inside the fireball of a nuclear detonation with a system similar to that used on Redwing.

16. An electrical recording system similar to that used on Project 5.9 in Redwing and with improvements indicated by Redwing experience should be capable of recording data accurately and reliably at slant ranges in the vicinity of 150 feet on yields comparable to Shot Erie.

17. Transistor oscillators may be capable of successful operation within the fireball of a nuclear detonation in a specimen of the Redwing type, under the condition that adequate shock mounting and thermal insulation are provided.

18. The velocity-distance impact gages which were adequately protected from the effects of overpressure and material ablation operated satisfactorily and yielded apparently reliable velocity versus distance data at least for the latter portions of these curves. No acceleration versus time values were obtained.

19. Ball-crusher gages may be successfully employed to observe experimentally peak fireball pressures and accelerations, provided the approximate shape of the dynamic input is known.

20. The method used to measure the peak temperature at various depths below the surface of the copper spheres was unsatisfactory.

21. Project 5.9 experience indicated that spherical specimens are best suited for total material ablation studies because of the unpredictable ballistic paths and resultant unknown engulfment times associated with nonspherical specimens.

22. The derived scaling, $(yield)^{1/3}$, of both mass loss and range is supported by the fact that the data from the higher yield Mohawk shot compared favorably with the data from the lower yield shots, Erie and Met, when this scaling method was used.

5.2 RECOMMENDATIONS

It is recommended that:

1. Project 5.9 data be used to further vulnerability studies of basic ballistic missile structures and materials to the fireball of a nuclear detonation.

2. Future programs similar to Project 5.9 consider instrumentation, both electrical and mechanical, of the type employed on Redwing for data collection within the fireball of a nuclear detonation.

3. Future programs similar to Project 5.9 determine experimentally the rate of material loss within and in the vicinity of a nuclear fireball so that the relative importance of ablation by vaporization and melting may be established.

4. Future tests include a number of spherical passive specimens exposed within the fireballs of a wide range of nuclear device yields for the determination and verification of metal loss versus range scaling methods.

5. Spherical specimens be used for total material ablation studies in all future tests similar to Project 5.9.

6. Future ablation theory development take into account the absence of significant corner rounding observed on the flat plates and cylindrical specimens exposed within the fireball of Shot Erie.

7. Future electrical recording within the fireball be made with a recorder specifically designed for this type of recording.

Appendix A

DETAILED DESCRIPTION OF SPECIMEN DAMAGE

A.1 SHOT ERIE SPECIMENS

In this appendix is to be found a brief description of the damage and surface conditions of each specimen, as well as photographs and/or profile drawings of the more unusual conditions.

A.1.1 Steel Spheres. Table A.1 is a summary of the depth of metal loss for all the steel spheres from Shot Erie. The sketch at the top of the table depicts the positions on the specimens where the measurements were made. The measurements on the right and left side refer to the specimen as it is viewed from the rear side looking toward the burst point. The measurements on the top and bottom were taken at the two points of intersection of the two lines from the burst point tangent to the spherical specimen and lying in a vertical plane through the center of the specimen.

Instrumented Sphere at 50-Foot Station. The sphere was still intact but was severely pockmarked on the side facing the burst point and the forward half of the outer shell had a crack approximately 10 inches long. In addition to the break in the outer shell, the inside sphere was significantly squeezed so that the cavity where the recorder set was reduced in diameter by as much as $\frac{1}{8}$ inch. The bolts which held the recorder cap were sheared and the lip around the recorder cap was broken. The $\frac{3}{4}$-inch-diameter battery holes around the sphere were deformed and squeezed out of round about $\frac{1}{8}$ inch.

The front half of the specimen lost an average of 0.2 inch more metal than the rear half. Figure 3.6 illustrates the variation of material loss in a vertical plane parallel to the direction of the shock wave propagation. The surface of the sphere was clean and free of any foreign material.

Instrumented Spheres at the 100-, 150-, and 250-Foot Stations. These were 12-inch-diameter spheres. The postshot surface conditions of all these specimens were similar in that they all had a thin coating of refrozen metal which was not bonded tightly to the sphere; they also had scratch marks

from impact with the ground. The sphere from the 100-foot station had a bolt missing from the main recorder cap, but other than that there was no structural damage to any of them.

With the exception of the area around the bolts which held on the various caps, the material loss from all these specimens was uniform. In the regions around the bolts there was more metal loss, and molten metal had been forced between the heads of the bolts and the sides of the caps.

Instrumented Sphere at 300-Foot Station. Material loss over this specimen was uniform and left the surface with only a small amount of unbonded refrozen metal. The refrozen metal was not in the form of a layer or coating, but rather was found along a few flow lines. The surface had a small number of scratch marks which cut through the flow lines.

Overpressure Spheres. Material losses from these specimens were also uniform over the entire surfaces. All six of the spheres had a thin layer of refrozen metal and scratch marks from the impact with the ground. Except for some crushing at the 50-foot station, there was no structural damage to any of these spheres. Figure A.1 is a composite photograph showing all the overpressure spheres after the ball-crusher gages had been removed.

Ten-Inch-Diameter Sphere at 50-Foot Station. The side of the sphere which faced the burst point had a dozen or so pockmarks, 4 were large, being about $1\frac{1}{2}$ inches in diameter and $\frac{5}{8}$ to $\frac{3}{4}$ inch deep. The forward side lost much more material than the rear side, and there was some displacement of material as can be seen in Figure A.2. The surface had a few flow lines and a large number of small pimples of refrozen metal. The impact with the ground caused some scratch marks which cut through the flow lines and pimples.

Ten-Inch-Diameter Sphere at 100-Foot Station. There were two pockmarks about $1\frac{1}{4}$ inches in diameter on the forward side. Except for these two pockmarks, the metal loss was uniform over the entire surface of the sphere. One half of the

TABLE A.1 SUMMARY OF DEPTH OF MATERIAL LOSS AT VARIOUS POINTS ON STEEL SPHERES EXPOSED TO SHOT ERIE
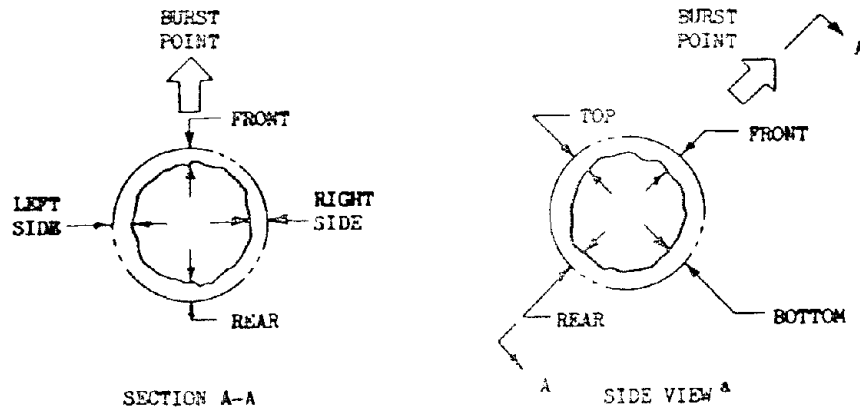
SECTION A-A   SIDE VIEW [a]

Type	Slant Range Nominal Feet	Slant Range Actual Feet	Front Inches	Back Inches	Rt. Side Inches	Lt. Side Inches	Top Inches	Bottom Inches	Average[b] Inches
Y	50	46.3	0.48	0.21	0.64	0.30	0.28	0.56	0.42
N	50	46.4	1.28[c]	0.38	0.08	1.00	0.68	0.24	0.51
O	50	46.2	1.26[c]	0.72	0.62	0.70	0.74	0.54	0.68
Q	50	44.9	1.35	1.08	1.16	1.07	1.16	1.02	1.14
M	100	97.5	0.40	0.28	0.44	0.32	0.30	0.28	0.26
X	100	97.9	0.20	0.18	0.10	0.17	0.20	0.19	0.25
X	150	159	0.16	0.14	0.15	0.18	0.18	0.20	0.20
X	200	205	0.17	0.18	0.19	0.19	0.17	0.24	0.21
X	250	257	0.12	0.14	0.13	0.16	0.21	0.17	0.18
X	300	306	0.14	0.20	0.08	0.20	0.20	0.19	0.20
Z	50	43.7	0.44	--	0.45[d]	--	0.26[e]	--	0.39
Z	100	97.7	0.39	0.17	0.38[d]	--	0.34[e]	--	0.29
Z	150	159	0.22	0.21	0.19[d]	--	0.22[e]	--	0.20
Z	200	204	0.20	0.23	0.24[d]	--	0.20[e]	--	0.17
Z	250	254	0.13	0.10	0.15[d]	--	0.18[e]	--	0.17
Z	300	306	0.20	0.12	0.26[d]	--	0.19[e]	--	0.16

[a] Vertical profile of sphere viewed normal to the direction of shock propagation.

[b] $\Delta R = R_o \left[1 - \left(\frac{W}{W_o} \right)^{1/3} \right]$

where: W_o = Pre-Shot Wt. (lbs) ΔR = Average Radius Loss (in)
        W = Post-Shot Wt. (lbs) R_o = Pre-Shot Radius (in)

[c] Data might be misleading due to pockmarks.

[d] Orientation of sphere could not be determined; this value is an average of right and left sides.

[e] Orientation of sphere could not be determined; this value is an average of the top and bottom.

sphere was covered with a $\frac{7}{32}$-inch layer of material which was not bonded tightly to the sphere. The side which did not have this layer had scratch marks from hitting the ground.

Eight-Inch-Diameter Sphere at 50-Foot Station. The front side was severely pockmarked but otherwise had almost uniform material loss. The surface of this specimen was clean and free of foreign material. There was no definite layer of refrozen metal, but there were a few ridges, i.e., flow lines, of resolidified metal. The scratch marks caused by the impact with the ground cut through these flow lines.

Four-Inch-Diameter Sphere at 50-Foot Station. The one 4-inch-diameter sphere recovered from the 50-foot station was found about 600 feet from its original position. This specimen lost 8.6 pounds of material, which was more than 90 percent of its original weight and more than half its diameter. The profile measurements show that there was about 0.3 inch more metal loss on the front side than on the rear. The front side was covered with flow lines of refrozen metal, and the rear side was well marked with cuts and scratches from the impact with the ground.

A.1.2 Composites. A summary of the average depth of metal loss at various cross sections along the specimen is presented in Table A.2. The locations of these sections are shown in the sketch accompanying the table.

Steel Composite Oriented Cone Forward at 50-Foot Station. Pressure forces caused extensive structural damage to the shell and also to the hardened steel insert. The insert was cracked at several places, and metal from the cone and hemisphere was extruded into the holes in the insert. Figure A.3 shows the cone end of the specimen. The five protrusions which were formed by metal, extruding into the insert, are to be noted. These extrusions were approximately $\frac{1}{8}$ to $\frac{3}{16}$ inch long. The extrusions on the hemispherical end were about $\frac{1}{32}$ inch long. The hemispherical end could not be unscrewed but had to be cut free of the cylinder.

Figure A.4 illustrates the large amount of metal lost at the junction of the hemisphere and the cylinder. Figure A.5 is a good example of the variation of the metal loss at the circular cross section on the hemisphere end of the cylinder. Except for some pockmarks, see Figure A.6, and some localized effects near the ends of the cylinder, there was equal material loss at any one cross section. The hemisphere and the cone had about the same depth of metal loss, but the cylinder had almost $\frac{1}{4}$ inch less. The surface of the cylinder was clean and did not have a layer of refrozen material.

Steel Composite Oriented Cone Forward at 100-Foot Station. Figure A.7 shows all that was recovered of this specimen. The light colored band around the middle is adhesive material from a piece of identification tape placed on the specimen at recovery. Since the hemisphere, cone,

and insert were not recovered, the weight loss could not be computed. The inside of the shell still had the original machine marks, and most of the threads on the hemispherical end retained their original profile.

Steel Composite Oriented Cone Forward at the 150-Foot Station. This specimen was found at a ground range of only 36 feet from its original position. The material loss, which amounted to $61\frac{1}{4}$ pounds, was not uniform but varied by as much as $\frac{1}{3}$ inch at various places. The surface was clean and smooth with a notable absence of scratch marks, flow lines, or refrozen metal.

Steel Composite Oriented Cone Forward at the 200-Foot Station. The cone end of the specimen was not recovered, but the hemisphere was still attached to the cylinder; the velocity-distance insert was separated from the shell and found nearby. The cylindrical portion had about equal material loss along its length, but there was more loss at the junction of the hemisphere and cylinder. The hemisphere had almost the same depth of loss as the cylinder.

Steel Composite Oriented Side On at the 50-Foot Station. This specimen, found at a ground range of 226 feet from its original position, was one of the most severely damaged specimens of those recovered. It had a weight loss of $45\frac{1}{4}$ pounds, the top rear quadrant, tangent to the blast, had several large pockmarks, and the bottom rear quadrant, which was shielded from the blast, was badly honeycombed. A photograph of the pockmarks is shown in Figure A.8 and the honeycombing in Figure 3.9. The original center of the specimen could not be located; therefore, the exact depth of metal loss could not be measured. Figure A.9 is a drawing of the profile measurement; the distorted shape of the circular sections is to be noted. The surface was clean and free of any foreign material or any unbonded layer of refrozen metal.

Steel Composite Oriented Side On at 100-Foot Station. There were a few pockmarks, 1 to $1\frac{1}{2}$ inches in diameter by $\frac{1}{4}$ inch deep, on the front side of the cylinder and cone, but otherwise the surface was smooth and clean and experienced an approximately uniform metal loss overall.

Steel Composite Oriented Side On at 150-Foot Station. Depth of material loss was about equal for the hemisphere, cylinder, and cone; but all three shapes lost about $\frac{1}{4}$ inch more on the front side than on the rear. There was a groove approximately $\frac{1}{8}$ to $\frac{1}{4}$ inch deep by 1 inch wide from the tip of the cone to the middle of the specimen on the top side and from the middle to the end of the hemisphere on the opposite side. This pattern was similar in location but not in magnitude to that shown in Figure A.7 for the cone-forward composite at 100 feet. There were flow lines of refrozen metal on most of the specimen; and part of the surface had ground impact induced cuts and scratches which cut through the flow lines indicating again that the surface refroze before the specimen hit the ground.

TABLE A.2   AVERAGE DEPTH OF METAL LOSS AT VARIOUS CROSS SECTIONS OF COMPOSITE SPECIMENS
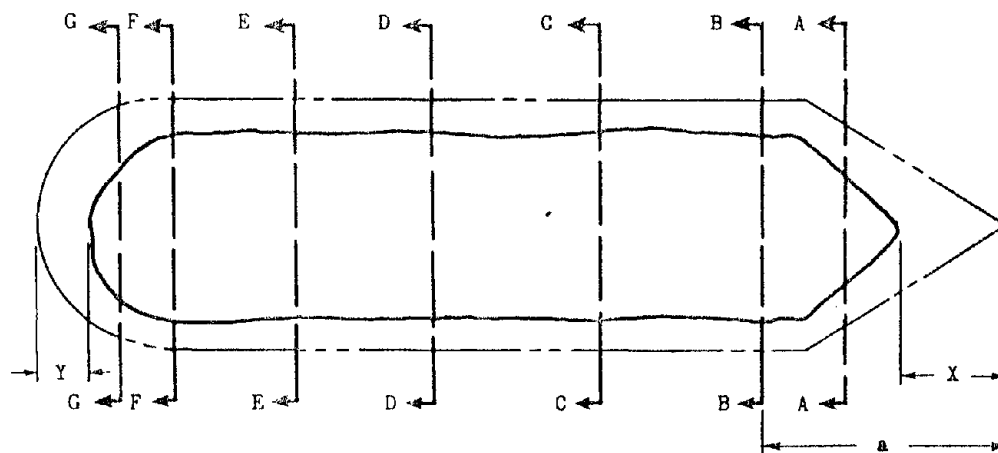
Orientation	Slant Range		Distance		Section												
					AA		BB		CC		DD		EE		FF		GG
	Nominal Ft.	Actual Ft.	X In.	Y In.	a In.	Loss In.	a In.	Loss In.	a In.	Loss In.	a In.	Loss In.	a In.	Loss In.	a In.	Loss In.	a In.	Loss In.
Cone-Forward	50	45.8	2.88	1.20	4.12	1.18	6.12	0.94	9.12	0.95	13.10	0.85	16.18	0.88	19.48	0.96	21.68	1.20
Cone-Forward	150	158.2	2.28	0.56	3.84	0.78	5.84	0.74	9.40	0.65	13.36	0.62	17.84	0.66	20.64	0.67	22.84	0.70
Cone-Forward	200	203.5	b	0.52	b	b	5.76	0.66	9.72	0.61	13.24	0.56	17.76	0.56	20.52	0.51	22.60	0.64
Side-On	100	97.5	1.68	0.72	3.28	0.44	5.60	0.48	10.64	0.47	13.92	0.44	18.92	0.42	21.44	0.45	22.68	0.45
Side-On	150	158.1	1.20	0.72	3.68	0.57	5.56	0.50	10.68	0.44	13.20	0.43	18.36	0.45	21.32	0.49	22.70	0.50
Side-On	200	203.6	0.36	0.32	3.36	0.17	4.96	0.24	10.64	0.29	12.88	0.27	18.44	0.44	21.04	0.36	22.76	0.63

a Distance from the original tip of cone.

b Cone was not recovered.

NOTE: The velocity-distance insert, cone, and sphere were not recovered for the cone-forward specimen at the 100 foot station. The side-on specimen at 50 feet had large pockmarks over the entire specimen.

Steel Composite Oriented Side On at 200-Foot Station. This specimen was found at a horizontal distance of 128 feet from its original position. The weight loss, only 27¾ pounds, was much less than that of the other side-on composites. The cone and sphere lost more material than the cylinder. The rounded end was no longer spherical but was more elliptical with the major axis coinciding with the axis of the cylinder. There was a sharp change in the depth of material loss at the junction of the cone and cylinder with the cone losing more than the cylinder. The surface was clean but had a few marks from the impact with the ground and some small flow lines of refrozen material.

A.1.3 Flat Plates. Table A.3 is a tabulation of the metal loss as determined from the profile measurements for the transversely grooved plates, and Table A.4 for the longitudinally grooved plate.

Steel Flat Plate Grooved Transversely at 50-Foot Station. The top of the grooves lost about 0.78 inch, and the bottom of the grooves and the plain side each lost an average of 0.56 inch. The surface was clean and free of foreign material.

Steel Flat Plate Grooved Transversely at 150-Foot Station. The top of the grooves had a metal loss of 0.72 inch, and the bottom of the grooves and the plain side each lost 0.54 and 0.52 inch, respectively. The surface was clean and showed no sign of an unbonded layer of refrozen metal.

Steel Flat Plate Grooved Transversely at 200-Foot Station. The top and bottom of the grooves lost an average of 0.18 and 0.12 inch of metal, respectively, and the plain side lost 0.19 inch.

Steel Flat Plate Grooved Longitudinally at 150-Foot Station. The plain side of the plate lost approximately ½ inch of material but the loss on the grooved side was not uniform. The tops of the grooves lost more than the bottoms, and both lost more toward the front of the plate than the rear. This variation is shown in Figure 3.11.

A.1.4 Laminated Cylinders. The average depth of metal loss at various cross sections along the cylinder is tabulated in Table A.5. The sketch at the top of the table shows the location of these cross sections.

Laminated Cylinder at 100-Foot Station, Twelve ⅛-Inch Laminations. Seven of the 12 laminations were completely missing, and part of the ninth was also missing; however, a small piece of the eighth lamination was still on the back side of the cylinder and was being held on by the orientation bolt. The specimen had a few pockmarks toward the middle of the cylinder; some of these were on the front and one was on the rear. Figure A.10 shows the pockmarks on the front side.

Laminated Cylinder at 150-Foot Station, Five ¼-Inch Laminations. Four

complete laminations and part of the fifth were missing. The fifth lamination did not have uniform material loss but lost more toward one end. Figure A.11 is a profile drawing of the specimen and shows the variation of material loss along the cylinder; it is noted that the steel core also lost more on the one end than it did on the other. Figure A.12 shows the irregular conditions on the surface and also the scratch marks on the side which hit the ground.

Laminated Cylinder at 150-Foot Station, Four ⅜-Inch Laminations. This specimen had between ¾ and 1 inch material loss. Figure A.13 shows the variation of material loss along the cylinder. There was more material lost on the front than on the rear; also, the front side had a few pockmarks, as shown in Figure A.14.

A.1.5 Ballistic and Dynamic-Pressure Cylinders. Table A.6 is a summary of the average depth of metal loss at various cross sections along the cylinder.

Ballistic Cylinders at 100-Foot Station. Figure A.15 is a profile drawing of the side-on cylinder which did not have a plastic disk, and Figure A.16 is of the side-on cylinder with the disk. The plastic disk was still bonded to the end of the cylinder which was oriented side-on. As can be seen in Figure A.17, the material loss on the plastic disk was irregular, but at no point did the disk burn completely through to the steel.

The cylinder oriented end-on with the plastic disk away from the burst point did not have the plastic disk attached when it was recovered; however, some of the bonding material was still stuck to the end of the specimen. Figure A.18 shows that the end which faced the burst point had much more material loss than any other part of the specimen. The surface of this specimen and also the other two ballistic cylinders had flow lines of resolidified steel. The scratch marks caused by the impact with the ground cut through the flow lines leaving sharp edges.

Dynamic Pressure Cylinders at the 50-Foot Station. The front of the cylinder was so distorted by the pressure forces that the postshot diameter was greater than the preshot. The rear of the specimen was not appreciably distorted, but its front had been compressed as much as ¼ inch. The rear cover plate was extruded 0.075 inch into the velocity distance insert, but the front of the cylinder was extruded as much as ½ inch into the insert. The hardened steel insert was broken and could not be removed from the shell; therefore, the front of the cylinder had to be cut off to study the extrusions on the front end. Figure A.19 is a profile drawing of the cylinder, and Figure A.20 shows the extrusions of the outer shell and the fracture of the hardened insert.

The surface of the cylinder was coated with a large amount of refrozen metal. One side of the cylinder was covered with pimples of metal, which looked like broken paint blisters, as seen in Figure A.21.

Dynamic Pressure Cylinder at 150-Foot Station. Figure A.22 is a profile drawing

100

TABLE A.3 SUMMARY OF DEPTH OF MATERIAL LOSS FOR FLAT PLATES GROOVED TRANSVERSELY

SLANT RANGE	X	Y	Z
43.7	2.72	4.84	7.06
156.0	1.88	5.36	7.96
201.0	2.26	5.28	7.80
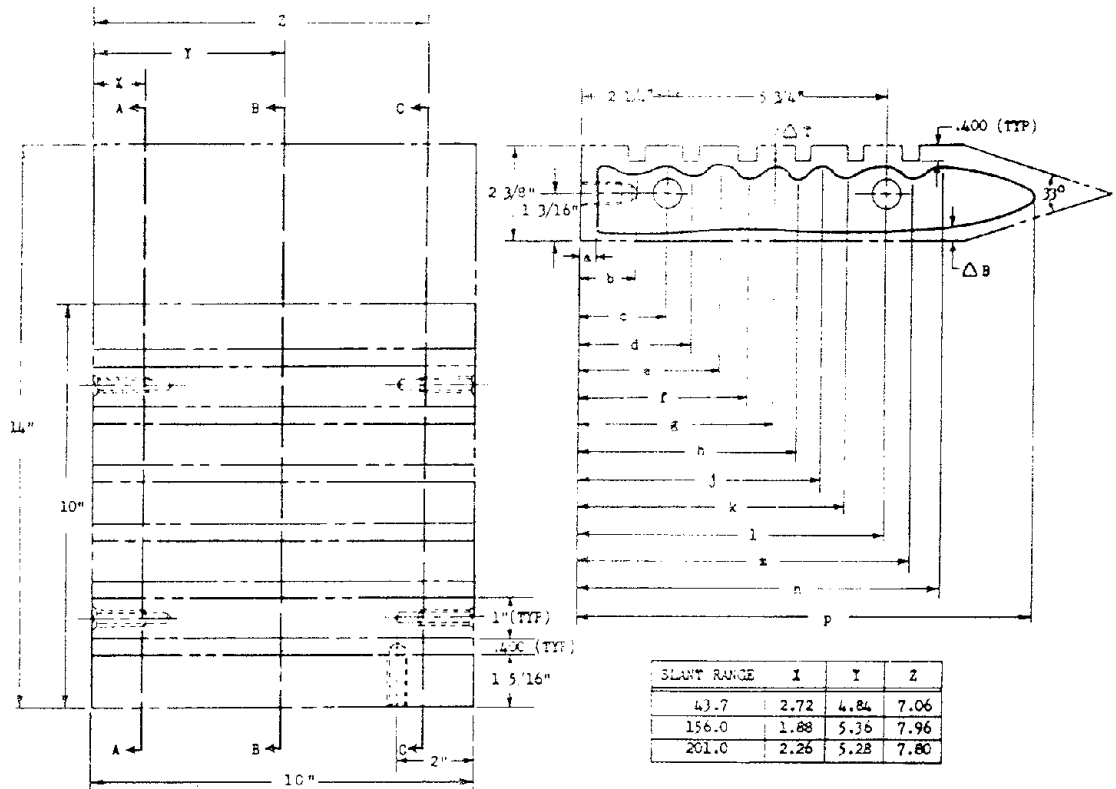
FLAT PLATE GROOVED TRANSVERSELY, 50 FOOT STATION

Section		a	b	c	d	e	f	g	h	j	k	l	m	n	p
AA	Location of Measurements (Dist. From End)	0.40	1.48	2.24	2.88	3.55	4.32	5.00	5.84	6.46	7.20	7.84	8.60	9.40	10.94
	Metal Loss, Grooved Side ΔT	—	0.62	0.68	0.54	0.64	0.50	0.64	0.48	0.72	0.62	0.88	0.76	0.96	—
	Metal Loss, Flat Side ΔB	—	0.54	0.64	0.64	0.64	0.64	0.54	0.64	0.64	0.60	0.56	0.54	0.46	—
BB	Location of Measurements (Dist. From End)	0.46	1.48	2.24	2.88	3.58	4.38	5.04	5.88	6.50	7.24	7.86	8.72	9.46	10.64
	Metal Loss, Grooved Side ΔT	—	0.54	0.70	0.50	0.68	0.50	0.70	0.54	0.80	0.62	0.92	0.82	1.00	—
	Metal Loss, Flat Side ΔB	—	0.64	0.62	0.62	0.64	0.62	0.62	0.58	0.58	0.54	0.54	0.50	0.42	—
CC	Location of Measurements (Dist. From End)	0.42	1.46	2.24	2.90	3.60	4.40	5.02	5.80	6.40	7.24	7.80	8.70	9.36	10.84
	Metal Loss, Grooved Side ΔT	—	0.60	0.74	0.52	0.72	0.52	0.74	0.60	0.80	0.66	0.90	0.74	1.00	—
	Metal Loss, Flat Side ΔB	—	0.70	0.70	0.70	0.66	0.56	0.54	0.62	0.62	0.60	0.58	0.54	0.48	—

FLAT PLATE GROOVED TRANSVERSELY, 150 FOOT STATION

Section		a	b	c	d	e	f	g	h	j	k	l	m	n	p
AA	Location of Measurements (Dist. From End)	0.46	1.48	2.22	2.90	3.58	4.36	5.00	5.76	6.50	7.08	7.74	8.52	9.40	11.54
	Metal Loss, Grooved Side ΔT	—	0.56	0.72	0.54	0.72	0.52	0.72	0.56	0.58	0.50	0.70	0.54	0.64	—
	Metal Loss, Flat Side ΔB	—	0.52	0.52	0.52	0.52	0.52	0.54	0.54	0.54	0.54	0.52	0.54	0.54	—
BB	Location of Measurements (Dist. From End)	0.36	1.44	2.24	2.90	3.50	4.28	5.02	5.70	6.44	7.12	7.84	8.60	9.26	11.74
	Metal Loss, Grooved Side ΔT	—	0.52	0.66	0.48	0.66	0.46	0.66	0.48	0.64	0.46	0.66	0.48	0.64	—
	Metal Loss, Flat Side ΔB	—	0.42	0.46	0.46	0.46	0.46	0.48	0.48	0.46	0.46	0.48	0.54	0.56	—
CC	Location of Measurements (Dist. From End)	0.38	1.38	2.22	2.86	3.50	4.26	5.00	5.70	6.44	7.10	7.72	8.52	9.28	11.72
	Metal Loss, Grooved Side ΔT	—	0.48	0.62	0.48	0.60	0.46	0.54	0.46	0.64	0.46	0.64	0.48	0.56	—
	Metal Loss, Flat Side ΔB	—	0.46	0.46	0.50	0.52	0.52	0.50	0.48	0.46	0.46	0.46	0.50	0.52	—

FLAT PLATE GROOVED TRANSVERSELY, 200 FOOT STATION

Section		a	b	c	d	e	f	g	h	j	k	l	m	n	p
AA	Location of Measurements (Dist. From End)	0.40	1.40	2.10	2.80	3.58	4.20	4.90	5.62	6.40	7.06	7.76	8.44	9.20	12.22
	Metal Loss, Grooved Side ΔT	—	0.28	0.32	0.26	0.36	0.24	0.36	0.24	0.36	0.26	0.38	0.26	0.40	—
	Metal Loss, Flat Side ΔB	—	0.42	0.42	0.42	0.42	0.42	0.40	0.38	0.38	0.36	0.36	0.36	0.36	—
BB	Location of Measurements (Dist. From End)	0.30	1.40	2.10	2.80	3.50	4.20	4.94	5.62	6.32	7.06	7.72	8.40	9.24	12.30
	Metal Loss, Grooved Side ΔT	—	0.26	0.36	0.26	0.36	0.24	0.36	0.24	0.36	0.26	0.38	0.26	0.42	—
	Metal Loss, Flat Side ΔB	—	0.42	0.40	0.38	0.36	0.34	0.34	0.34	0.34	0.34	0.34	0.36	0.36	—
CC	Location of Measurements (Dist. From End)	0.32	1.46	2.14	2.84	3.52	4.28	4.92	5.62	6.40	7.04	7.72	8.48	9.00	12.30
	Metal Loss, Grooved Side ΔT	—	0.24	0.36	0.24	0.36	0.24	0.36	0.26	0.38	0.26	0.38	0.26	0.40	—
	Metal Loss, Flat Side ΔB	—	0.42	0.42	0.42	0.42	0.40	0.38	0.36	0.38	0.36	0.34	0.38	0.40	—

TABLE A.4 SUMMARY OF DEPTH OF MATERIAL LOSS FOR FLAT PLATE GROOVED LONGITUDI-
NALLY, 150-FOOT STATION
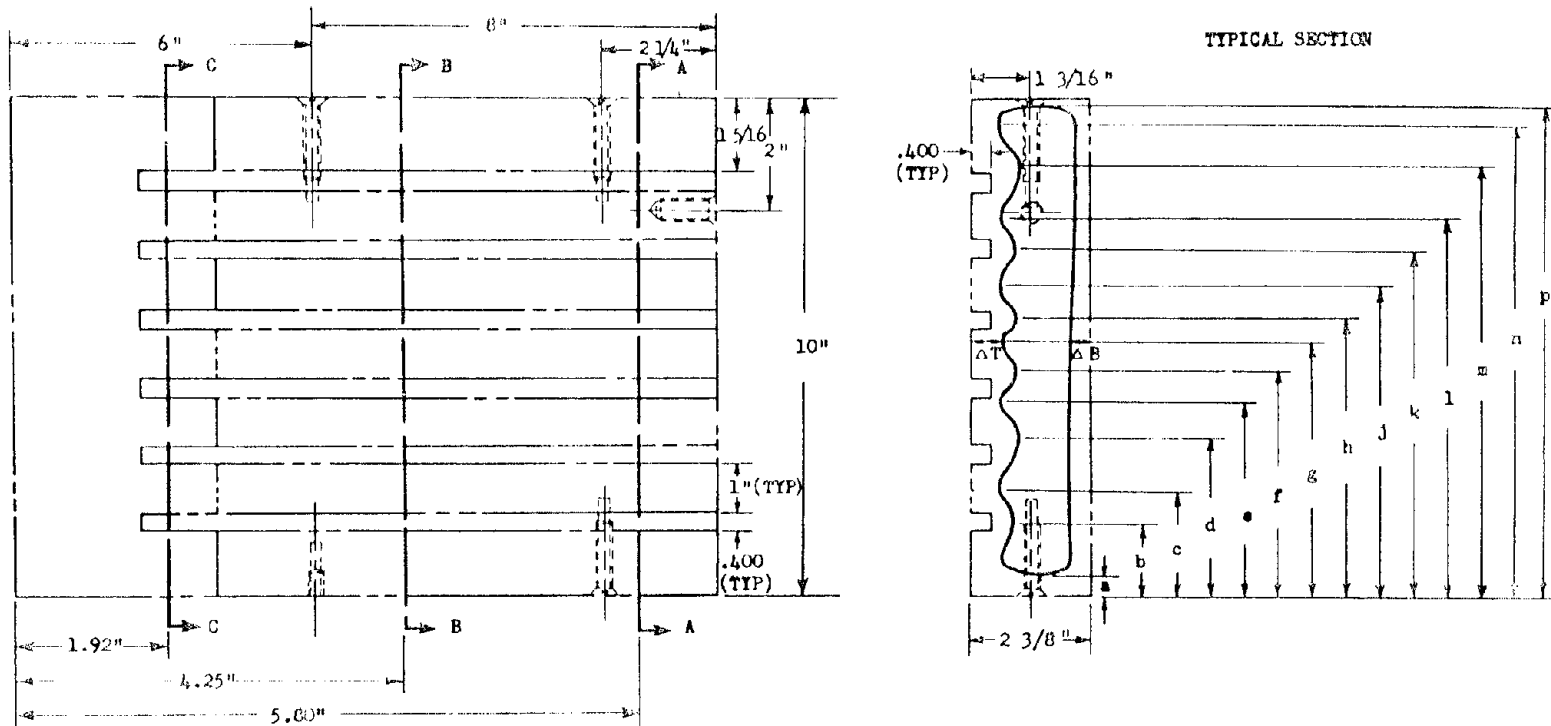
Section		a	b	c	d	e	f	g	h	j	k	l	m	n	p
AA	Location of Measurements (Dist. From Side)	0.42	1.44	2.22	3.00	3.56	4.16	4.96	5.70	6.30	6.94	7.80	8.40	9.26	9.54
	Metal Loss, Grooved Side △T	--	0.52	0.68	0.50	0.72	0.54	0.74	0.54	0.76	0.50	0.64	0.48	0.56	--
	Metal Loss, Flat Side △B	--	0.50	0.50	0.50	0.48	0.48	0.48	0.48	0.50	0.50	0.54	0.54	0.56	--
BB	Location of Measurements (Dist. From Side)	0.46	1.40	2.20	2.84	3.50	4.16	4.96	5.60	6.26	6.92	7.70	8.40	9.28	9.56
	Metal Loss, Grooved Side △T	--	0.62	0.80	0.60	0.82	0.68	0.86	0.62	0.78	0.54	0.74	0.58	0.56	--
	Metal Loss, Flat Side △B	--	0.50	0.50	0.50	0.50	0.50	0.50	0.50	0.50	0.48	0.46	0.46	0.46	--
CC	Location of Measurements (Dist. From Side)	0.54	1.52	2.14	2.80	3.60	4.36	5.00	5.64	6.30	6.92	7.66	8.40	9.20	9.50
	Metal Loss, Grooved Side △T	--	0.70	0.94	0.70	0.90	0.72	0.82	0.68	0.86	0.64	0.78	0.56	0.68	--
	Metal Loss, Flat Side △B	--	0.56	0.56	0.56	0.56	0.56	0.56	0.54	0.54	0.52	0.52	0.52	0.54	--

TABLE A.5   AVERAGE DEPTH OF METAL LOSS AT VARIOUS CROSS SECTIONS OF THE LAMINATED
CYLINDERS

BURST POINT
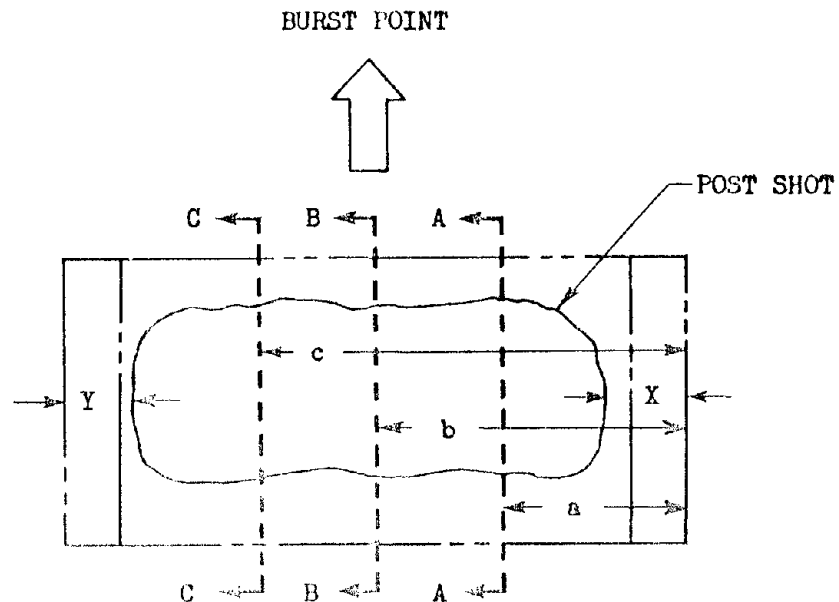
Laminations		Slant Range		Section Location			Metal Loss				
Thickness Inches	Number	Nominal Feet	Actual Feet	a Inches	b Inches	c Inches	X Inches	Y Inches	A Inches	B Inches	C Inches
1/8	12	100	95.9	4.16	6.44	8.18	0.94	1.18	1.07	1.09	1.06
1/4	5	150	156.1	3.06	5.08	8.08	1.32	0.96	1.06	1.07	1.06
3/8	4	150	156.2	3.82	5.72	7.54	1.30	0.96	0.88	0.88	0.84

Note: Metal loss X and Y are losses on end of cylinder. Metal loss A, B, and C are average losses at
cross sections.

TABLE A.6 SUMMARY OF AVERAGE DEPTH OF METAL LOSS AT VARIOUS CROSS SECTIONS ALONG BALLISTIC AND DYNAMIC PRESSURE CYLINDERS

BALLISTIC CYLINDERS

DYNAMIC PRESSURE CYLINDERS
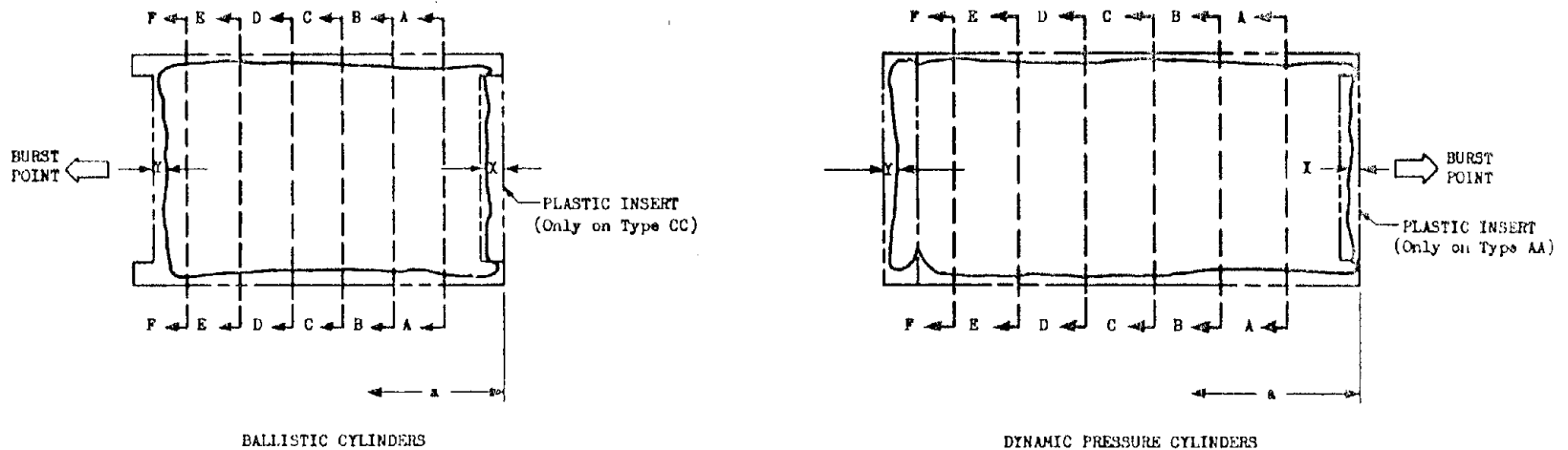
| Specimen | | Slant Range | | | Distance | | Section | | | | | | | | | | | |
Type	Code	Nominal Ft.	Actual Ft.	Orientation	X In.	Y In.	AA a In.	AA Loss In.	BB a In.	BB Loss In.	CC a In.	CC Loss In.	DD a In.	DD Loss In.	EE a In.	EE Loss In.	FF a In.	FF Loss In.
Ballistic Cylinder	BB	100	97.4	Side-On	0.50	0.28	0.88	0.40	2.50	0.34	4.02	0.34	6.00	0.30	7.80	0.35	10.24	0.40
Ballistic Cylinders (With Plastic Insert)	CC	100	97.4	Side-On	0.15b	0.42	0.50	0.32	1.98	0.34	3.74	0.37	6.76	0.42	8.74	0.43	10.80	0.48
	CC	100	95.4	End-On	c	0.56	0.62	0.56	1.86	0.35	3.86	0.36	6.88	0.31	8.88	0.37	9.74	0.67
Dynamic Pressure Cylinders	U	50	43.8	End-On	d	0.48	2.60	0.12	3.40	0.32	5.98	0.50	6.92	0.47	8.86	0.47	11.40	0.45
	U	150	158.6	End-On	0.61	0.30	0.88	0.58	3.76	0.47	4.76	0.45	8.64	0.42	10.64	0.40	12.64	0.36
	U	250	254.5	End-On	0.23	0.17	0.38	0.25	3.44	0.22	4.88	0.21	8.40	0.21	10.40	0.22	12.40	0.25
Dynamic Pressure Cylinders (With Plastic Insert)	AA	150	158.0	End-On	c	0.34	0.56	0.37	1.80	0.38	3.80	0.37	9.32	0.42	10.80	0.41	12.80	0.46
	AA	150	158.5	End-On	0.19b	0.16	0.50	0.36	3.76	0.34	5.50	0.35	8.00	0.33	10.50	0.35	12.52	0.37

a Distance from the original end of cylinder.
b Loss on plastic disk.
c Plastic insert was not recovered.
d End of cylinder was distorted by blast.

of this specimen and shows the variation of material loss about the specimen. The front of the cylinder had more material loss than the sides or the rear, and the sides of the cylinder had more loss toward the front than rear. The surface of the cylinder, as seen in Figure A.23, had an interesting flow pattern of refrozen metal and was covered with blisters (as seen in Figure A.24) similar to the cylinder at the 50-foot station. On the rear and sides of the cylinder there were a few cuts and scratches which cut through the flow lines and blisters.

Dynamic Pressure Cylinder at 250-Foot Station. Except for a slight rounding at the ends, the material loss on the sides of the cylinder was uniform. The material loss, Figure A.25, along the sides of the cylinder was 0.2 inch, and the loss on the front and rear was 0.26 and 0.12 inch, respectively. The surface of the specimen was covered with a rusty shell of refrozen metal which was about $\frac{1}{32}$ inch thick and which was not bonded to the cylinder.

Dynamic Pressure Cylinders With Plastic Disks at 150-Foot Station. There were two cylinders exposed at the 150-foot station which had material losses of $32\frac{1}{4}$ and $28\frac{1}{2}$ pounds. The plastic disk was missing from the one which lost $32\frac{1}{4}$ pounds, and the surface where the plastic had been bonded was covered with flow lines and blisters of refrozen metal, but there was no measurable metal loss. The cylindrical surface was free of foreign material and had a flow pattern similar to that shown in Figure A.23.

The cylinder which lost $28\frac{1}{2}$ pounds of material still had the plastic disk attached to it; however, the disk was not bonded to the steel. The sides of the cylinder had markings similar to those on the other two cylinders at the 150-foot station. The plastic lost an average of 0.19 inch of material; the solid steel end lost 0.16 inch, and the sides of the cylinder lost about 0.30 inch.

A photograph of the exposed face of the plastic disk is shown in Figure A.26. Profiles of both the cylinders which had plastic disks are shown in Figure A.27.

A.1.6   Material Evaluation.   Table A.7 lists some of the representative depth of material loss measurements for material spheres. The sketch on the table depicts the locations of these measurements on the sphere.

Plastic Sphere at 150-Foot Station. Only about $\frac{1}{2}$ of this specimen was recovered. The specimen broke apart along a horizontal plane. The surface of the specimen was badly damaged and severely canyoned, as shown in Figure 3.12. The depth of material loss was measured as 0.047 inch on the plastic and 0.070 inch on the steel locking nut which was still attached to the sphere. The surface of the canyons, as well as the exposed surface on the inside of the sphere, was charred to a depth of about $\frac{1}{64}$ inch, indicating that the sphere broke apart while it was still in the fireball.

Plastic Sphere at 250-Foot Station. There was little damage to this sphere. The section which faced the burst point had some shallow sections broken out, and the surface was charred to a depth of about $\frac{1}{32}$ inch. The mounting bolt shown in Figure 3.13 was still attached to the sphere.

Graphite Spheres. Three pieces of graphite were recovered, but they could not be identified as to exposure ranges. Two of the pieces fitted together to form part of a sphere. From the recovery location it is believed that they came from the 250-foot station, but positive identification could not be made. There were some small pieces missing from the surface of the specimen portions recovered, which were believed to have been chipped off by the impact with the ground. If there was any material loss due to the fireball environment, it was so small that it was not measurable.

Copper Sphere at 50-Foot Station. The surface of the specimen was relatively clean, with only a small amount of resolidified material on it. Figure A.28 shows the variation of metal loss in a plane parallel to the shock wave. The metal loss was least in the vertical plane passing through the burst point and the center of the specimen and was greater in specimen sections parallel to this plane, increasing as the distance of the sections from the central vertical plane increased. These sections remained approximately circular; although the horizontal sections were somewhat elliptical, with their major axes in the central vertical plane.

Copper Sphere at 100-Foot Station. Material loss was uniform and left the specimen still quite spherical. Part of the specimen was coated with a layer of refrozen slag, but the rest of the surface was clean and appeared to have been swept clean of molten copper by impact with the ground. Figure A.29 is a photograph of $\frac{1}{2}$ of the sphere and slag.

Copper Sphere at 150-Foot Station. The sphere, as listed in Tables 3.8 and A.7, with a weight loss of $56\frac{1}{2}$ pounds was believed to be from the 150-foot station, but there was the possibility that it could have been from the 200-foot station; however, the recovery location, weight loss, and that portion of the identification plug which was legible all indicated that it was from the 150-foot station. The surface had some small flow lines of resolidified copper but not a complete layer of refrozen metal. The metal loss was not uniform over the specimen but had a variation similar to that on the copper sphere at the 50-foot station. Figure A.30 shows this variation as viewed from the burst point.

Copper Sphere at 200-Foot Station. The copper sphere listed in Tables 3.8 and A.7 with a weight loss of 42 pounds was believed to be from the 200-foot station; however, it might possibly have been from the 150-foot station. Part of the sphere was covered with a mixture of copper and slag, but the remainder of the specimen was free of foreign material. It appeared that the sphere was covered with a layer of molten copper which was wiped away

TABLE A.7 SUMMARY OF DEPTH OF MATERIAL LOSS AT VARIOUS POINTS ON MATERIAL SPHERES
EXPOSED TO SHOT ERIE

SECTION A-A   SIDE VIEW [a]
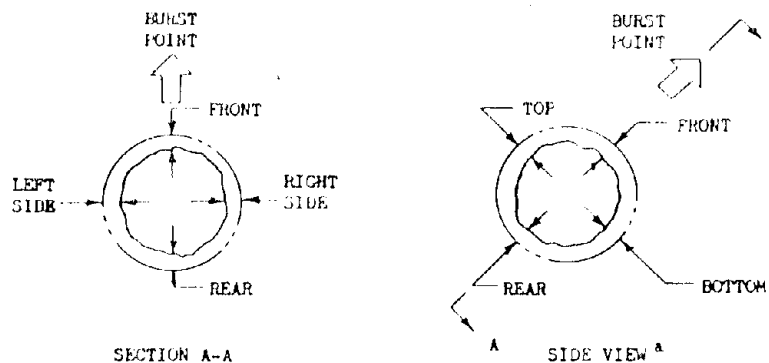
Type	Material	Slant Range		Material Loss						
		Nominal Feet	Actual Feet	Front Inches	Back Inches	Rt. Side Inches	Lt. Side Inches	Top Inches	Bottom Inches	Average[b] Inches
G	Plastic	250	256.6	0.00	0.02	0.04	0.04	0.02	0.02	0.02
I	Molybdenum	100	95.4	0.28	0.36	0.16	0.38	0.24	0.26	0.24
I	Molybdenum	200	203.9	0.18	0.18	0.20	0.24	0.08	0.24	0.18
J	S. Steel	100	97.4	0.38	0.36	0.64[c]	0.46	0.38	0.34	0.34
J	S. Steel	200	203.8	0.40	0.16	0.18	0.30	0.28	0.28	0.22
K	Titanium	100	95.3	0.70	0.56	0.60	0.54	0.80	0.58	0.56
K	Titanium	200	201.6	0.52	0.28	0.38	0.46	0.42	0.36	0.35
L	Copper	50	44.7	1.64	1.68	1.34	1.42	1.32	1.29	1.27
L	Copper	100	95.3	0.94	0.92	0.76	0.76	0.82	0.64	0.79
L	Copper	150	156.1	1.60	0.84	0.66	1.36	1.54	1.20	1.19
L	Copper	200	201.6	0.80	0.70	0.82	0.80	0.80	0.68	0.80
L	Copper	250	254.4	0.74	0.54	0.72	0.72	0.68	0.64	0.68

[a] Vertical profile of sphere viewed normal to the direction of shock wave propagation.

[b] $\triangle R = R_0 \left[1 - \left(\frac{W}{W_0} \right)^{1/3} \right]$

where: W_0 = Pre-Shot Wt. (lbs) $\triangle R$ = Average Radius Loss (in.)
        W = Post-Shot Wt. (lbs) R_0 = Pre-Shot Radius (in.)

[c] End of mild steel plug.

from the side that hit the ground. The metal loss was relatively uniform, leaving the sphere still quite spherical.

Copper Sphere at 250-Foot Station. The sphere hit some solid object which gouged the surface, as shown in Figure A.31. The metal loss was slightly more on the front and sides of the specimen than on the rear.

Molybdenum Sphere at 25-Foot Station. Figure A.32 shows the section of this sphere which was recovered. The depth of metal loss was determined by measuring the profile of the recovered part and then finding the radius of curvature. Using this method, the metal loss was estimated to be 0.74 inch in a radial direction. Assuming equal material loss over the entire surface of the sphere, the weight loss of the entire specimen, had it remained in one piece, would have been approximately 45 pounds.

The portion of the sphere recovered was from the rear of the specimen, since it contained the orientation bolt, which was always positioned away from the burst point.

The inside of the specimen showed signs of melting which would indicate that the specimen broke apart before it was buried in the ground. The surface was pitted with small irregularities but the finish was smooth.

Molybdenum Sphere at 100-Foot Station. Metal loss was uniform in a vertical plane parallel to the blast, but in the vertical plane normal to the blast the one side lost 0.2 inch more than the opposite side. Figure A.33 shows the variation of material loss in the two planes.

The surface of the specimen, Figure A.34, was relatively clean but had many stream lines of refrozen metal. There was one small area which had a few scratch marks; this area was also the only area which had any foreign material adhered to it.

Molybdenum Sphere at 200-Foot Station. Material loss was uniform over the entire surface of this specimen and amounted to $12\frac{3}{4}$ pounds. There were two cracks in the surface of the specimen, one of which extended through 360 degrees in a horizontal plane and the other for about 15 degrees in a vertical plane. The surface had scratch marks which indicated the point of contact with the ground. There was a thin layer, about 0.010 inch thick, of resolidified material on part of the specimen.

Stainless Steel Sphere at 25-Foot Station. This specimen, like the molybdenum sphere at the 25-foot station, was broken apart, and only the rear section was found. By measuring the profile and finding the radius of curvature, the radius appeared to have increased instead of decreased; therefore, due to the distortion of the specimen, the depth of material loss could not be found. Figure A.35 is a photograph of that portion which was recovered. The inside and outside of the specimen looked about the same regarding surface conditions,

so that it appeared that the specimen broke apart while it was still in the fireball.

Stainless Steel Sphere at 100-Foot Station. The specimen had three pockmarks on the front side, but otherwise the material loss was uniform, being about 0.35 inch at any point on the specimen. Figure A.36 is a plot of a vertical profile. Also shown in the same figure is a $\frac{1}{32}$ to $\frac{1}{16}$ inch thick layer of refrozen metal which covered about $\frac{1}{2}$ the specimen surface but was not bonded tightly thereto. The other half was clean and had cuts and scratches on it, indicating the point of impact with the ground. It appeared that the entire surface of the sphere was covered with a layer of molten metal which the impact with the ground removed on the side of contact. This specimen was machined from a billet which had some flaws in it. These flaws were in the form of a group of small holes which ran through the center of the billet. The flaws were drilled out and a mild steel plug about $\frac{3}{4}$ inch in diameter was pressed in their place. The plug was machined with the sphere so that the exposed end had a spherical radius and was flush with the surface of the sphere. Postshot inspection of the specimen showed that there was what appeared to be a pockmark exactly centered on the end of the pin. This pockmark was about $1\frac{1}{4}$ inches in diameter and $\frac{1}{4}$ inch deep; however, it was not known whether this was a pockmark of the same type as those which appeared on the other parts of this specimen and on several of the others or whether it was due to some phenomenon associated with the mild steel plug being pressed in the stainless steel.

Stainless Steel Sphere at 200-Foot Station. Metal loss on this specimen was relatively uniform with slightly more on the front face, as shown in Figure A.37. Weight loss was $11\frac{3}{4}$ pounds, which was an average reduction in radius of 0.22 inch.

About half the specimen was clean and had a smooth finish but was pockmarked with small pits. The other half had some refrozen metal in the form of flow lines which looked like thick paint smears. This refrozen metal was bonded tightly to the sphere.

Titanium Sphere at 100-Foot Station. The side of the sphere which hit the ground, as indicated by the scratches and cuts (see Figure A.38) was free of foreign material or a large amount of refrozen material, but the opposite half was covered with a layer of resolidified material. Apparently the entire surface was covered with a molten layer when contact was made with the ground, but this layer was wiped off as the sphere penetrated.

The overall material loss was uniform except for the thickness of the refrozen layer on the one half. The weight loss of 16 pounds indicated an average reduction of 0.56 inch in the radius.

Titanium Sphere at 200-Foot Station. The material loss on the side facing the burst point was slightly more than on the side away from the burst point. This variation of material loss is shown in Figure A.39. The face of the sphere which hit the

107

ground had several deep cuts and scratches on it (also shown in Figure A.39); otherwise the surface was clean and had only a small amount of refrozen metal on it.

Tantalum-Copper Cylinder at 100-Foot Station. Weight loss of this cylinder as given in Table 3.8 included the weight loss of the copper, tantalum, and steel. No attempt was made to separate the material loss for each of the individual items. Variation of material loss along the cylinder can be seen in Figure A.40. Because of the bent condition of the specimen, the original profile of the specimen is not shown; however, the cylinder was originally 18 inches long and 6 inches in diameter, constructed of two steel end caps, each 3 inches thick, and three 4-inch-thick copper cylinders. When the cylinder was bent, the ends of the sections were then exposed, with the result that the material loss was irregular. All the tantalum was gone from the specimen. The rear side of the three copper sections had been shortened by slightly more than $\frac{1}{2}$ inch, with the result that the loss of the copper as measured from Figure A.40 may not have been the true material loss.

Tantalum-Copper Cylinder at 200-Foot Station. The weight loss given in Table 3.8 is the combined loss of the steel, copper, and tantalum. Figure A.41, the postshot profile measurement, shows the large variation of material loss. As shown by the profile, there was more material lost at the center of the cylinder than at either end. The copper section which was covered with 0.100 inch of tantalum appeared to have about the same loss as the section which was not covered. Because of the protection afforded to the outer copper cylinders by the steel end caps, the planned detailed analysis of the metal loss experienced by each cylinder was not undertaken.

Bakelite Cylinder at 200-Foot Station. The cylinder was broken in two, and only part of it was recovered. The exposed surface of the specimen lost about $\frac{1}{8}$ inch of material. Figure A.42 is a profile drawing and photograph of the specimen; note in the figure that the aluminum bolt in the end of the cylinder had little material loss.

Specimens With Ceramic Inserts. Three of the six cylinders which held the special purpose alloys and ceramics were recovered. These were the cylinder at the 100-foot station and both cylinders at the 200-foot station.

The specimens, after they were returned from the test site, were sent to the General Electric Company, which had supplied the samples, for analysis. The following was taken from a letter received from the Materials Studies Aerosciences Laboratory of the General Electric Company, dated 25 June 1957.

This letter gives the final observations on samples supplied by the Missile and Ordnance Systems Department of the General Electric Company for exposure to atomic blasts in Project Red-

wing. The list of materials tested and method of exposure are given in G.E. Report #57JUS7, dated June 13, 1956.
... The original intention had been to remove the samples from the cylinders and spheres after the test, measure their loss of weight and dimensions, and possibly make metallographic examination of those samples which might be expected to show a change in structure. This became impossible for several reasons. The sample holders had been made of high carbon steel, and this was hardened during the exposure, making machining operations difficult. In addition, the units had become coated with fused sand, whose clean removal presented problems. Moreover, some of the samples retained a considerable level of activity for months after the test, complicating any work to be done on them. The dosage level a few inches from some samples was in the 30-50 milliroentgen range. This report, therefore, is limited to photographs of the recovered materials, showing their present condition, and notes on the condition of each sample. It is believed that this will at least serve to distinguish between the more resistant and less resistant materials. . .

Figure A.43 shows two of the cylinders, one from the 100-foot station and one from the 200-foot station, and Table A.8 the observations and relative ratings as made by the General Electric Company. This table lists the specimens exposed to Shot Erie as well as Shot Mohawk. The Mohawk data is presented on the same table with the Erie data as an aid in making comparisons of the various inserts.

A.2 SHOT MOHAWK SPECIMENS

The depths of metal loss at some typical points on the spheres are tabulated in Table A.9. The measurements were taken from the profile data. The analysis of the ceramic inserts in the 9-inch-diameter spheres is presented in Section A.1.6, Table A.8, along with the inserts from the Shot Erie test.

A.2.1 Steel Spheres. Ten-Inch-Diameter Steel Sphere at 545-Foot Range, Right Side of Tower. This was one of the two 10-inch spheres from the 150-foot level on the specimen tower and was found 210 feet from the base of the tower. Material loss was relatively uniform and amounted to $50\frac{1}{4}$ pounds. There were two peculiar grooves, about $\frac{1}{16}$ inch deep and $\frac{1}{2}$ to $\frac{3}{4}$ inch wide, around this specimen and also around the other three solid steel spheres exposed at the 150-foot level. These grooves were parallel to each other and about $1\frac{1}{2}$ inches apart. In all cases the mounting bolt was between the grooves; however, there was no correlation of the plane of the grooves with the direction of the shock wave. Figures A.44 and A.45 are illustrations of these grooves.

Ten-Inch-Diameter Steel Sphere at 545-Foot Range, Left Side of Tower. This specimen was exposed at the 150-foot level and was found 175 feet from the tower. The sphere had 40 pounds of material loss in a uniform fashion except for the double groove, shown in Figures A.44 and A.45, which ran around it. The surface was clean and free of pockmarks or scratches.

TABLE A.8 VISUAL ANALYSIS OF CERAMIC AND ALLOY SAMPLES

MATERIAL	COMMENTS At 100 ft. Range	RATING	COMMENTS At 200 ft. Range	RATING	COMMENTS At 545 ft. Range	RATING
Mo+Cr Plate	Considerable Evaporation	Good			Some Evaporation and Melting at Edges	Very Good
$Al_2O_3 \cdot TiO_2$			Melted and Evaporated Below Plate	Poor	Some Evaporation (Sand Encrusted)	Good
Mo			Considerable Even Evaporation	Good	Some Evaporation at Edges	Good
S-816 Co - Base Alloy	Gone	----				
MgO+Binder (Norton)			Shocked and Evaporated Flush; Some Melting	Poor	Lost 1/4 Inch; Some Melting	Good
M-252 Ni-Base Alloy			Considerable Evaporation; Half Gone	Fair		
"Hydrocal" Pottery Plaster and Graphite	Gone	----			Gone	----
$BN+Si_3N_4$			Gone	----	Gone	----
Cu			Evaporated or Sheared; Some Melting	Fair		
Refrax 20 - SiC Bonded With Si_3N_4	Some Residue in Bottom of Hole	----			Residue in Hole	Poor
Q - Felt+Polyester			Evaporated Flush	Poor	Lost 1/2 Inch	Fair
Graphite			Top Gone	Poor		
$Al(OH)_3$+Fiberglas+Polyester	Gone	----				
B_4C+Polyester			Gone	----	Gone	---
Carboloy (GE Tungsten Carbide Cermet)			Shocked or Spalled; Some Melting	Fair	Some Evaporation at Edges	Very Good
Sintered and Extruded Alum. + Al_2O_3 - Powder Metal Product	Gone	----	Sheared	Poor		
Phenolic+Asbestos Felt			Some Charring and Spalling, Excellent Condition	Very Good		
Graphite+Cr Plate	Gone	----	Top Gone	Poor	Some Evaporation at Edges	Very Good
MgO+Binder (Carborundum)			Gone	---	Residue in Hole	Poor
K162B Kentanium (TiC Cermet)	Exposed Part Evaporated or Sheared Flush	Poor	Sheared Flush; Some Fusing	Poor	Lost 1/8 Inch, Some Spalling	Good
Glass Cloth and Melamine			Sheared and Evaporated Flush	Poor	Residue in Hole	Poor
Durhy-Si Impregnated into SiC	Evaporated Half Exposed Portion	Fair	Sheared or Shocked; Some Fusing	Poor	Lost 1/8 Inch	Good
Durhy-Si Impregnated into SiC					Some Evaporation (Sand Encrusted)	Good
Glass Mat and Polyester			Gone	---	Evaporated 1/4 Inch (Some Large Chips or Breaks)	Fair
Cu+Cr Plate	Melted and Evaporated Flush	Poor	Melted Flush	Poor	Sheared or Evaporated 1/2 Inch	Fair
Mo, Ceramic Coated					Lost 1/4 Inch, Some Melting	Good
Mo, Ceramic Coated					Some Evaporation (Sand Encrusted)	Good
Molded Compound Phenolic Asbestos			Sheared or Evaporated Flush	Poor		
Ni+10% (Vol.) Al_2O_3					Lost 1/4 Inch From Top, Some Melting	Good
SiC (KT Fine)					Residue in Hole	Poor
SiC (KT Fine)					Lost 1/2 Inch From Top of Sample	Fair
Quartz Rod					Some Evaporation and Spalling Around Sides	Good
MgO+ZrO_2					Residue in Hole	Poor
Al_2O_3 (Norton)					Some Residue in Hole	Poor
ZrO_2 (Carborundum)					Some Evaporation at Corners	Good
Rokide C Coated Graphite					Some Evaporation and Melting	Very Good

NOTE: Specimens exposed at 100 ft. and 200 ft. were from the Erie test and specimens exposed at 545 ft. were from the Mohawk test.

TABLE A.9 SUMMARY OF DEPTH OF MATERIAL LOSS AT VARIOUS POINTS ON SPHERES EXPOSED
TO SHOT MOHAWK

BURST POINT

FRONT

LEFT SIDE

RIGHT SIDE

REAR

SECTION A-A

BURST POINT

A

TOP

FRONT

REAR

BOTTOM

A   SIDE VIEW [a]
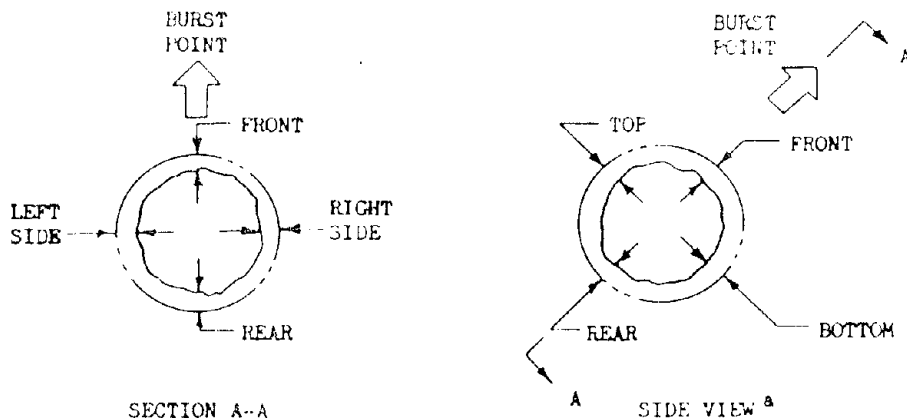
Type	Nominal Slant Range Feet	Material Loss						
		Front Inches	Back Inches	Rt. Side Inches	Lt. Side Inches	Top Inches	Bottom Inches	Average[b] Inches
N	545	0.64	0.58	0.84	0.76	0.76	0.76	0.64
N	545	0.44	0.56	0.50	0.52	0.56	0.72	0.50
N	575	0.06	0.10	0.08	0.08	0.04	0.12	0.05
N	575	0.24	0.36	0.24	0.44	0.18	0.44	0.26
O	545	0.44	0.46	0.48	0.56	0.48	0.56	0.45
O	545	0.42	0.48	0.30	0.50	0.48	0.52	0.41
GG	545	1.10	0.86	1.06	1.08	1.20	0.86	0.88

[a] Vertical profile of sphere viewed normal to the direction of shock wave propagation.

[b] $\Delta R = R_o \left[1 - \left(\frac{W}{W_o} \right)^{1/3} \right]$

where: W_o = Pre-Shot Wt. (lbs) ΔR = Average Radius Loss (in.)

W = Post-Shot Wt. (lbs) R_o = Pre-Shot Radius (in.)

Eight-Inch-Diameter Steel Sphere at 545-Foot Range, Right Side of Tower. This sphere was exposed at the 150-foot level and was found 175 feet from the base of the specimen tower. The metal loss, 23 pounds, was uniform except for the double groove which extended around the specimen. Figures A.44 and A.45 show the variation of metal loss and the orientation of the double groove. There were no scratch marks or flow lines on the surface.

Eight-Inch-Diameter Steel Sphere at 545-Foot Range, Left Side of Tower. The specimen was found 205 feet from its original position and had a metal loss of 21 pounds. The metal loss was uniform around the sphere except for the same double grooves.

Nine-Inch-Diameter Steel Sphere at 545-Foot Range, Right Side of Tower (Ceramic Insert Sphere). This specimen had a uniform metal loss of 28 pounds and was found at a ground range of 180 feet from the specimen tower. The surface was covered with a thin layer of rusted material.

Nine-Inch-Diameter Steel Sphere at 545-Foot Range, Left Side of Tower (Ceramic Insert Sphere). This specimen was found 180 feet from the base of the specimen tower with a uniform metal loss of $29\frac{1}{2}$ pounds. There was a thin crust, about $\frac{1}{64}$ inch thick, which had rusted; this crust was not bonded tightly to the surface.

Ten-Inch-Diameter Steel Sphere at 575-Foot Range, Right Side of Tower. This sphere, exposed at the 70-foot level, had little metal loss, only $4\frac{1}{4}$ pounds, and was found 270 feet from the tower. The surface was clean, smooth, and free of any foreign material.

Ten-Inch-Diameter Steel Sphere at 575-Foot Range, Left Side of Tower. This specimen was also exposed at the 70-foot level but had a metal loss of $21\frac{1}{2}$ pounds. It traveled the farthest, 420 feet, of any of the specimens exposed to Shot Mohawk. The surface of this specimen had an interesting flow pattern of refrozen metal. These flow lines started at the two poles of the specimen and spiraled around, ending in a line at the equator; it thus appears that these lines were formed by molten metal being thrown to the equator by centrifugal force, as seen in Figure A.46.

A.2.2 Aluminum Sphere. Ten-Inch-Diameter Aluminum Sphere at 545-Foot Range. This sphere was exposed to the Mohawk fireball at the 150-foot level on the specimen tower. The weight loss of $22\frac{1}{2}$ pounds was about 0.3 inch greater on the front side than on the rear. One interesting observation was that the mounting bolt broke just outside the locking nut; then, as the aluminum was removed, more and more of the steel mounting bolt was exposed, with the result that there was a large variation in material loss on the bolt. Figure A.47 shows the mounting bolt and sphere.

50 FT   100 FT   150 FT   200 FT   250 FT   300 FT
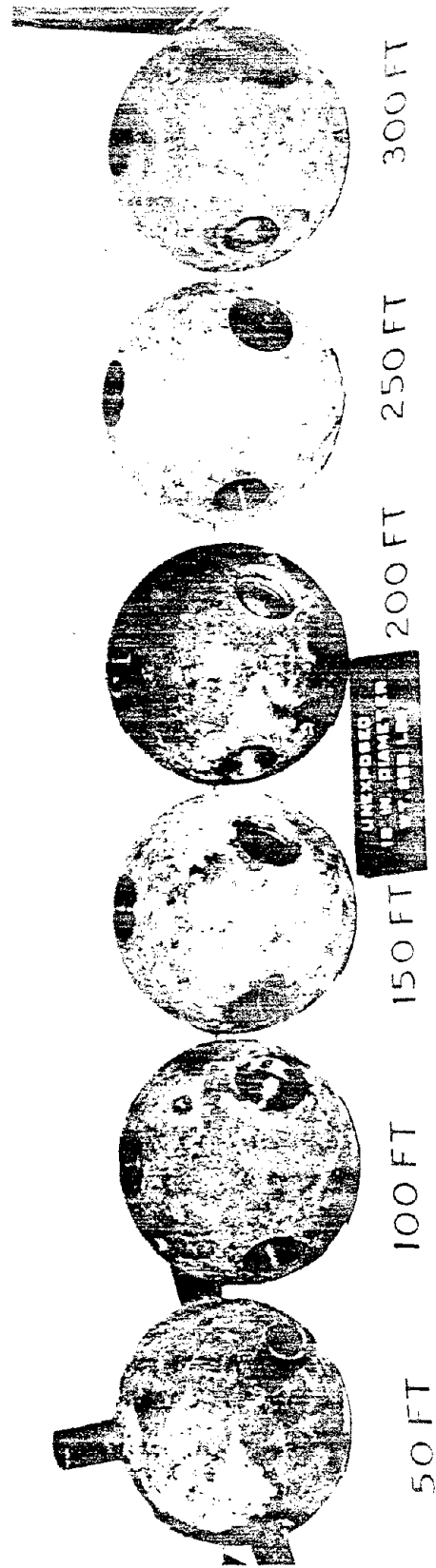
Figure A.1 Overpressure spheres with ball-crusher gages removed.
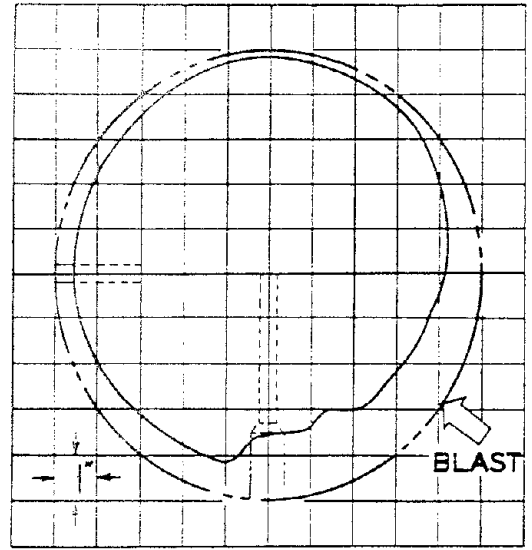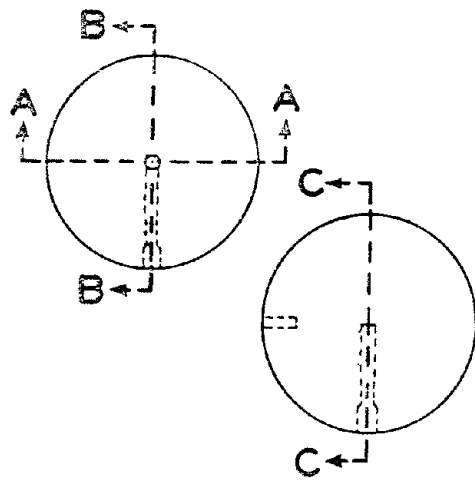
Section BB
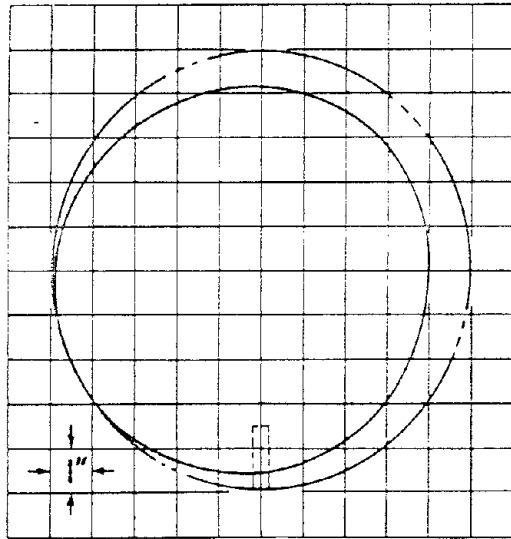
Section AA
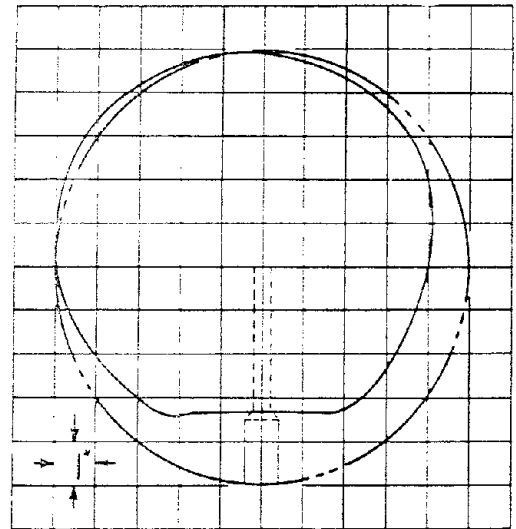
Section CC

Figure A.2 Ten-inch-diameter steel sphere, 50-foot station, Shot Erie.
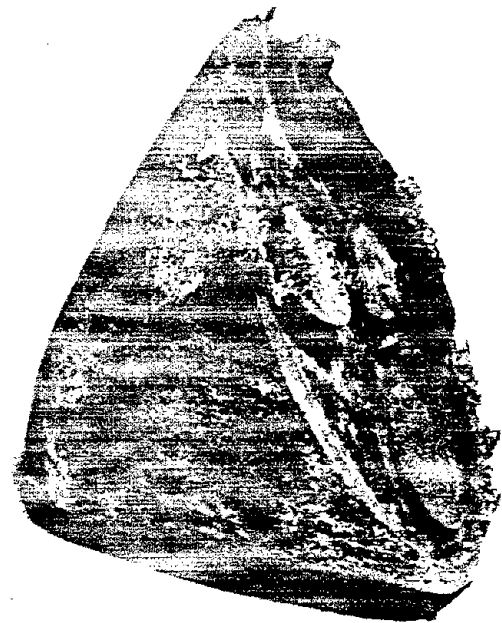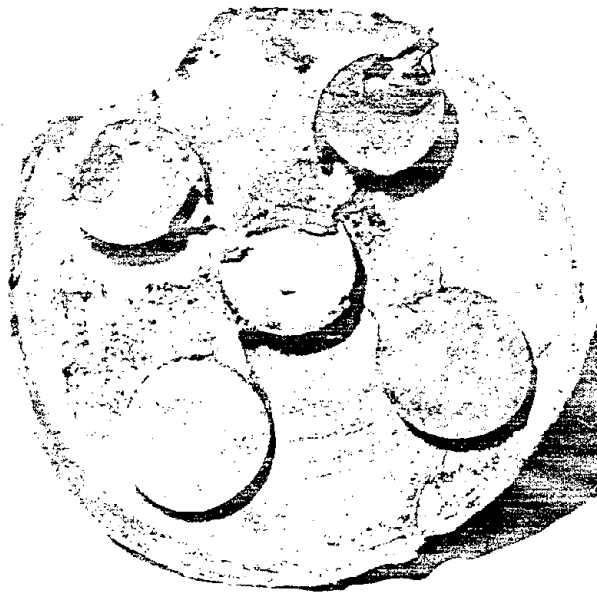
Figure A.3   Cone end of composite specimen, oriented cone forward, 50-foot station.
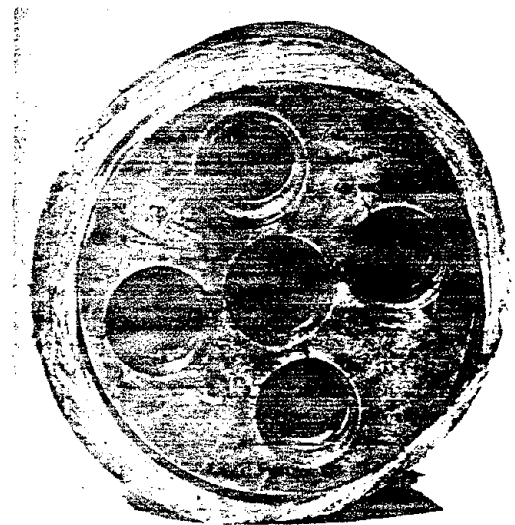
Figure A.4   Sphere end of composite specimen, oriented cone forward, 50-foot station.

Figure A.5   Sphere end of composite specimen, oriented cone forward, 50-foot station.

Figure A.6   Steel composite oriented cone forward, 50-foot station.

Figure A.7   Steel composite oriented cone forward at the 100-foot station.

Figure A.8   Side-on composite, 50-foot station. (note pockmarks).

115
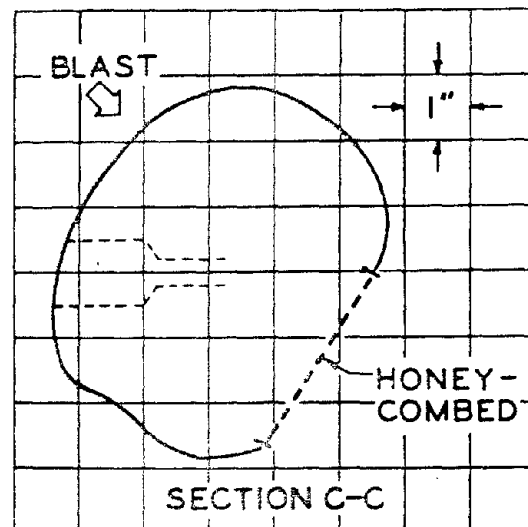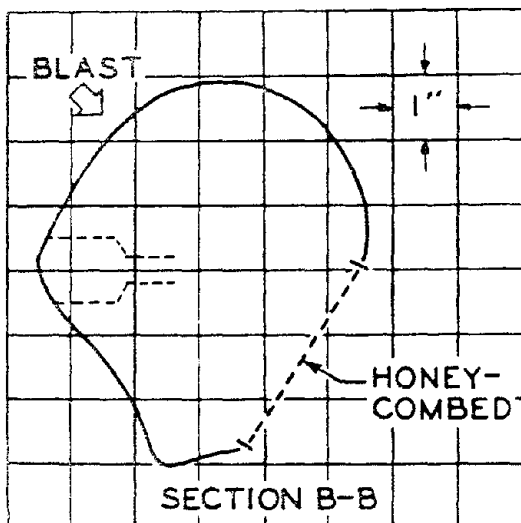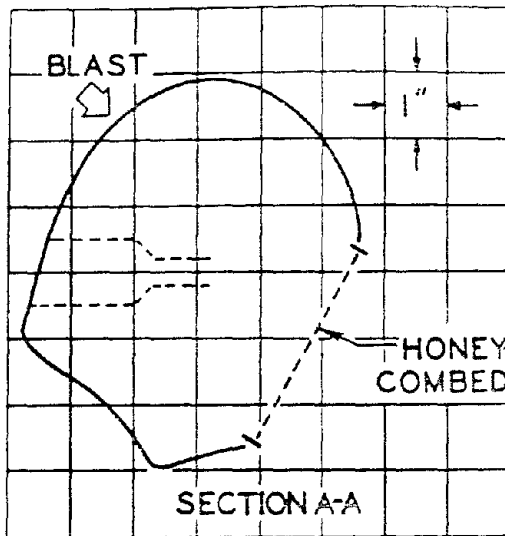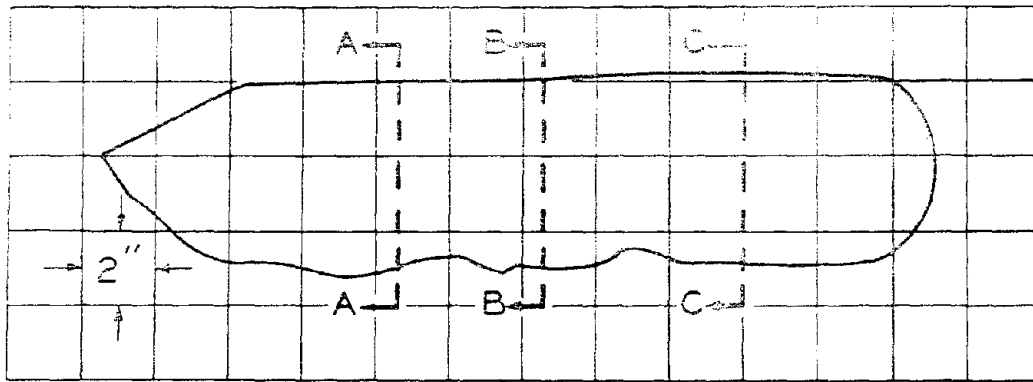
Figure A.9 Side-on composite, 50-foot station.

116

Figure A.10   Laminated cylinder, 100-foot station, twelve $\frac{1}{8}$-inch laminations.
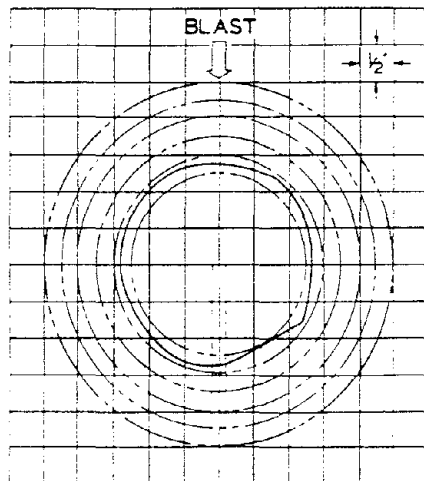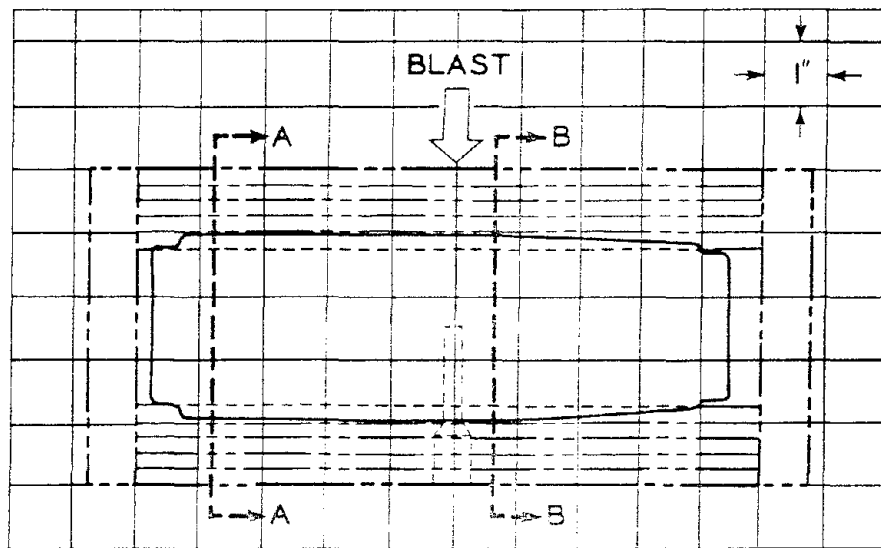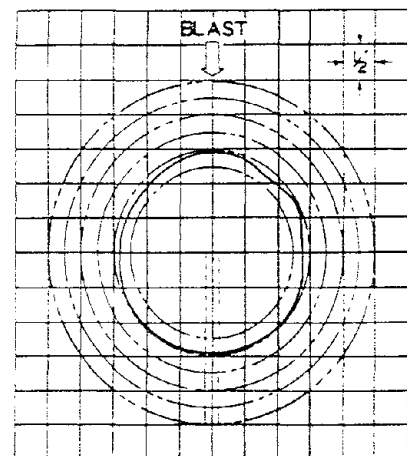
Section AA

Section BB

Figure A.11   Laminated cylinder, 150-foot station, five $\frac{1}{4}$-inch laminations.

Figure A.12 Laminated cylinder, 150-foot station, five $\frac{1}{4}$-inch laminations.

Section AA

Section BB
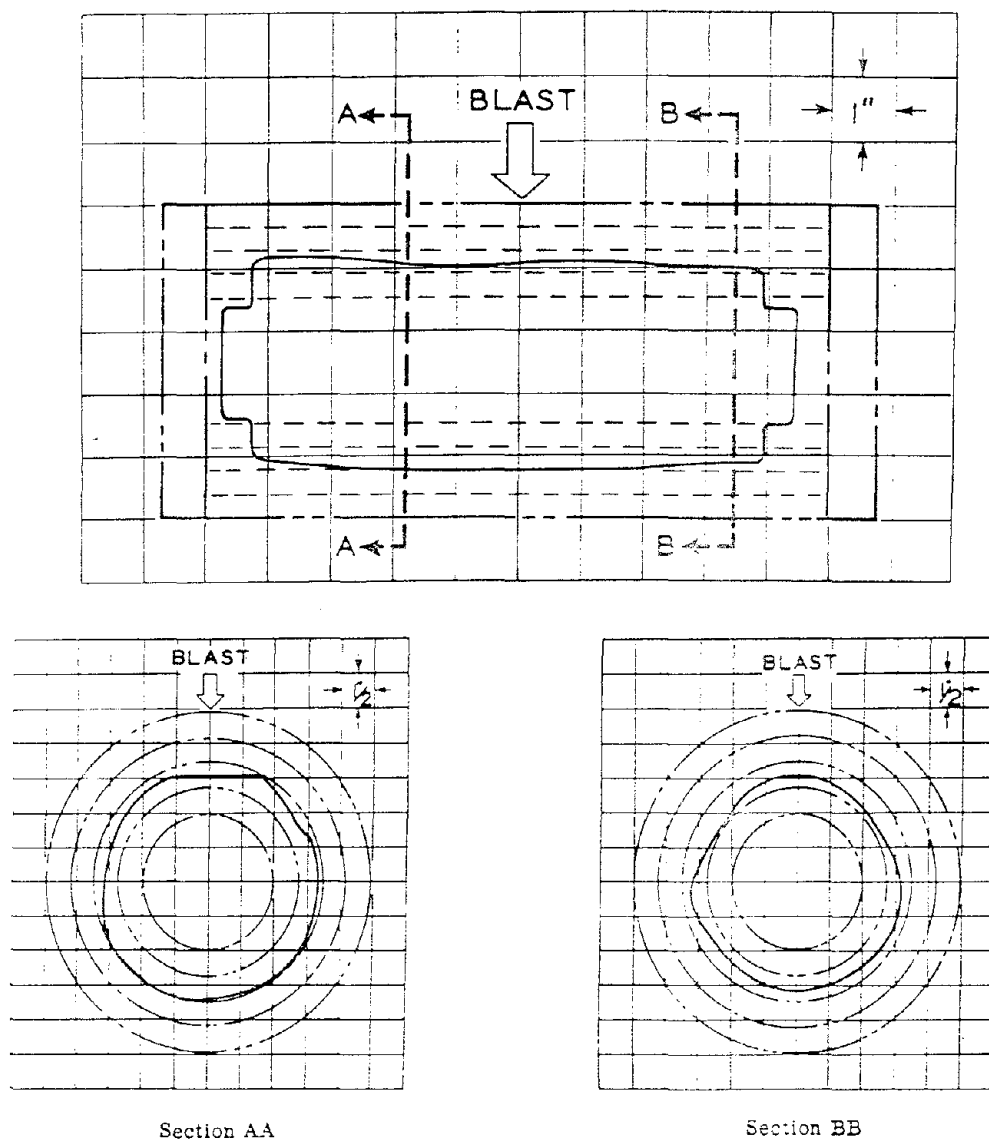
Figure A.13 Laminated cylinder, 150-foot station, four $\frac{3}{8}$ inch laminations.

118

Figure A.14   Laminated cylinder, 150-foot station, four ³⁄₈-inch laminations.
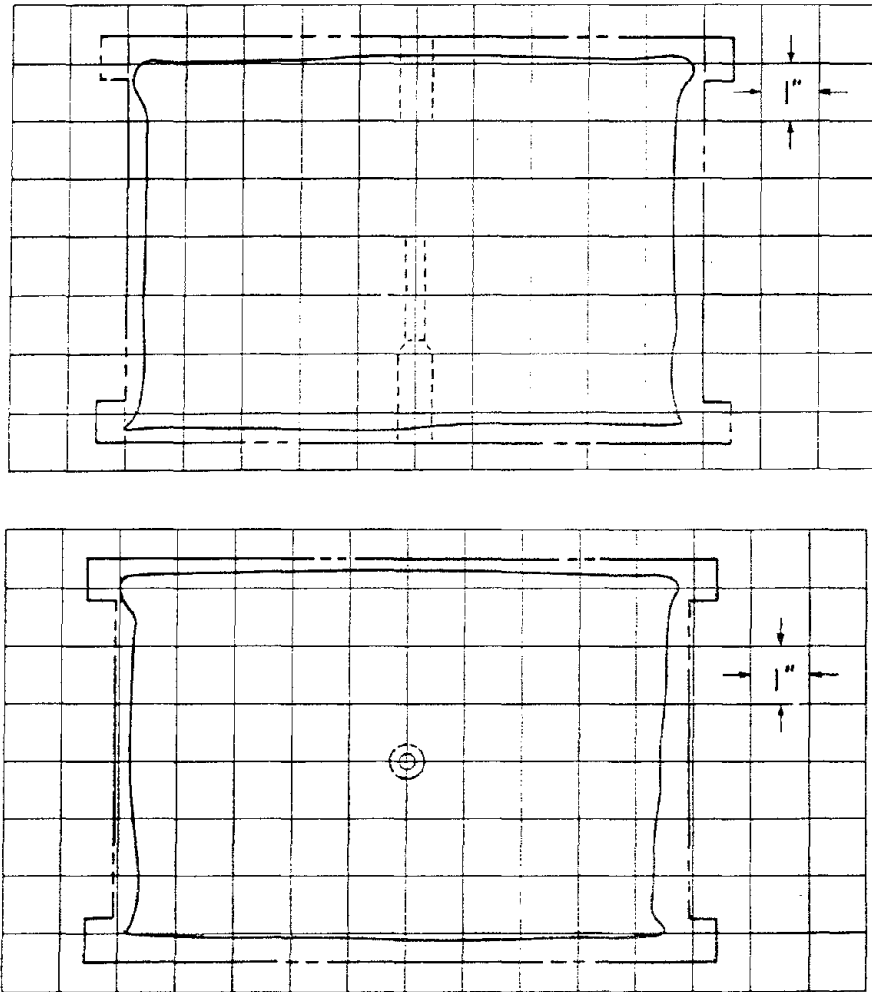
Figure A.15   Ballistic cylinder without plastic, side-on, 100-foot station.

119
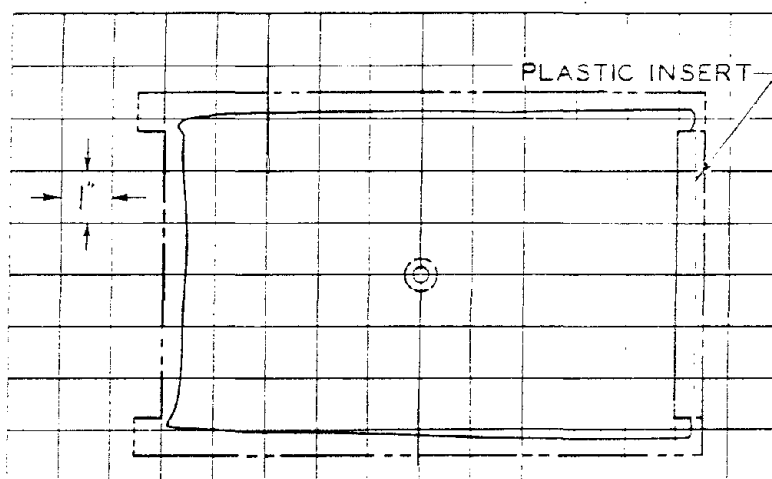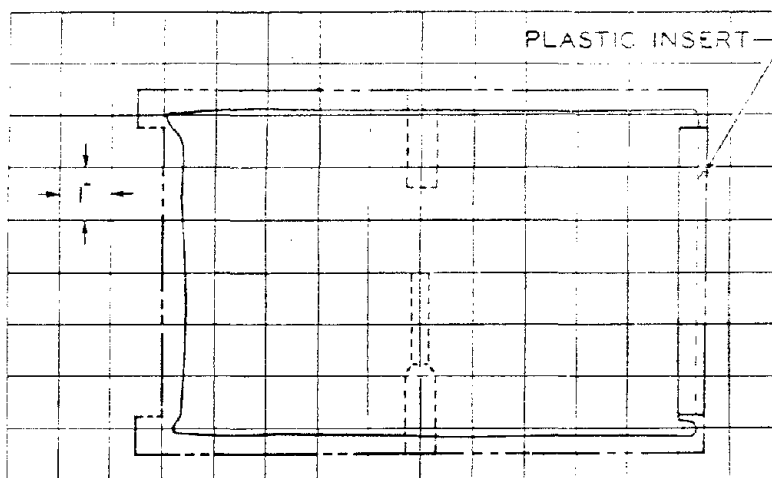
Figure A.16   Ballistic cylinder with plastic, side-on, 100-foot station.

Figure A.17   Plastic disk from side-on
ballistic cylinder, 100-foot station.

120
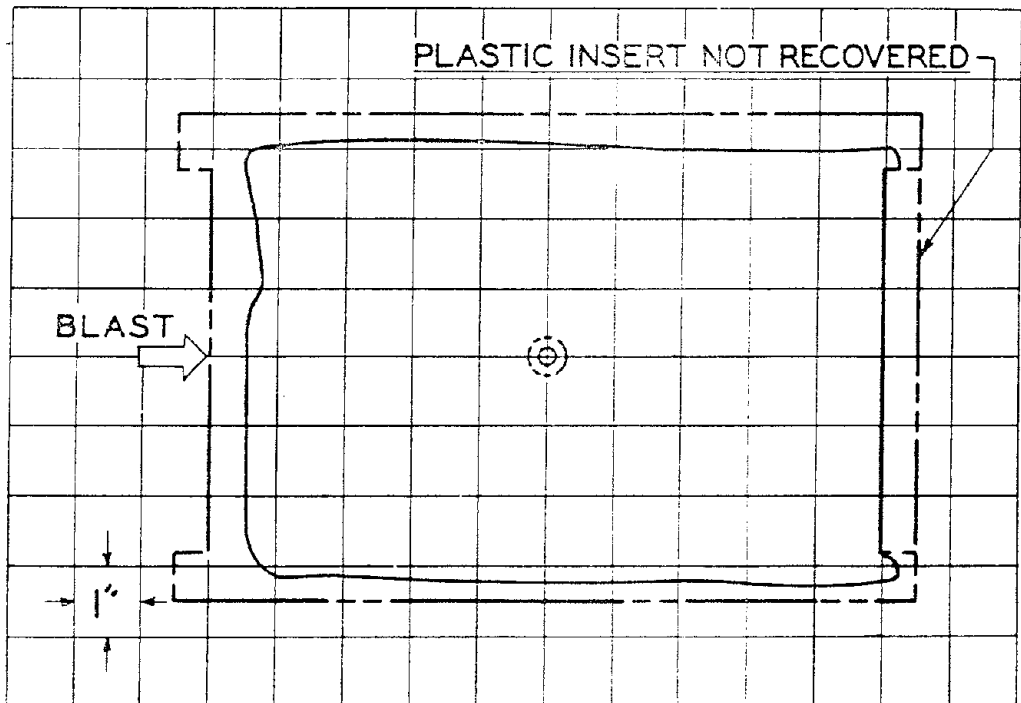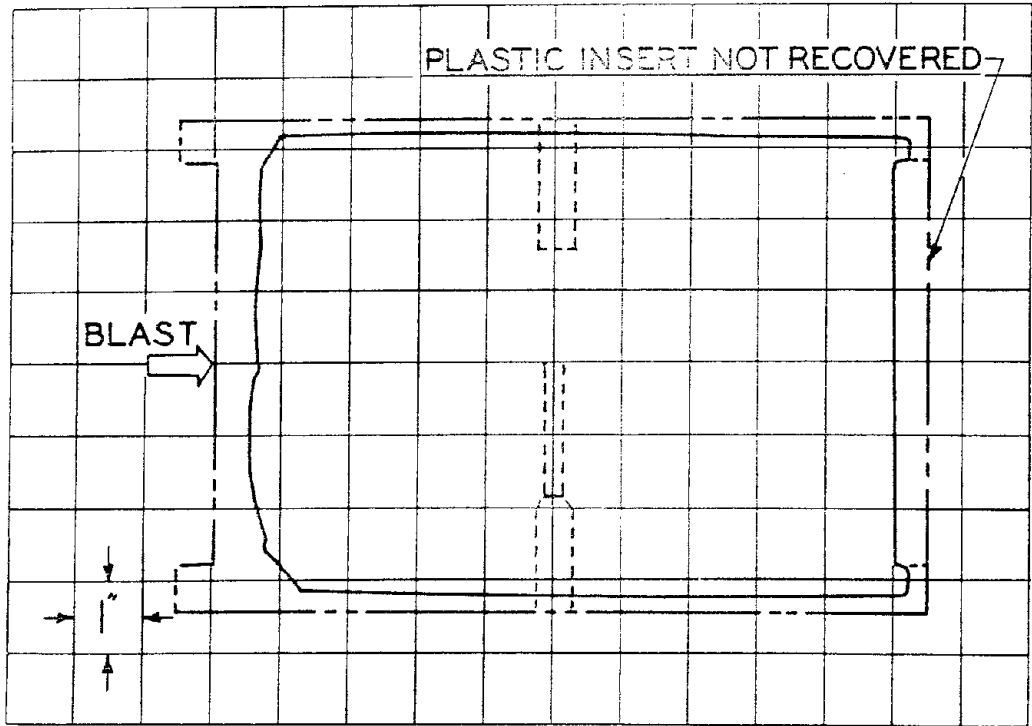
Figure A.18   Ballistic cylinder with plastic, end-on, 100-foot station.
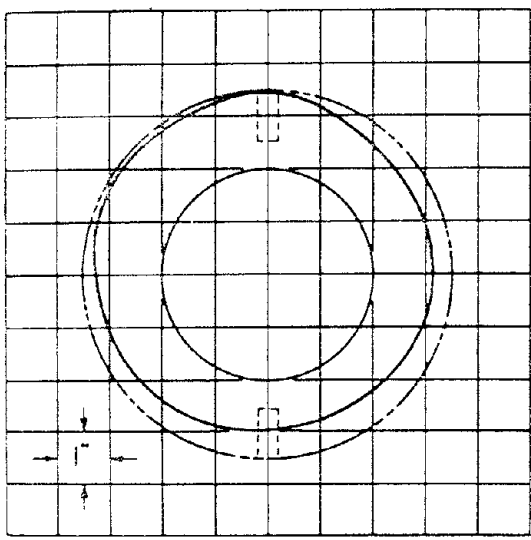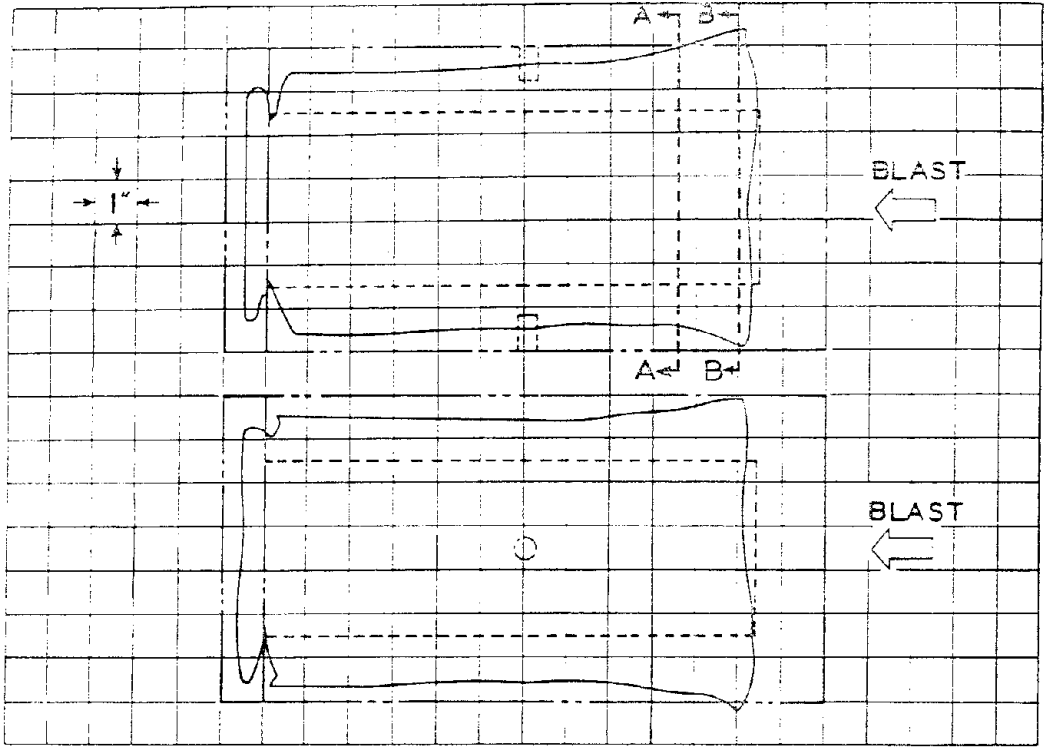
Section AA
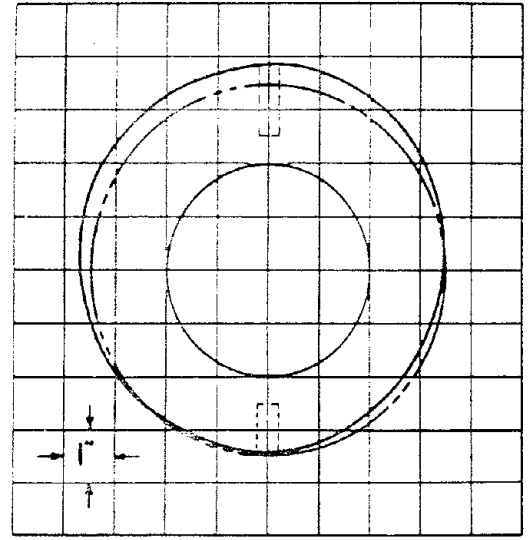
Section BB

Figure A.19 Dynamic pressure cylinder, 50-foot station.
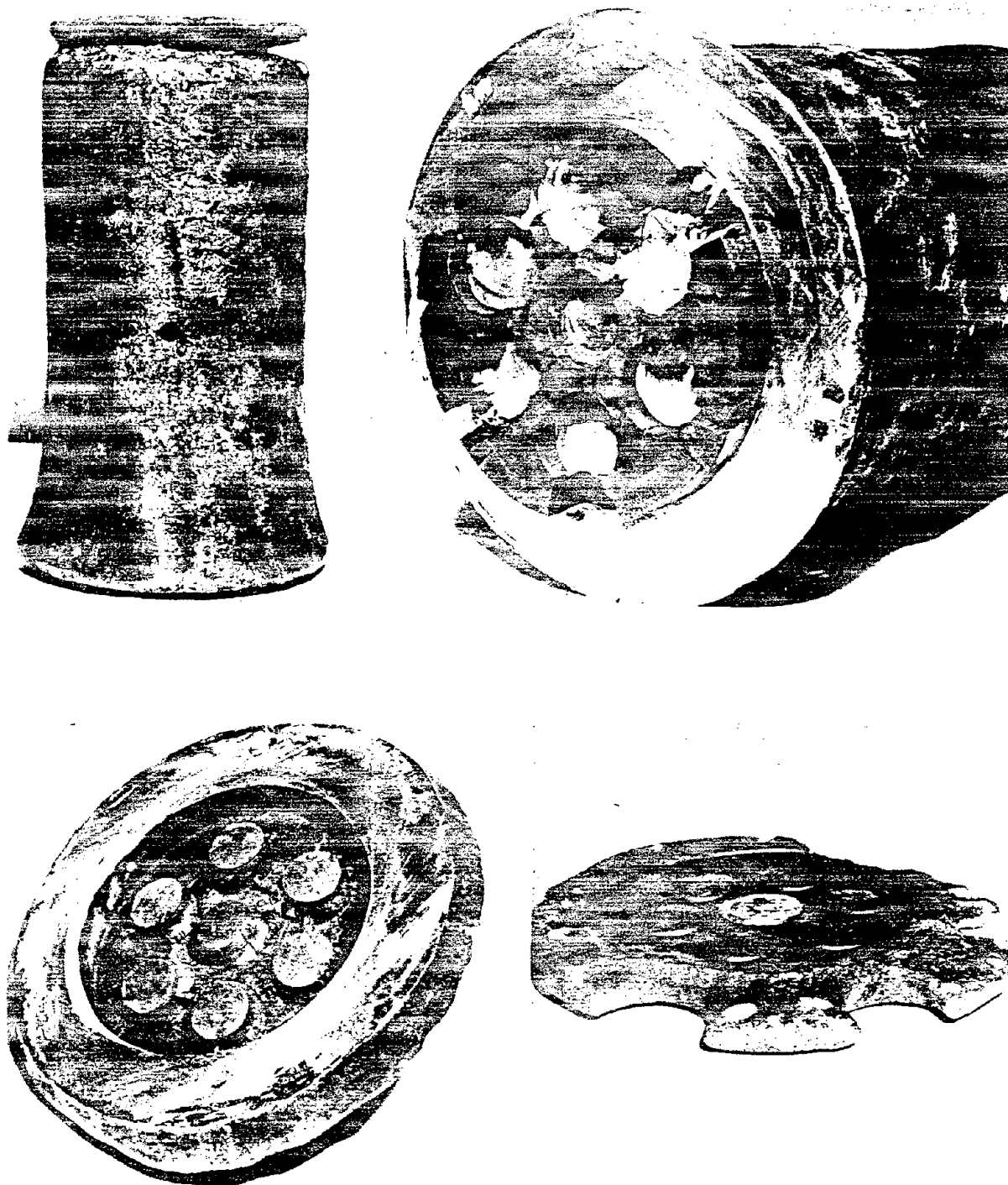
Figure A.20   Dynamic pressure cylinder, 50-foot station.

123

Figure A.21 Dynamic pressure cylinder, 50-foot station (note blisters on the surface).
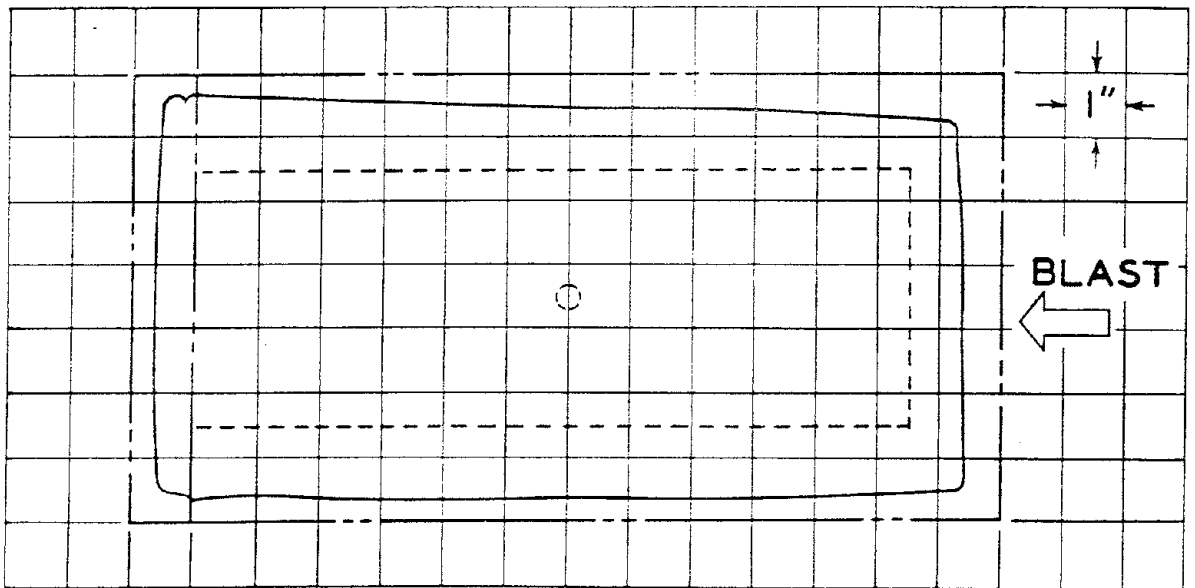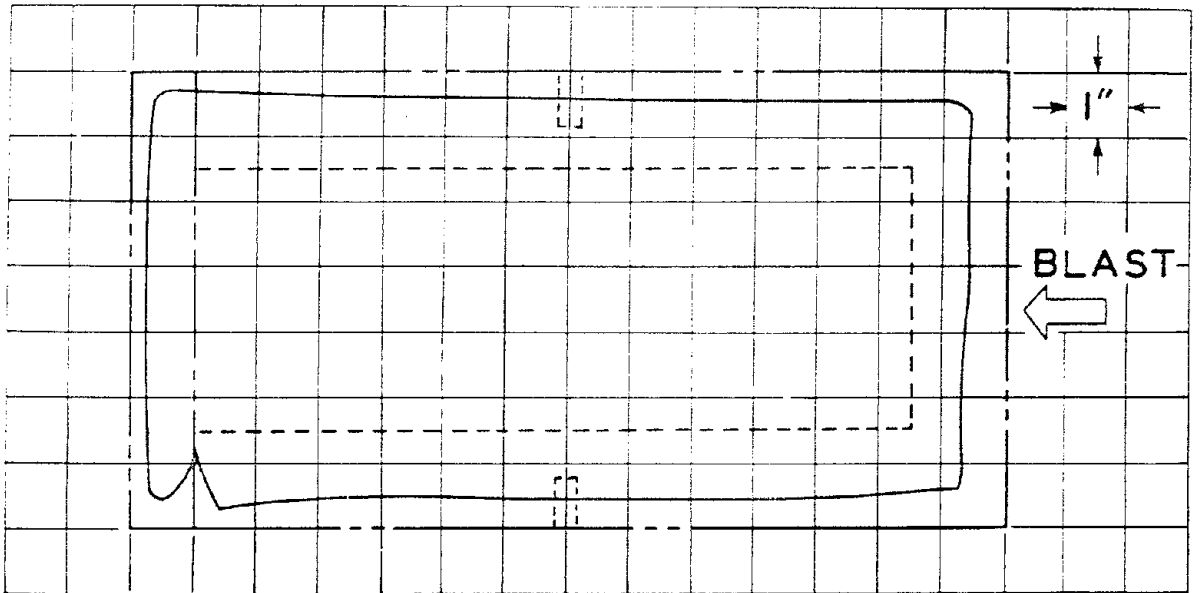
Figure A.22   Dynamic pressure cylinder, 150-foot station.
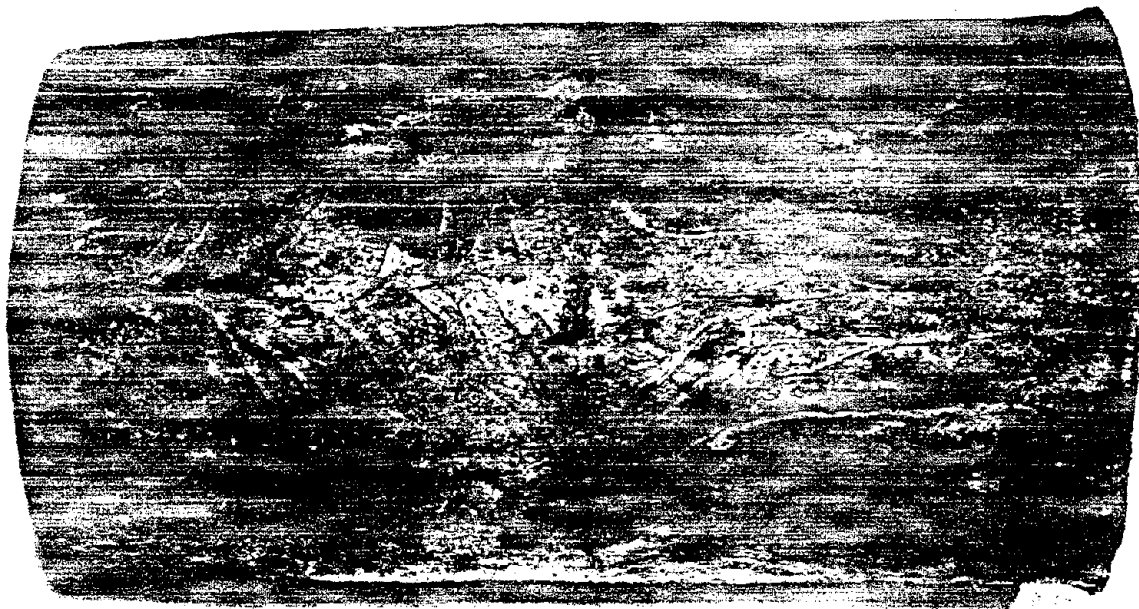
Figure A.23 Flow pattern on dynamic pressure cylinder, 150-foot station.
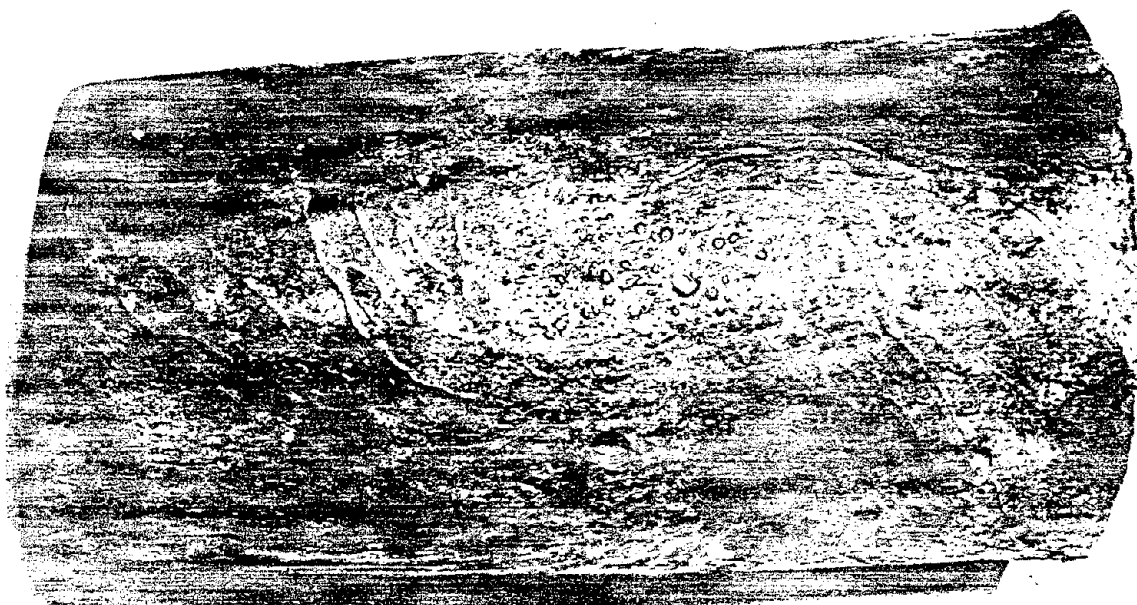
Figure A.24 Dynamic pressure cylinder, 150-foot station (note blisters on the surface).
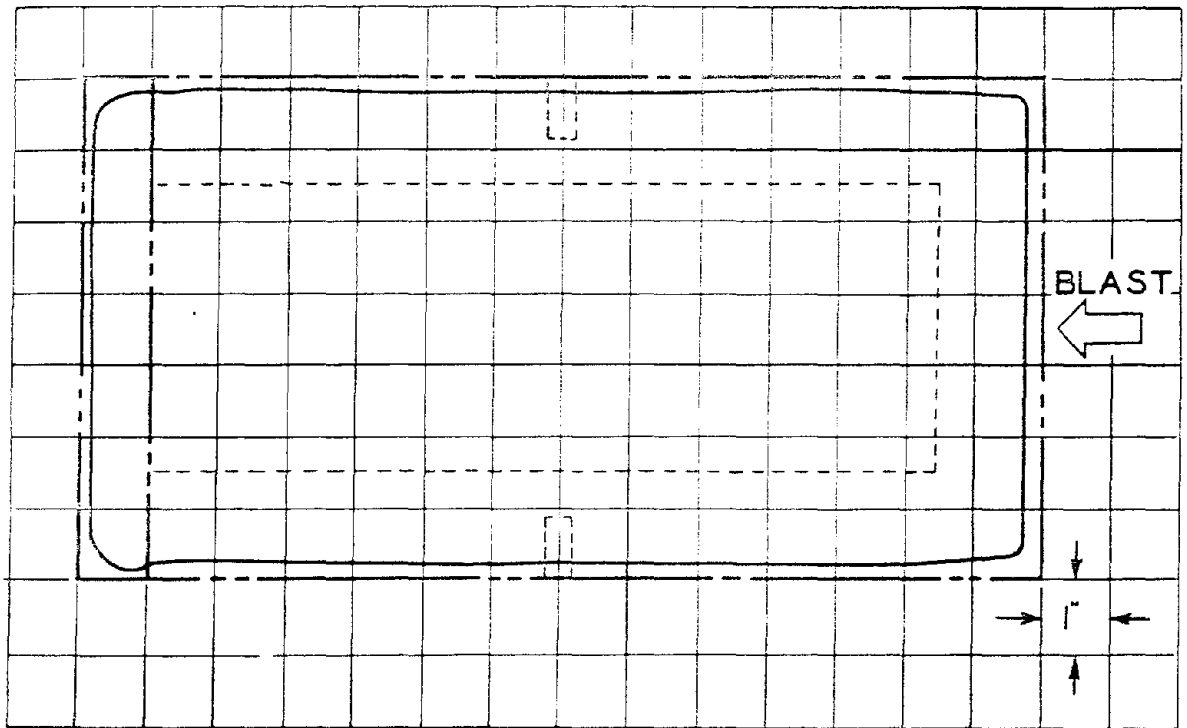
Figure A.25 Dynamic pressure cylinder, 250-foot station.
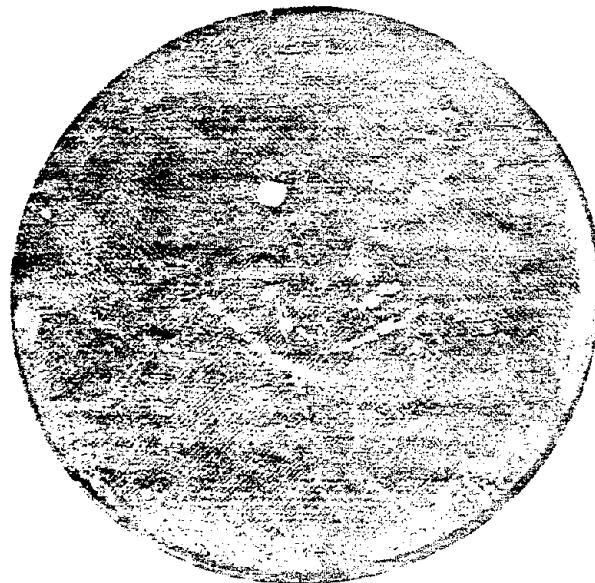
Figure A.26 Plastic disk from dynamic pressure
cylinder, 150-foot station.

127
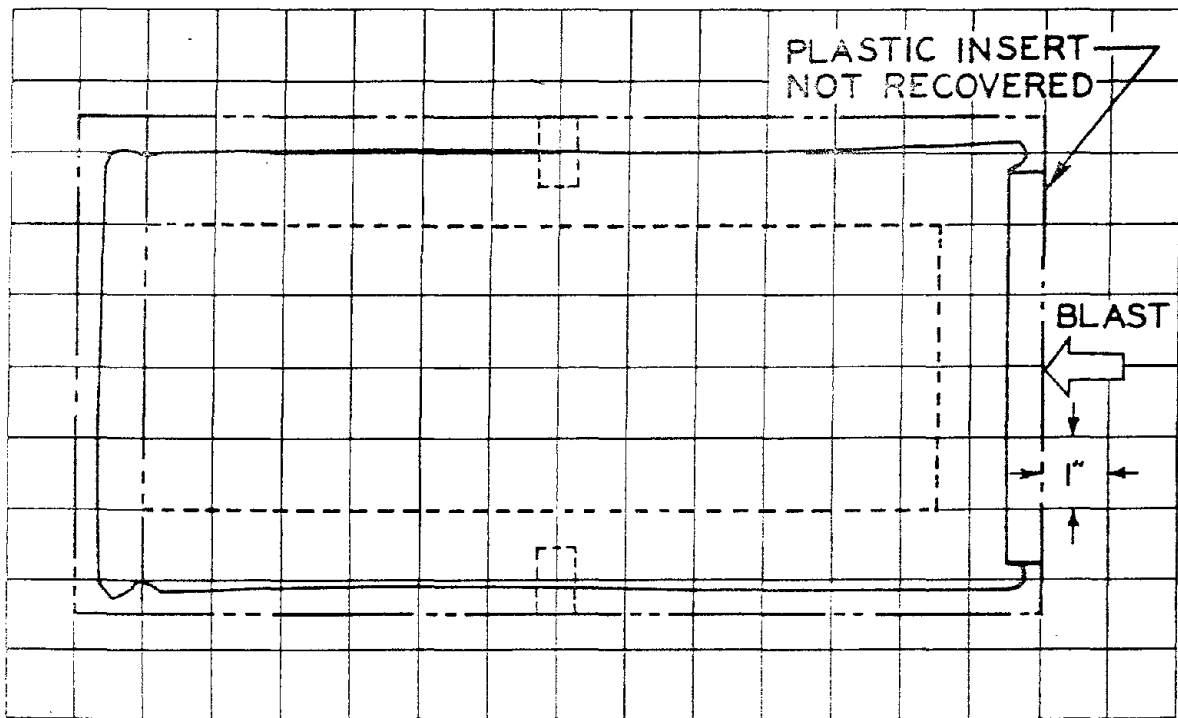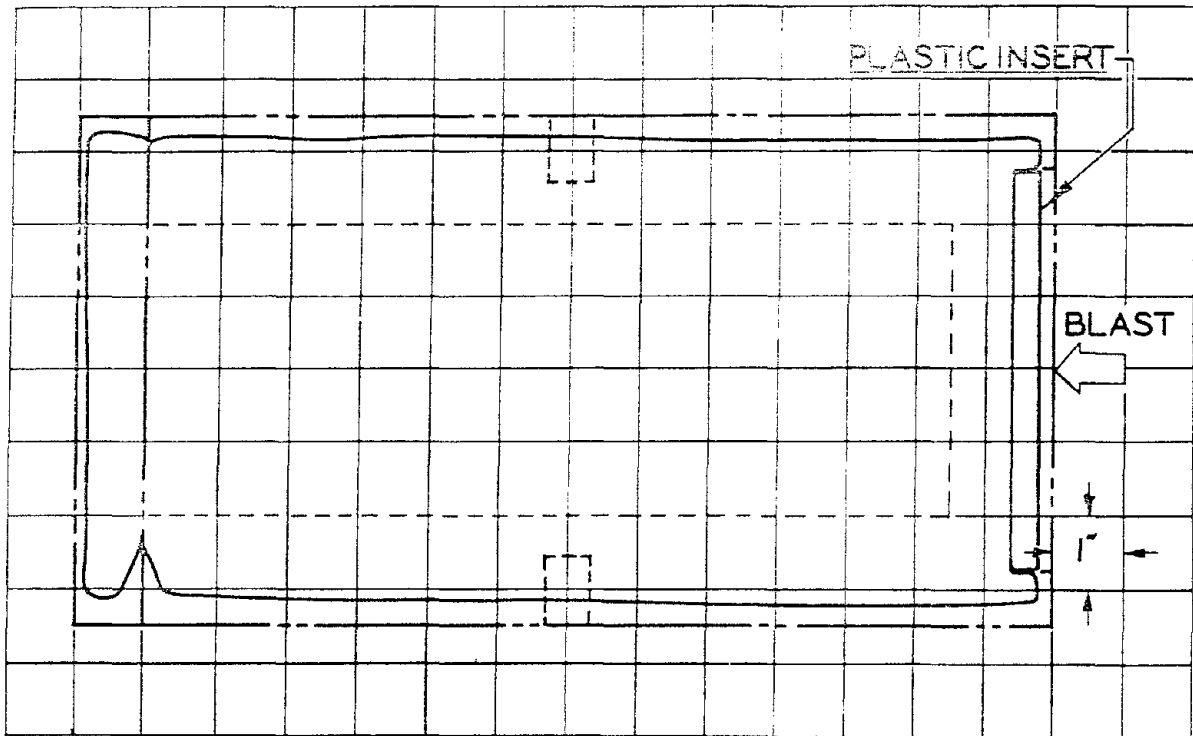
Figure A.27 Dynamic pressure cylinders with plastic disks, 150-foot station.
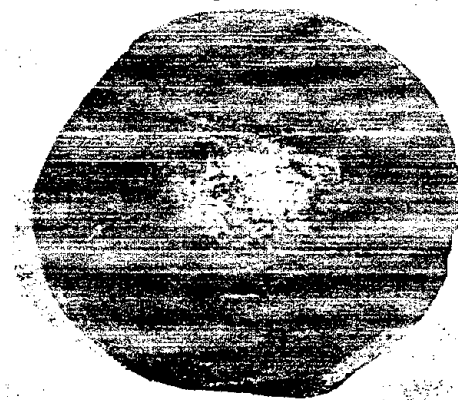
Figure A.28   Copper sphere, 50-foot station.
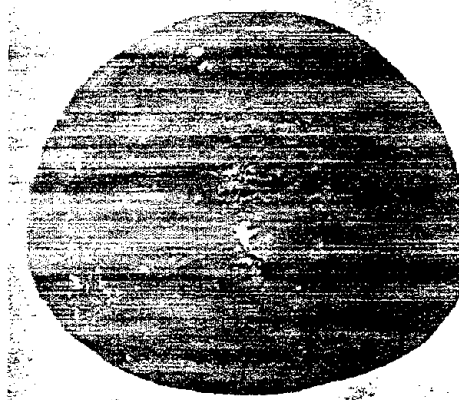
Figure A.29   Copper sphere, 100-foot station.

Figure A.30   Copper sphere, 150-
foot station. Cut in right side was
made after the test to relieve pres-
sure on peak temperature pin so
that it could be removed.

Figure A.31   Copper sphere, 250-foot station.

Figure A.32   Molybdenum sphere, 25-foot station.

129
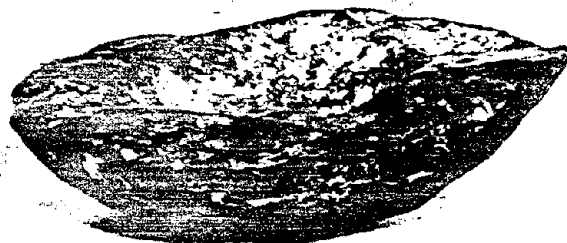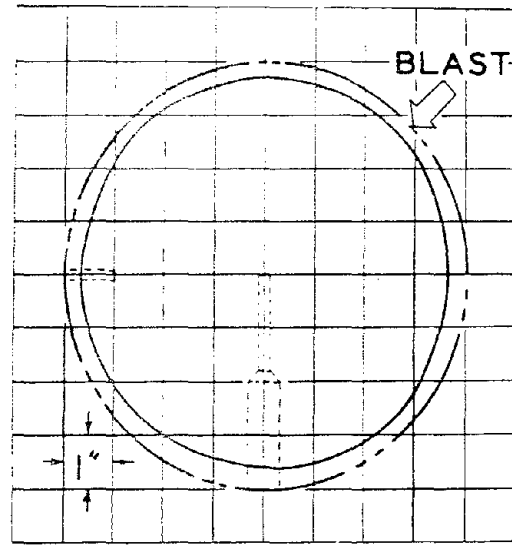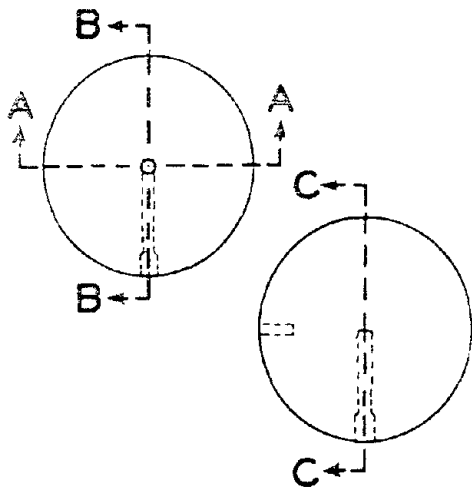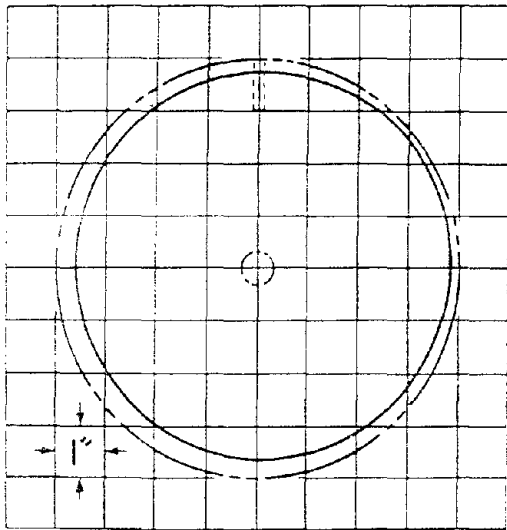
Section BB
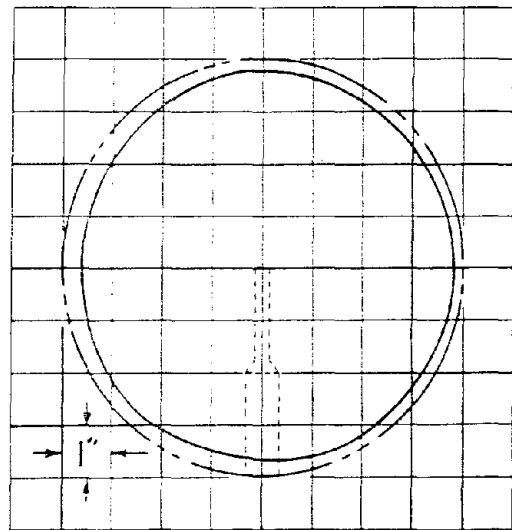
Section AA   Section CC

Figure A.33   Molybdenum sphere, 100-foot station.

Figure A.35   Stainless steel sphere, 25-foot station.

Figure A.34   Molybdenum sphere, 100-foot station.
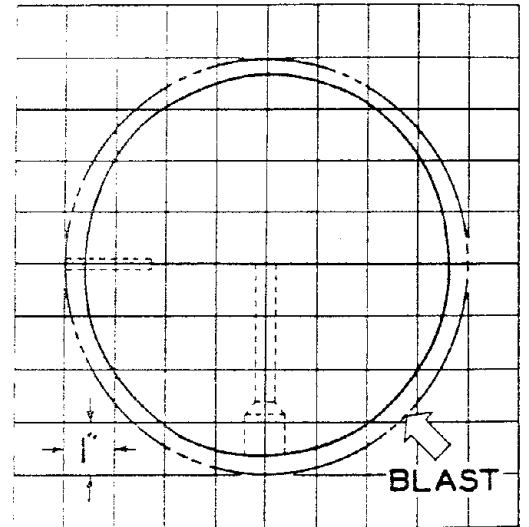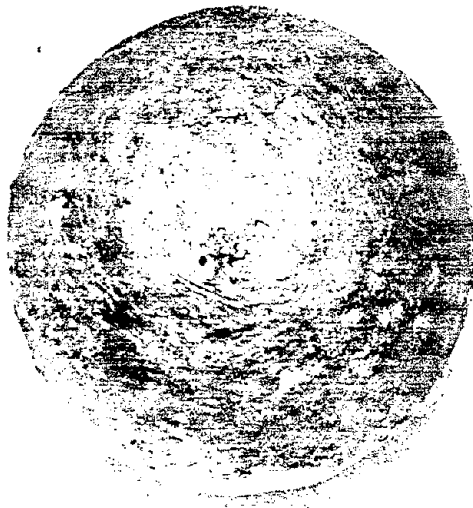
Figure A.36   Stainless steel sphere, 100-foot station.
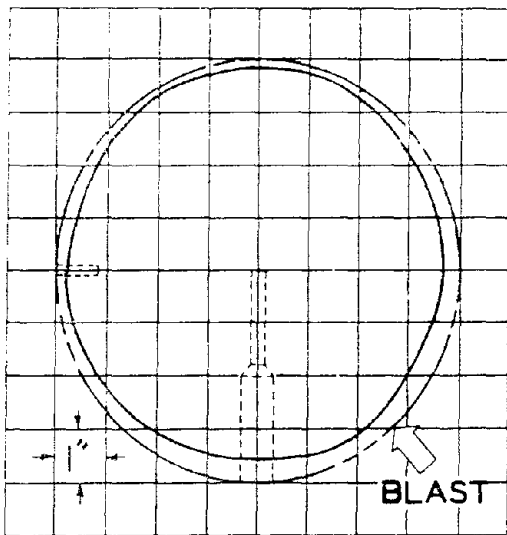
Figure A.37 Stainless steel sphere, 200-foot station.

Figure A.38 Titanium sphere, 100-foot station.
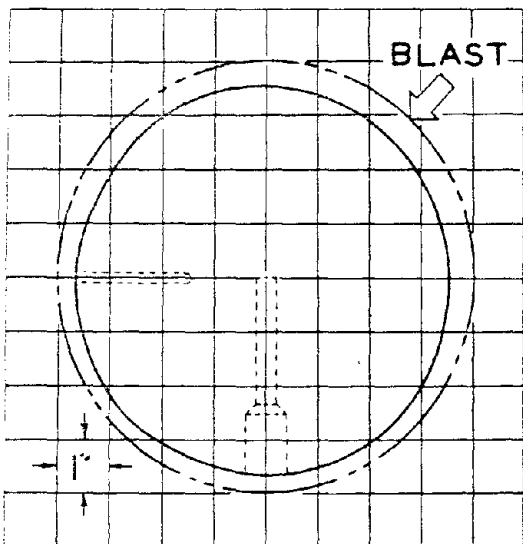
Figure A.39 Titanium sphere, 200-foot station.
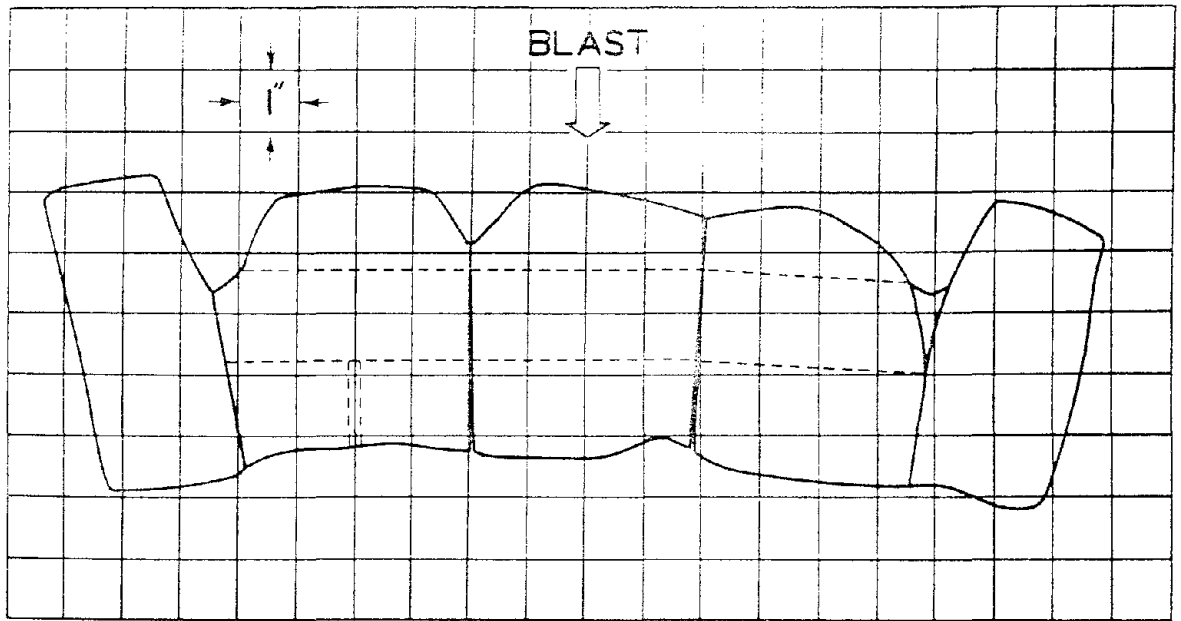
Figure A.40   Tantalum-copper cylinder, 100-foot station.
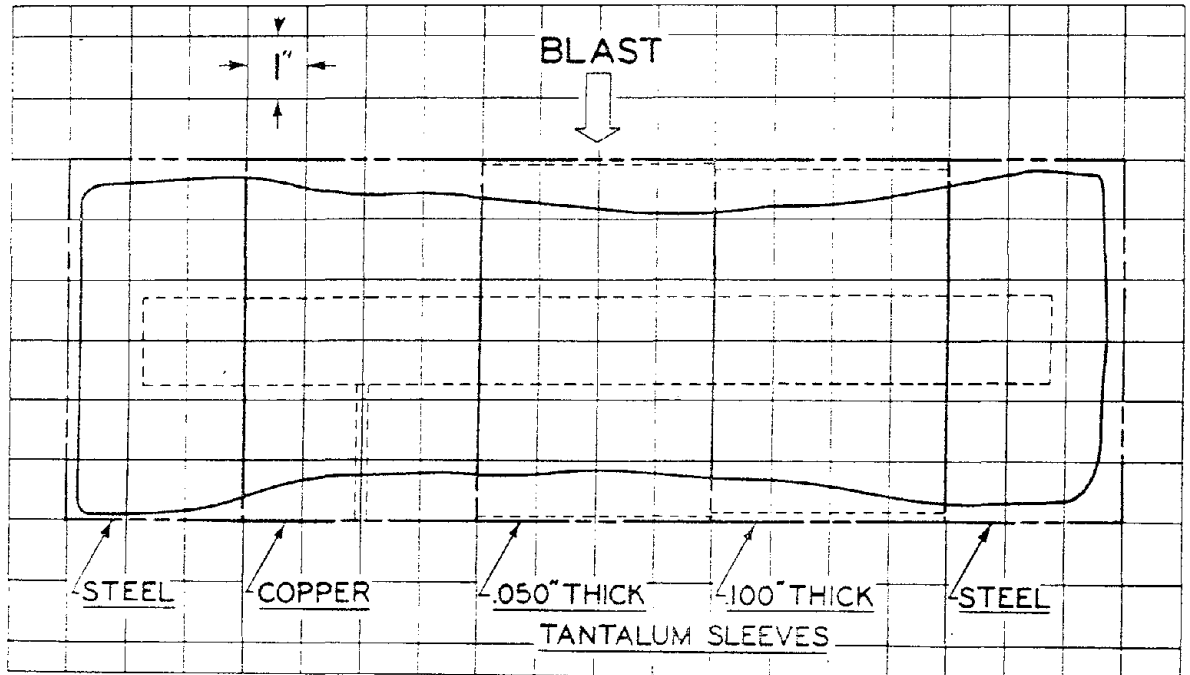
Figure A.41   Tantalum-copper cylinder, 200-foot station.

133
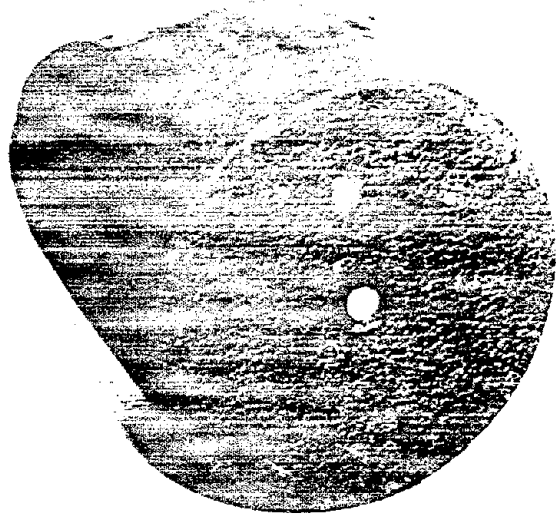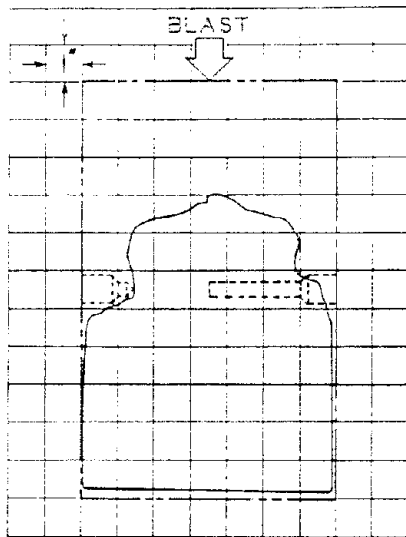
Figure A.42   Bakelite cylinder, 200-foot station.
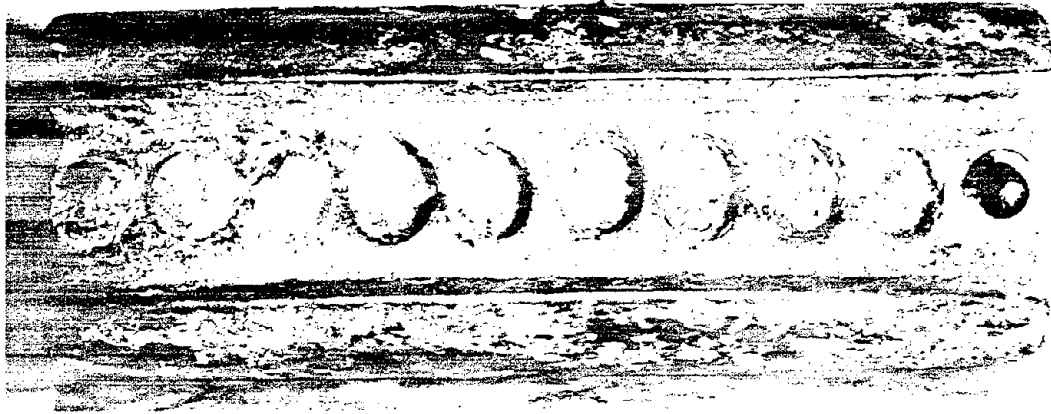
Station 100
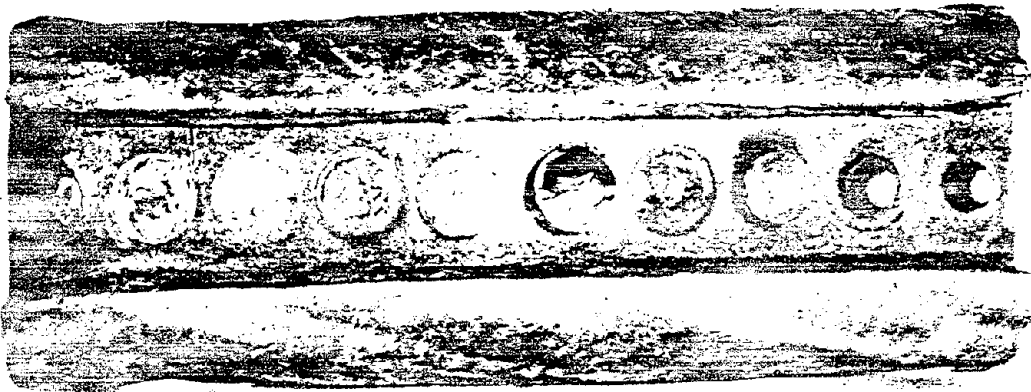
Station 200

Figure A.43   Cylinders with ceramic and special alloy samples.

134
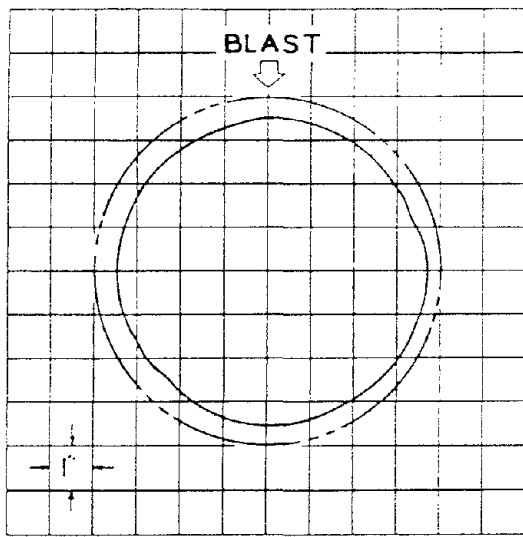
10-Inch Diameter, Left Side
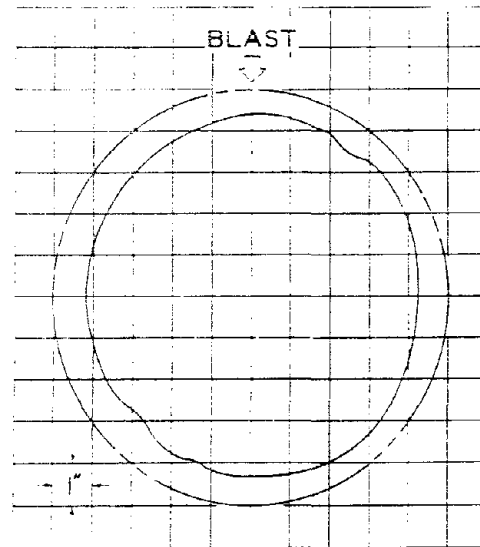
10-Inch Diameter, Right Side
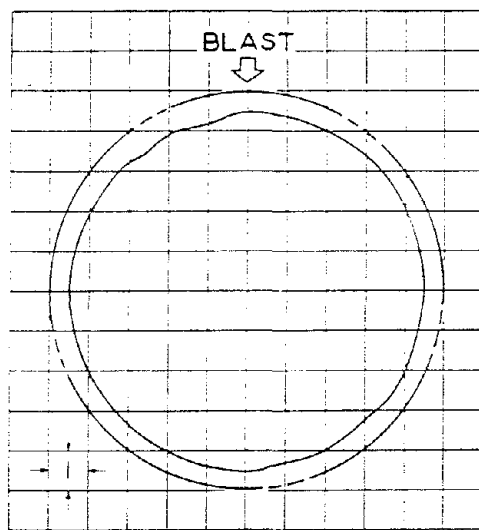
8-Inch Diameter, Left Side
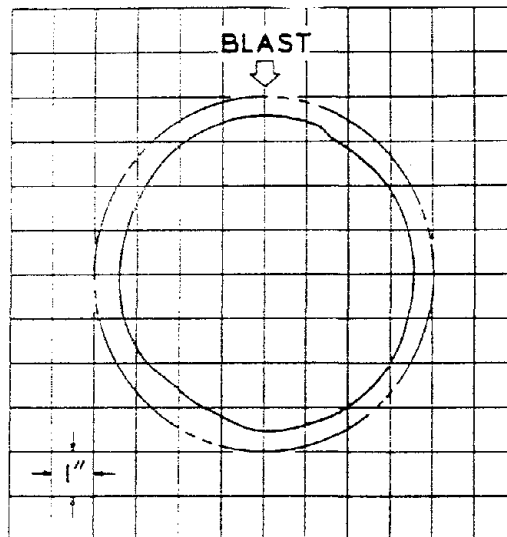
8-Inch Diameter, Right Side

Figure A.44 Steel spheres, 545-foot range, Shot Mohawk.

135
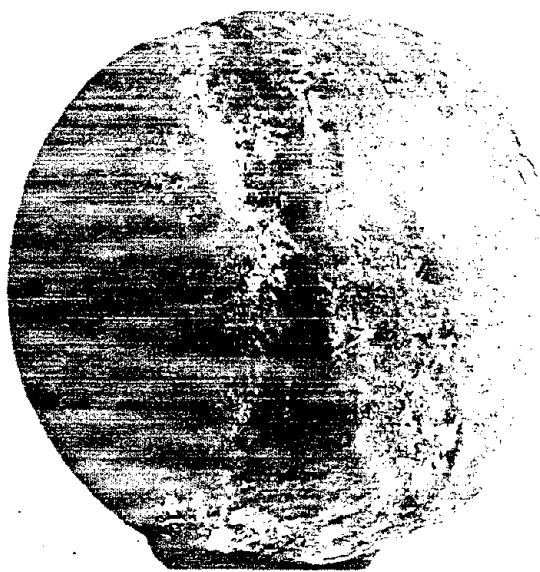
10-Inch Diameter, Right Side

10-Inch Diameter, Left Side
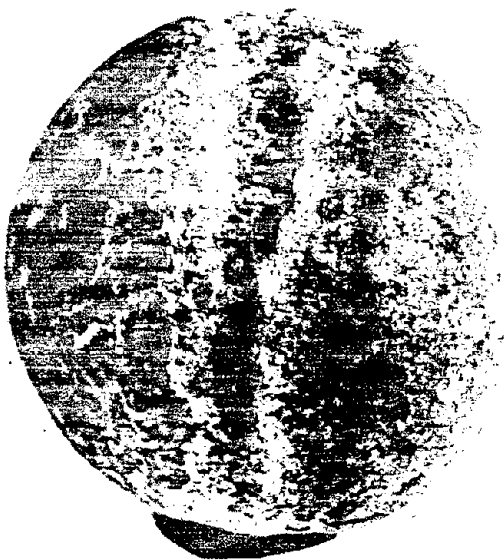
8-Inch Diameter, Left Side
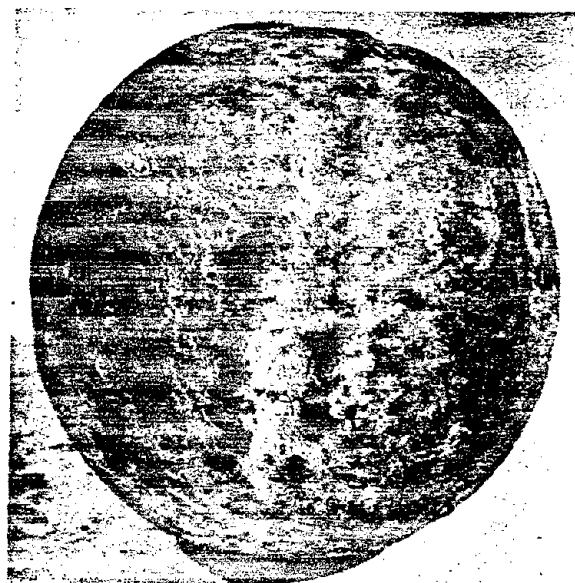
8-Inch Diameter, Right Side

Figure A.45   Steel spheres, 545-foot range, Shot Mohawk (note the double grooves).

136
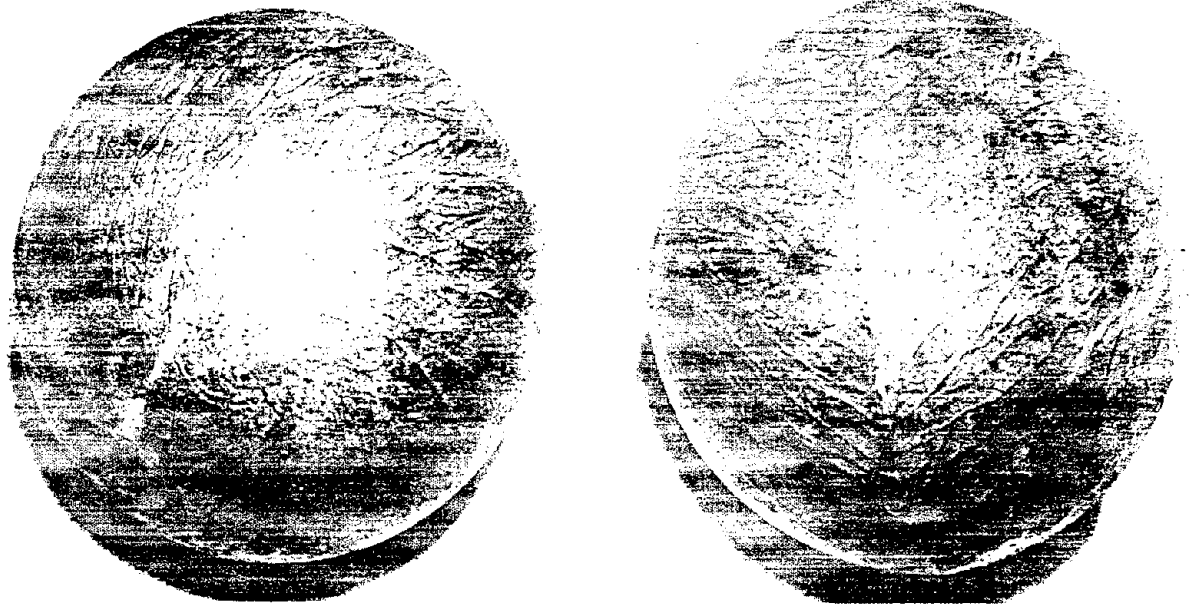
Figure A.46 Ten-inch-diameter steel sphere, 575-foot range, left side of tower, Shot Mohawk.
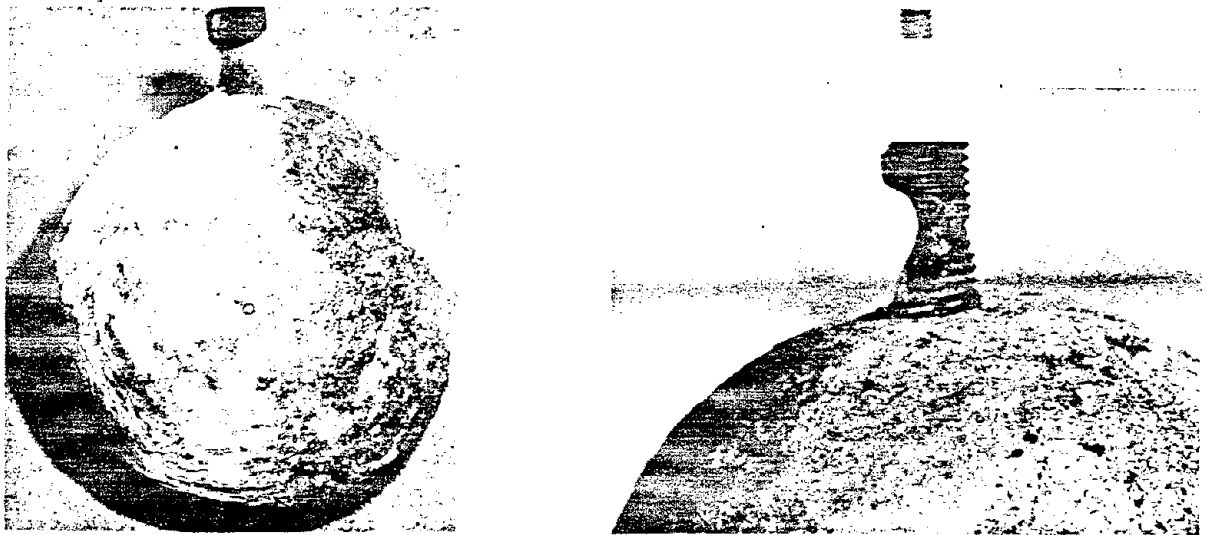
Figure A.47 Ten-inch-diameter aluminum sphere, 545-foot range, Shot Mohawk. Note mounting bolt. The blast came from the left in the right photograph.

Appendix B
ELECTRICAL RECORDING WITHIN THE FIREBALL

B.1 INTRODUCTION

The problems involved in collecting data inside a nuclear fireball by electrical means can best be indicated by listing the more important environmental conditions in which such a recording system must operate. Theoretical analysis of the fireball of a 20 kt nominal atomic bomb at sea level yields the following environmental conditions:

1. Temperature ranging from about 150,000C to 5,000C,

2. Overpressure up to 20,000 atmospheres,

3. Neutron bombardment at high flux rates and totals up to 10^{17} neutrons/cm^2.

4. Gamma radiation in excess of 2×10^6 r,

5. Powerful electromagnetic radiation of various wave lengths.

The above environment results in the specimen responses of up to 1 inch metal loss due to the high temperature, accelerations on the order of 100,000 grams due to the shock wave and dynamic pressure, and overpressure crushing. The specimen container must be designed to withstand all these effects and protect the recorder and other equipment from the fireball environment. The recorder must be of a rugged design capable of withstanding the high acceleration and nuclear radiation from which the container cannot shield it.

Six instrumented specimens, each containing a miniature tape recorder, were exposed inside the fireball of Shot Erie. Five were spheres 12 inches in diameter and were exposed at slant ranges of 100, 150, 200, 250, and 300 feet from the detonation point. The sixth specimen was a 16-inch-diameter sphere and was exposed at a slant range of 50 feet.

The object of this appendix is to describe and evaluate the electrical recording system and to suggest improvements for future designs.

B.2 PROCEDURE

Since this was one of the first attempts to make electrical measurements inside the fireball, it was decided to keep the specimen as simple as possible.

Various specimen configurations were considered and a spherical shape was chosen because the drag coefficient was independent of specimen orientation and also because it was structurally capable of withstanding large overpressure crushing forces. Since the ballistics of a sphere are somewhat predictable, location and recovery of the specimen after the test would also be facilitated.

A tape recorder was selected as the best method of electrical recording inside the fireball. Other recording methods were undesirable because of their vulnerability to such things as high level gamma radiation and large accelerations. The only available recorder which appeared suitable for these requirements was the North American Instruments (NAR) miniature recorder. It combined small size with operation at relatively high accelerations. Direct recording, without amplifiers, of low power thermocouples had been accomplished with this recorder using a dc erase of a prerecorded signal. The fact that no amplification was required to record low power dc signals on magnetic tape made it ideal for this project's specimen.

Phenomena selected for measurement were specimen accelerations, depth of surface melting as a function of time, and specimen temperature at selected depths below the surface.

B.2.1 Container. Design of the spherical specimen container was guided by several considerations: (1) it had to be adequately housed to protect the recorder and other equipment from the extreme environment of the fireball. (2) it had to have sufficient surface area to permit mounting of the various sensing transducers, and (3) it had to be as small as practical, consistent with recorder size and requirements in (1) and (2) above.

Figure B.1 shows the container design selected for all ranges except the closest. It was spherical in shape, 12 inches in diameter, and fabricated from high strength steel. Machining tolerances on the external caps and cap seats were held quite close to

138

prevent the large pressures from forcing the high temperature gases inside the container. The design was such that overpressure would press the caps tighter into their seats, thus making a better seal and also removing much of the stress on the cap securing bolts.

The main body of the container and all external caps were made of 4340 steel heat treated to a yield strength of 200,000 psi or more. Since the strongest specimen possible would have been a solid sphere, the container was designed to approach this ideal as closely as feasible. The main container body was fabricated from a solid steel billet, and a minimum amount of steel was removed from the inside. Consideration of the machining costs, wiring space, and equipment mounting space caused some voids which were filled with a foam-in-place plastic called Eccofoam.

A specimen larger than 12 inches in diameter was required at the 50-foot range because: (1) a large amount of metal loss was expected. (2) increased strength was required to withstand the overpressure crushing, and (3) the mass of a larger specimen would cause smaller accelerations. This closest instrumented specimen (50-foot slant range) was a 16-inch diameter sphere. Essentially, it was one of the 12-inch spheres described above with a 2-inch thick shell completely enclosing it, as shown in Figure B.2. The shell was in two pieces which screwed together. The two half shells were machined to close tolerances, heat treated to a yield strength of 200,000 psi or better, and finally ground on their inside surface to fit very tightly over the 12-inch inner sphere. These close tolerances were necessary so that during the overpressure loading the shell would transfer part of the load to the inner sphere, and during the high acceleration the sphere would have maximum bearing area on the shell.

B.2.2 Recorder. A miniature tape recorder manufactured by North American Instruments, Inc. was selected as the specimen recorder. The reasons for the selection should become apparent after studying the recorder characteristics listed below:

1. Satisfactory operation while under axial accelerations up to 500 grams and angular accelerations up to 200 radians/sec².

2. Small size, approximately 4 inches in diameter by 6 inches in length, including batteries.

3. Eight information channels on ½-inch magnetic tape.

4. Employment of a recording system which could record small dc currents without the aid of amplifiers.

The North American Recorder (NAR) as shown in Figure B.3 used as a recording medium ½-inch Mylar magnetic recording tape. Eight information channels were recorded on this tape by two recording heads each containing four channels. The two heads were arranged so that the four channels from one head were recorded between the channels of the

other. One head, odd numbered channels 1, 3, 5, and 7, was designed to operate with thermocouples and depth-of-melt transducers, cf., Section B.2.3, and had channels with approximately 12.5 ohms resistance and 30 mh inductance. The head with even numbered channels 2, 4, 6, and 8, was designed to operate with accelerometer transducers and the time base oscillator; and had a resistance and inductance of approximately 35 ohms and 130 mh, respectively. The recorder was driven by a small ungoverned 12-volt dc motor which ran at approximately 12,000 rpm. The effect of the inherent speed variations of such a system was minimized by the recording system used. Power to drive the recorder was furnished by eight small Yardney silvercels. The high speed of the drive motor was reduced to that required for driving the tape by a series of pulleys which used O rings for drive bolts, also shown in Figure B.3. The tape transport mechanism was protected by a phenolic cylinder surrounded by a heavy steel case. The drive motor and silvercels were encased in a potting material called lockfoam.

The direct recording of low power fluctuating direct currents on magnetic tape was accomplished by using these currents to partially erase prerecorded alternating current signals. The procedure was as follows: a test tape was prerecorded with an alternating current of constant frequency and amplitude; this prerecorded tape was then transported past the recording head while the fluctuating direct current was flowing, causing the prerecorded signal to be erased in proportion to the current through the recording head. Each head contained a bias winding which was energized by a direct current to a point on the hysteresis curve which provided approximately linear modulation by the recording current. The system, as outlined above, would record low power direct current signals without amplification of any kind.

The frequency response of such a system was dependent on two factors: the prerecorded signal frequency, and the characteristics of the particular recording circuit. The maximum frequency that could be used for prerecording was a function of tape speed and recording head gap length. A frequency of 1,250 cps was obtained with a tape speed of 3.75 in./sec and a recording head gap length of one mil. This was the practical upper limit of the prerecorded frequency under the recording conditions listed above. The prerecorded frequency imposed a ½-cycle rise time limitation on the modulating signal, which for 1,250 cps yielded a rise time of 0.4 msec. The time constant of the complete recording system was dependent on the impedance of the recorder head, transducer, and other components in the circuit. The circuit with a large ratio of resistance to inductance would have the best frequency response. The time constant of the accelerometer and thermocouple circuits used with the NAR was approximately 1.39 msec. Thus, 3.2 msec were required for the recording current, and hence the signal applied to the tape, to reach 90 percent of maximum and 4.17 msec to

139

reach 95 percent of maximum, if a step function were applied: if a sine wave were applied to the recording head, the peak current would fall to 90 percent of the dc value as the frequency was increased from zero to 55 cps, provided the peak of the alternating voltage had been held at the dc value.

B.2.3 Transducers.
Time-history measurements of specimen acceleration, depth of melting of the specimen's surface, and temperatures at various depths below the surface were made by the instrumented spheres. Table 2.2, in Section 2.4, lists the data recorded on each channel of the recorder for all ranges.

Each instrumented sphere contained two accelerometers: one measured the acceleration along the radial line from the burst point through the specimen, and the other measured acceleration, due to the reflected shock, normal to the first but still in the plane of the shot tower and the specimen. Statham Laboratories Type A5A-1000-50 accelerometers were used for all specimens. This instrument was of the unbonded strain gage type and had a range of ±1,000 grams. The natural frequency was 2,100 cps, and it was damped with a silicone fluid (DC-200) to 65 percent of critical. Power for the accelerometers was supplied by mercury cells. Figure B.7 is a schematic showing the manner in which the accelerometers and mercury cells were connected into the recording circuit. Calibration of each accelerometer channel was accomplished by introducing given millivolt steps into the recording head and measuring the resultant deflection on the play-back oscillograms. This information, combined with the calibration factor relating grams and millivolts supplied with each instrument, permitted a calibration curve of grams versus millivolts to be drawn for each channel.

The depth-of-melt (DOM) transducer was designed to put out a pulse when the melting of the specimen had reached a predetermined depth below the surface. It consisted of two conductors insulated from each other and installed at the desired depth below surface. These conductors were connected in series with a recording channel and battery so that, when the melting had reached that particular depth, the molten metal would complete the circuit and record a pulse on the tape. The DOM transducers were made from Ceramo thermocouple wire which had the conductors encased in ceramic insulation inside a stainless steel sheath. Figure B.4 shows the DOM transducer and the manner in which it was mounted in the specimen. One specimen contained three DOM transducers at various depths, connected to a single recording channel through an appropriate resistance network. The closing of the contacts of each transducer produced a pulse of a distinctive height and thus recorded the time at which melting reached that depth. The only calibration required for a single DOM channel was the determination of the polarity of the signal produced when the two conductors were shorted. Calibration of the triplet DOM channel,

however, required the determination of the relative pulse heights from each channel as well as the polarity of the signals.

The thermocouple transducers were of the chromel-alumel type and were also made from the Ceramo wire described above. The stainless steel sheath and ceramic were cut away from the wires on one end for a distance of 0.020 inch, as shown in Figure B.4. These wires were then forced into good mechanical and electrical contact with the specimen at the particular depth where the temperature measurement was desired. The method of mounting is also shown in Figure B.4. The alumel lead from the thermocouple was connected to a relatively massive piece of alumel which served as a cold junction and was located directly behind the thermocouple installation. Figure B.7 indicates the manner in which the thermocouples were wired into the recording circuit. Calibration of the thermocouple channels was accomplished by accepting the standard chromel-alumel thermocouple tables (compiled in 1935 by the Bureau of Standards) of millivolts versus temperature and establishing the millivolt sensitivity of each channel by the method described for the accelerometers. Table B.1 presents the depths below the surface of the DOM and thermocouple channels.

The primary timing reference consisted of a 1,000 cps transistor oscillator which furnished timing information that was relatively independent of external influences. Figure B.7 contains a wiring diagram of the transistor oscillator. Because of the probable vulnerability of transistors to neutron bombardment, a secondary timing reference was incorporated in the specimen. It consisted in recording the output of a pulse transformer connected in series with the armature of the tape drive motor. Although this furnished no independent time base information, it was installed to back up the transistor oscillator just after time zero when the neutron bombardment occurred. In the course of preshot testing, it was noted that the pulse timing circuit was sensitive to rapid accelerations of the specimen. In view of this, it was hoped that some additional information, such as shock arrival time and ground impact time, could be obtained from this channel.

B.2.4 Complete Specimen.
An exploded cutaway view of the complete specimen is shown in Figure B.5. The starter assembly shown in this drawing was used to start the recorder, connect the bias batteries, and apply battery power to the accelerometers. The large accelerations to which the specimen would be subjected rendered impossible the use of most standard type switches because of their vulnerability to momentary contact opening. The switching method chosen was designed to be resistant to acceleration effects, and it consisted of a standard cannon connector which was forced and held together with a threaded rod driven by a small direct current motor. Although the external portion of the starter was swept away by the fireball, the remaining part of the

140

TABLE B.1 DEPTHS IN INCHES BELOW SURFACE OF SPECIMENS AT WHICH DEPTH-OF-MELT TRANSDUCERS AND THERMOCOUPLES WERE LOCATED

Station	50	100	150	200	250	300
Measurement	Note 1	Note 2	Note 1	Note 1	Note 1	Note 1
Independent Depth-of-Melt Transducers	0.100 0.200 0.350 0.500	0.140	0.050 0.100 0.150 0.250	0.035	0.015	0.010
Triplet Depth-of-Melt Transducers		0.070 0.140 0.210				
Thermocouples				0.020 0.070 0.140	0.015 0.030 0.060	0.010 0.020 0.040

Note 1, This instrumentation existed on side of specimen only.
Note 2, Duplicate instrumentation on both side and rear of this specimen.

threaded rod provided a plug which protected the interior of the specimen from overpressure and hot gases. This design provided a positive action switch unaffected by acceleration, and thus eliminated the need for holes through the specimen surface for electrical conductors of a conventional type switch.

Figure B.5 also illustrates the manner in which the accelerometers were mounted in the specimen. This mounting was designed, first, to make the accelerometer an integral part of the specimen, so that it would experience the same accelerations; and second, to make the accelerometer easily removable for calibration and inspection purposes. Electrical connection to the accelerometer was accomplished by connecting Sealectro Manufacturing Company's SKT-1 teflon socket terminals to the instrument and supporting them with Eccofoam FP, a foam-in-place liquid resin manufactured by Emerson and Cuming, Inc. The mating Sealectro plugs (FT-M-2) were mounted on a phenolic block and molded into the accelerometer cavity with Eccofoam, as shown in Figure B.6. The Eccofoam served a two-fold purpose: first, it filled all voids, since it was foamed in place with a material which would absorb shock; and second, it gave support to all wiring in the voids into which it was molded, as also illustrated in Figure B.6.

The recorder was mounted on the recorder cap with a $\frac{1}{8}$-inch disk of lead between the recorder and cap to act as a shock absorber. All electrical connections between the recorder and the sphere were made by a master connector located on the battery end of the recorder. This master connector mated with its counterpart when the recorder and recorder cap were inserted into the sphere. The design of this connection was such that when the recorder cap was in place and held tightly by its retaining bolts, the two halves of the master connector were held tightly

together. Orientation of the master connector plug and socket was obtained from an indexing pin which had to be aligned before the recorder cap would seat into the sphere. The specimen was designed to be oriented with the recorder cap pointing toward the burst point. Thus, the acceleration of the specimen from the shock wave would cause the recorder and sphere half of the master connector to exert a force toward the recorder cap. It was not desirable to have the recorder itself support this load, so a recorder jacket was designed to transfer the master connector load directly to the recorder cap. The recorder jacket was a steel sleeve surrounding the recorder and bearing on the master connector and recorder cap, as shown in Figure B.6. A secondary function of the recorder jacket was to provide an enclosed area which would contain the wiring and supporting Eccofoam.

Power for the accelerometers and depth-of-melt transducers was supplied by Type RM-601R mercury cells manufactured by the P. R. Mallory Company. Lead wires were soldered to the cells, and they were packaged in groups of two, end to end, inside a phenolic tube. Eccofoam was used to fill all the voids around the cells and make a solid package which could be slipped into the battery mounting holes located between the recorder cap retaining bolt holes, as shown in Figure B.5. These battery packs were designed to press tightly into the specimen so there would be no movement under high accelerations. The battery wiring was contained in the shoulder offset around the top of the recorder cavity into which all of the battery holes had an opening. Wiring from the batteries to the switch and from the transducers to the master connector was run between the recorder jacket and the specimen container wall, and then Eccofoam was foamed into this space to support the wiring and make the whole assembly solid.

141

	Preshot			Postshot	
Slant Range					
Actual, feet	Nominal, feet	Diameter, inches	Weight, pounds	Weight, pounds	Observations
46.3	50	16	584.5	496.3	Pockmarked, cracked around periphery, recorder cap extruded, inside sphere indicates crushing failure.
97.9	100	12	225	194.8	Small pockmarks, one recorder cap retaining bolt missing, no apparent cracks, structurally sound.
158.9	150	12	225	200.5	No apparent cracks, no retaining bolts missing, structurally sound.
205.2	200	12	225	199.8	Structurally sound.
257.1	250	12	225	202.3	Structurally sound.
306.4	300	12	225	200.0	Structurally sound.

A complete wiring diagram of a typical instrumented specimen is presented in Figure B.7.

B.3 RESULTS

This section presents only specimen damage results as determined from posttest laboratory analyses of the components and, in general, does not reflect the actual operating characteristics thereof. The time history data which were recorded by the specimens were presented in Section 3.3 of the main report.

Shot Erie was detonated on the 31st of May 1956 and the yield was determined to be 15.5 kt. The high level of residual radiation prevented immediate specimen recovery; however, 1 instrumented sphere was recovered 1 week after the shot. All remaining instrumented specimens were recovered approximately 4 months after the shot. The specimens were opened by drilling out the bolts holding the recorder cap, by welding a section of pipe onto the cap, and then by pulling it from the specimen. This method worked satisfactorily for all 12-inch specimens.

The 16-inch instrumented sphere was recovered on the 10th of October. It was cracked around its periphery where the two half shells were screwed together. An attempt was made to unscrew the outside shells, but only about a half turn could be made. Ultimately, a chisel was used first to pry off a portion of the cracked periphery and then to pry apart the two hemispheres.

High temperature and nuclear radiation had caused the magnetic tape to become brittle at Stations 50, 100, and 150. It was impossible to remove the tape

from the take-up reels of these recorders without breaking it into small pieces. The tape at Station 50 had also been crushed by the phenolic protective covers.

The three remaining tapes from Stations 200, 250, and 300 were capable of being played back. The Station 200 recorder had stopped upon being engulfed by the shock wave, and the tape yielded little information. The Station 250 tape was the only tape to run completely through the recorder. The high temperatures experienced by this recorder, however, caused the oxide on the magnetic tape to transfer from its normal position on the tape to the back of a preceding layer on the take-up reel. This transferred oxide side was played back along with the normal side and the combined information reduced. Some distortions of the information were evident, due to the transfer, but the information appeared reasonably good. The Station 300 tape ran for approximately 6 seconds after time zero (the specimen took approximately $1\frac{1}{2}$ seconds to hit the ground). Heat damage to the recording tape was evident but had only minor effect on the recorded information. It is believed that this station yielded reasonably good data.

B.3.1 Container Damage. A summary of container damage is presented in Table B.2.

The 16-inch specimen at Station 50 sustained considerable damage. In addition to a weight loss of 88 pounds, the outside shell was cracked and pockmarked, as shown in Figure 3.5 of the main report. The inside sphere sustained no metal loss but was cracked and extruded by the pressures and accelerations. In particular the recorder cap was extruded approximately $\frac{1}{16}$ inch into the recorder cavity by the

dynamic pressure of the shock wave. The inside sphere experienced a crushing force sufficient to distort the mercury battery holes and crack out their sides. This crushing force caused by the overpressure has been calculated to have been in excess of 135,000 psi and could have been much greater.

The 12-inch specimen at Station 100 sustained approximately 30 pounds metal loss and lost one recorder cap retainer bolt but otherwise experienced no serious mechanical damage. The remaining specimens, Stations 150 through 300, sustained metal loss as listed in Table B.2, Container Damage Summary, but otherwise were structurally unharmed.

One of the primary container functions was recorder protection. The degree of damage to the 16-inch specimen at Station 50 indicated that it did not give adequate protection to the recorder. The cracks in the outer shell definitely permitted the hot, high pressure gases inside the fireball to come in contact with the inside sphere. It is possible, but questionable, that the cracks in the inner sphere permitted a significant quantity of these hot gases to get into the recorder cavity. The 12-inch specimens at Stations 100 through 300 withstood the environmental forces at their respective ranges and provided adequate structural protection for their recorders.

B.3.2 Recorder Damage. The overall damage sustained by the North American Instruments recorders at the various ranges is illustrated in Figure B.8. The damage spread was from an essentially unharmed recorder at the farthest (300-foot) range to a completely disintegrated recorder at the closest (50-foot) range.

Table B.3 is a breakdown of component damage with respect to the damage mechanism. Since certain types of damage are difficult to attribute to particular damage mechanisms, the author presents Table B.3 with the qualification that it be considered as an opinion only.

Recording Tape. The primary damaging mechanism to the Minnesota Mining and Manufacturing Company Type 120 AM Mylar magnetic recording tape was heat. Three shot tapes (Stations 300, 250, and 200) were capable of being played back after the shot and these tapes showed no appreciable deterioration of the recorded signals. All three of these tapes exhibited heat blocking, which is a transfer of oxide from its normal position on the tape to an adjacent turn of tape on the reel. This heat blocking occurs when the 120 AM tape is subjected to temperatures in the range of 250 to 400 F. Prolonged exposure to these temperatures also causes the tape to become brittle. However, the brittleness exhibited by the three outermost shot tapes did not materially interfere with their playback. The remaining three shot tapes (Stations 150, 100, and 50) were so brittle that they would break into little pieces when an attempt was made to unwind them from the reels. Nuclear radiation, as well as heat, can cause Mylar tape to become brittle, and this may have been a contributing factor on these three tapes.

Motors. The recorder motors were manufactured by Globe Industries, and this company conducted tests on each motor, after exposure in the fireball, to evaluate damage. The following is a summary of this evaluation.

Station 250 and 300 motors were the only ones in operational condition after the detonation, and the Station 250 motor was considered marginal. The remaining four motors were not operational and showed an increase in damage as the exposure range became shorter.

Acceleration was probably the primary damaging mechanism, although neutron and heat damage contributed significantly at the closer ranges. Stations 50 and 100 motors were so badly damaged that they could not be dismantled and their components inspected. The manufacturer expressed the opinion that it was doubtful whether any motor could be built to withstand such treatment.

Acceleration was responsible for bearing failure and sticking brushes on the motors at Stations 150 and 200.

Station 150 was the only inspected motor which exhibited armature rubbing. This was probably the result of the rupturing of the main bearing housing. All permanent magnets, which could be tested, showed no deterioration in strength.

Neutron damage was evident in the electrical insulation. The insulation of the motors at Stations 150, 200, and 250 failed when 500 volts ac to ground were applied. The Station 300 motor passed this test but showed a ground at 1,000 volts alternating current. This is considered normal for this type motor.

The damage to the commutators of Station 150 and 200 could probably be attributed to heat. These commutators exhibited charred insulation, thrown solder, and commutator bars which had turned blue from heat. The heat which caused the damage could have been generated by electrical arcing.

Tape Transport. In general, the capstan assembly adequately performed its function of providing smooth power to transport the tape. Its major failing was expanding of the neoprene rubber tubing of the pinch roll, so that it became loose on its metal spindle. It is believed that heat was the main cause of this damage, since laboratory tests showed that a temperature of 400 F would cause this type of expansion. Nuclear radiation could have also contributed to the loosening of the neoprene, which was observed in varying degrees on all exposed recorders. It is the opinion of the author that the reason the recorder from Station 300 ran only 6 seconds after time zero was because the loose neoprene pinch roll caused it to jam; however, this occurred after all significant data had been recorded. At Station 250, all the tape ran through the recorder, but the neoprene tubing on the pinch roll was observed to be loose.

The fluid clutches of the take-up reels apparently operated satisfactorily for the three stations where tapes were capable of being played back. The primary damage was the increase in viscosity of the

143

Recorder Components	Heat Est. Peak Temp. Rise °F x 10²						Acceleration Est. Peak Acc. In G's x 10³						Radiation					
	10	7	6	5	4	2.5	70	67	27	11	5	2						
	Stations						Stations						Stations					
	50	100	150	200	250	300	50	100	150	200	250	300	50	100	150	200	250	300
Tape Recording Tape (120 AM)	H	H	H	M	M	L	H	OK	OK	OK	OK	OK	?	OK	OK	OK	OK	OK
Motor Overall Condition	H	H	H	H	OK	OK	H	H	H	M	OK	OK	H	H	M	L	OK	OK
Bearings	M	M	OK	OK	OK	L	H	H	H	H	OK	OK	OK	OK	OK	OK	OK	OK
Brushes	OK	OK	OK	OK	OK	OK	H	H	H	M	L	OK	OK	OK	OK	OK	OK	OK
Commutator	H	H	H	H	OK	OK	H	H	H	H	OK	OK	OK	OK	OK	OK	OK	OK
Insulation	H	H	H	H	OK	OK	H	H	H	H	OK	OK	H	M	L	L	L	OK
Tape Transport Capstan Assembly	H	H	H	L	OK	OK	H	H	M	L	OK	OK	H	H	M	M	L	L
Pulleys and Pulley Support	OK	OK	OK	OK	OK	OK	H	M	OK	OK	OK	OK	OK	OK	OK	OK	OK	OK
"O" Ring Drive Belts	H	?	?	OK	OK	OK	OK	OK	OK	OK	OK	OK	H	M	M	L	L	OK
Pay-Out and Take-Up Reels	?	OK	OK	OK	OK	OK	H	OK	OK	OK	OK	OK	OK	OK	OK	OK	OK	OK
Fluid Clutch	?	OK	OK	OK	OK	OK	H	OK	OK	OK	OK	OK	H	M	L	OK	OK	OK
Melamine Base Plate	H	H	L	OK	OK	OK	H	H	M	L	L	OK	H	H	H	M	L	OK
Electronic Components Recording Heads	H	H	M	M	M	M	H	H	H	M	OK	OK	?	?	?	?	OK	OK
Attenuating Resistors, Wire	H	H	M	L	L	L	?	OK	OK	OK	OK	OK	H	M	L	L	L	L
Wiring Insulation	H	H	M	L	L	OK	?	?	OK	OK	OK	OK	H	M	M	L	L	OK
Master Connector Material	OK	OK	OK	OK	OK	OK	L	OK	OK	OK	OK	OK	L	OK	OK	OK	OK	OK
Teflon Plugs and Sockets	L	OK	OK	OK	OK	OK	OK	OK	OK	OK	OK	OK	M	OK	OK	OK	OK	OK
Timing Circuits Complete Transistor Oscillator	H	H	M	?	?	OK	H	H	M	M	M	L	H	H	M	L	L	M
Transistors, CK-722	H	H	H	M	?	OK	H	H	H	M	M	?	H	?	?	OK	OK	OK
Capacitors, Ceramic	H	?	OK	OK	OK	OK	H	?	OK	OK	OK	OK	?	?	OK	OK	OK	OK
Transformers	H	H	?	OK	OK	OK	?	?	?	OK	OK	OK	?	?	M	L	L	OK
Resistors, Carbon	H	M	OK	OK	OK	OK	H	?	OK	OK	OK	OK	?	?	OK	OK	OK	OK
Power Silvercels	H	H	H	H	M	M	?	?	?	?	OK	OK	?	?	?	?	OK	OK
Mercury Cells	H	H	H	H	L	L	?	?	?	?	OK	OK	?	?	?	?	OK	OK
Container & Mounting Main Supporting Deck	OK	OK	OK	OK	OK	OK	H	M	L	OK	OK	OK	OK	OK	OK	OK	OK	OK
Phenolic Protective Cover	H	L	OK	OK	OK	OK	H	H	M	L	OK	OK	?	?	?	OK	OK	OK
Steel Protective Cover	L	OK	OK	OK	OK	OK	H	M	L	L	OK	OK	OK	OK	OK	OK	OK	OK
Load Disk Shock Absorber	H	H	H	H	L	OK	?	?	?	M	L	OK	OK	OK	OK	OK	OK	OK
Eccofoam	H	H	H	M	L	L	?	?	?	OK	OK	OK	?	?	?	?	L	L

OK - No Damage
L - Light Damage, Operational
M - Medium Damage, Not Operational
H - Heavy Damage, Not Operational

144

silicone fluid used in the clutch. This was probably caused by nuclear radiation and it became progressively worse for each closer range. The clutch at Station 100 was considered to be too stiff for satisfactory operation. It was also noted that the orientation of the clutch was such that acceleration would cause the silicone fluid to be driven out from between the rotating parts, thus making the clutch ineffective.

The melamine base plate, which was part of the main load carrying structure and which was used as thermal insulation between the main recorder deck and the outside case was one of the weaker components in the recorder. It satisfactorily withstood the inputs at Stations 300 and 250, only. The primary damage was delamination, probably caused by acceleration and nuclear radiation. The plate at Station 200 was only partially delaminated, the one at Station 100 was in poor condition, and the one at Station 50 was almost completely disintegrated. At the closer ranges, Stations 50 and 100, heat was undoubtedly a contributing factor to the damage of the melamine base plate.

The recording heads appeared essentially undamaged at Stations 250 and 300. The primary damage was caused by acceleration which forced the phenolic protective cover to compress the recording head cases and distort the recording channels. This compression was apparent on all recording heads at Stations 200, 150, 100, and 50, and increased progressively as the range decreased. There was also damage from the heat to which the heads were subjected at Stations 50, 100, and 150. This heat caused the potting material, supporting each channel in the head, to become fluid and run out any opening in the head casing, causing the channels to become misaligned and thereby reducing the recording efficiency. It is the opinion of the author that, after shock arrival, the heads were useless for recording purposes at Stations 150, 100, and 50, and questionable at Station 200.

The resistors used in the recording circuits for attenuation and impedance adjustment were of the wire wound type manufactured by the Sprague Electric Company under the name of Blue Jackets. Postshot inspection of these resistors from all the spheres indicated that in general the vitreous enamel coating on them had melted, but otherwise they were in good condition. This melting would have required a temperature of 650C and other components in close proximity to the resistors indicated that this temperature had not been reached. An analysis of the vitreous enamel insulation showed that it contained from 1 to 10 percent boron. Melting of the vitreous enamel coating was therefore attributed to neutron bombardment of the boron and its subsequent alpha decay. Calculation of the effect of this heating on recording, due to resistance changes, indicated that the error introduced would be less than 10 percent. Although the resistors were not destroyed from an operational viewpoint and the neutron damage to the vitreous enamel coating, their use in future specimens of this type is not recommended.

The insulation of the wire used in the North American Recorder was of the thermoplastic type. This insulation held up satisfactorily at Stations 200, 250, and 300. There is serious doubt as to its adequacy at the remaining three stations. The main causes of damage seemed to be heat and nuclear radiation. Heat probably was the main cause of the deterioration of the insulation at Stations 50, 100, and 150. The insulations at Stations 200, 250, and 300 showed discoloration and some brittleness, which could have been caused by nuclear radiation.

The master connector was made of phenolic with an asbestos filler, Type AA. This material probably stood up better than any other nonmetallic material in the entire specimen. It was one of the few components from the recorder at Station 50 which experienced such minor damage that it could be used again. The only noticeable change was a darkening of color from heat or nuclear radiation and a slight bowing probably due to acceleration.

The teflon plugs and sockets used to make the electrical connections from the recorder to the specimen sustained little damage. A color change was observed at some of the stations farther out, but Station 50 was the only one with any appreciable damage. This consisted of swelling which could have been due to heat, radiation, or both.

Transistor Oscillator. Postshot laboratory tests showed that all six oscillators were inoperative upon recovery. Here again it should be pointed out that the damage results presented below are merely those determined by these posttest analyses and are not, in general, concerned with the operation of the components. Structurally, the oscillators at Stations 50 and 100 were almost completely destroyed by heat and, consequently, no shock damage could be observed. Heat damage to the oscillators from Stations 150 through 300 varied from medium to light and in only two cases, Stations 200 and 250, was there conclusive evidence of shock damage. This damage was manifested at Station 250 as a severe crack in the plastic potting material; the two portions of the oscillator were held together only by the internal wires and components. At Station 200 the potting material was also cracked although not as severely. The various components of the oscillators were removed, with some difficulty, from the potting material and individual tests were performed to ascertain the damage sustained by each component. The results of these tests are discussed below.

The transistors used in the oscillator were Type CK-722. All the transistors successfully removed from the potting material were inoperative. The emitter and collector junctions of the Station 300 transistors were severely degraded and showed rectification ratios of only three or four. Transistors from Stations 100 and 150 exhibited visible evidence of high temperature exposure; on the other hand, those from Stations 200, 250, and 300 had evidently

145

not been exposed to such high temperatures. Observable damage sustained by the transistors was of the type that could have been caused by heat, nuclear radiation, or both.

Capacitors used in the oscillator were of the ceramic disk type. No capacitor data was obtained from Station 50 because of the extensive heat damage and from Station 100 because of an open circuit. At the remaining stations, 150, 200, 250, and 300, the disk capacitors were in operational condition and apparently unharmed.

Transformers used in the oscillators were of the subminiature type especially designed for transistor circuits. Transformers in the oscillators at Stations 50 and 100 were found to be inoperative after the test because of the extensive heat damage. Posttest measurements on the transformers at Stations 150, 200, and 250 showed that the primary windings were essentially unharmed and that the secondary windings had open circuits. The transformer at Station 150 showed evidence of minor heat damage. The Station 300 transformer was essentially unharmed by the test.

Carbon resistors used in the oscillator apparently suffered no physical damage or resistance changes at Stations 100 through 300. No data was obtained from the Station 50 oscillator. Resistors from Stations 100, 200, and 300 were checked and found to be good after the test; and, although Stations 150 and 250 resistors were broken during the process of removal from the potting material, they appeared physically unharmed.

Batteries. Primary damage mechanism of the silvercel was heat. Laboratory tests showed that the silvercel cases were deformed when the cell was heated to approximately 250F for 15 minutes. The electrolyte boiled at about the same temperature. The cells were further tested by heating them from 300 to 350F for about 40 minutes. This resulted in severe damage, which completely ruined the cells as a source of electrical power. The damage level of this second test closely approximated that at Station 200 and was not much worse than the damage observed at Stations 250 and 300. The silvercels at Stations 150, 100, and 50 were damaged to such an extent by the heat that they were almost unrecognizable. Because of the severe heat damage, the extent of the acceleration and nuclear radiation damage could only be estimated.

Mercury cells apparently were physically unharmed at Stations 250 and 300. The effects of radiation and heat at these stations are unknown. At Station 200 the mercury cell in the battery container used as bias supply was badly damaged. The inside portion was pushed out from the bottom of the steel case approximately $\frac{1}{4}$ inch. This type of damage probably was caused by nuclear radiation or heat, which built up an internal pressure and thereby forced the inside of the cell out, for it is doubtful that the acceleration could have brought this about. Another verification of the internal pressure theory

was obtained from the damage to the mercury cells used for accelerometer power. They were located in holes between the recorder cap bolt holes in the main specimen body. The cells were completely enclosed by the specimen, except for small openings for the wires which connected the cells to the accelerometers. Postshot inspection of the specimens exposed at Stations 50 and 150 resulted in the discovery of holes in the sides of the mercury cell cases adjacent to the openings through which had passed the connecting wires from the cells. Around the edges of these holes jagged metal from the mercury cells protruded, indicating that the holes were the result of internal pressure. The mercury bias cell in the recorder at Station 150 was completely disintegrated from heat or radiation.

Container and Mounting. The main supporting deck of the recorder was essentially undamaged at Stations 200, 250, and 300. Acceleration loading, which was the only mechanism to damage the main supporting deck, caused the deck to dish in approximately $\frac{1}{16}$ inch at Station 150, $\frac{1}{4}$ inch at Station 100, and $\frac{3}{4}$ inch at Station 50. The total damage at Station 150 was relatively minor, but the deck was definitely damaged beyond repair at Station 50.

The phenolic protective cover was essentially undamaged at Stations 250 and 300. The primary damage mechanism was acceleration loading. The Station 200 cover showed some cracks, but the damage was minor. The covers at Stations 150 and 100, however, showed extensive cracking and chipping of the phenolic but they were still in one piece. The cover at Station 50 was broken into many pieces, closely resembling charcoal in appearance, indicating extensive heat damage. The effects of heat, and possibly radiation, were also noticeable at Station 100 and to a lesser degree at Station 150 in the form of a color change and some blistering.

Damage to the steel protective cover was probably due exclusively to the acceleration loading. Stations 250 and 300 covers were undamaged, and the only damage sustained by the covers of Stations 150 and 200 was a slight dishing in of the top where they were bearing on the lead disk shock absorber. The top of the cover at Station 100 was dished in approximately $\frac{1}{8}$ inch, and most of the bolts holding the main supporting deck to the steel protective cover were sheared. The cover was badly damaged at Station 50; its top was separated from the cylindrical portion and badly dished. The cylinder was bowed out in a manner which indicated that it had been subjected to an axial load greater than it could support. Some portions of the cover were discolored from heat and some were covered with molten lead.

The lead disk used as a shock absorber for the recorder was essentially undamaged at Station 300. Station 250 showed some extrusion of the lead around the mounting holes, due to acceleration, as well as a few places where the heat had caused the lead to melt. Extrusion by acceleration was evident at Station 200, along with extensive melting caused by the

146

Station	Orientation	Damage mechanisms			Total prompt damage[a]
		Heat	Acceleration	Radiation	
50	Radial	H	H	H	H
	Normal	H	H	H	H
100	Radial	M	H	H	H
	Normal	H	H	H	H
150	Radial	L	H	M	H
	Normal	M	H	M	H
200	Radial	L	L	L	L
	Normal	L	OK	L	L
250	Radial	OK	OK	OK	OK
	Normal	OK	OK	OK	OK
300	Radial	L	OK	OK	OK
	Normal	L	OK	OK	OK

[a]Damaged before or during shock engulfment.
OK, No damage
L, Light Damage (Operational)
M, Medium Damage (Not operational)
H, Heavy Damage (Not operational)

heat. Extrusion effects caused by the acceleration were obliterated by the extensive melting at Station 150, and the lead had been completely melted at Stations 50 and 100.

B.3.3 Transducer Damage. Transducers used in the instrumented spheres can be divided into two divisions: accelerometers, and thermocouple type transducers which include thermocouples and depth-of-melt instruments.

Accelerometers. Damage to the Statham accelerometers ranged from essentially unharmed instruments at Stations 250 and 300 to heavily damaged instruments at Stations 50 and 100. Table B.4 breaks down the accelerometer damage according to mechanism and exposure range.

The heavy acceleration damage experienced by Stations 50, 100, and 150 accelerometers consisted of deformed cases, broken electrical insulators, deformed strain wire supports, and sheared bolts which held the back plate in place. The normal accelerometers at Stations 50 and 100 were permanently bent along their wide axis, and this bending could have been caused only by the large accelerations experienced by the specimens. The main supporting lugs of the radial accelerometers, which were loaded in shear, showed no evidence of failure. The radial accelerometer at Station 200 sustained light acceleration damage in the form of one broken insulator. The normal accelerometer at Station 200 and both accelerometers at Stations 250 and 300 showed no evidence of any damage caused by acceleration.

Heat damage to the accelerometers in the form of melted solder (causing electrical circuits to become open or shorted) and charred components such as wire insulation and resistors was evident from Sta-

tion 50 through 300 as noted in Table B.4. Charring of components was the principle heat damage mechanism at Stations 50, 100, and 150, and melting solder was the predominant mechanism at Stations 200, 250, and 300. It should be noted that the heat damage was probably a delayed effect, since the peak temperature was not reached until some time after the specimen was in the ground, and therefore would not have prevented the instrument from functioning normally during the period of interest.

Thermocouples and Depth-of-Melt. In general, the thermocouples and depth-of-melt transducers sustained no unexpected damage. The metal loss of the specimens in the vicinity of the transducers was generally greater than the thickness of the diaphragm behind which the transducer was located for the ceramo end was visible on many specimens. At Stations 200, 250, and 300, the magnesium oxide insulation was apparently unharmed, and the chromel-alumel wires were in good condition on most of the transducers. Most of the transducers on the specimens at Stations 50, 100, and 150 were ob-

147

scured by foreign material, but the ones which could
be inspected appeared to be in reasonably good con-
dition.

B.4 DISCUSSION

A total of 10 time-history curves, recorded inside
the fireball, is presented in Section 3.3 of the main
report. These consist of two acceleration and three
temperature time-history curves each from Stations
250 and 300. The accuracy and reliability of the data
from Station 250 were materially reduced by the heat
blocking sustained by the recording tape. The data
collected by Station 300 was also impaired by heat
damage to the recording tape but to a lesser degree.

Although these data have a relatively low accuracy
and reliability compared to data collected under less
severe environmental conditions, there is general
overall consistency and reasonable correlation with
some known values, such as shock arrival time.

B.4.1 Damage Mechanism. Table B.5 presents a
summary of the damage sustained by the major com-
ponents of the instrumented spheres in Operation
Redwing. The table separates the damage according
to heat, acceleration loading, and nuclear radiation,
as well as according to range within these general
damage mechanisms. Overpressure crushing was
not listed, since it was only significant on the 16-
inch specimen at the 50-foot range.

Heat damage was most significant on the recorder
and recording tape and to a lesser degree on the
transistor oscillators and accelerometers as indi-
cated in Table B.5. Since it is improbable that neu-
tron heating contributed significantly to the total heat
input of the specimen, with the possible exception of
the 50-foot station, the heat damage would not have
occurred until well after the specimen had completed
its recording and was in the ground. Table B.5,
therefore, contains a Total Damage column as well
as a Total Prompt Damage column. It should be
noted, however, that the existence of damage to the
recording tape is significant, rather than the time at
which the damage was sustained.

Acceleration damage was significant on the re-
corder, accelerometers, and transistor oscillators.
Figure B.9 illustrates the type of damage sustained
by the recorder and accelerometers. Analysis of this
damage, along with the determination of the static
strength of the various damaged components, yielded
maximum and minimum values for the acceleration
which caused the damage. Figure B.9 explains the
manner in which the acceleration damage values were
calculated and presents these maximum and mini-
mum values for each instrumented sphere. It should
be noted that the peak accelerations listed in this
table refer to the specimen proper. The recorder
may have experienced a significantly lower peak ac-
celeration, since it was supported on a lead sheet,
which, through extrusion, would have reduced the
peak acceleration. A good example of this is the Sta-

tion 100 specimen which, according to Figure B.9,
experienced a peak acceleration between 82,000 and
55,000 grams; however, the recorder case which
buckles at 24,000 grams showed no sign of failure.

Nuclear radiation damage was evident on the re-
corder, accelerometers, transistor oscillator, and
recording tape as listed in Table B.5. Because of the
difficulty in separating nuclear radiation damage
from other damage mechanisms, the component dam-
age listed in Table B.5 should be considered only as
the author's best estimate.

Prior to this test, one of the big unknown factors in
electrical recording within the fireball was the pos-
sible effect on the recording system of the electro-
magnetic energy released by the detonation. Inspec-
tion of the recorded signals in the vicinity of time
zero at Stations 200, 250, and 300 showed, in general,
little disturbance on the accelerometer and thermo-
couple channels. The depth-of-melt and motor timing
channels showed definite time zero disturbances, but
these were of such small amplitude that they caused
no recording circuit damage. It is evident, therefore,
that under similar exposure conditions the electro-
magnetic energy from a detonation comparable to
Shot Erie would not seriously damage electrical re-
cording specimens similar to those used on Redwing
at slant ranges beyond 200 feet.

B.4.2 System Evaluation. The Operation Red-
wing test showed that it is feasible to record data
electrically inside the fireball of a nuclear detona-
tion with a system similar to that used on Operation
Redwing. It is believed that there are no insurmount-
able obstacles to recording data with an improved
system of this type at slant ranges in the vicinity of
150 feet for device yields comparable to Shot Erie.

The following is an evaluation of each component in
the system:

Container (Specimen Body)
1. The containers at Stations 100 through 300
structurally withstood the fireball environment.
2. The Station 50 container did not give adequate
structural protection to the recording system.
3. All six containers provided inadequate thermal
protection for their recorders.
4. It is evident that the containers at Stations 200,
250, and 300 provided adequate electromagnetic
shielding for their respective recording systems.

Recorder
1. Assuming that heat damage was not a prompt
mechanism, the NAR recorder (exclusive of record-
ing tape) operated satisfactorily at Stations 250 and
300.
2. Acceleration effects were the most important
reason the recorder at Station 200 did not operate
satisfactorily.
3. Acceleration and nuclear radiation were the
major reasons the recorders failed at Stations 50,
100, and 150. Neutron heating, a prompt mechanism,
may have been important at Station 50.

148

TABLE B.5   DAMAGE MECHANISM SUMMARY

System Component	Heat Station						Acceleration Loading Station						Nuclear Radiation Station						Total Damage Station						Total Prompt Damage * Station					
	50	100	150	200	250	300	50	100	150	200	250	300	50	100	150	200	250	300	50	100	150	200	250	300	50	100	150	200	250	300
Container							X												X						X					
Recorder	X	X	X	X	X	X	X	X	X	X			X	X	X				X	X	X	X	X		X	X	X	X		
Recording Tape	X	X	X	X	X		X						X						X	X	X	X	X		X					
Transistor Oscillator	X	X	X	X			X	X	X	X	X		X	X	X				X	X	X	X	X	X	X	X	X	X	X	X
Accelerometer	X	X	X				X	X	X				X	X	X				X	X	X				X	X	X			
Thermocouple & Depth-of-Melt																														

X - Not Operational
Blank - Operational
* - Damaged Before Or During Shock Engulfment

4. The recording tape at Stations 250 and 300 experienced heat damage to the extent that it significantly reduced the accuracy and reliability of the data.

Transistor Oscillator

1. It is highly probable that none of the six transistor oscillators operated completely through the period of interest.

2. Two oscillators, Stations 200 and 250, operated through time zero and stopped at shock arrival.

3. The Station 300 oscillator stopped at time zero.

Transducers

1. The accelerometers used in this system operated satisfactorily at Stations 250 and 300 but not at the closer stations.

2. In general, this type of accelerometer was unsatisfactory for measurements of this nature because of its low electrical output and the viscosity changes of the silicone damping fluid caused by the neutron bombardment.

3. The thermocouple and depth-of-melt transducers mechanically withstood the environment of their respective stations and operated satisfactorily at the stations from which data were obtained. It is possible that the thermocouple channels may have had intermittent contact with their diaphragms during the period of interest.

B.4.3 System Improvement. Since the Operation Redwing test was one of the first attempts to record data electrically within the fireball of a nuclear detonation, it follows that the system used was necessarily a first approximation to the problem. Although the Operation Redwing system achieved only moderate success in the recording of data, it provided an appreciation of the type and magnitude of the problems encountered in such data collection, which could be obtained in no other manner. The important modifications of the Operation Redwing system, as indicated from Operation Redwing experience, are discussed in the following paragraphs.

The Operation Redwing containers could be improved in two ways: (1) give more thermal protection to the recorder, and (2) provide a better method of reducing the peak acceleration experienced by the recorder. The thermal protection of the recorder could be improved by covering the outside of the container with some heat resistant material such as phenolic resin. The recorder could be further protected from the heat by surrounding it with a low heat conductive material inside the container. These two improvements would materially decrease the heat problems in future container designs. The acceleration of the whole specimen, assuming it is approximately the size and shape of the Operation Redwing specimens, is determined by the slant range and device yield of the particular exposure. Since the specimen acceleration cannot be reduced, the only way the peak acceleration experienced by the recorder can be reduced is to allow relative motion between the recorder and the specimen. This move-

ment should be allowed while accelerating the recorder at some relatively low constant rate. Thus, the recorder will attain the velocity of the specimen without experiencing the large, damaging, peak acceleration of the specimen.

Since the North American Miniature recorder (NAR) was not designed for recording in the extreme environment of the fireball, it had some components which would not withstand the inputs associated with this type of recording. It is, therefore, suggested that future attempts at recording within the fireball should be made with a recorder specifically designed for this type of recording. Table B.3, Recorder Damage Summary, indicates the areas where improvements in a new recorder design could be made. This table indicates that the major portion of the damage at Stations 150, 200, 250, and 300 was due to heat and acceleration. An improved container design could reduce these damage mechanisms, leaving nuclear radiation as the only mechanism which cannot be substantially reduced. Selection of proper materials in designing an improved recorder could probably reduce this damage to the point where successful recording at 150 feet from a shot of comparable yield would be feasible. An increased frequency response should be a design requirement for such an improved recorder, and a temperature resistant recording tape should be used for all future tests. A transistor oscillator, properly shock mounted, thermally insulated, and using radiation resistant transistors, may be capable of furnishing time base information for future recorders.

A different type of accelerometer from that used on Operation Redwing should be used in future tests. This accelerometer should operate on direct current, have a relatively high electrical output, high frequency response, and should not use silicone fluid as a damping medium. The only modification suggested for the thermocouple transducer is an improved mount to prevent possible intermittent contacts. Since depth-of-melt transducers do not yield as much information as thermocouples, it is suggested that only thermocouples be installed for this type of information.

If the above improvements were made in a future recording system, it should be capable of recording data at slant ranges in the vicinity of 150 feet on yields comparable to Shot Erie.

B.5 CONCLUSIONS AND RECOMMENDATIONS

B.5.1 Conclusions

1. The Operation Redwing test has shown that it is feasible to record data electrically inside the fireball of a nuclear detonation with a system similar to that used on Operation Redwing.

2. An electrical recording system similar to that used by Project 5.9 in Operation Redwing and with improvements indicated by Operation Redwing experience should be capable of recording data at slant

ranges in the vicinity of 150 feet on yields comparable to Shot Erie.

3. The containers gave adequate structural protection for the recording system at all stations except Station 50.

4. Adequate electromagnetic shielding was provided by the containers for slant ranges of at least 200 feet.

5. All six containers provided inadequate thermal protection for their recorders.

6. Exclusive of recording tape, the North American recorder operated satisfactorily at Stations 250 and 300 and the remaining recorders failed because of acceleration and nuclear radiation effects.

7. The recording tape experienced heat and nuclear radiation damage of varying degrees in all specimens; however, data were obtained from the tapes at Stations 200, 250, and 300.

8. With adequate precautions, transistor oscillators may be capable of operation within the fireball of a nuclear detonation in a specimen of the Operation Redwing type.

9. Reliable and accurate temperature measurements using thermocouples should be feasible within the fireball of a nuclear detonation employing the method used in the Operation Redwing test.

10. The accelerometers used in the Operation Redwing specimens were unsatisfactory for measurements of this type.

B.1.2 Recommendations. It is recommended that:

1. Future programs concerned with effects and phenomena within or near the fireball of a nuclear detonation consider the use of an electrical recording system similar to the Operation Redwing system for data collection.

2. In future designs the thermal characteristics of the container be improved to give more thermal protection to the recorder.

3. In future designs the acceleration experienced by the recorder should be reduced by some method, such as allowing relative moment between the specimen and the recorder.

4. Future attempts to electrically record within the fireball should be made with a recorder specifically designed for this type of recording.

5. Temperature resistant magnetic recording tape should be used for all future magnetic data recording within the fireball.

6. Thermocouples should be used as transducers for temperature measurements similar to those made within the fireball of Shot Erie by Project 5.9 on Operation Redwing.

7. For acceleration measurements in future tests similar to Project 5.9, only accelerometers specifically designed for their function should be employed.
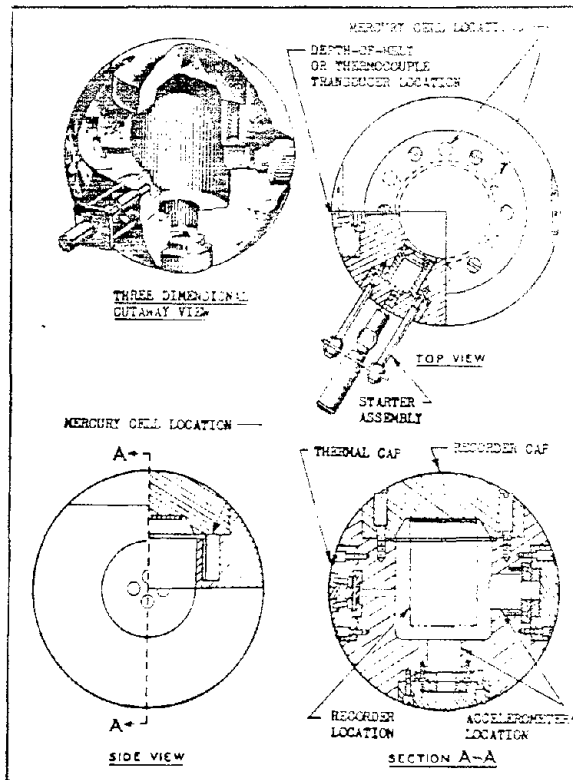
Figure B.1 Twelve-inch instrumented sphere container.

BURST POINT

RECORDER

ACCELEROMETER

STARTER

12-Inch Instrumented Sphere

BURST POINT

INNER SPHERE

STARTER

16-Inch Instrumented Sphere
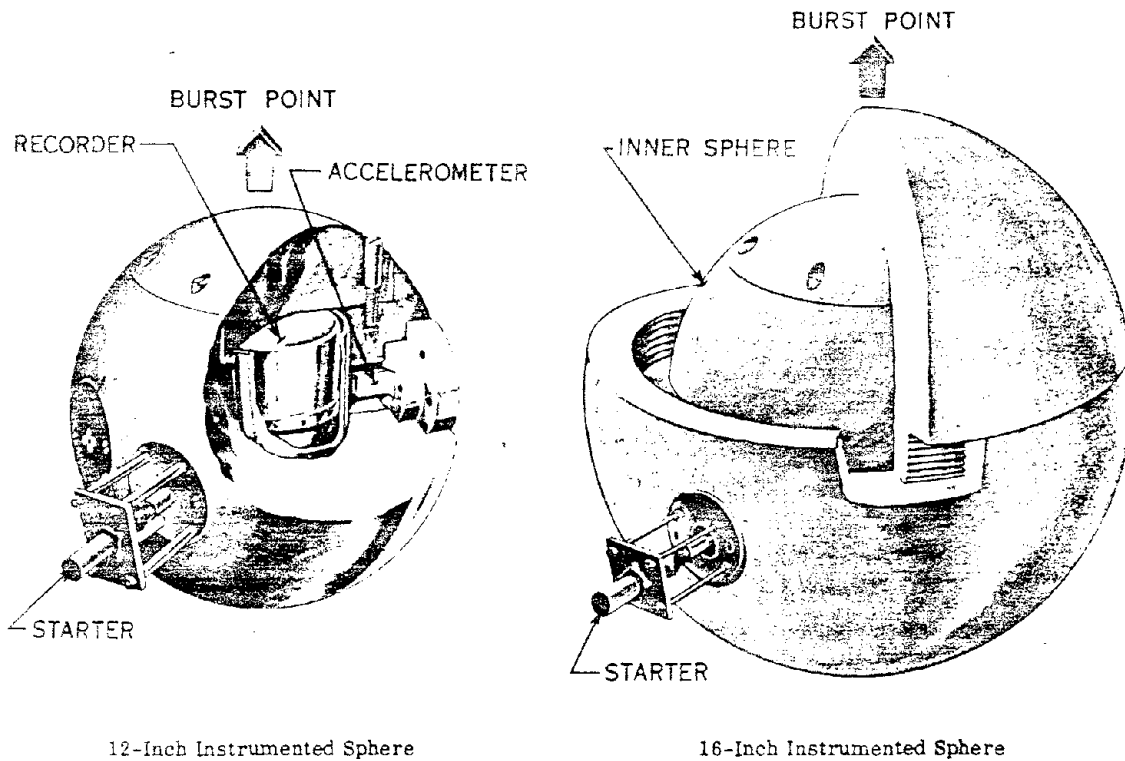
Figure B.2 Instrumented spheres.

152
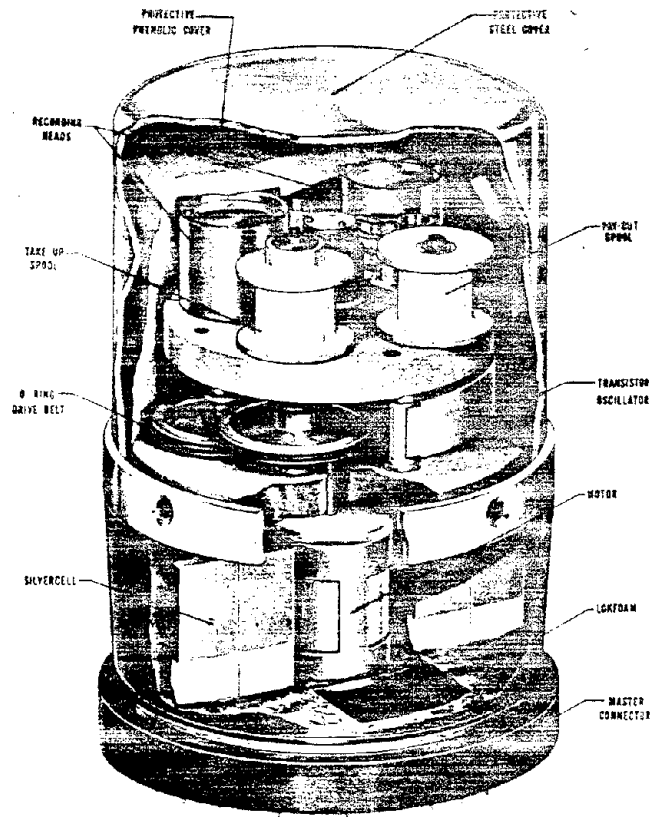
Figure B.3   North American miniature recorder.

CERAMO

.020

RETAINING
SCREW

PLUG

THERMOCOUPLE

CAP

THERMOCOUPLE   DEPTH OF MELT   TYPICAL INSTALLATION
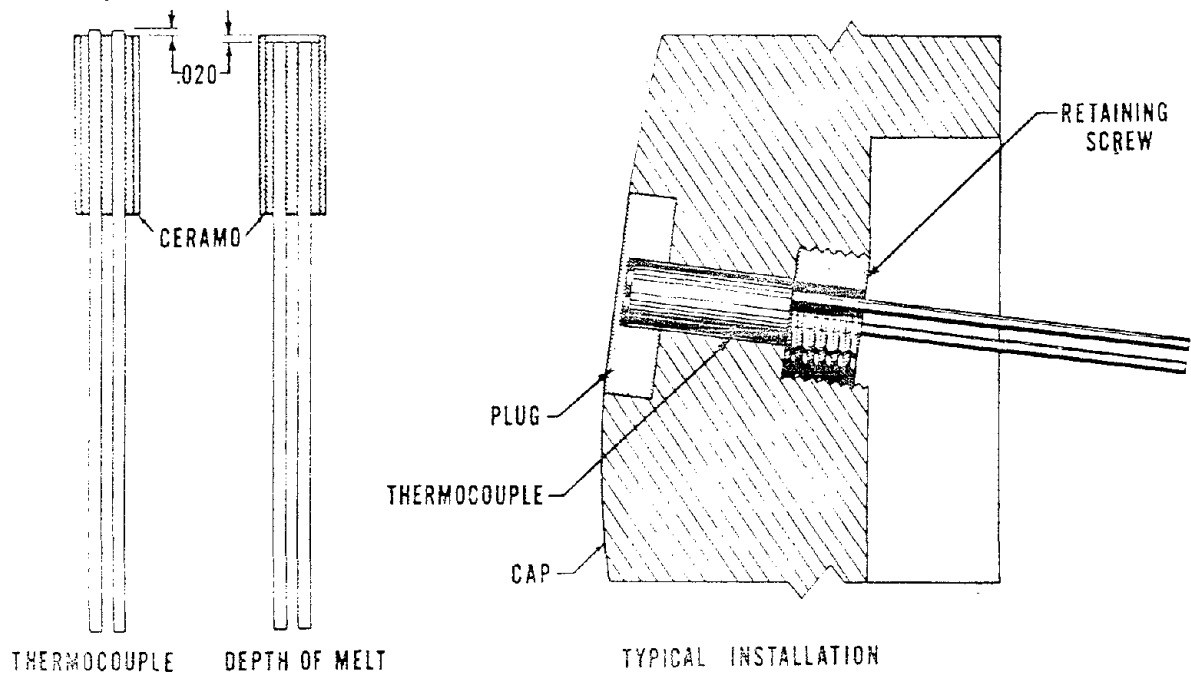
Figure B.4   Design and installation of thermocouple and depth-of-melt transducers.

153
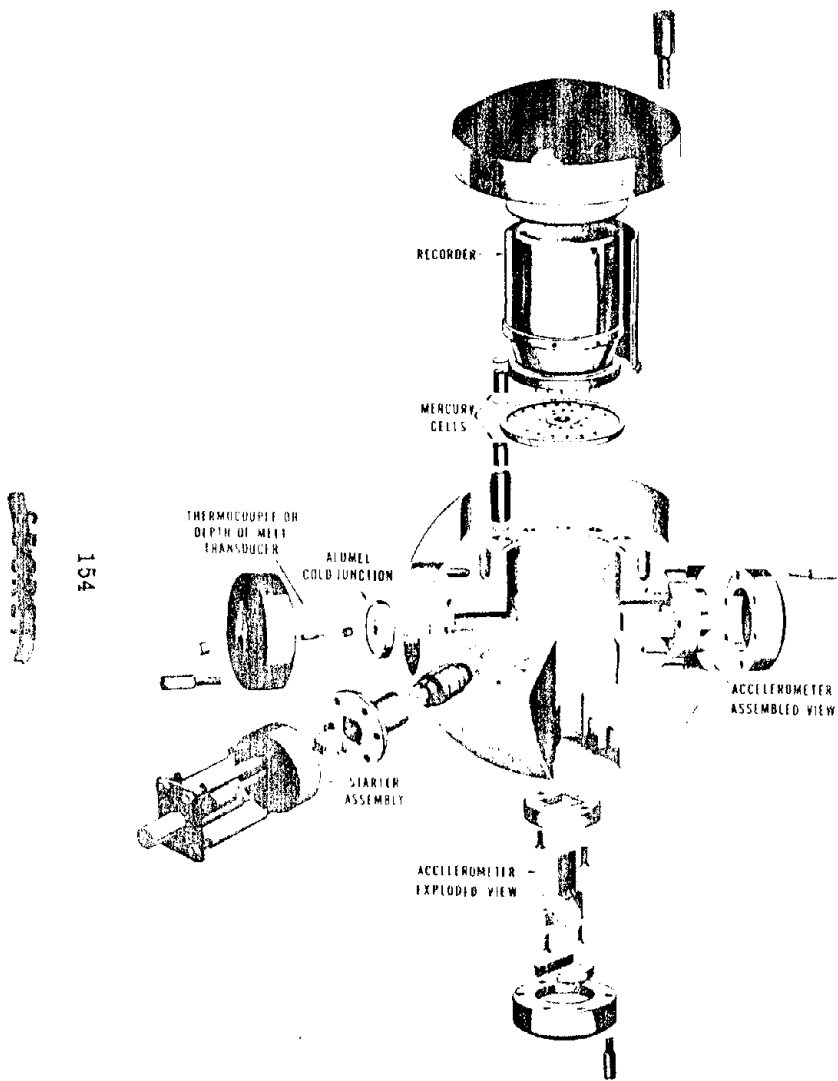
Figure B.5 Exploded view of a typical 12-inch instrumented sphere.

RECORDER

MERCURY
CELLS

THERMOCOUPLE OR
DEPTH OF MELT
TRANSDUCER

ALUMEL
COLD JUNCTION

ACCELEROMETER
ASSEMBLED VIEW

STARTER
ASSEMBLY

ACCELEROMETER
EXPLODED VIEW
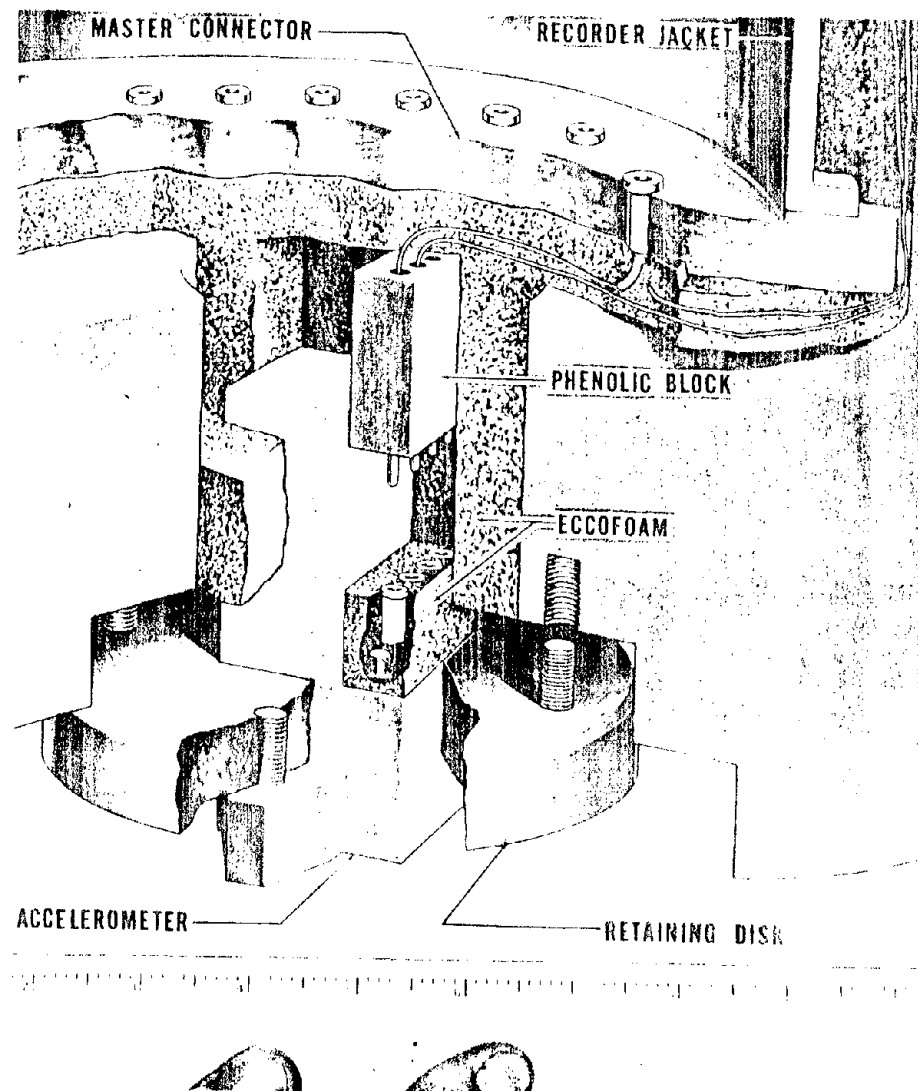
Figure B.6 Typical accelerometer installation showing eccofoam.

MASTER CONNECTOR

RECORDER JACKET

PHENOLIC BLOCK

ECCOFOAM

ACCELEROMETER

RETAINING DISK
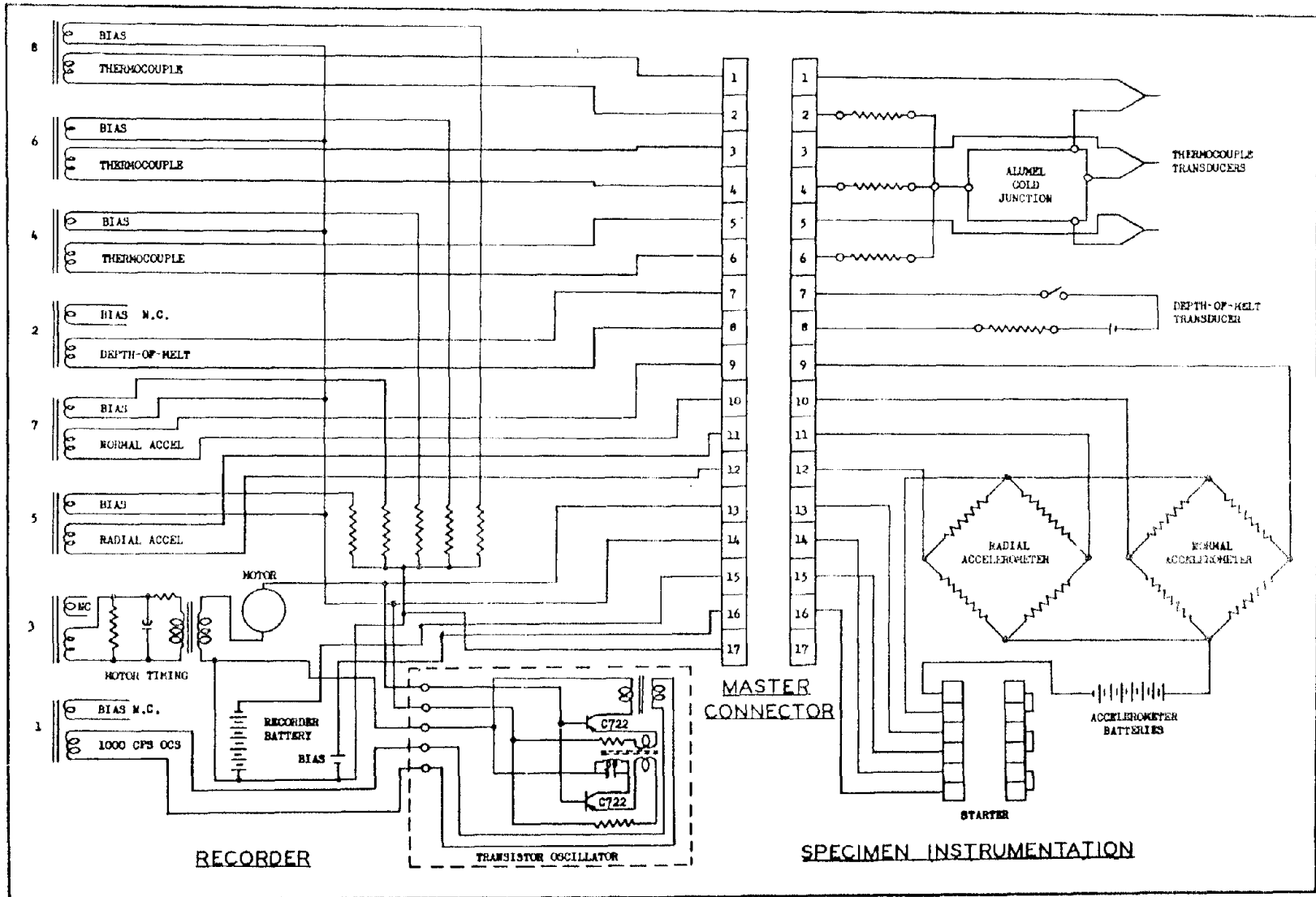
Figure B.7   Schematic wiring diagram of a typical 12-inch instrumented sphere.
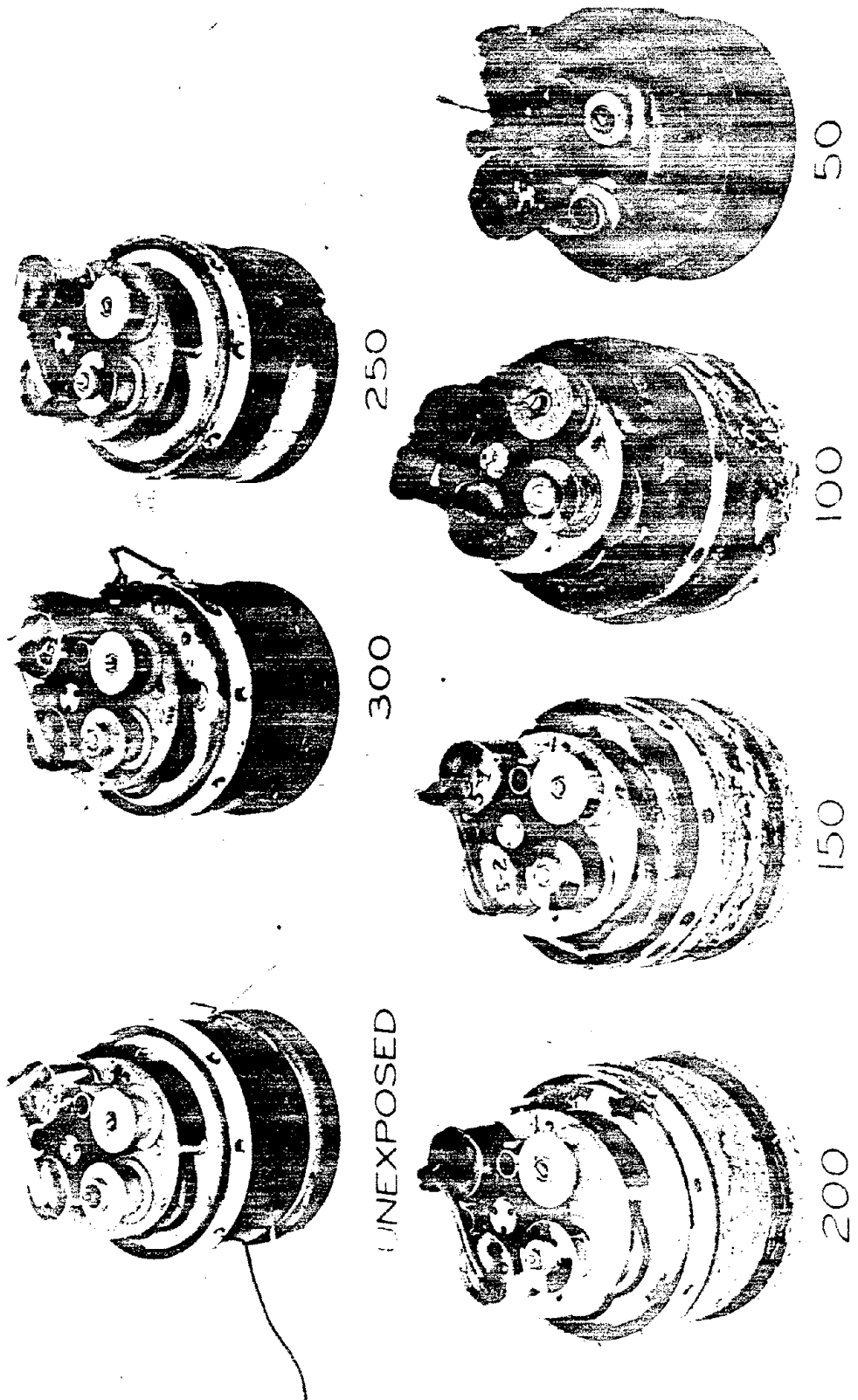
Figure B.8 Miniature recorder damage at Stations 50 through 300.

50

100

150

200

250

300

UNEXPOSED

ASSUMING ACCELEROMETER CASE TO BE A SHORT CANTILEVER BEAM WITH POINT LOADS (WEIGHT OF COMPONENTS & EXTENDED PORTION OF CASE ACTING THROUGH THEIR RESPECTIVE CENTROIDS), STATIC ANALYSIS THEN YIELDS A MINIMUM VALUE OF 55,000 G'S ±20% REQUIRED TO PERMANENTLY BEND THE CASE.

PERMANENT CASE BENDING REQUIRES 55,000 G'S ±20%.

BLAST

NORMAL ACCELEROMETER

1/8" LEAD SHOCK ABSORBER PLATE

STATIC ANALYSIS OF ACCELERATION REQUIRED TO EXTRUDE LEAD PLATE AT RECORDER CASE TOP YIELDS A MINIMUM VALUE OF 1,800 G'S ±10%.

RECORDER

INERTIA OF ACCELEROMETER TENDS TO MAKE IT REMAIN STATIONARY WHILE THE MOUNTING RING ACCELERATES IN A DIRECTION PARALLEL TO THE BLAST, THUS IT WOULD CAUSE BENDING OF THE NORMAL ACCELEROMETER'S CASE AND SHEARING OF THE RADIAL ACCELEROMETER'S MOUNTS.

LEAD PLATE SHOWING EXTRUSION

ACCELEROMETER MOUNTING RING

RADIAL ACCELEROMETER

BUCKLED RECORDER CASE REQUIRED 24,000 G'S ±10%.

MOUNTS WILL SHEAR AT 82,000 G'S ±10%.

ASSUMING RECORDER CASE TO BE A SHORT THIN-WALLED CYLINDER IN COMPRESSION, WITH A PLATE FIRMLY ATTACHED TO ONE END; STATIC ANALYSIS OF THE ACCELERATION REQUIRED TO BUCKLE THE CASE YIELDS A MINIMUM VALUE OF 24,000 G'S ±10%.

STATIC ANALYSIS OF THE ACCELERATION REQUIRED TO SHEAR ACCELEROMETER MOUNT (DOUBLE SHEAR) YIELDED A MINIMUM VALUE OF 82,000 G'S ±10%.

OBSERVED DAMAGE						
SPECIMEN STATIONS IN FT.	50	100	150	200	250	300
ACCELEROMETER MOUNT SHEARED	NO	NO	NO	NO	NO	NO
ACCELEROMETER CASE BENT	YES	YES	NO	NO	NO	NO
RECORDER CASE BUCKLED	YES	NO	NO	NO	NO	NO
LEAD IMPACT PLATE EXTRUDED	YES	YES	YES	YES	YES	NO

ESTIMATED SPECIMEN ACCELERATION		
STA.	MAXIMUM ACCELERATION	MINIMUM ACCELERATION
50	82,000 G'S ±10%	55,000 G'S ±20%
100	82,000 G'S ±10%	55,000 G'S ±20%
150	55,000 G'S ±20%	1,800 G'S ±10%
200	55,000 G'S ±20%	1,800 G'S ±10%
250	55,000 G'S ±20%	1,800 G'S ±10%
300	1,800 G'S ±10%	

Figure B.9   Recorder and accelerometer acceleration damage.

Appendix C

VELOCITY-DISTANCE IMPACT GASSES

C.1 OBJECTIVE

The ultimate objective of the velocity-distance instrumentation was the obtaining of a plot of actual specimen velocity versus specimen traveled distance from which a specimen acceleration versus time plot could be derived by the method presented in Section C.2.5.

C.2 PROCEDURE

The manner by which the velocity versus distance data were obtained involved the use of impact gages. The gage was a device for measuring the relative velocity, at the time of contact, between the impact block and the plunger. It was an energy absorbing instrument based upon the empirical fact that, when a freely supported hardened steel plunger penetrates a soft aluminum block, the penetration is some function of the change in kinetic energy of the plunger. The instrument consisted of a soft metallic impact block and a steel tube, which were integral parts of the test specimen, and a hardened steel plunger which rested freely in the tube at a preset distance from the impact block. As the specimen accelerated in a direction parallel to the axis of the tube, the specimen, the impact block, and the tube moved; however, the plunger, due to its inertia, was assumed to remain stationary. After the specimen had moved a distance equal to the initial distance between the block and plunger, the plunger would contact the block and be accelerated until it reached the same velocity as the specimen. The force required to accelerate the plunger would cause it to penetrate the soft target block, and the magnitude of penetration was an indication of the change in velocity of the plunger. The degree of penetration, however, was not only a measure of the velocity of the target block at impact, but also a measure of the acceleration of the target block during penetration. To obtain velocity versus distance data, plungers were set at various initial distances from the target block and the depths of penetration were

measured. These penetrations were then compared to the calibration data and a so-called calibration velocity, which was that velocity required to yield the same penetration, was determined. Since the calibration was performed with zero acceleration on the target block, these calibration velocities then had to be corrected to eliminate the effects of the acceleration during penetration. Figure C.1 is a sketch of a specimen with seven plungers, each set at a different distance from the block.

C.2.1 Theory. This section is intended to present the theory involved in determining the true velocity versus distance data from test data which contains the effects of acceleration during penetration in addition to the impact velocity effects. To facilitate discussion, it is desirable to establish the nomenclature listed in Table C.1.

The depth of penetration is related to the displacement of the specimen and plunger by the following relationship:

$$\delta = X_s - X_p + \text{const.} \qquad (C.1)$$

where the constant generalizes the equation for any reference plane. Differentiating Equation C.1 with respect to time gives relationships involving velocity and acceleration.

$$\dot{\delta} = \dot{X}_s - \dot{X}_p, \qquad (C.2)$$

and

$$\ddot{\delta} = \ddot{X}_s - \ddot{X}_p. \qquad (C.3)$$

From the calibration data, it is possible with certain assumptions to write an explicit expression of force as a function of penetration (Section C.2.2). Since this is the only force acting on the plunger (neglecting friction), one has $\ddot{X}_p = F(\delta)/m_p$. Rewriting Equation C.3 and using the above expression,

$$\ddot{\delta} + \frac{F(\delta)}{m_p} = \ddot{X}_s. \qquad (C.4)$$

158

TABLE C.1   NOMENCLATURE

C_d	coefficient of drag
F	instantaneous force on the plunger during penetration
$\bar{F}$	average force on the plunger during penetration
P	force on specimen
S_n	normalized displacement
V_c	velocity indicated by calibration data for a given depth of penetration
V_n	normalized velocity
V_0	actual velocity of specimen at the time of contact with the plunger
X_s	displacement of specimen
$\dot{X}_s$	dX_s/dt velocity of specimen
$\ddot{X}_s$	d^2X_s/dt^2 acceleration of specimen
X_p	displacement of plunger
$\dot{X}_p$	dX_p/dt velocity of plunger
$\ddot{X}$	d^2X_p/dt^2 acceleration of plunger
δ	depth of penetration of plunger into the target block
$\dot{\delta}$	$d\delta/dt$ velocity of penetration
$\ddot{\delta}$	$d^2\delta/dt^2$ time rate of change of velocity of penetration
a	projected frontal area
k	velocity constant
k_1	scaling factor
m_p	mass of plunger
m_s	mass of specimen
n	exponential velocity constant
q	dynamic pressure
w_s	weight of specimen

Integrating Equation C.4 with respect to δ between the limits of zero and maximum penetration (δ_{max}),

$$\int_0^{\delta_{max}} \ddot{\delta}d\dot{\delta} + \int_0^{\delta_{max}} \frac{F(\delta)}{m_p} d\delta = \int_0^{\delta_{max}} \ddot{X}_s d\delta. \qquad (C.5)$$

An energy balance on the plunger, neglecting minor effects, shows that

$$\int_0^{\delta_{max}} F(\delta)d = \frac{1}{2}m \ V_c^2. \qquad (C.6)$$

Consequently Equation C.5 becomes

$$\frac{\dot{\delta}^2}{2}\bigg|_0^{\delta_{max}} + \frac{V_c^2}{2} = \int_0^{\delta_{max}} \ddot{X}_s d\delta. \qquad (C.7)$$

Substituting the limits into Equation C.7 and noting that $(d\delta/dt)_{\delta_{max}} = 0$ and that $(d\delta/dt)_{\delta_0} = V_0$, one has

$$-\frac{V_0^2}{2} + \frac{V_c^2}{2} = \int_0^{\delta_{max}} \ddot{X}_s d\delta, \qquad (C.8)$$

which is equivalent to

$$V_0^2 = V_c^2 - 2 \int_0^{\delta_{max}} \ddot{X}_s d\delta. \qquad (C.9)$$

Thus Equation C.9 gives a relationship between the velocity of the specimen (V_0) at the time of contact with the plunger, the indicated impact velocity or calibration velocity (V_c) as determined from the amount of penetration δ_{max}, and the acceleration $\ddot{X}_s$ on the specimen during the time the plunger is penetrating. Consequently, it can be seen that, if there is any appreciable acceleration, $\ddot{X}_s$, on the specimen, the calibration velocity will not equal the velocity of the specimen at the time of contact but must be corrected by an amount equal to the last term on the right side of Equation C.9.

C.2.2   Calibration. Calibration of the impact gages was completed for impact velocities from 20 to 300 ft/sec. This range was covered using four different plunger diameters varying from 0.105 to 0.404 inch in diameter and machined as shown in Figure C.2. The impact blocks for this calibration were made of 2S aluminum $\frac{1}{2}$ and 1 inch thick by $\frac{7}{8}$ inch in diameter and held in a steel fixture, shown in Figure C.3, which allowed only unidirectional deformation of the blocks.

For the calibration, the impact blocks were held stationary and the plungers shot into them. The plungers were fired in a tube using a modified 12-gage shotgun shell with the shot replaced by wadding, and the velocity was varied by using various amounts of gun powder in the shells. The velocity of each plunger was determined by measuring the time required for the plunger to travel over a 6-inch-gage distance located close to the impact block. This was accomplished by using two small light rays impinging on photocells which were used to start and stop an electronic timer. Figure C.4 is an overall photograph of the calibration equipment. The light source and photocells can be seen in the figure. The light rays were directed across the tube and into the path of the plunger so that as the plunger traveled along the tube it interrupted the first ray starting the timer and then the second ray which stopped the timer. The timer, therefore, recorded the time required for the plunger to travel the distance between the light rays. The distance between the rays divided by the time was the velocity of the plunger.

Special care was exercised to ensure that all of the aluminum blocks were held in the fixture with the same degree of confinement.

Figure C.5 is a plot of the penetration as a function of plunger velocity for $\frac{1}{2}$-inch-thick target blocks, and Figure C.6 for 1-inch-thick blocks. As can be seen from the log-log plots, the data are represented by a straight line of the form,

$$V_c = k\delta^n. \qquad (C.10)$$

Equations of these straight lines are given in Table C.2.

The selection of the proper material for the impact block, as well as the weight and diameter of the plungers, was also part of the calibration. A plunger weight of approximately 0.2 pound was chosen, then various

159

TABLE C.2 EQUATIONS OF PENETRATION AS A FUNCTION OF PLUNGER VELOCITY

Plunger diameter, inches	Plunger weight, pounds	Impact block thickness, inches	Equation, $V_c = k\delta^{n}$[a]
0.105	0.1932	$\frac{1}{2}$	$V_c = 191\ \delta^{0.563}$
0.155	0.1948	$\frac{1}{2}$	$V_c = 261\ \delta^{0.543}$
0.252	0.1992	$\frac{1}{2}$	$V_c = 413\ \delta^{0.572}$
0.404	0.2097	$\frac{1}{2}$	$V_c = 746\ \delta^{0.587}$
0.105	0.1932	1	$V_c = 197\ \delta^{0.587}$
0.155	0.1948	1	$V_c = 277\ \delta^{0.582}$
0.252	0.1992	1	$V_c = 426\ \delta^{0.556}$
0.404	0.2097	1	$V_c = 685\ \delta^{0.587}$

[a] V_c is in ft/sec; δ is in inches.

alloys of aluminum and steel were tested, using a selected range of plunger diameters to determine which combination would produce penetrations between 0.10 and 0.30 inch for velocities from 50 to 300 ft/sec. The 2S aluminum impact blocks with plunger diameter from 0.1 to 0.4 inch were selected on the basis of the above requirements.

From the calibration data it is possible, assuming that the force on the plunger is a function only of the penetration, to obtain a relationship between the force and the amount of penetration. The above assumption is not necessarily correct since the force could also be a function of the rate of penetration in a manner similar to the increase in the yield stress of a materials test specimen with increased rates of loading. It is believed, however, that over the range of velocities encountered, this dependence would be small and has been neglected. From the calibration data therefore,

$$V_c = 12k\delta^{n}$$

where

$$V_c = \text{in/sec}$$

and

$$\bar{F}\delta_{max} = \tfrac{1}{2}\ m_p V_c^2$$

$$\bar{F}\delta_{max} = 72\ m_p k^2 \delta_{max}^{2n},$$

$$\bar{F} = 72\ m_p k^2 \delta_{max}^{2n-1}. \qquad (C.11)$$

Since

$$\int_0^{\delta_{max}} F(\delta)d\delta = \bar{F}\delta_{max}$$

$$\frac{d \int_0^{\delta_{max}} F(\delta)d\delta}{d\delta_{max}} = \frac{d(\bar{F}\delta_{max})}{d\delta_{max}}$$

$$F(\delta_{max}) = \bar{F} + \delta_{max}\frac{d\bar{F}}{d\delta_{max}} \qquad (C.12)$$

and substituting from Equation C.11,

$$F(\delta_{max}) = 72\ m_p k^2 \delta_{max}^{2n-1} + (2n-1)\ 72\ m_p k^2 \delta_{max}^{2n-1}$$

$$F(\delta_{max}) = (1 + 2n - 1)\ 72\ m_p k^2 \delta_{max}^{2n-1}$$

$$F(\delta_{max}) = 144\ m_p k^2 \delta_{max}^{2n-1} \qquad (C.13)$$

where: n = constant from Table C.2,
k = constant from Table C.2,
m_p = mass of plunger (lb-sec^2/in.),
$F(\delta_{max})$ = force on plunger at maximum penetration (lb),
δ = penetration (in.)

Now, since it has been assumed that the force on the plunger is a function of penetration (δ) only, then the forces at maximum penetration are merely individual points on a more general curve of force versus penetration and this general curve is identical with the plot of Equation C.13. Thus, the assumption amounts to the same as the statement

$$F(\delta_{max}) = F(\delta) \qquad (C.14)$$

Equation C.14 states that the force on the plunger at any point along its penetration is the same as that which would have acted on the plunger at that point had the plunger contacted the target block with a lower impact velocity and had its maximum penetration at the point under discussion. Comparing Equations C.13 with C.11, it is noted that

$$F(\delta_{max}) = 2n\bar{F}, \qquad (C.15)$$

which shows that the force at maximum penetration is a constant times the average force during penetration. Since n is greater than $\frac{1}{2}$, the force during penetration is continually increasing, as would be expected under the initial assumption of the discussion.

Equation C.13 is the force-penetration relationship referred to in Section C.2.1 and is used to solve Equation C.4.

C.2.3 Design Conditions. Since the container housing the aluminum blocks and plungers, called the insert, was completely enclosed by the specimen, it required no additional protection from the hot gases.

However, it had to withstand the crushing effect and acceleration forces; therefore, the inserts at the 25- and 50-foot ranges were made of hardened tool steel. All other inserts were made of mild carbon steel.

C.2.4 Prediction of Velocity versus Distance Curves.

It was necessary to estimate the velocity-distance curve for each specimen to select the proper size plungers for the various specimens. The following method was used for this estimation.

The acceleration of the specimen is given by the following equation:

$$\ddot{X}_s = \frac{C_d g a q}{w_s}, \tag{C.16}$$

and

$$\dot{X}_s = \int_0^t \ddot{X}_s dt = \frac{g}{w_s} C_d a \int_0^t q dt, \tag{C.17}$$

also

$$X_s = \frac{g}{w_s} C_d a \int_0^t \int_0^t q dt dt. \tag{C.18}$$

The above equations assume that: (1) C_d is constant for any one specimen, (2) the specimen velocity is low in comparison to the particle velocity of the shock wave, and (3) the impulse imparted to the specimen by the diffraction of the shock wave was negligible.

Time-history dynamic-pressure curves were obtained from Problem "M" for a 20 kt device at ranges of 350, 400, and 450 feet. These curves were then mechanically integrated to obtain the first and second integrals of the dynamic pressure. The ranges and times of these curves were then scaled for a 10 kt device by the cube root method.

$$Range_{10} = k_1 Range_{20};$$

$$Time_{10} = k_1 Time_{20};$$

$$\text{where } k_1 = \left(\frac{10}{20}\right)^{1/3}$$

Solving Equations C.17 and C.18 for the same time intervals will yield a velocity-displacement curve. Figure C.7 is a plot of the normalized velocity versus slant range for normalized displacements up to 2 inches. Curves of velocity versus displacement for any specimen can be obtained by the use of Figure C.7 and the following two equations:

$$\dot{X}_s = 0.178 \frac{a C_d}{w_s} V_n, \tag{C.19}$$

$$X_s = 0.0525 \frac{a C_d}{w_s} S_n, \tag{C.20}$$

where: V_n = normalized velocity (lb-sec/ft²),
$\dot{X}_s$ = actual velocity (ft/sec),
S_n = normalized displacement (lb-sec²/ft²),
X_s = actual displacement (in.)
a = projected frontal area (in.²),
w_s = specimen weight (lb).

C.2.5 Conversion of Velocity versus Distance Curves to Acceleration versus Time Curves.

Given any velocity versus distance curve, it is possible to determine an acceleration versus time curve by a relatively simple mathematical manipulation.

Since,

$$\ddot{X} = \frac{d^2 X}{dt^2},$$

$$\ddot{X} = \frac{d(dX/dt)}{dt};$$

$$\ddot{X} = \frac{d(dX/dt)}{dX} \frac{dX}{dt},$$

therefore

$$\ddot{X} = \frac{\dot{X} d\dot{X}}{dX}. \tag{C.21}$$

The acceleration of the specimen at any point on the curve is then equal to the product of the velocity and slope of the velocity-distance curve at that point. Since time is equal to distance divided by velocity, if constant velocity is assumed for small increases in the distance traveled, then

$$t = \frac{dX_1}{\dot{X}_1} + \frac{dX_2}{\dot{X}_2} + \ldots + \frac{dX}{\dot{X}}. \tag{C.22}$$

where $\dot{X}_1, \dot{X}_2 \ldots \dot{X}_n$ are the average velocities during the distance changes dX_1, dX_2, and dX_n, respectively. Solving C.21 and C.22 at the same point on the velocity-distance curve will give the coordinates of a point on the acceleration-time curve.

C.3 RESULTS

Seven of the 11 specimens containing velocity impact gages recovered from Shot Erie yielded reliable data. Only one of the recovered specimens failed to yield useful data because of the malfunctioning of the gage itself. Exclusive of gage malfunction, overpressure and material ablation were the chief causes of gage failure. The specimens were constructed either of steel or aluminum and were exposed at ranges from 25 to 250 feet; however, none of the aluminum specimens were recovered, apparently because they were destroyed by material ablation. The recovered specimens which gave reliable results were originally located at Stations 150, 200, and 250 feet.

The specimen which did not yield useful data because of malfunctioning of the gages either had the target blocks and plungers misaligned or the plunger tips bent prior to impact, since the plungers penetrated in a skew manner. In another specimen, two of the four plungers penetrated the full depths of the target blocks and, although this was not a gage malfunction, the actual impact velocity could not be accurately determined.

161

C.4 DISCUSSION

The depth of penetration of the plunger into the target block was a function of the impact velocity between the plunger and target block and also a function of the target block acceleration. It was necessary to eliminate the effects of target block acceleration from the plunger data to describe the velocity of the target block as a function of its traveled distance. An immediate observation was apparent; i.e., for the plunger initially in contact with the target block, the impact velocity was zero; thus, the true velocity versus traveled distance relationship must pass through the zero point. The depth of penetration of that plunger was therefore a measure of the acceleration only.

The method selected to calculate the true velocity versus distance data from the velocity impact data involved an iteration process operating on two equations already derived in Section C.2.1, Equations C.4 and C.9. Since extensive numerical calculations were involved, use was made of the Datatron Electronic Data Processing System. The procedure was as follows: the indicated velocity versus preset distance curve was plotted from the velocity-impact data and was assumed to be the true curve; acceleration versus time data were computed by the methods presented in Section C.2.5. Equation C.4 was then solved using the calculated acceleration-time data yielding the penetration (δ) as a function of time. Having the two desired variables, penetration and acceleration, as functions of a third variable, time, it was possible to obtain the desired relationship of acceleration as a function of penetration. This relationship was then integrated over the entire penetration as indicated in Equation C.9 and the correction was applied to the calibration velocity versus distance curve. Using the corrected velocity versus distance curve, the entire procedure was repeated until subsequent corrections yielded by application of Equation C.9, and applicable to the original data, V_c versus X_s, remained relatively unchanged.

The method of positioning the plungers in the specimens at preset distances could have affected the depth of penetration readings for the plungers initially in contact with the target blocks. Solid metal spacers were used to position the plungers; consequently, if overpressure were sufficiently large and the specimens sufficiently compressed, the initial plunger could conceivably have slightly penetrated the target block. This penetration would be additive to the penetration due to acceleration.

Ground impact of the specimen could also tend to increase the depth of penetration readings, depending upon the angle of impact and the deceleration involved. It has been computed, however, that for the large diameter plunger (0.404 inch), a specimen acceleration of 25,000 grams would be required to produce additional penetration, assuming the plunger remains in contact with the target block after the initial penetration. Ground impact was consequently regarded as insignificant.

C.5 CONCLUSIONS AND RECOMMENDATIONS

C.5.1 Conclusions

1. The velocity-impact gages which were adequately protected from the effects of overpressure and material ablation of the specimen performed their functions as anticipated and yielded apparently reliable data.

2. Only extremely large specimen accelerations during plunger penetration appreciably affect the indicated velocity values as determined from the depth of penetration and the calibration data. For example, for a plunger 0.404 inch in diameter, an average specimen acceleration of 9,000 grams during penetration would result in only a 10 percent reduction in the indicated velocity value.

C.5.2 Recommendations

1. It is recommended that future programs consider the use of velocity-distance impact gages to measure specimen velocity as a function of distance within the fireball of a nuclear detonation.

2. In an effort to eliminate possible overpressure effects upon the readings of the plungers in contact with the target blocks, it is recommended that spring type spacers be used with spring constants sufficiently low so that the spacers would deform before plunger penetration would occur.

3. It is further recommended that more plungers be utilized in each gage to determine more accurately the shape of the indicated velocity versus distance curve, especially at preset distances close to the target blocks, a region of high acceleration.
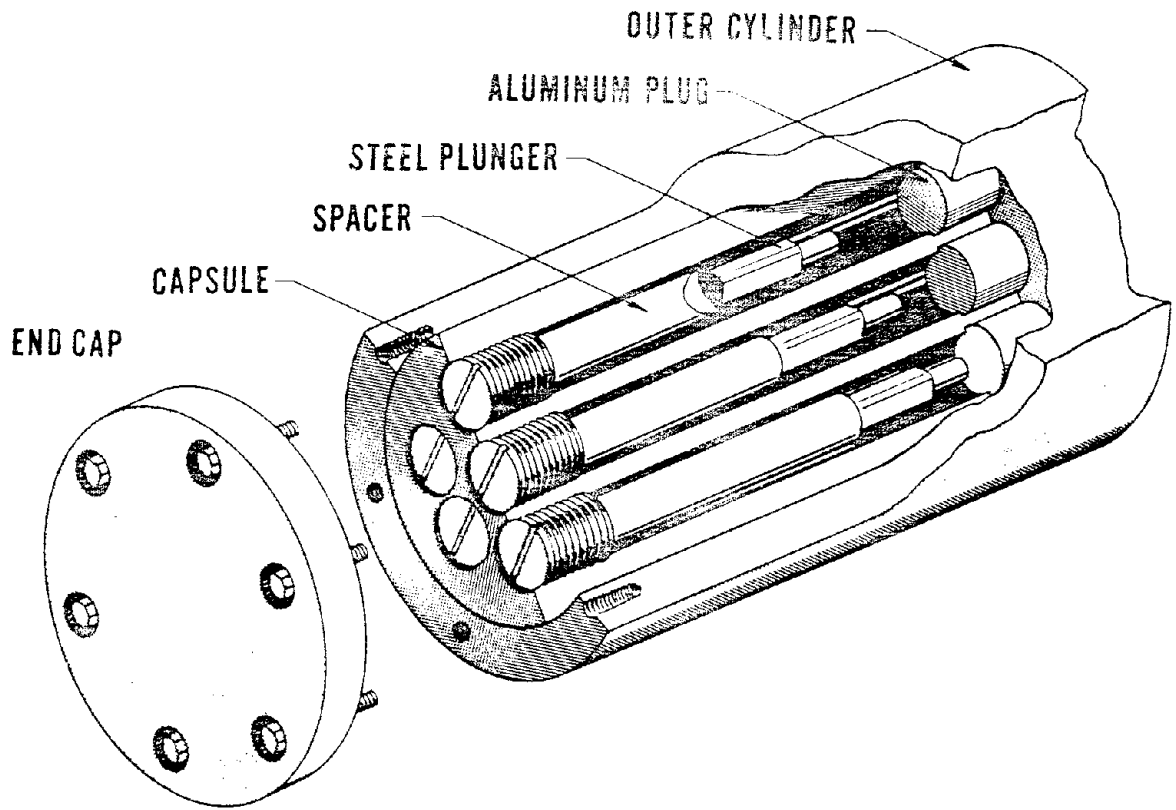
Figure C.1   Typical velocity-distance impact gage installation.
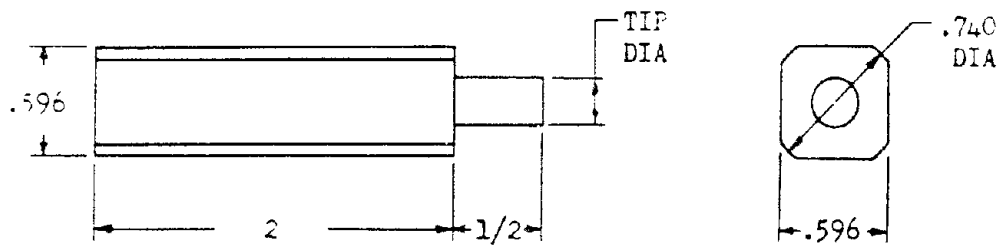
Figure C.2   Typical plunger depicting general machined dimensions.

163

TARGET BLOCK   RETAINER PLUG

.876 DIA   .750 DIA   1 1/2 DIA
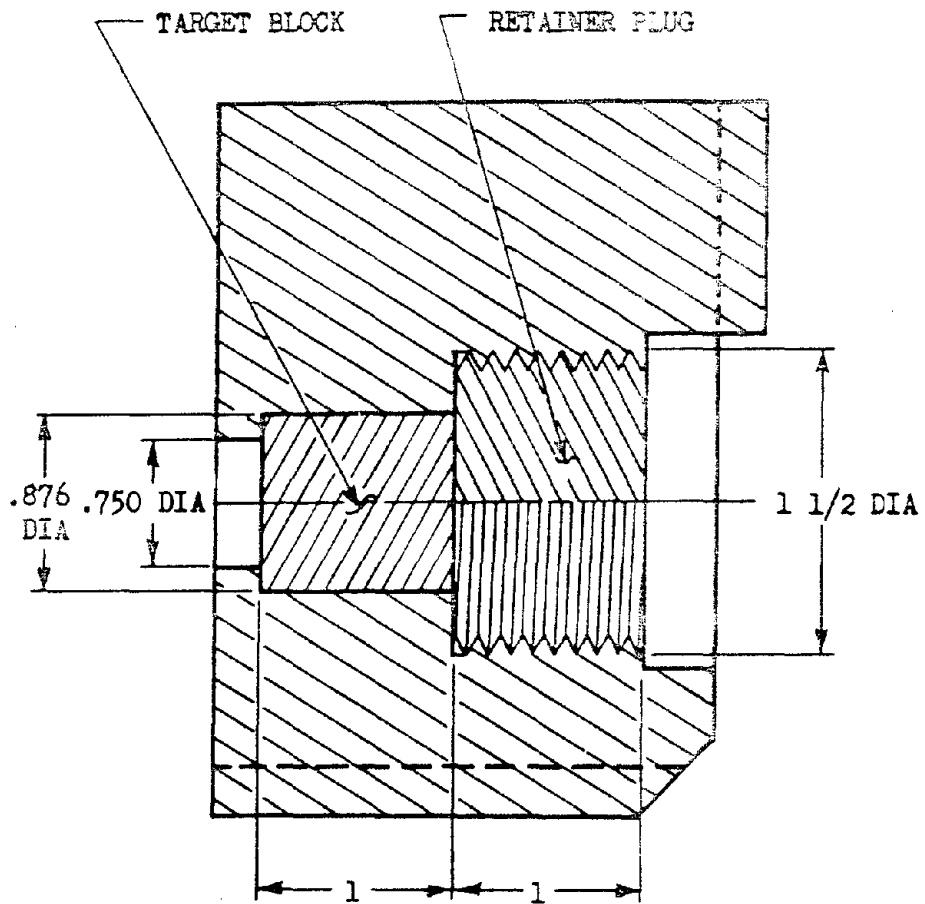
Figure C.3   Section drawing of target block holding fixture.
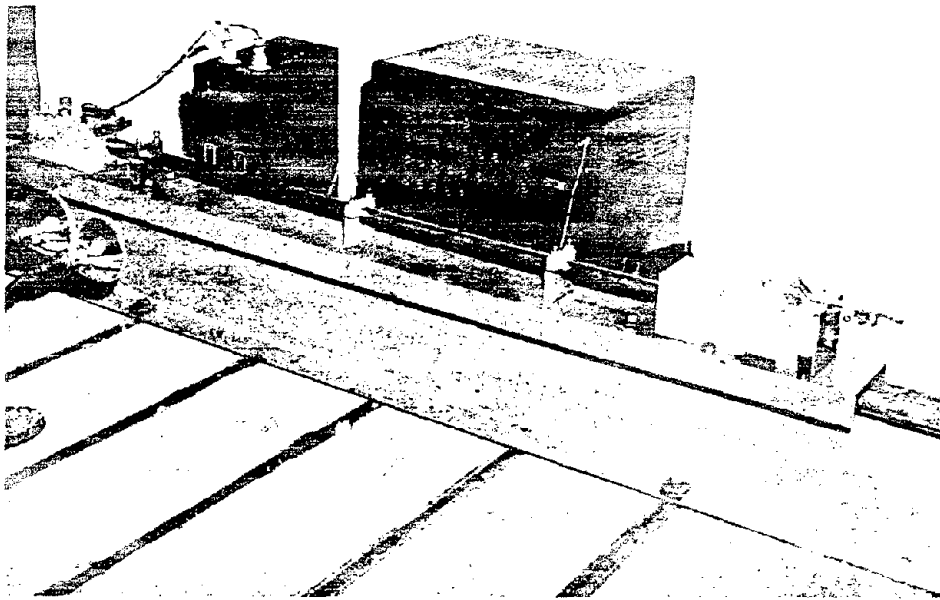
Figure C.4   Equipment used for calibration of velocity-distance impact gages.
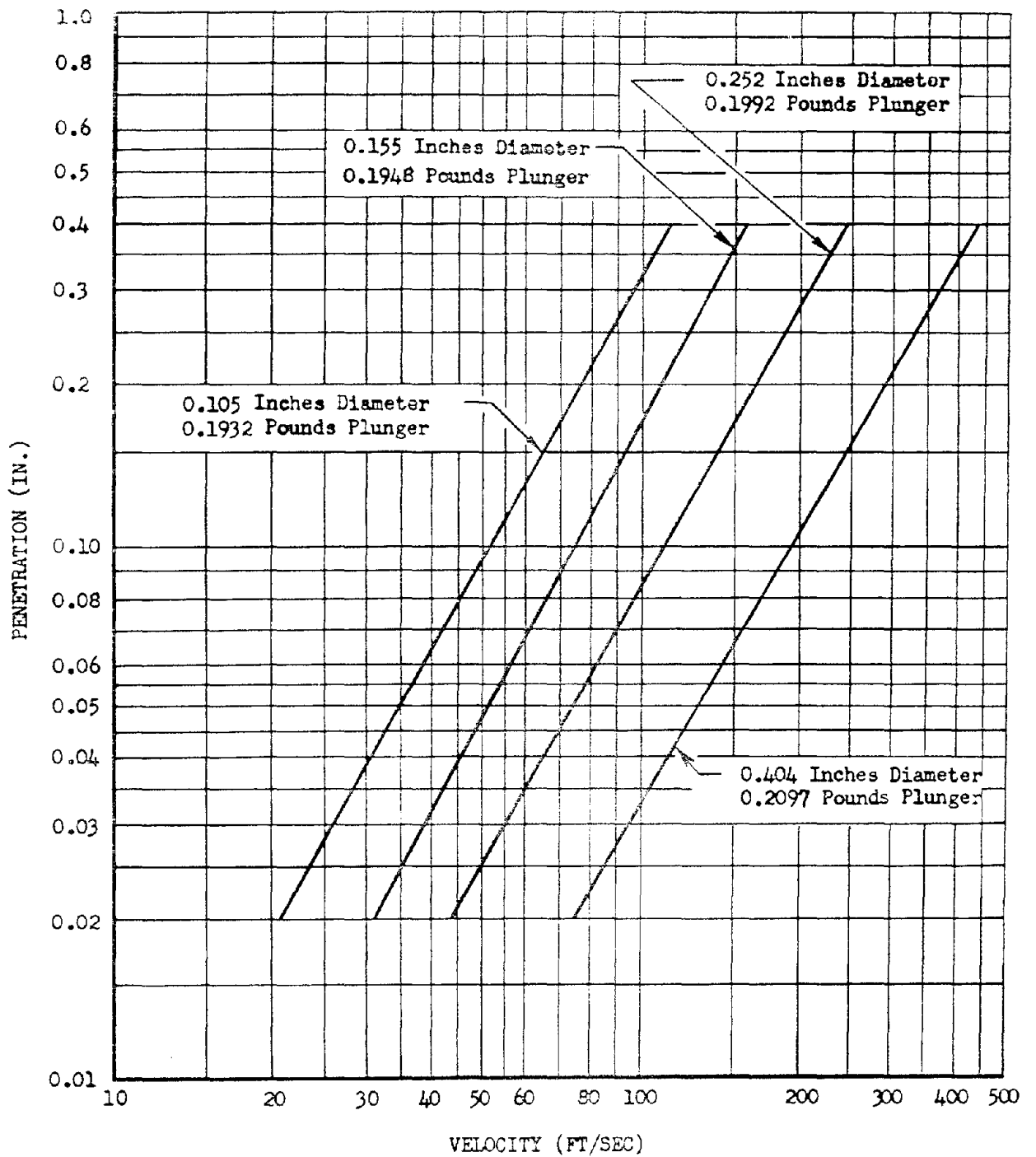
Figure C.5 Penetration versus velocity for ½-inch-thick 2S aluminum impact blocks.
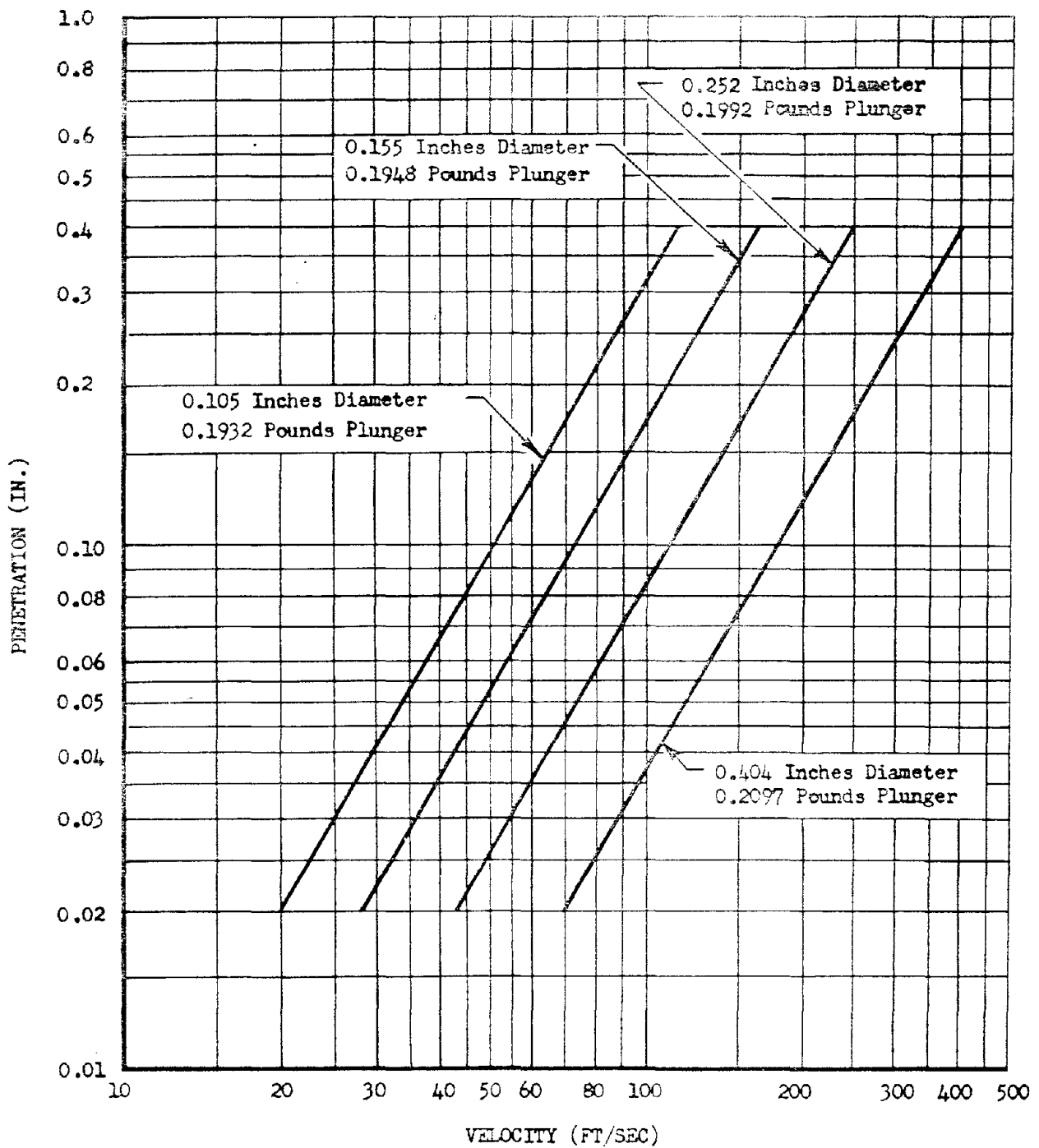
Figure C.6   Penetration versus velocity for 1-inch-thick 2S aluminum impact blocks.
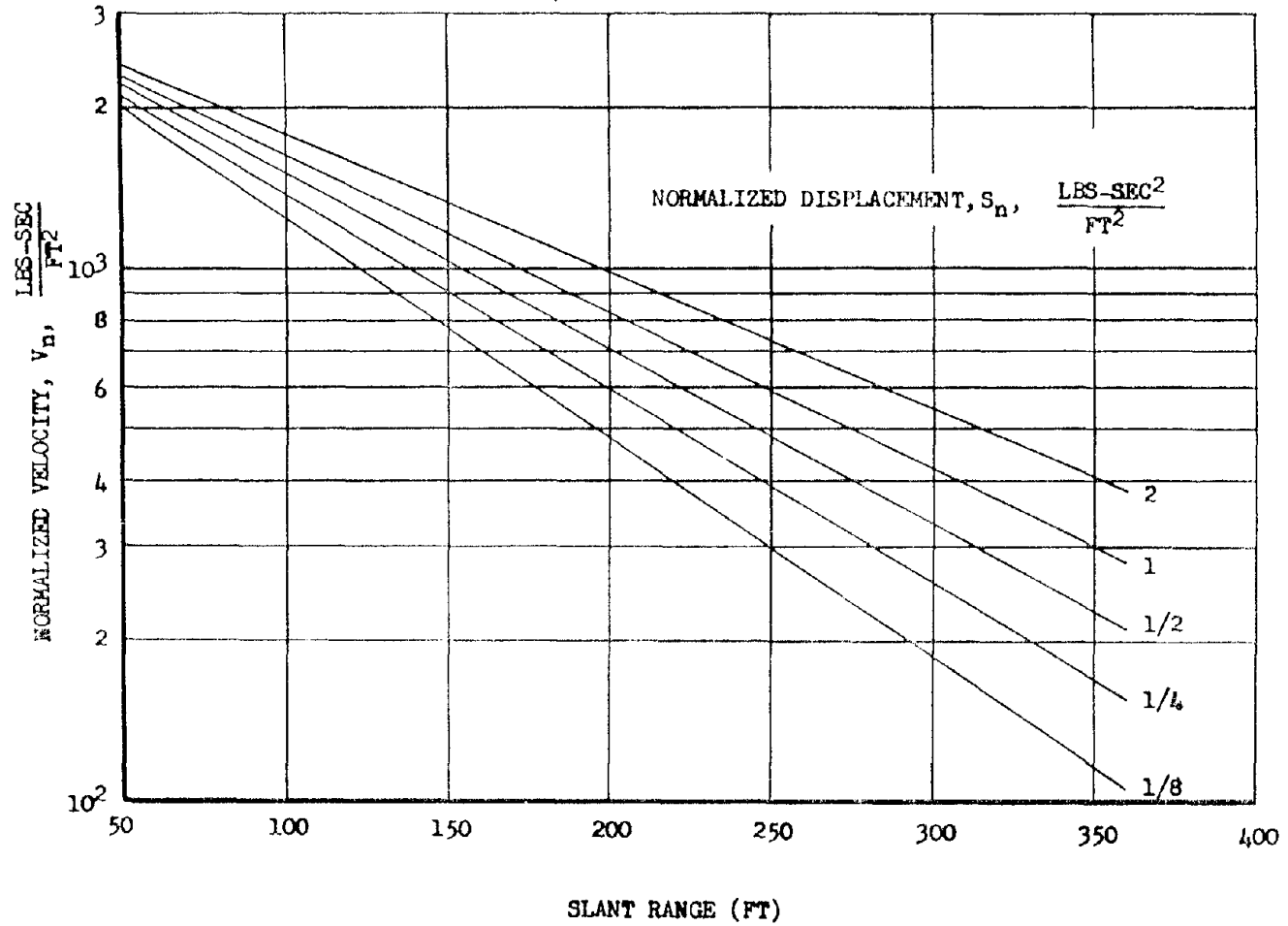
Figure C.7 Normalized velocity as a function of slant range for normalized displacement up to 2 inches for a 10 kt yield.

Appendix D

BALL-CRUSHER GAGES FOR MEASUREMENT OF PRESSURE AND ACCELERATION WITHIN THE FIREBALL OF A NUCLEAR DETONATION

D.1 INTRODUCTION

As part of its work on Air Force Contract No. AF 33(616)-3155, Allied Research Associates, Inc. was given the responsibility for the design and calibration of the pressure gages and accelerometers to be installed in six of the specimens exposed by Project 5.9 and the analysis of the results of this exposure. The results of this work have been published as Reference 1, WADC TR 57-188 Pt I. This appendix summarizes the more important topics contained therein.

D.2 THEORY AND DESIGN DETAILS

A simple type of mechanical gage which appeared likely to yield good results for both pressure and acceleration measurements was the ball-crusher gage. This was a gage in which a soft metal ball was deformed by a piston, the magnitude of the deformation of the ball being a measure of the magnitude of the force applied to the piston. The ball-crusher gage was first developed by the U. S. Navy in 1941 and is now used by the Navy as a standard device for measuring forces in the near vicinity of an explosion, particularly underwater explosions. The inherent accuracy of the device is such that errors of less than 10 percent may be expected when it is used to measure pressures in underwater explosions or strong shock front overpressures.

This gage is a simple device for measuring the maximum value of an applied static load. It is a peak reading instrument based upon the largely empirical fact that, when an annealed copper or aluminum ball is crushed between two flat parallel surfaces, the permanent or inelastic deformation of the ball is linear with the applied load. This linearity holds for

deformations as large as 30 percent of the initial ball diameter. Since the inelastic deformation remains after the load is removed, and may be relatively large, measurements of the deformation provide a convenient means for determining the maximum value of the applied force. The copper ball thus behaves as an irreversible linear spring. A deformation constant equivalent to a spring constant may be defined in terms of force per unit displacement. These deformation constants were determined for each gage by static loading. When the external force is applied slowly or statically, the peak force can be determined directly from the deflection; however, if the externally applied load varies rapidly, the dynamic response characteristics of the gage must be considered. In the Operation Redwing test, the load applied to the gages was rapid; therefore, the dynamic response of the gages had to be determined to interpret any experimental data obtained from the gages. Past and present experiments have shown that the dynamic spring constant (determined from the rapid loading of the balls, through dropping a weight) was approximately 18 percent greater than the static spring constant.

Since the deflection of the ball in the ball-crusher gage was proportional to the force applied to it, the ball was in effect a linear spring. Thus, the response of a mass bearing upon a ball to an applied external force function may be likened to the response of the identical mass supported by a spring equivalent to the ball.

In the light of the ball-spring analogy, the differential equation of the ball-crusher gages may be written as

$$m\ddot{X} - KX = F_0 f(t), \qquad (D.1)$$

where: m = the mass of the piston plus $\frac{1}{3}$ the mass of the ball (lbs),

X = the displacement of piston (in.)

K = the dynamic ball deformation constant (lbs/in.)

F_0 = the maximum value of the forcing function, F(t), (lbs),

and

f(t) = the non-dimensional forcing function
$f(t) = F(t)/F_0$.

The general solution of (D.1) is of the form

$$X = \frac{\omega F_0}{K} \int_0^t f(t') \sin \omega(t - t') \, dt', \qquad (D.2)$$

where t' is a variable of integration, and ω the equivalent natural gage frequency, $\sqrt{K/m}$, (radians/sec).

It is customary to compare the response of such a system to that which it would have if the forcing function were a step function.

It has been shown in Reference 1 that normalizing the response with respect to a unit step function, the relationship between the maximum deformation, X_{max}, and the peak applied force, F_0, is given by:

$$X_{max} = \frac{2}{K} \gamma \, F_0, \qquad (D.3)$$

where

$$\gamma = \frac{\omega}{2} \int_0^{t_1} f(t') \sin \omega(t_1 - t') \, dt', \qquad (D.4)$$

and t_1 is the time of maximum deformation. Hence, once a normalized driving function f(t) is assumed, the relative response of the gage can be determined by evaluating γ at t_1 for the assumed driving function.

The ball-crusher gages utilized in recording the experimental data in Shot Erie are shown in Figures D.1 and D.2. Figure D.1 shows a typical pressure gage, and Figure D.2 shows a complete acceleration unit consisting of two ball-crusher accelerometers. The pressure and acceleration gages were designed to withstand the pressures and temperatures predicted at specified ranges within the fireball of a 10 kt nuclear explosion, since this was the estimated yield of Shot Erie. The gages of the 50-foot station were constructed of special tool steel to withstand the predicted pressures at this station. The procedure used in estimating the fireball pressure is presented in Reference 1. The estimation is based on the solution of the spherical shock wave problem as given by G. I. Taylor and H. L. Brode. Since the pressure gages were located at various slant ranges from the center of the burst, the gages contained different sized copper or aluminum balls, so that sufficiently large deformations for accurate measuring would be obtained in the linear region. These ball sizes were determined by using the estimated value of the peak shock front overpressure at various slant ranges and assuming the dynamic input into the gages to be a Taylor Wave. This postulated Taylor Wave gave the time history of the overpressure at a fixed point in space. The ball sizes varied from 0.375 inch diameter at the outermost station to 1.000-inch diameter at the innermost station.

The accelerometer used the same diameter copper ball, 0.500 inch, for all stations, since the estimated range of ball deformation fell within the linear region. These deformations were calculated by assuming that the peak accelerations received by the spheres would be caused by the material velocity of the shock wave.

D.3 RESULTS

All six spheres containing the ball-crusher gages were recovered. The gages were removed by welding a length of pipe to the gage and unscrewing it. During removal of the gages, most of the outside threads were galled or stripped by the slag material that had been deposited in the outermost threads. The rubber O rings at the base of the threads were still in their original condition, and the outside of the gage base showed no discoloration that would indicate extremely high temperatures within the spheres. Disassembly of the gages indicated that the O rings on the pistons provided adequate seals in preventing the hot gases from being forced into the ball chambers. The crushed balls and their rubber grommets were also in excellent condition, as was the base of the gages. The flats on the deformed balls were parallel; thus accurate measurements of the deformations were obtained.

The previous remarks exclude the pressure gages and the acceleration unit at the 50-foot station, since only one of the gages was removed from this specimen. This gage was removed in pieces with the base of the gage remaining wedged in the sphere. Only the head of the gage was removed, exposing the crushed ball, which was picked out of the base. The head of the gage as well as the base was cracked in several places, and the piston was broken into several pieces. The bottom section of the piston was found in the base of the gage, but the top section was not located. During the initial attempt to remove this gage by unscrewing it, a section of the top of the gage was broken off with the pipe welded to it. An inspection of this exposed surface revealed that there were visible cracks throughout the gage. After removal of the head of the gage by cutting the sphere away with a torch, the base was found to be cracked in three places. The anvil face of the base was cracked along a centerline causing nonparallel forces on the deformed ball. By taking the average of several measurements, deformation data was obtained from this ball.

D.4 METHOD OF ANALYZING EXPERIMENTAL DATA

In this section the generalized response of the ball-crusher gage presented in Section D.2 is utilized in predicting the response of this gage to a variety of

169

postulated inputs. For each of these postulated inputs the procedure is as follows: from theory and perhaps the use of certain assumptions, the time history of each of these inputs is derived. For each of these inputs it is convenient to assume a peak pressure or acceleration to be an unknown parameter. Once the shape of the assumed input is known, it is a simple matter to derive a functional relationship between the observed ball deformation and the unknown parameter, using the technique presented in Section D.2.

The following pressure time histories have been calculated in an effort to cast light on which of the postulated phenomena actually did occur within the fireball. In general, of course, the pressure measured by the ball-crusher gage is the sum of the various postulated pressure phenomena. However, certain of these phenomena may be too small in magnitude or too rapid in time to be sensed by the instrument; hence, the division of phenomena given below.

1. Taylor Wave, Figure D.3A,
2. Isobaric Sphere Pressure, Figure D.3B,
3. Blow-Off Pressure, Figure D.3C,
4. Diffraction Pressure, Figure D.3D,
5. Acceleration Loading, Figure D.4.

The details of these phenomena are discussed in Reference 1. The relative response of the ball-crusher gage to various pressure inputs is presented in Figure D.5. The slant ranges in the figure are for a gage having a period of 0.75 msec. Figure D.6 shows the relative response to diffraction and gust loading accelerometers with a period of 0.803 msec.

D.5   ANALYSIS OF EXPERIMENTAL DATA

After removal of the copper and aluminum balls from the pressure and acceleration ball-crusher gages, the deformation of each ball was measured. These deformations are given in Table D.1. Included in this table are the slant ranges of the sphere, size and material of the balls, and the position of each gage in its respective sphere.

The experimental data were analyzed by using the different dynamic gage responses for the various postulated inputs to the gages to determine the peak value of the forcing functions. The deformations were first reduced to give an equivalent static force by using the experimentally determined deformation constant for each size ball and material. Table D.2 gives these equivalent static forces and the deformation constant used in calculating these values of force from the data given in Table D.1. The peak pressures and accelerations may be calculated for the various postulated inputs by correcting the forces in Table D.2 for the dynamic response characteristics of the gages to these inputs. Specifically,

$$F_0 = \frac{F}{2\gamma},$$ (D.5)

where: F_0 = Peak force,
        F = Equivalent static force from Table D.2.

Figure D.5 gives the various pressure response characteristics and is used to calculate the parameter of the peak pressure distribution. This value of the peak pressure is given in Table D.3 and presented in Figure 3.29 for two of the postulated inputs, the Taylor Wave and the blow-off pressure plus the Taylor Wave. Figure D.3 shows the postulated acceleration input, and Figure D.6 is used to calculate the value of the parameter of this distribution which is taken to be the peak of the gust plus diffraction acceleration and the peak of the gust only. Tables D.3 and 3.9 summarize these data.

D.6   CORRELATION OF EXPERIMENTAL DATA

In this section the peak pressures and accelerations determined from the experimental data in Section D.5 are compared with postulated theoretical predictions. This method of correlation is used since the shape of actual dynamic input into the gages is, a priori, unknown.

In correlating the experimental pressure data given by gages with theoretical peak pressure, the peak pressure observed by the gages was determined by correcting the experimental ball deformations for the dynamic response characteristics of the gages to the postulated blow-off pressure and Taylor Wave input. These observed peak pressures are shown in Figures D.7A and D.7B as a function of the slant range location of the gages. The theoretical peak pressures for the same slant ranges are values of the peak shock front overpressure (Figure D.7A) and overpressure plus blow-off pressure (Figure D.7B), calculated from relationships set forth in Reference 1. From comparison of these observed and theoretical values of peak pressure, it is noted that most of the observed data points lie below the curve of theoretical peak pressure, especially the smaller slant range points in Figure D.7B.

Comparing Figures D.7A and D.7B, which differ only in that Figure D.7B includes the blow-off pressure as given by Figure D.3C, it can be seen that the agreement between theory and experiment is approximately the same in both cases at the longer ranges. This is due to the fact that the gage was capable of seeing the initial peak shock, which rises above the postulated blow-off pressure peak. It should perhaps be pointed out that the data at the 50-foot station is given partly by the fact that the ultimate strength of the steel used in the gage (250,000 psi) was exceeded by the pressure loading. This gives a lower bound on the observed peak pressure at this location. In addition, a crude measurement was made on one of the aluminum balls. Since the anvil was cracked, this measurement must also be considered as a lower bound.

It can also be seen from the data that there is a variation in observed pressures at any one station. At most a factor of three between the lowest value and the highest value was found. Several possible sources of these variations have been investigated

TABLE D.1 EXPERIMENTAL BALL-CRUSHER GAGE DATA, SHOT ERIE

Range, feet	Gage No.	Ball size, inch	Material	Deformation, δ, inch	Location of gages (rear view)
50	-	1.0000	Al	~0.250	
100	5	1.0000	Al	0.0156	
	6	1.0000	Al	0.0342	
	11	1.0000	Cu	0.0548	
	14	1.0000	Cu	0.0623	
	Accel.	0.5000	Cu	0.1440	
150	18	1.0000	Cu	0.0514	
	19	1.0000	Cu	0.0436	
	21	1.0000	Cu	0.0489	
	2	0.5000	Cu	0.0565	
	Accel.	0.5000	Cu	0.0998	
200	10	0.6250	Cu	0.0338	
	17	0.6250	Cu	0.0503	
	16	0.3750	Cu	0.0718	
	22	0.3750	Cu	0.0329	
	Accel.	0.5000	Cu	0.0687	
250	8	0.5000	Cu	0.0232	
	9	0.5000	Cu	0.0371	
	4	0.3750	Cu	0.0364	
	12	0.3750	Cu	0.0285	
	Accel.	0.5000	Cu	0.0339	
300	3	0.5000	Cu	0.0170	
	7	0.5000	Cu	0.0401	
	13	0.3750	Cu	0.0152	
	15	0.3750	Cu	0.0145	
	Accel.	0.5000	Cu	0.0167	
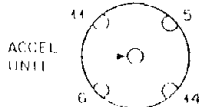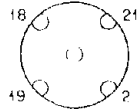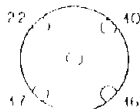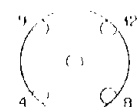
TABLE D.2 EQUIVALENT STATIC FORCE (F) AND DEFORMATION CONSTANT (K) CALCULATED FROM BALL DEFORMATION DATA GIVEN IN TABLE D.1

Range, feet	Gage No.	K (lb/in.)	F, pounds
50	-	4.8×10^5	$\sim 1.20 \times 10^5$
100	5	4.8×10^5	7.50×10^3
	6	4.8×10^5	1.64×10^4
	11	7.0×10^4	3.83×10^3
	14	7.0×10^4	4.36×10^3
	Accel.	3.5×10^4	5.05×10^3
150	18	7.0×10^4	3.59×10^3
	19	7.0×10^4	3.05×10^3
	21	7.0×10^4	3.42×10^3
	2	3.5×10^4	1.98×10^3
	Accel.	3.5×10^4	3.49×10^3
200	10	4.4×10^4	1.49×10^3
	17	4.4×10^4	2.21×10^3
	16	2.6×10^4	1.87×10^3
	22	2.6×10^4	8.56×10^2
	Accel.	3.5×10^4	2.41×10^3
250	8	3.5×10^4	8.12×10^2
	9	3.5×10^4	1.30×10^3
	4	2.6×10^4	9.46×10^2
	12	2.6×10^4	7.42×10^2
	Accel.	3.5×10^4	1.19×10^3
300	3	3.5×10^4	5.95×10^2
	7	3.5×10^4	1.40×10^3
	13	2.6×10^4	3.95×10^2
	15	2.6×10^4	3.77×10^2
	Accel.	3.5×10^4	4.17×10^2

TABLE D.3 PEAK PRESSURE AND ACCELERATION FOR VARIOUS DYNAMIC INPUTS AS CALCULATED FROM EXPERIMENTAL DATA

			Pressures		
		Taylor Wave		Blow Off + Taylor Wave	
Gage No.	T/t_0	γ	P_s(psi)	γ	P_s(psi)
–	1.88	0.35	3.88×10^5	0.49	2.77×10^5
5	0.36	0.66	1.28×10^4	0.72	1.18×10^4
6	0.36	0.66	2.81×10^4	0.72	2.58×10^4
11	0.89	0.48	9.02×10^3	0.61	7.10×10^3
14	0.89	0.48	1.03×10^4	0.61	8.11×10^3
18	0.31	0.70	5.73×10^3	0.74	5.42×10^3
19	0.31	0.70	4.86×10^3	0.74	4.60×10^3
21	0.31	0.70	5.45×10^3	0.74	5.15×10^3
2	0.41	0.64	3.49×10^3	0.71	3.15×10^3
10	0.18	0.81	2.06×10^3	0.81	2.06×10^3
17	0.18	0.81	3.07×10^3	0.81	3.07×10^3
16	0.23	0.77	2.76×10^3	0.78	2.76×10^3
22	0.23	0.77	1.26×10^3	0.78	1.26×10^3
8	0.114	0.88	1.03×10^3	0.88	1.03×10^3
9	0.114	0.88	1.65×10^3	0.88	1.65×10^3
4	0.131	0.86	1.25×10^3	0.86	1.25×10^3
12	0.131	0.86	9.81×10^2	0.86	9.81×10^2
3	0.073	0.94	7.23×10^2	0.94	7.23×10^2
7	0.73	0.94	1.71×10^3	0.94	1.71×10^3
13	0.84	0.92	4.89×10^2	0.92	4.89×10^2
15	0.84	0.92	4.67×10^2	0.92	4.67×10^2

		Acceleration				
Station		100	150	200	250	300
Gust	γ	0.41	0.76	0.86	0.91	0.91
	n(G's) (Peak)	2.81×10^4	1.03×10^4	6.27×10^3	2.89×10^3	1.035×10^3
Gust plus diffraction	γ	0.195	0.43	0.57	0.60	0.52
	n(G's) (Peak)	5.9×10^4	1.82×10^4	9.46×10^3	4.43×10^3	1.81×10^3

and ruled out as negligible or not consistent with the experimental data. One source investigated was the possibility that the shock front intersected the plane of the gages at an angle differing from zero degrees. The possibility of the shock front not being parallel to the plane of the gages would cause dynamic pressures and conventional shock diffraction effects to be observed by the gages in addition to the peak shock front pressures. It was found from photographs of the fireball, at various times up to breakaway, that the shock front was indeed not parallel to the plane of the shock front. However, this source of the variations was ruled out because the pressures recorded by the gages on the spheres did not follow any set pattern of high and low values as would be expected from the geometry of such a situation. Another possibility for these variations could be due to differences in the materials used in the gages, notably the balls, or imperfections in the manufacturing of the balls. In this case, tests and experiments performed on balls made from the same batch of metal used in the balls of the gages showed that any material differences or imperfections in the balls themselves were negligible. It was found that crushing dozens of these balls statically and dynamically gave consistent deformation results (within 1 percent) for a wide range of loads.

One possible explanation of this variation in observed pressure is the extension of the shock front of the fireball locally around the spherical specimen, causing local pressures that may vary in magnitude by factors of 2 or 3. This phenomenon would be caused by the local preheating of the air surrounding the sphere due to radiation from the shock front. The mechanism for this preheating is that a small amount of metal is vaporized from the surface of the specimens and advances into the air at sonic velocities, effectively heating this air. The higher air temperature increases the local shock front propagation velocity, and the shock front then extends from the surface of the fireball toward the sphere. When the shock front extension reaches the sphere it advances around the surface in an irregular shaped front causing different shock diffraction effects on various sections of the surface. This phenomenon is analogous to the formation of spikes from the fireball along the guy wires from the shot tower or down the shot tower itself and is, therefore, expected to be as unpredictable and unstable as the spikes.

The accelerations observed by the gages have been compared with the theoretical accelerations the spheres received from the shot gust loading. These theoretical accelerations were determined from equations given in Reference 1 for the dynamic pressure pulse and the diffraction loading. These observed and theoretical peak accelerations are shown in Figure D.8 as a function of slant range. Only the gust loading has been considered since, as indicated in Figure D.6, the gage is not sufficiently fast to respond to the diffraction phase. It can be seen from Figure D.8 that

the agreement between the theoretical gust-induced accelerations and the measured data is excellent.

D.7 CONCLUSIONS AND RECOMMENDATIONS

D.7.1 Conclusions

1. It has been shown that ball-crusher gages may be successfully employed to experimentally record fireball pressures and accelerations under the adverse conditions encountered in the fireball. The damage to most of the gages was limited to the outer surfaces; the interior sections were unaffected by the extremely high pressures and temperatures. The gages at the 50- and 100-foot stations were damaged internally, since the ultimate strength and the yield strength, respectively, of the materials used, were exceeded.

2. The response of the ball-crusher gages used in this study was dependent upon the shape of the dynamic input. However, by quantitatively examining various possible inputs, it was determined that the Taylor Wave similarity solution plus a blow-off pressure of the order of the isobaric sphere pressure satisfactorily described most of the observed phenomena.

3. It was noted that the experimental points at any one slant range gave a variation between readings of about a factor of three. It is believed that this variation can be explained by the spike or shock front extension phenomenon which is analogous to the observable unstable spike of the fireball along a guy wire and the Taylor Instability.

From the experimental data and close examination of the gage responses to various dynamic inputs (Table D.3 and Figure D.5) it was determined that the blow-off pressure on iron was not much greater than the peak shock front overpressure for most ranges at sea-level altitude, although experimental evidence for its existence was given. It is believed that from the evidence indicated by the lower bound of the pressure on the sphere at Station B the blow-off pressure was significant at this location. However, the fluctuations in the data from the other gages (caused by the spikes) only permit one to state that the blow-off pressure is not much greater than the peak shock overpressure. It is also noted that the gage modified with the plastic material gave observed pressures approximately the same as the other gages. This indicated that there was no appreciable dependence of observed pressure on material atomic weight.

4. The observed accelerations were corrected for the gage response by assuming a gust loading input. The resultant correlation between the theoretical values of peak accelerations and the experimentally observed peak accelerations was close.

D.7.2 Recommendations. In view of the results of the analysis of this experiment with ball-crusher gages to obtain fireball pressures and acceleration,

it is recommended that these gages be designed to cover a greater range of response times or periods. This will enable the faster gages to observe the peak caused by the diffraction shocks and dynamic pressure inputs as well as the peak shock front overpressure. The slower gages can be designed so that they will be able to observe the effects of blow-off pressure and possibly give more information on the order of magnitude of this pressure. With proper instrument location on the specimen, it may be possible to determine the existence and location of the spike phenomenon on the surface of the specimen.

ANVIL

NEOPRENE WASHER

BALL (Cu or Al)

CYLINDER

O-RING SEALS

PISTON

PACKING
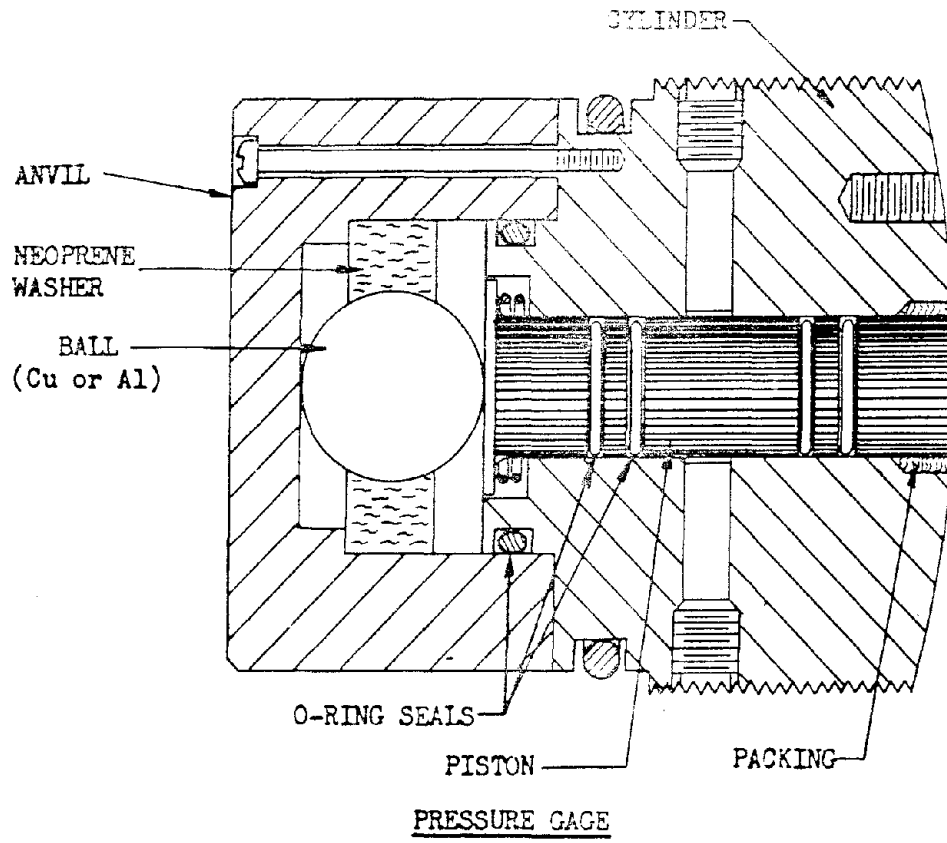
PRESSURE GAGE

Figure D.1 Ball-crusher pressure gage.

CYLINDER END

PISTON

O-RING SEAL

NEOPRENE WASHER

BALL (Cu or Al)

BODY

ANVIL END
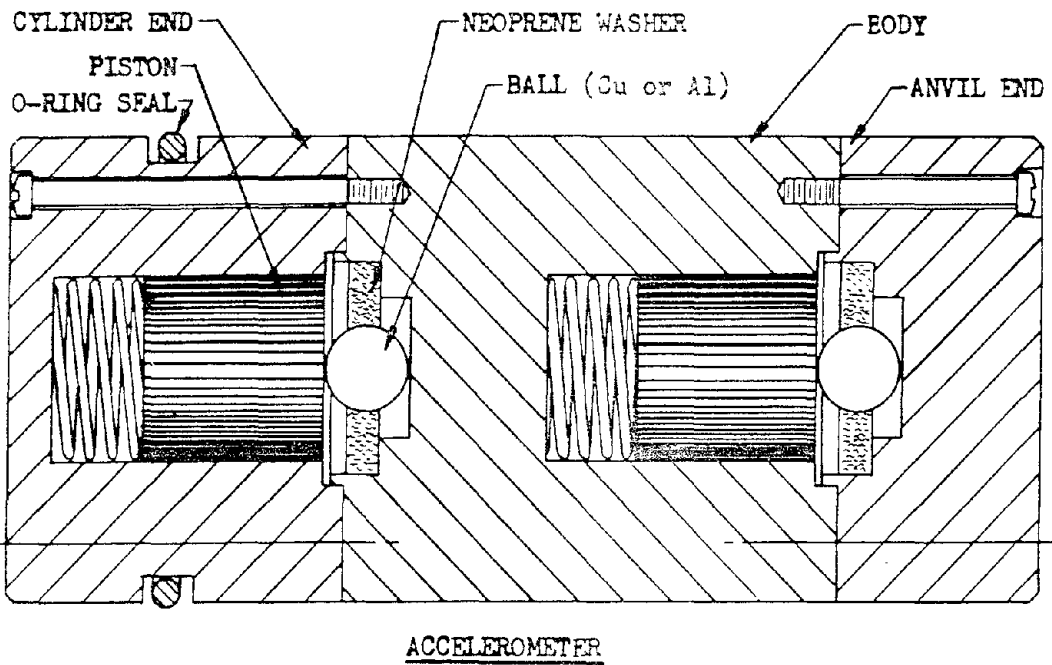
ACCELEROMETER

Figure D.2 Ball-crusher accelerometer unit.

P = PRESSURE

P_S = PEAK SHOCK PRESSURE

t = TIME AFTER SHOCK ARRIVAL

t_o = TIME OF SHOCK ARRIVAL

A. TAYLOR WAVE, P_S

B. ISOBARIC SPHERE, P_{IB}

$P_{IB}/P_S \simeq 0.42$

C. BLOW-OFF PRESSURE, P_{BO}

$P_{BO} + P_{IB}/P_S \simeq 0.60$

D. DIFFRACTION PRESSURE, P_D

$P_D/P_S \simeq 4.0$

DIFFRACTION

TAYLOR WAVE
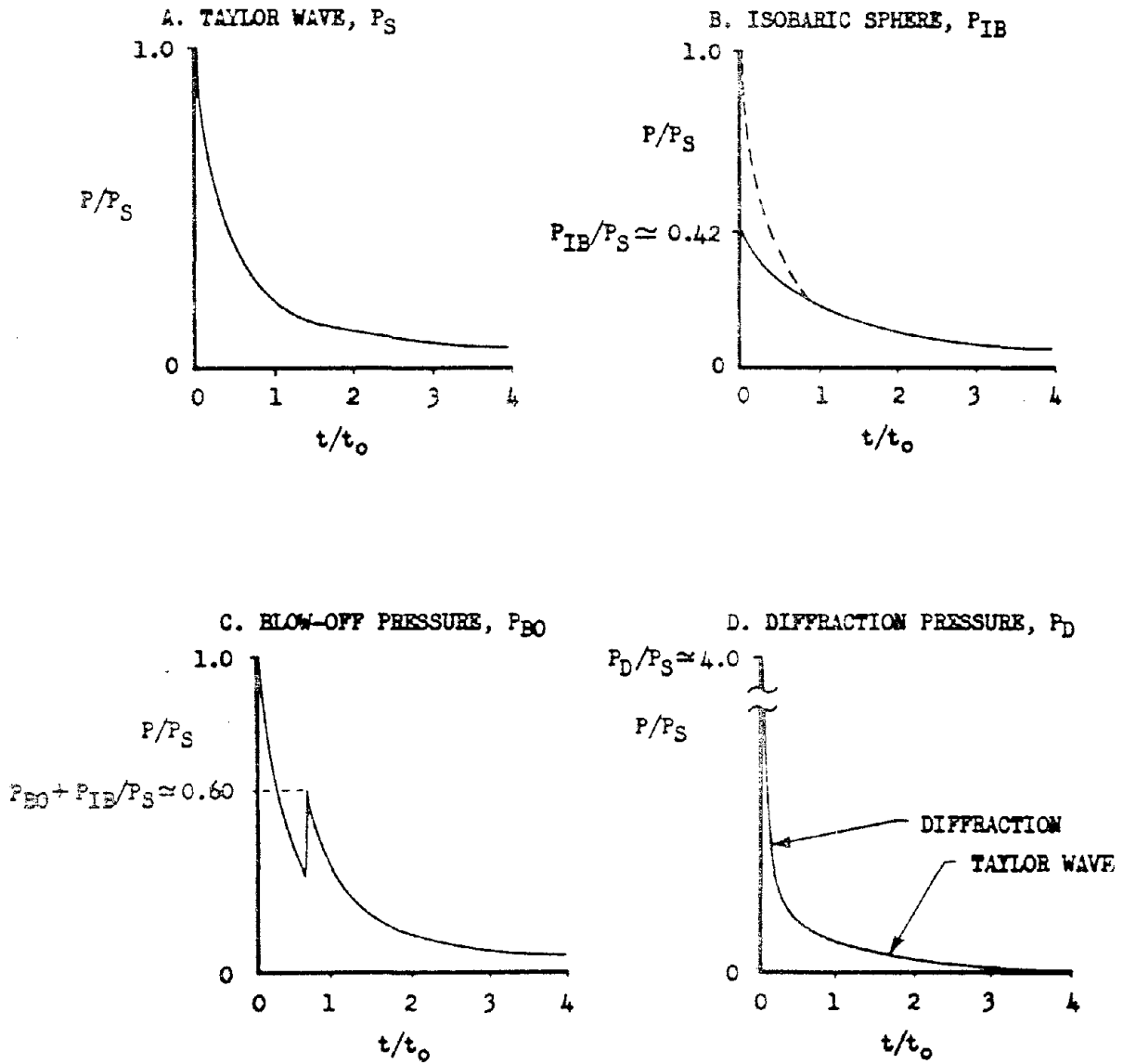
REFERENCE:
WADC TR 57-188 Pt I

Figure D.3   Nondimensional forcing functions at a fixed range.

176
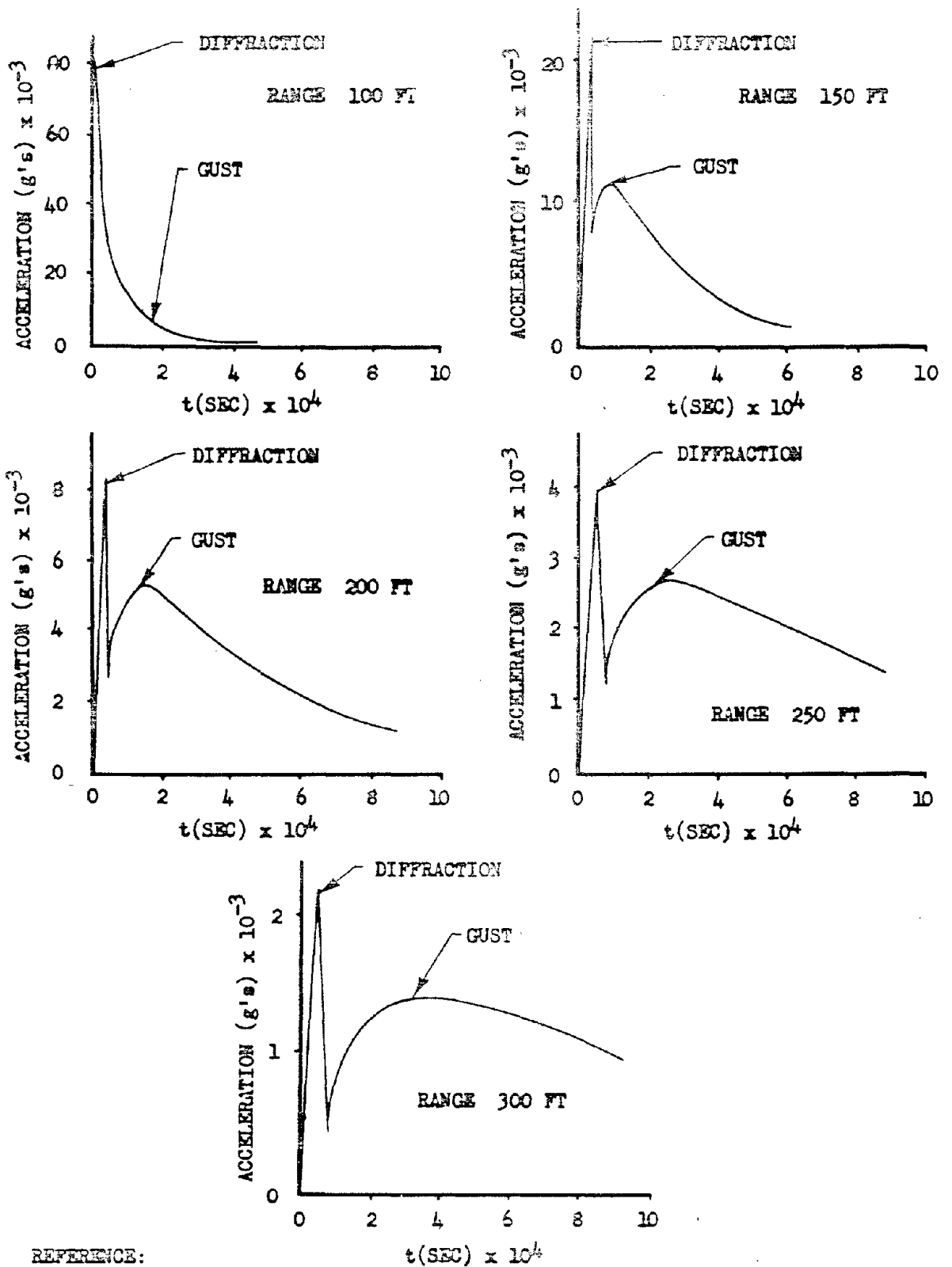
REFERENCE:
WADC TR 57-188 Pt I

Figure D.4 Postulated acceleration versus time after shock arrival.
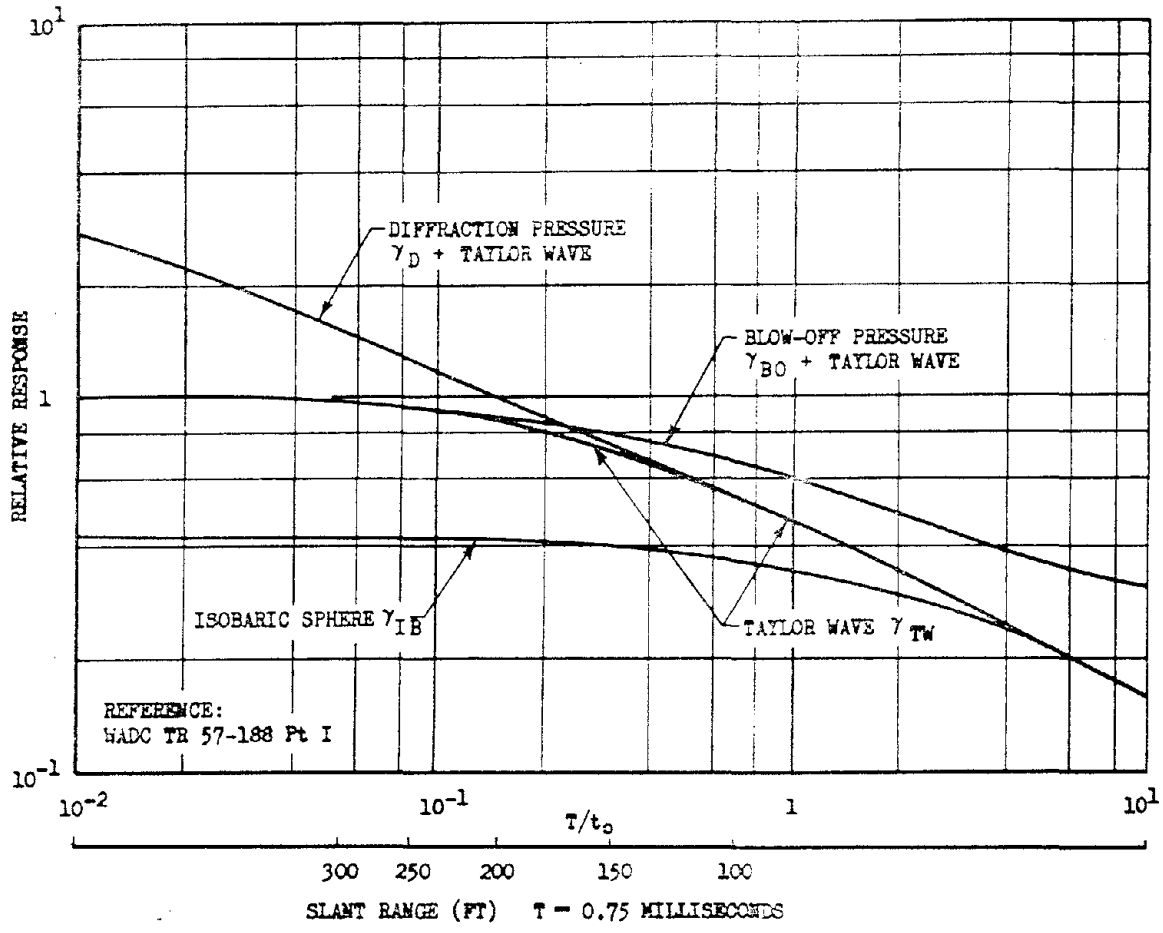
Figure D.5   Relative response of ball-crusher gage to various inputs. Relative response, γ versus ratio of gage period (T) to time of shock arrival (t_0), T/t_0.
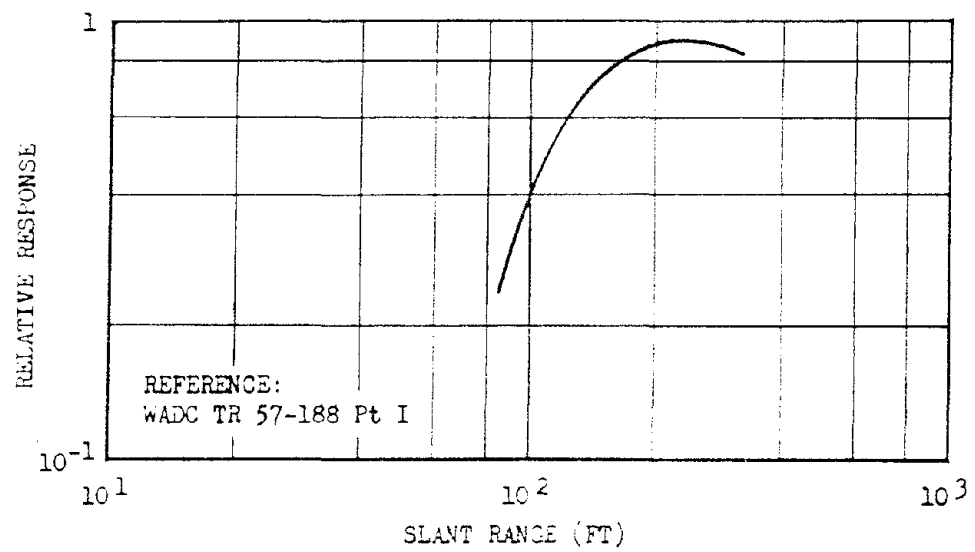
Figure D.6   Ball-crusher gage relative response to diffraction and gust loading accelerations. Relative response versus slant range.

A. TAYLOR WAVE

B. BLOW-OFF PRESSURE PLUS TAYLOR WAVE
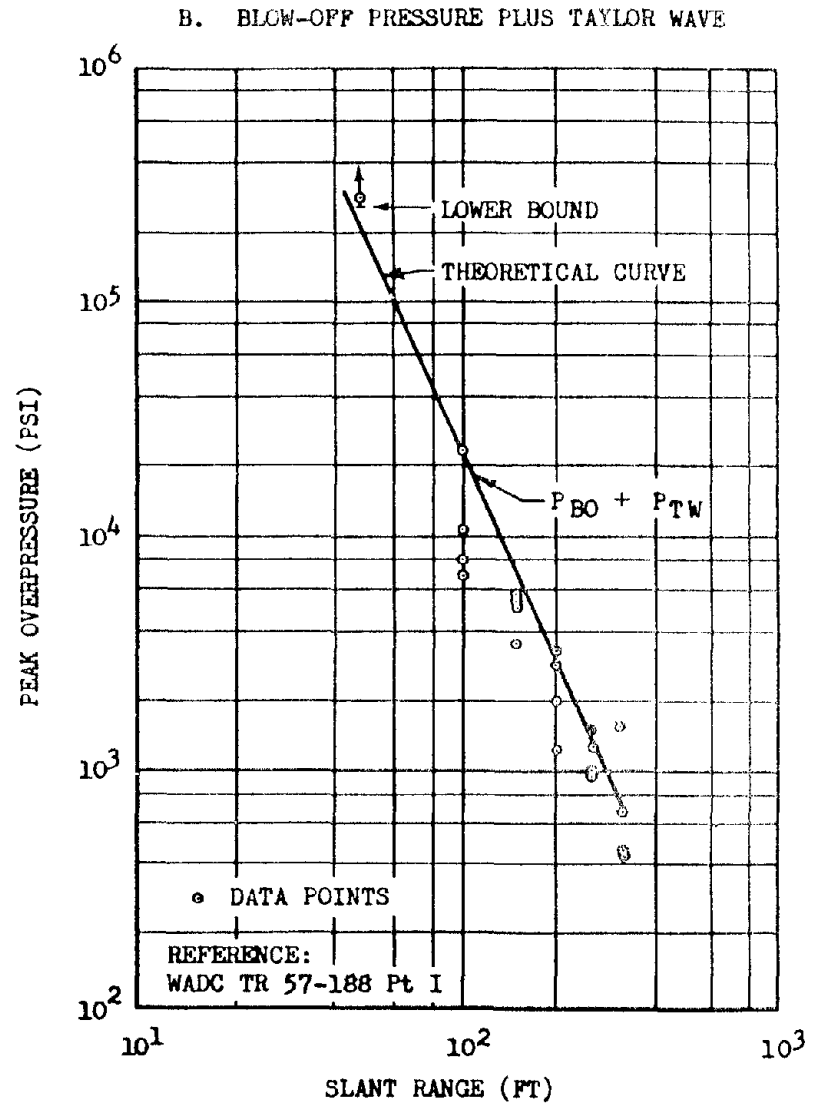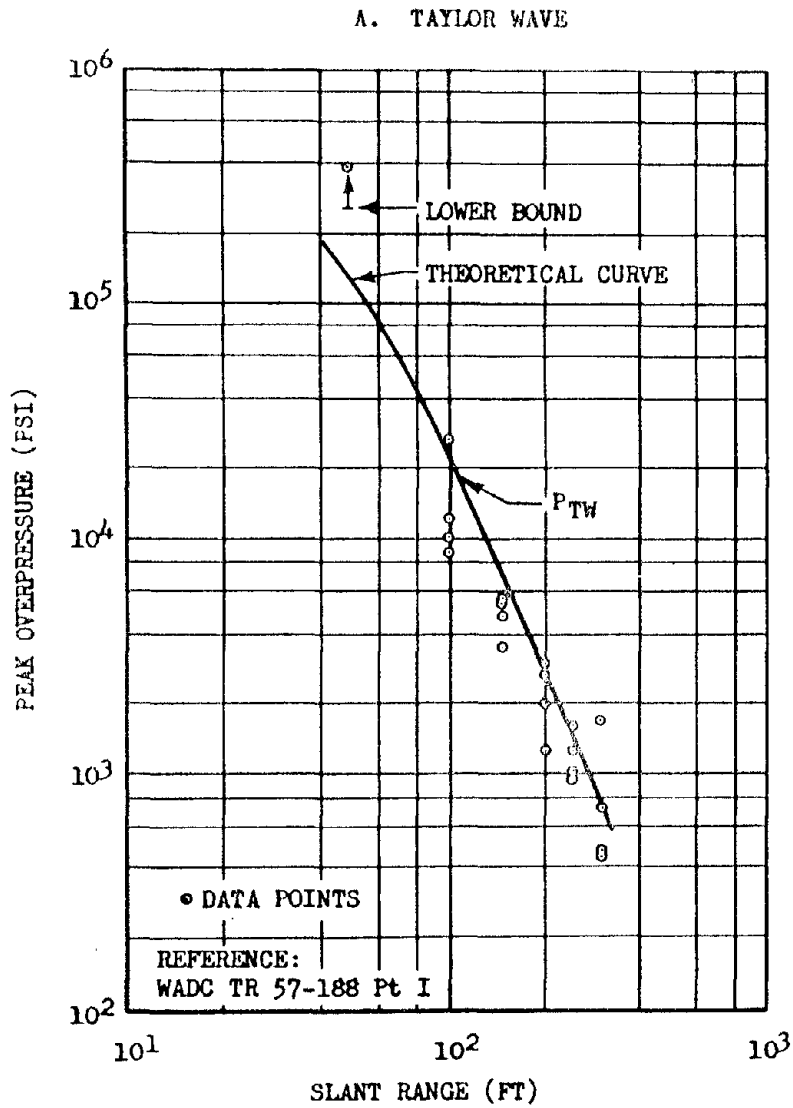
Figure D.7 Observed peak pressure versus slant range.
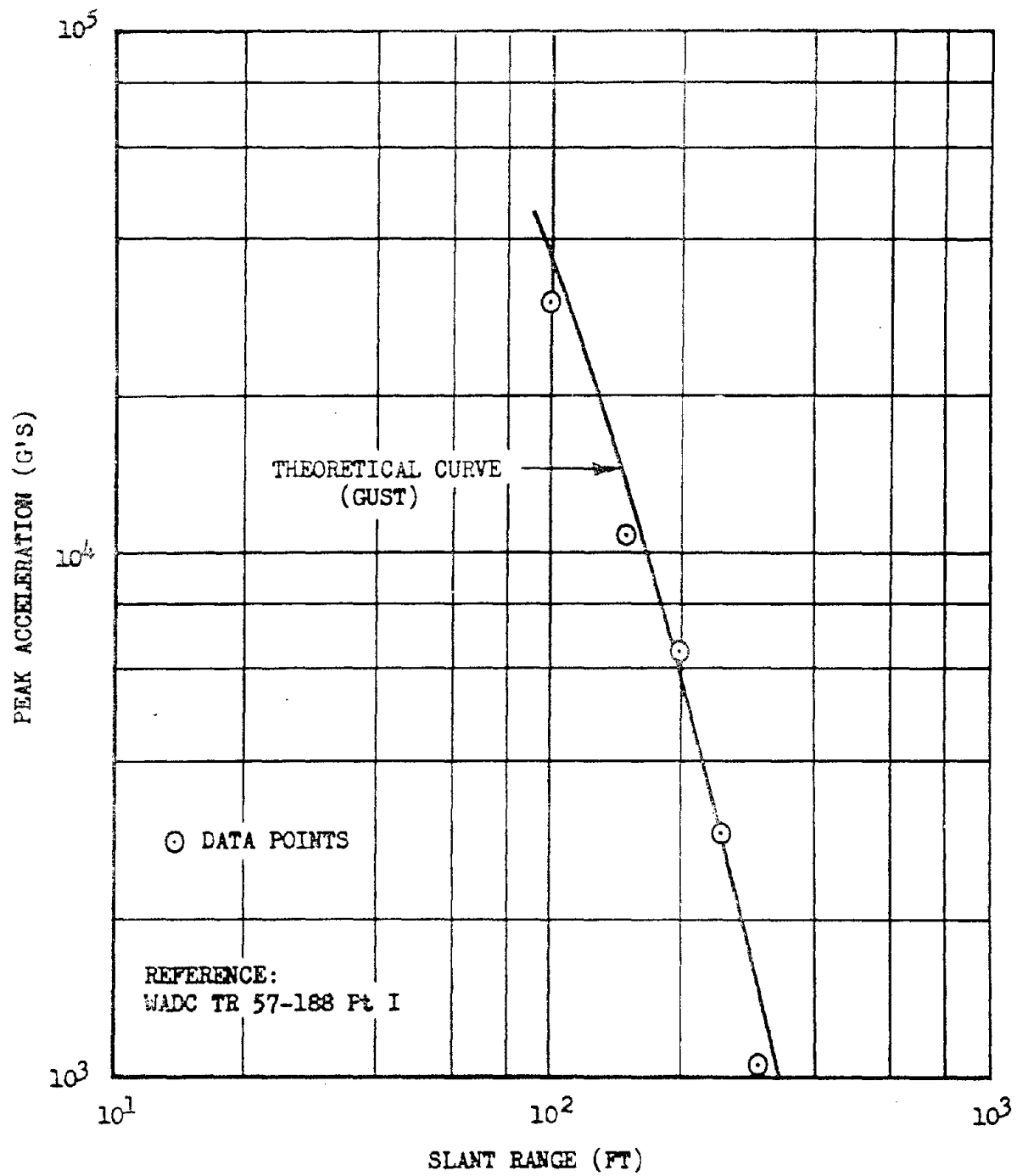
Figure D.8 Observed peak acceleration versus slant range.

REFERENCES

1. Martin Annis and Calvin Y. Sing; (S) The Measurement of Thermal and Hydrodynamic Phenomena Associated with the Fireball of a Nuclear Detonation. Part I Analysis of Experimental Fireball Pressure and Acceleration Data, Allied Research Associates, Inc., WADC Technical Report 57-188 Pt. 1, September 1957, Secret Restricted Data.
2. Martin Annis, Daniel J. Fink, and Arthur B. Cicero; (S) The Fireball and Associated Radiation Transport Phenomena with Application to the Destruction of ICBM Re-Entry Body, Allied Research Associates, Inc., Document No. ARA-286, 24 May 1956, Secret Restricted Data.
3. AFSWP; (U) Capabilities of Atomic Weapons, TM 23-200, November 1957, Confidential.

DISTRIBUTION

Military Distribution Category 52

ARMY ACTIVITIES

1. Deputy Chief of Staff for Military Operations, D/A, Washington 25, D.C. ATTN: Dir. of SW&R
2. Chief of Research and Development, D/A, Washington 25, D.C. ATTN: Atomic Div.
3. Assistant Chief of Staff, Intelligence, D/A, Washington 25, D.C.
4. Chief of Engineers, D/A, Washington 25, D.C. ATTN: ENGTB
5-6. Office, Chief of Ordnance, D/A, Washington 25, D.C. ATTN: ORDTN
7. Chief of Transportation, D/A, Office of Planning and Int., Washington 25, D.C.
8-10. Commanding General, U.S. Continental Army Command, Ft. Monroe, Va.
11. Director of Special Weapons Development Office, Headquarters CONARC, Ft. Bliss, Tex. ATTN: Capt. Chester I. Peterson
12. President, U.S. Army Artillery Board, Ft. Sill, Okla.
13. President, U.S. Army Air Defense Board, Ft. Bliss, Tex.
14. President, U.S. Army Aviation Board, Ft. Rucker, Ala. ATTN: ATBG-DG
15. Commandant, U.S. Army Command & General Staff College, Ft. Leavenworth, Kansas. ATTN: ARCHIVES
16. Commandant, U.S. Army Air Defense School, Ft. Bliss, Tex. ATTN: Command & Staff Dept.
17. Commandant, U.S. Army Artillery and Missile School, Ft. Sill, Okla. ATTN: Combat Development Department
18. Commandant, U.S. Army Aviation School, Ft. Rucker, Ala.
19. Commandant, U.S. Army Ordnance School, Aberdeen Proving Ground, Md.
20. Commandant, U.S. Army Ordnance and Guided Missile School, Redstone Arsenal, Ala.
21. Commanding General, U.S. Army Chemical Corps, Research and Development Comd., Washington 25, D.C.
22-23. Commanding Officer, Chemical Warfare Lab., Army Chemical Center, Md. ATTN: Tech. Library
24. Commanding Officer, Diamond Ord. Fuze Labs., Washington 25, D.C. ATTN: Chief, Nuclear Vulnerability Br. (230)
25-26. Commanding General, Aberdeen Proving Grounds, Md. ATTN: Director, Ballistics Research Laboratory
27-28. Commanding General, U.S. Army Ord. Missile Command, Redstone Arsenal, Ala.
29. Commander, Army Rocket and Guided Missile Agency, Redstone Arsenal, Ala. ATTN: Tech Library
30. Commanding General, White Sands Proving Ground, Las Cruces, N. Mex. ATTN: ORDBS-OM
31. Commander, Army Ballistic Missile Agency, Redstone Arsenal, Ala. ATTN: ORDAB-HT
32. Commanding General, Ordnance Ammunition Command, Joliet, Ill.
33. Commanding Officer, USA Transportation Research Command, Ft. Eustis, Va. ATTN: Chief, Tech. Info. Div.
34. Commanding Officer, USA Transportation Combat Development Group, Ft. Eustis, Va.
35. Director, Operations Research Office, Johns Hopkins University, 6935 Arlington Rd., Bethesda 14, Md.
36. Commander-in-Chief, U.S. Army Europe, APO 403, New York, N.Y. ATTN: Opot. Div., Weapons Br.

NAVY ACTIVITIES

37. Chief of Naval Operations, D/N, Washington 25, D.C. ATTN: OP-03EG
38. Chief of Naval Operations, D/N, Washington 25, D.C. ATTN: OP-75
39. Chief of Naval Operations, D/N, Washington 25, D.C. ATTN: OP-922G1

40-41. Chief of Naval Research, D/N, Washington 25, D.C. ATTN: Code 811
42-43. Chief, Bureau of Aeronautics, D/N, Washington 25, D.C.
44-48. Chief, Bureau of Aeronautics, D/N, Washington 25, D.C. ATTN: AER-AD-41/20
49. Chief, Bureau of Ordnance, D/N, Washington 25, D.C.
50. Chief, Bureau of Ordnance, D/N, Washington 25, D.C. ATTN: S.P.
51. Director, U.S. Naval Research Laboratory, Washington 25, D.C. ATTN: Mrs. Katherine H. Cass
52-53. Commander, U.S. Naval Ordnance Laboratory, White Oak, Silver Spring 19, Md.
54. Director, Material Lab. (Code 900), New York Naval Shipyard, Brooklyn 1, N.Y.
55. Commanding Officer, U.S. Naval Mine Defense Lab., Panama City, Fla.
56-57. Commanding Officer, U.S. Naval Radiological Defense Laboratory, San Francisco, Calif. ATTN: Tech. Info. Div.
58. Commanding Officer, U.S. Naval Schools Command, U.S. Naval Station, Treasure Island, San Francisco, Calif.
59. Superintendent, U.S. Naval Postgraduate School, Monterey, Calif.
60. Commanding Officer, Nuclear Weapons Training Center, Atlantic, U.S. Naval Base, Norfolk 11, Va. ATTN: Nuclear Warfare Dept.
61. Commanding Officer, Nuclear Weapons Training Center, Pacific, Naval Station, San Diego, Calif.
62. Commanding Officer, U.S. Naval Damage Control Tng. Center, Naval Base, Philadelphia 12, Pa. ATTN: ABC Defense Course
63. Commanding Officer, Air Development Squadron 5, VX-5, China Lake, Calif.
64. Director, Naval Air Experiment Station, Air Material Center, U.S. Naval Base, Philadelphia, Pa.
65. Commanding Officer, U.S. Naval Air Development Center, Johnsville, Pa. ATTN: NAS, Librarian
66. Commanding Officer, Naval Air Sp. Wpns. Facility, Kirtland AFB, Albuquerque, N. Mex.
67. Commander, U.S. Naval Ordnance Test Station, China Lake, Calif.
68. Commandant, U.S. Marine Corps, Washington 25, D.C. ATTN: Code AO3E
69. Director, Marine Corps Landing Force, Development Center, MCS, Quantico, Va.
70. Commanding Officer, U.S. Naval CIC School, U.S. Naval Air Station, Glynco, Brunswick, Ga.

AIR FORCE ACTIVITIES

71. Assistant for Atomic Energy, HQ, USAF, Washington 25, D.C. ATTN: DCS/O
72. Hq. USAF, ATTN: Operations Analysis Office, Office, Vice Chief of Staff, Washington 25, D. C.
73-74. Air Force Intelligence Center, HQ. USAF, ACS/I (AFCIN-3V1) Washington 25, D.C.
75. Director of Research and Development, DCS/D, Hq. USAF, Washington 25, D.C. ATTN: Guidance and Weapons Div.
76. The Surgeon General, HQ. USAF, Washington 25, D.C. ATTN: Bio.-Def. Pre. Med. Division
77. Commander, Tactical Air Command, Langley AFB, Va. ATTN: Doc. Security Branch
78. Commander, Air Defense Command, Ent AFB, Colorado. ATTN: Assistant for Atomic Energy, ADLDC-A
79. Commander, Hq. Air Research and Development Command, Andrews AFB, Washington 25, D.C. ATTN: RDRWA
80. Commander, Air Force Ballistic Missile Div. HQ. ARDC, Air Force Unit Post Office, Los Angeles 45, Calif. ATTN: WDSOT

183

FC04601011

SECRET

SECRET

RESTRICTED DATA

FC 0 4 6 0 1011